SUSTAINABLE DESIGN OF HYDROCARBON REFRIGERANTS APPLIED TO THE HERMETIC COMPRESSOR

NIGEL P. GARLAND

Thesis submitted in partial fulfilment of the requirements of
Bournemouth University for the degree of Doctor of Philosophy

November 2004

Bournemouth University
In collaboration with the
Engineering and Physical Sciences Research Council
(Design for Whole Lifecycle Programme)
Calor Gas Refrigeration
Plint and Partners

Abstract

International environmental concern led to the control and phase out of traditional chlorofluorocarbon refrigerants (CFCs) under the terms of the Montreal protocol. CFCs used in domestic applications were initially replaced with hydrofluorocarbons (HFCs) such as R134a which has a zero ozone depletion potential (ODP). The use of HFCs has also come under scrutiny as they have high global warming potential (GWP) and inferior thermodynamic and lubricating properties and have been replaced by hydrocarbon (HC) refrigerants such as R600a in much of the domestic European and Asian markets. Despite this, there has been little research into the long-term environmental consequences of their application.

Domestic refrigeration compressors were analysed to ascertain the tribological contact conditions for both R600a and R134a systems. A novel pressurised micro-friction test machine was developed to simulate the tribological conditions of the critical components using aluminium on steel samples. Refrigerant charges of R600a with mineral oil (MO) and poly-ol-ester (POE) lubricant and R134a with POE were tested for their tribological performance within the test rig. Experimental tribological information is presented from the physical test procedures to establish wear mechanisms and friction coefficients within the critical components. The tribological performance is used to predict deterioration in energy consumption and system durability.

Results indicate that for higher contact stresses R600a MO charges provide a lower wear regime than R600a and R134a POE charges. At lower contact stresses the R600a and R134a POE charges provide a very low wear, very low friction regime. Despite this, the R134a compressors critical component contact conditions lead to a faster deterioration in durability, hence increase in energy consumption compared to the R600a system.

Publications resulting from thesis

Nigel P. Garland and Mark Hadfield, "Tribological Analysis of Hydrocarbon Refrigerants Applied to the Hermetic Compressor" In Press, Tribology International, Journal.

Nigel P. Garland and Mark Hadfield, "Environmental Implications of Hydrocarbon Refrigerants Applied to the Hermetic Compressor", In Press, International Journal of Materials and Design.

Nigel P. Garland and Mark Hadfield "Tribological Analysis of Hydrocarbon Refrigerants Applied to the Hermetic Compressor", December 2003, Mission of Tribology Research 12, Institution of Mechanical Engineers.

Nigel P. Garland and Mark Hadfield "In-use Tribological Analysis of Hydrocarbon Refrigerants Applied to the Hermetic Compressor", Tribology in Environmental Design 2003, Professional Engineering Publishing Ltd, London, pp. 193-203, 2003. ISBN: 1-86058-415-2

M. Hutchings, S. Lewarne, K. Norman, N. Garland, M. Hadfield and G Howard "Educational challenges of web-based studies in sustainable development" Design and Manufacturing for Sustainable Development 1st International Conference, Liverpool, June 2002, PEP Publications, ISBN 1 86058-396-2

Publications resulting from thesis

Nigel P. Garland and Mark Hadfield, "Tribological Analysis of Hydrocarbon Refrigerants Applied to the Hermetic Compressor" In Press, Tribology International, Journal.

Nigel P. Garland and Mark Hadfield, "Environmental Implications of Hydrocarbon Refrigerants Applied to the Hermetic Compressor", In Press, International Journal of Materials and Design.

Nigel P. Garland and Mark Hadfield "Tribological Analysis of Hydrocarbon Refrigerants Applied to the Hermetic Compressor", December 2003, Mission of Tribology Research 12, Institution of Mechanical Engineers.

Nigel P. Garland and Mark Hadfield "In-use Tribological Analysis of Hydrocarbon Refrigerants Applied to the Hermetic Compressor", Tribology in Environmental Design 2003, Professional Engineering Publishing Ltd, London, pp. 193-203, 2003. ISBN: 1-86058-415-2

M. Hutchings, S. Lewarne, K. Norman, N. Garland, M. Hadfield and G Howard "Educational challenges of web-based studies in sustainable development" Design and Manufacturing for Sustainable Development 1st International Conference, Liverpool, June 2002, PEP Publications, ISBN 1 86058-396-2

List of Contents

List of Tables

List of Figures

List of Equations

Acknowledgement

I would like to acknowledge the help and guidance provided throughout the course of this thesis by my academic supervisor. Professor Mark Hadfield has provided both whilst remaining detached enough for me to make my own judgements and, occasionally, my own mistakes.

I also acknowledge the financial support provided by the Engineering and Physical Sciences Research Council (EPSRC) through their *Design for Whole Lifecycle Programme*.

I would also like to express my gratitude toward George Plint of Phoenix Tribology Ltd for the manufacture and supply of the test equipment without which this project would not have been possible. Thanks also go to F.J. Engineering Ltd for the manufacture and supply of the physical test samples used throughout this project. I would like to thank Daniel Colbourne of Calor Gas Refrigeration Ltd for supplying the refrigerants and providing safety training for the handling of hydrocarbon refrigerants.

I also acknowledge the help of Dr Robert Bulpett of the Experimental Techniques Centre, Brunel University for the SEM imaging and EDX analysis. Thanks also go to the staff of Tolpuddle House for all the help with equipment fabrication and modification.

A special thanks goes to Mrs Jacqui Holmes for answering the how, who, when, can you? type questions.

Finally, a big thank you goes to Anna, who was my girlfriend at the start of this project and wife before the end. Her support throughout the past three years has been invaluable, greatly appreciated and very thoughtful.

Nomenclature

a	Radius of contact (unit)
A_a	Apparent area of contact (m^2)
A_b	Axial cross section area, small end/gudgeon pin bearing (mm^3)
A_f	Area of contact separated by boundary film (m^2)
A_m	Area of metal to metal contact (m^2)
A_p	Piston area (mm^3)
A_r	Real area of contact (m^2)
α	Lubricant pressure-viscosity coefficient (m^2/N)
b	Contact width (m)
b_h	Half the contact width (m)
d	Wear depth at small end bush (mm)
β	Fractional film defect
E'	Effective elastic modulus (Pa)
E_1 and E_2	Elastic modulus of the contacting surfaces (Pa)
F	Frictional force (N)
f_{ff}	Friction coefficient when boundary film separation is complete
f_{mf}	Friction coefficient for unlubricated contacts
f_t	Total friction coefficient
H	Flow hardness of the softer surface, material hardness (Pa)
h	Wear depth at small end bush (m)
h_o	Minimum film thickness (m)
k	Dimensional wear coefficient ($mm^3\ N^{-1}\ m^{-1}$)
K	Probability factor (dimensional wear coefficient)
l	Sliding distance, gudgeon pin sliding distance (m)
l_b	Contact length (m)
l_c	Sliding distance during compression (m)
l_h	Half the contact length (m)
l_p	Length of pin sample wear scar (mm)
l_s	Sliding distance during suction (m)
λ	Specific film thickness ratio
μ	Friction coefficient
M_p	Material removed from pin sample (mm^3)

M_r	Material removed from small end bearing (mm^3)
η_o	Lubricant viscosity (Pa s)
P	Contact stress (pressure)
P_a	Apparent contact stress (Pa)
P_c	Power used during compression stroke (W)
P_d	Dissipated energy (W)
P_r	Real contact stress (W)
P_s	Power recovered during suction stroke (W)
P_t	Total energy (W)
P_u	Useful energy (W)
P_1	Pressure at beginning of cycle (Bar)
P_2	Pressure at discharge (Bar)
P_3	Pressure within the compression chamber (Bar)
Q_r	Real contact stress Ratio
R_e	Relative radius of the contact surfaces (m)
R_1 and R_2	Radius of contacting surfaces (m)
R_{sk1} and R_{sk2}	R.M.S. of the surface roughness' (m)
t_c	Duration during compression (s)
t_s	Duration during suction (s)
τ	Shear strength of the softer material (Pa)
U	Surface velocity (ms^{-1})
υ_1	Pouisons ratio for the small end bearing
υ_2	Pouisons ratio for the gudgeon pin
V	Wear volume (mm^3)
V_c	Volume within the compression chamber (mm^3)
V_e	Effective wear volume (mm^3)
V_d	Volume of refrigerant discharged (mm^3)
V_f	Wear volume, area of contact separated by boundary film (mm^3)
V_{ff}	Wear volume when boundary film separation is complete (mm^3)
V_l	Long wear volume (mm^3)
V_m	Wear volume, area of metallic contact (mm^3)
V_{mf}	Wear volume for unlubricated contacts (mm^3)
V_r	Volume of material removed (m^3)
V_s	Short wear volume (mm^3)
V_t	Total wear volume (mm^3)

V_1	Volume at bottom of piston stroke (crank angle 0°) (mm^3)
V_2	Volume at top of piston stroke (crank angle 180°) (mm^3)
ΔV_2	Change in volume at top of piston stroke (mm^3)
W	Contact load (N)
w	Load per unit width (N)
w_c	Piston load during compression (N)
W_p	Load on piston (N)
w_s	Piston load during suction (N)
ω	Wear rate, material removed per unit sliding distance ([length]^2)
Y_s	Yield strength of the softer material (Pa)

1 Introduction

1.1 Background to Research

1.1.1 Hydrocarbon Refrigerants

The traditional refrigerants for use in domestic refrigeration applications have, until the mid 1990s, been chlorofluorocarbons (CFCs). The use of these compounds was the primary cause of ozone depletion in the upper atmosphere and were controlled, limited and finally phased out under the terms of the Montreal protocol. CFCs used in domestic applications were initially superseded by hydrofluorocarbon (HFC) refrigerants such as R134a. The replacement refrigerant was selected for the similarity of its thermodynamic performance and its zero ozone depletion potential. The refrigerants zero ODP and lower global warming potential provided, what seemed, an ideal solution with apparently reduced environmental burden. The reality was that the thermodynamic performance was inferior to its predecessor, whilst the refrigerant charge failed to lubricate as effectively as the CFC charge. This in turn led to a higher environmental burden with increased energy consumption negating any direct environmental benefit in replacing the CFC refrigerant. As a solution, European domestic refrigeration has moved increasingly to hydrocarbon (HC) refrigerant R600a and is now the dominant technology (Meyer 1996).

The use of HCs as refrigerants is not new, Ammonia was used long before the advent of CFC compounds for the refrigeration industry. What is relatively new is the use of flammable HC compounds such as Butane, Isobutane, Propane and their blends as a zero ODP, low GWP alternative to CFCs and HFCs (Granryd 2000). The ODP of a refrigerant is an index number (by weight of product) with the CFC refrigerant R11 (CFC11) rated at 1, whilst the GWP relates (again by weight) to CO_2 and are classified under the Kyoto agreement as greenhouse gasses (Cranvey 1997) (Table 1.1).

Refrigerant	Technology	ODP	GWP
R11	(CFC)	1	4000
R12	(CFC)	1	8500
R134a	(HFC)	0	1300
R717 (Ammonia)	(HC)	0	0
R600a (Isobutane)	(HC)	0	3
R290 (Propane)	(HC)	0	3
R600a/R290 Blend	(HC)	0	3

Table 1.1 Refrigerant ODP & GWP

1.1.2 The Hermetic Compressor

The most commonly used type of compressor used in the domestic refrigeration market is of the hermetic reciprocating compressor design originally introduced by General Electric in 1927. The basic design has changed little over the years and varies only slightly between manufacturers. The unit consists of a simple reciprocating piston in cylinder design, coupled via a connecting rod to a crankshaft. The inlet/outlet valves are of the reed type mounted in a simple cylinder head. The crank is driven directly by a single-phase electric motor. To prevent refrigerant leakage over time (service life of 10-20 years is typical) the whole is sealed in a hermetic chamber containing the refrigerant and lubricant charge. In this configuration, no external dynamic seals are required therefore little likelihood of a refrigerant leakage occurring during normal operation.

1.1.3 Aims of the Investigation

The environmental impact of a hermetic refrigerator compressor employing hydrocarbon refrigerant and compatible lubricant combinations was assessed from a tribological viewpoint. This included testing under pressurised/depressurised conditions using a novel micro-friction test rig. Sustainable development of the hermetic compressor was evaluated using Life Cycle Analysis (LCA) tools in terms of the friction and durability of the mechanical system for a number of scenarios. These included alternative operational timeframes for the products in-use phase (hence electricity fuel mix and subsequent emissions profile) and alternative lubricants (hence wear

regime, durability and product longevity). The overall scheme for the thesis investigation can be encompassed within a flow-chart (Figure 1.1).

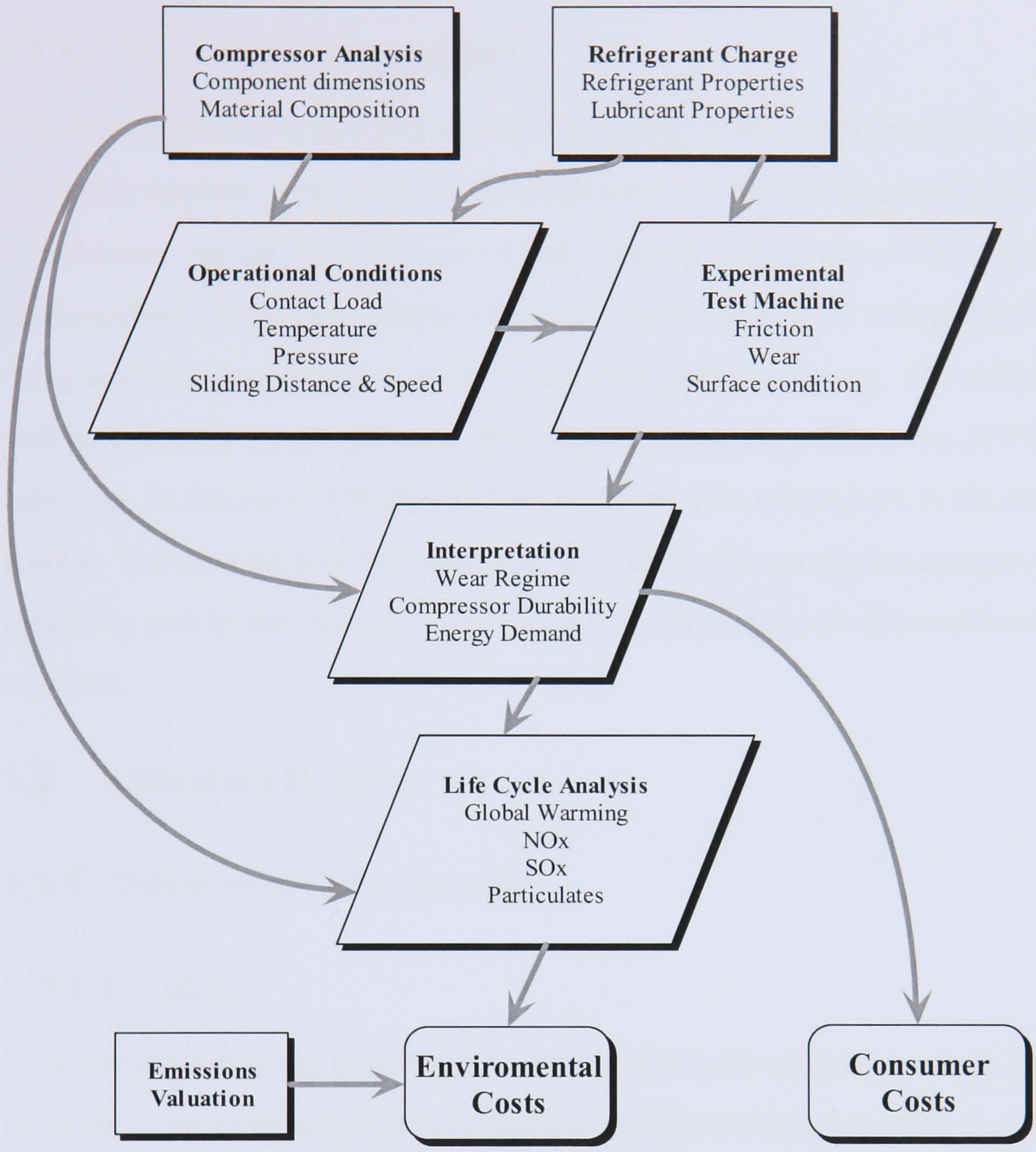

Figure 1.1 Flow chart encompassing theses scheme

1.1.4 Objectives of the Investigation

- Design, development and manufacture of a novel pressurised micro-friction machine.
- Quantify and assess the tribological performance of hydrocarbon refrigerant/lubricant combinations under simulated operational conditions (liquid/vapour phases) using the micro-friction machine.
- Ascertain the compressors long-term durability and performance characteristics from tribological data.
- Perform Life Cycle Analysis of a hermetic compressor to quantify the important in-use environmental impacts of hydrocarbon refrigerants.

- Monetarisation of environmental impacts to assess the total economic, health and environmental cost of the product.

1.1.5 Scope of the Investigation

The Investigation for this project will be limited to the environmental and economic aspects of sustainable development; it is not anticipated that the social issues arising from the use of hydrocarbon refrigerants will be addressed. Hydrocarbon refrigerant R600a will be compared with HFC refrigerant R134a using a novel, purpose built, pressurised reciprocating test rig. The refrigerants will be tested for their influence upon the tribological performance of POE lubricant, in the case of R600a and R134a, and with mineral oil in the case of R600a. The data gained from the tests will be used to gauge the products longevity and in-use energy profile for a life cycle analysis and cost benefit analysis.

1.2 Literature Review

1.2.1 Tribological Considerations

1.2.1.1 Wear

Wear within a bearing or contact is conditional upon contact pressure, lubricant properties, temperature, surface roughness and material properties. It is the relationship between these properties that dictates lubricant film thickness, surface separation, lubrication regime and wear mechanism. All machine finished surfaces have a surface roughness, typified by hills and valleys or asperities. As the two surfaces of a contact come together the asperities deform elastically to support the load. As the load increases the asperities deform plastically resulting in localised welding at the asperity junctions. The weld junctions continue to make and break as the surfaces slide across each other resulting in adhesive wear or scuffing (Stolarski 1996). Although equations are provided for friction, wear and lubrication, they are for guidance only since the surface conditions and lubricant properties are subject to change throughout the operation of the bearing contact. Ultimately, wear at contacting surfaces is likely to be a combination of, but not limited to, those described here.

1.2.1.2 *Adhesive wear*

Adhesive wear is the result of localised welding between the sliding surfaces of a bearing or contact. The surface asperities displacing the lubricant molecules as they come into contact. The asperities deform elastically and, as the asperity contact load increases they begin to deform plastically, if localised conditions permit welding may occur at their junctions. As the two surfaces separate the welds tend to break, away from the junction, causing material deposition from one (softer) material surface to the other (harder) surface (Stolarski 1989) (Figure 1.2). If adhesive wear is the result of a breakdown of lubricating film separation the wear can be described as scuffing (Williams 1994).

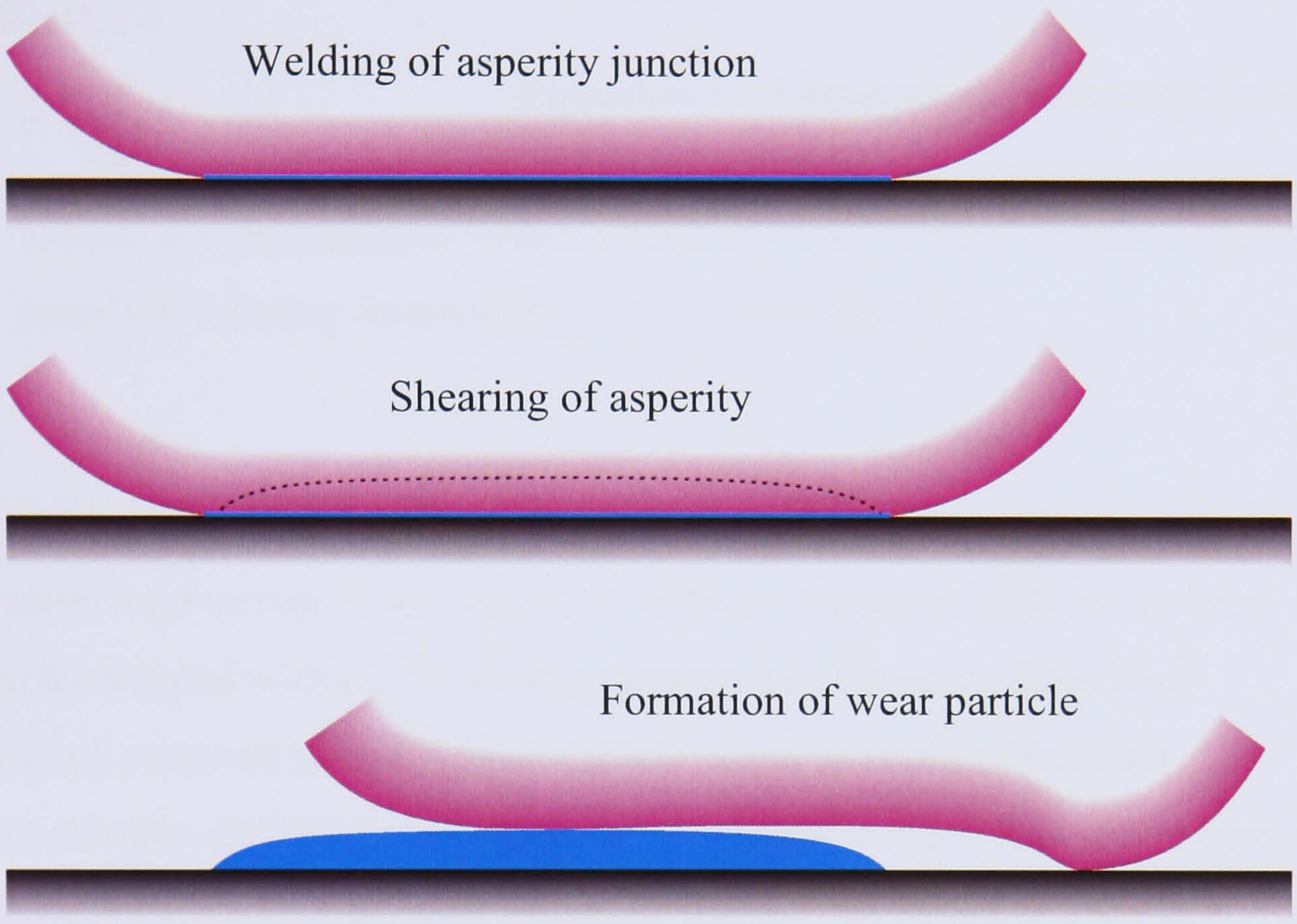

Figure 1.2 Adhesive wear particle formation

For the calculation and subsequent interpretation of wear the Archard wear equation is commonly used. In its original form (Archard 1953) the equation describes probability of creating a wear particle of radius a from sliding a single contact of the same radius through a distance of $2a$ (Equation 1.1):

$$\omega = KP/3a$$ **Equation 1.1 Original Archard wear equation**

Where: ω = wear rate (material removed per unit sliding distance); P = contact pressure; a = radius of contact; K is the Probability factor.

Taking all the individual sliding contacts into account and relating to the real area of contact under sliding conditions arrives at the most commonly used variant (Equation 1.2):

$$V = KlA_r = Kl\frac{W}{Y_s}$$

Equation 1.2 Archard wear equation

Where: V = volume of material removed (mm^3); l = sliding distance (m); A_r = real area of contact (m^2); W = contact load (N); Y_s = yield strength of the softer surface (Pa); K = dimensionless wear coefficient.

Often more useful for the evaluation of wear data is the dimensional wear coefficient *k:*

$$k = \frac{V}{lW}$$

Equation 1.3 Dimensional wear coefficient

Where: k = dimensional wear coefficient (mm^3/Nm); V = wear volume (mm^3); l = sliding distance (m); W = contact load (N).

1.2.1.3 Abrasive wear

Abrasive wear occurs when the rough surface of a harder material or hard particles trapped within it (two body abrasion) or between (three body abrasion), removes particles from another, often as result of external contamination (Williams 1994). Three body wear is much less severe than two body as the particles can break down, be filtered out, or act as a surface separation. Abrasive wear can take place as plastic flow, brittle fracture or as a combination of both (Hutchings 1992). If a trapped particle is significantly harder than the counter-face it will indent the surface causing plastic flow, if the particle is less than 1.2X the hardness of the surface, it will itself be blunted and not indent the counter-face (Hutchings 1992). The former is unlikely to be severe since harder external contaminants (silica grits) are unlikely to be present in a sealed system such as the hermetic compressor (Ciantar 2000). However it is likely that phases of harder material present in either counter face or work hardened wear particles could induce abrasive wear. Whilst plastic flow from trapped particles may not be significant, they may cause brittle fracture of both the embedded face and the counter-face (Hutchings 1992).

1.2.1.4 Chemical wear mechanisms

Chemical wear is the wear of materials by chemical reaction (wholly or partly) between the contact surfaces or between the surfaces and another reactive agent. The reactive agent may be a lubricant additive or a compound present in the operational environment. Chemical wear is normally characterised by the formation of a reacted film layer on sliding contact surfaces. Under these conditions the film layer may influence the sliding contact in a number of ways (Stachowiak and Batchelor 2001):

- A durable film may prevent further corrosion and result in low wear rates.
- A weak film may be removed quickly resulting in high wear rates.
- Resultant wear may be the sum of the adhesive and chemical actions.
- Wear products may react with the lubricant to produce low friction soaps.

Lubricant anti-wear and extreme pressure additives are typically designed to react chemically with the worn contact surfaces to produce the reacted film layers. At lower loads the creation of high viscosity metallic soaps from the reacted surfaces may support the contact load within the boundary regime and prevent further wear (Stachowiak and Batchelor 2001). The reacted soap layers typically have a higher melting point than the original lubricant and continue to provide film separation at temperatures beyond that of the lubricant with non-reactive surfaces (Williams 1994). At higher loads lubrication by sacrificial film may dominate. Here a durable reactive film may be created on the contact surfaces, replenishing itself at a faster rate than it can be removed. If the loads are too high the layer may be removed faster than it can be replenished, resulting in higher wear rates. If the selection of lubricant and additive package is not carefully matched to the contact materials and operating conditions, wear rates may be much higher than non-additised packages.

Ester based lubricants have been found to react with aluminium wear surfaces producing very low friction and wear rates at low loads with a sudden transition to very high wear rates at higher loads (Montgomery 1965). At lower loads the wear rates were lower than those found for mineral oil lubricated contacts producing smooth wear surfaces on both the aluminium and steel

counterfaces. At higher loads the wear rates were much higher than those recorded for the MO but the contact surfaces were again left smooth. Further inspection of the steel surfaces revealed little material removal, rather the valleys between asperity peaks had been filled. Friction coefficients at the lower loads were found to be as low as 0.01 whilst for the higher loads coefficients as high as 0.2 were recorded.

Lubricant anti-wear and extreme pressure additives containing phosphorous based compounds were also found to increase wear rates within aluminium-steel contacts (Wan Yong and Qunji 1995). Under the test conditions endured, phosphate additives reduced the friction coefficient whilst phosphite additives increased the friction coefficient compared to pure base-stock. Both types of additive showed an increase in wear rates when compared to base-stock.

1.2.1.5 Friction

As discussed previously (1.2.1.2) when two surfaces are brought together the asperities will deform locally, increasing the real area of contact. The real area of contact is a function of the material yield strength of the softer surface and the applied load:

$$A_r = \frac{W}{Y_s}$$ **Equation 1.4 Real area of contact**

Where: Ar = real area of contact; W = applied load; Y_s = yield strength.

The contact surfaces may promote localised welding or adhesion at the junction between the asperities, deformation of the softer surface or a combination of the two. In each case, shearing of the junction will be required to promote lateral movement of the surfaces. For welded asperities (adhesive wear), the shear strength of the junction or the softer material will dominate. Therefore for frictional conditions where adhesive wear is the major component the shear strength of the softer material can be used, with the real area of contact, to calculate the friction force:

$$F = A_r \tau$$ **Equation 1.5 Friction force**

Where: Ar = real area of contact; F = frictional force (N); τ = shear strength of the softer material (Pa).

The ratio of friction force to the load applied is the coefficient of friction:

$$\mu = \frac{F}{W}$$

Equation 1.6 Friction coefficient

Where: F = frictional force; W = applied load; μ = friction coefficient.

Substituting the friction force according to the preceding equations (Equation 1.4, Equation 1.5) the frictional coefficient can be expressed in terms of material yield strength and shear strength.

$$\mu = \frac{\tau}{Y_s}$$

Equation 1.7 Friction coefficient from material properties

Therefore for a low friction coefficient the surfaces should present a low shear strength and high hardness. For most materials these attributes are exclusive and are normally found to be in the ratio of about 0.2.

Although friction and wear are inexorably linked, an increase in wear does not infer an increase in friction. In boundary lubricated steel contacts, changing the test lubricant from polyalphaolefin (PAO) to synthetic ester (SE) results in a reduction of friction but a substantial increase in wear rates (Kassfeldt, Norrby et al. 2000). However, a constant level of friction is usually indicative of a constant rate of wear, any fluctuation being allied to a change in lubrication regime or surface film (Plint 2000).

1.2.1.6 Lubrication

Within a bearing or sliding contact the main purpose of the lubricant is to provide asperity separation through the creation of a lubricating film, the thickness of which depends upon the contact pressure (or load per unit width), velocity and lubricant absolute viscosity. Point contact experiments (Archard and Kirk 1960) have found that lubricating films can persist at low speed lightly loaded conditions whilst at higher speeds plastic flow of hardened steel can occur before film breakdown. For elastohydrodynamic contacts, the film thickness h_o can be calculated for smooth surfaces (Stolarski 1989):

$$h_o = 4.9\frac{\eta_o U R_e}{w}$$

Equation 1.8 Simple elasto-hydrodynamic film thickness

Where: h_o = minimum film thickness (m); η_o = lubricant viscosity (Pa s); U = surface velocity (ms^{-1}); w = load per unit width (N); R_e = Relative radius of the contact surfaces (m):

$$R_e = 1\Big/\left(\frac{1}{R_1} - \frac{1}{R_2}\right)$$

Equation 1.9 Relative radius

Where: R_1 and R_2 = Radius of the contact surfaces (m).

From the equation it is clear that increasing the viscosity, surface velocity, or relative radius (hence contact area), or reducing the contact loading, will lead to an increase in lubricant film thickness. Rearranging to present the group $\eta_o U/p$ where p is the contact pressure provides the Stribeck number. Plotting friction coefficient against this group results in the Stribeck curve (Figure 1.3) and shows that under elastohydrodynamic conditions friction falls proportionally to a reduction in the Stribeck number. As the Stribeck number falls a transition is reached where contact between surfaces occurs and friction begins to rise. As the load is supported increasingly by the surfaces, so the friction coefficient rises until the load is supported entirely by the surfaces. Beyond this point the hydrodynamic characteristics of the contact no longer influence friction at the contact.

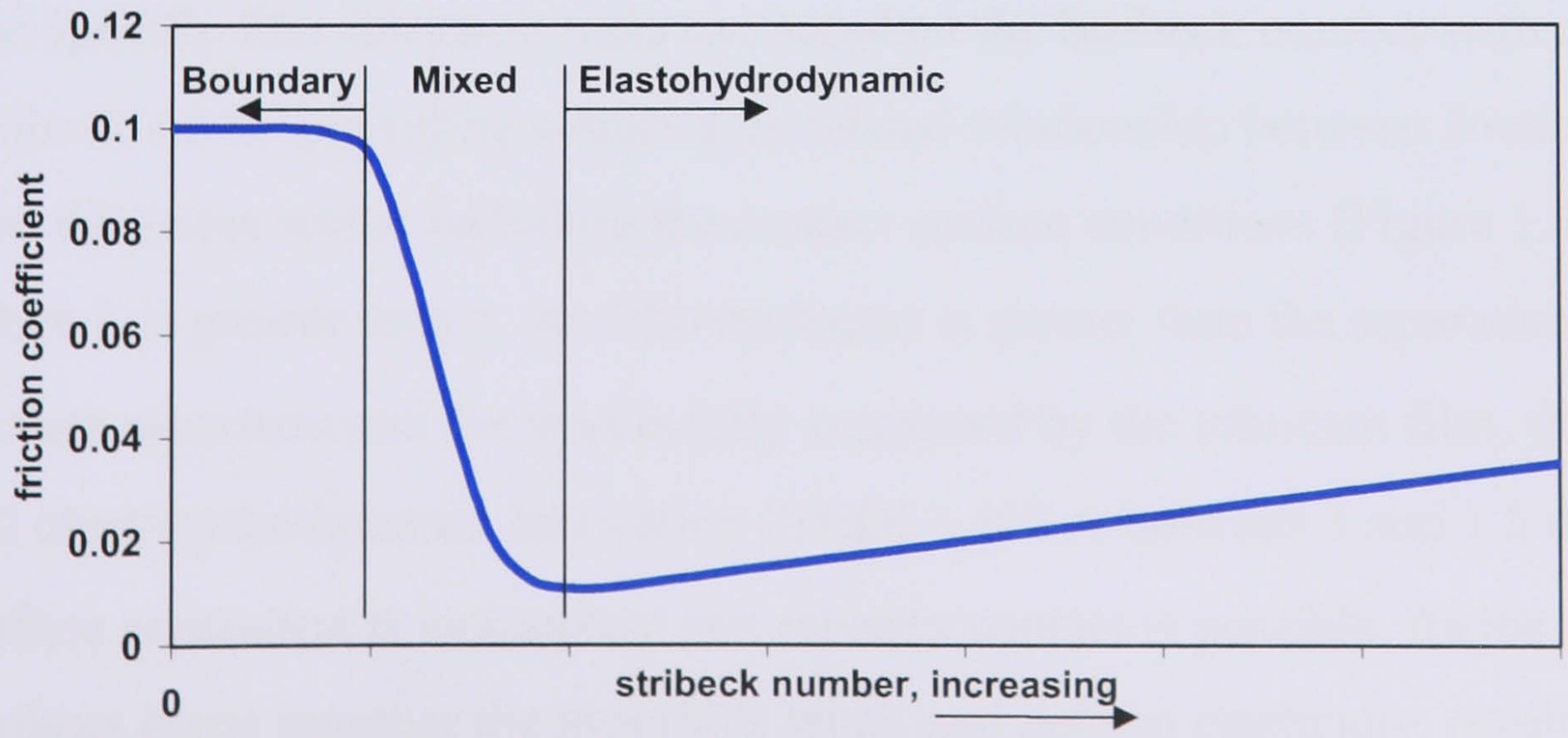

Figure 1.3 Stribeck curve

The simple EHD equation (Equation 1.8) fails to account for the localised increase in lubricant viscosity that can occur at high pressures and velocities, with the subsequent increase in film thickness. To this end a modified EHD power equation is available (Hamrock and Dowson 1979):

$$h_o = 3.63R_e\left(\frac{V\eta_o}{E'R_e}\right)^{0.68}(\alpha E')^{0.49}\left(\frac{W}{E'R_e^{\,2}}\right)^{-0.073}\left(1-e^{-0.68k}\right)$$

Equation 1.10 Elasto-hydrodynamic lubrication

Where: α = pressure-viscosity coefficient (m^2/N); E' = effective elastic modulus (Pa):

$$E' = 1\Big/\left(\frac{1-\upsilon_1^{\,2}}{E_1}+\frac{1-\upsilon_2^{\,2}}{E_2}\right)$$

Equation 1.11 Effective elastic modulus

Where E_1 and E_2 = Elastic modulus of the surfaces (Pa); υ_1 and υ_2 = Pouisons ratio for the surfaces.

The film thickness calculated for smooth surfaces can be used in conjunction with the R.M.S. of the surface roughness to calculate the specific film thickness (λ) proposed by Bodensiek (Bodensiek 1965):

$$\lambda = \frac{2h_o}{\left(R_{sk1}+R_{sk2}\right)}$$

Equation 1.12 Specific film thickness ratio

Where: R_{sk1} and R_{sk2} are the R.M.S. of the surface roughness' (m); λ = specific film thickness ratio.

The specific film thickness ratio can supplant the Stribeck number within Stribeck curve, providing a more generalised relationship between friction and film thickness whilst including the contact surface conditions (Figure 1.4). When λ is greater than 3, the film thickness is greater than the separation of surface asperities and the load is fully supported by the lubricant film, this is full elastohydrodynamic lubrication (EHDL). If λ is between 3 and 1.5 the surface separation is incomplete and asperity contact is possible. As the surfaces come together the asperities touch and deform elastically, resulting in mixed or partial elastohydrodynamic lubrication.

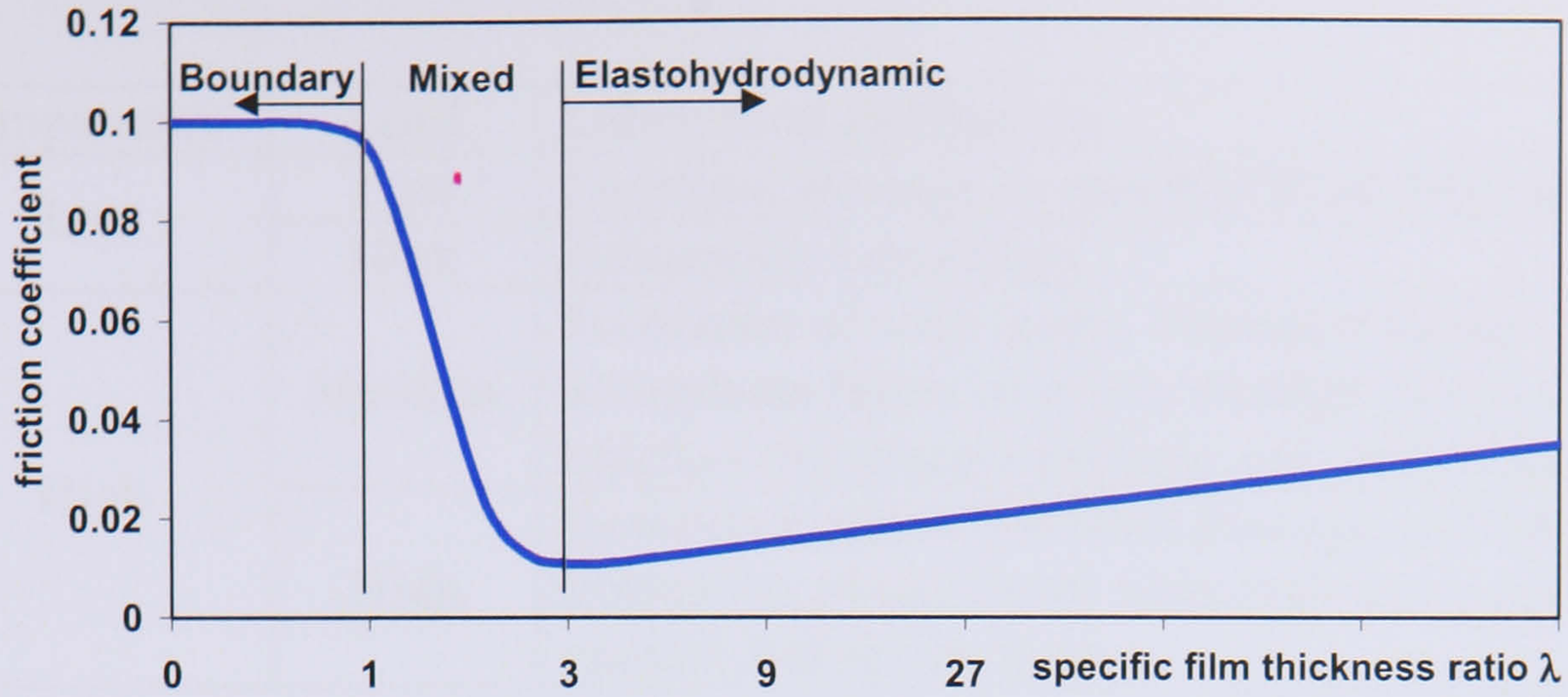

Figure 1.4 Friction coefficient relative to specific film thickness

Here the load is increasingly shared with the asperities as λ reduces resulting in some glazing but no detrimental effects to the bearing performance. If the surfaces are brought even closer together and λ is between 1.5 and 1, surface glazing and distress will occur, together with an increase in bearing friction. If λ falls below 1, the load is supported almost entirely upon the asperities resulting in deformation and wear. At this point the task of the lubricant is no longer to provide a lubricant film, but to provide a boundary film to prevent the surface asperities from adhering, it is here that scuffing or adhesive wear occurs (Stolarski 1996).

1.2.1.7 Boundary lubrication

The equations for adhesive wear volume (Equation 1.2) and friction force (Equation 1.5) have shown that both friction force and wear are proportional to the real area of contact. If the surfaces can be prevented from adhering, reducing the area of contact subject to localised welding, both friction and wear can be reduced. The equation for the coefficient of friction from material properties (Equation 1.7) has shown that for a low coefficient of friction, it would be desirable to have both low shear strength and a high hardness. Since these are incompatible a low shear strength layer attached to a hard contact surface would be suffice to reduce the friction coefficient and is the principle behind boundary lubrication (Stachowiak and Batchelor 2001). Effective boundary lubrication can be initiated by a number of distinct mechanisms, each within particular temperature and contact pressure ranges: (Table 1.2) adapted from (Stachowiak and Batchelor 2001).

Temperature	Load	Lubrication mechanism.
Low	Low	Localised increase in viscosity at surface contact.
	High	Adsorption lubrication.
High	Medium	Formation of soap layers, viscous material or amorphous layers of debris through chemical reaction of lubricant package and contact surface.
	High	Reaction between lubricant package and surface. Formation of sacrificial films preventing metallic contact and severe wear.

Table 1.2 Categorisation of boundary lubrication mechanisms

For low temperature contacts, a localised increase in viscosity can prevent surface contact at low loads. Linear hydrocarbon polar molecules align perpendicular to the surface, attracting further layers to form a protective film. The layers, however, do not persist beyond contact pressures of 2 MPa or temperatures of 50°C (Fuks 1962). More effective for low temperatures (up to 150°C) is adsorption lubrication which can provide film separation up to loads or 1 GPa. A single layer of polar lubricant additive is adsorbed onto the surface. Bonding between the polar end group and the substrate is strong, whilst the hydrocarbon chain repels. This repulsion provides for a low shear strength interface between the surfaces, hence low friction and wear characteristics (Stachowiak and Batchelor 2001).

For higher temperature, medium load contacts, chemical reaction between the lubricant components and the surfaces can initiate the formation of low shear products at the surface. These may be formed by the reaction between substrate and fatty acid additive to produce a metallic soap film at the surface. The soap film is generally more viscous than the original lubricant package, therefore increasing the load carrying capacity at the contact. Alternatively, an amorphous layer may be constructed from finely ground reacted debris particles entrained within the contact. In either case the result film, whilst significantly thicker than those resulting from adsorption lubrication, require material contribution from the sliding surfaces. For higher loads, lubrication by sacrificial films (extreme pressure lubrication) can prevent excessive surface wear. Under sliding contact oxidised surface layers are removed to present a nascent surface. This surface attracts the additive package, typically sulphur, phosphorous or a combination, which in turn reacts with the surface to form a

durable film layer. Both high temperature mechanisms are also discussed in chemical wear (1.2.1.4).

For the domestic hermetic compressor, boundary lubrication is typically found at the gudgeon pin/small end bearing contact. With CFC based refrigeration systems boundary lubrication regime was provided by chlorine within the refrigerant compound acting as an extreme pressure lubricant. HFCs on the other hand were unable to form a durable boundary layer under the same operating conditions and suffered from Adhesive wear (Na, Chun et al. 1998) (Mizuhara, Akei et al. 1994).

1.2.1.8 Fractional Film Defect

From the concept of adhesive wear (1.2.1.2) it is clear that unlubricated contacts can wear by adhesion and promote higher friction regimes. Additionally, the concept of boundary lubrication films (1.2.1.7) has shown how separation of the surfaces with a low shear film can prevent wear and reduce friction. In many cases, the boundary lubrication of contacts can be found somewhere between these actions, with the load being shared between the boundary film and the contacting surfaces, the ratio of which is the fractional film defect (Equation 1.13, Figure 1.5) (Stolarski 1996).

$$\beta = \frac{A_m}{A_r}$$

Equation 1.13 Fractional film defect

$$A_f = A_r - A_m$$

Where: β = fractional film defect; A_m = Area of metal to metal contact (m^2); A_r = real area of contact (m^2); A_f = Area of contact separated by boundary film (m^2).

Since $A_m \leq A_r$ then β will be in the range 0-1. From the equation it is clear that when $\beta = 0$ there is no metallic contact and the load will be carried entirely by the boundary film, therefore friction and wear characteristics will be equal to that of a contact where the boundary film is complete. Conversely, when $\beta = 1$, there is no boundary separation of surfaces and the friction and wear characteristics will be that of an unlubricated contact.

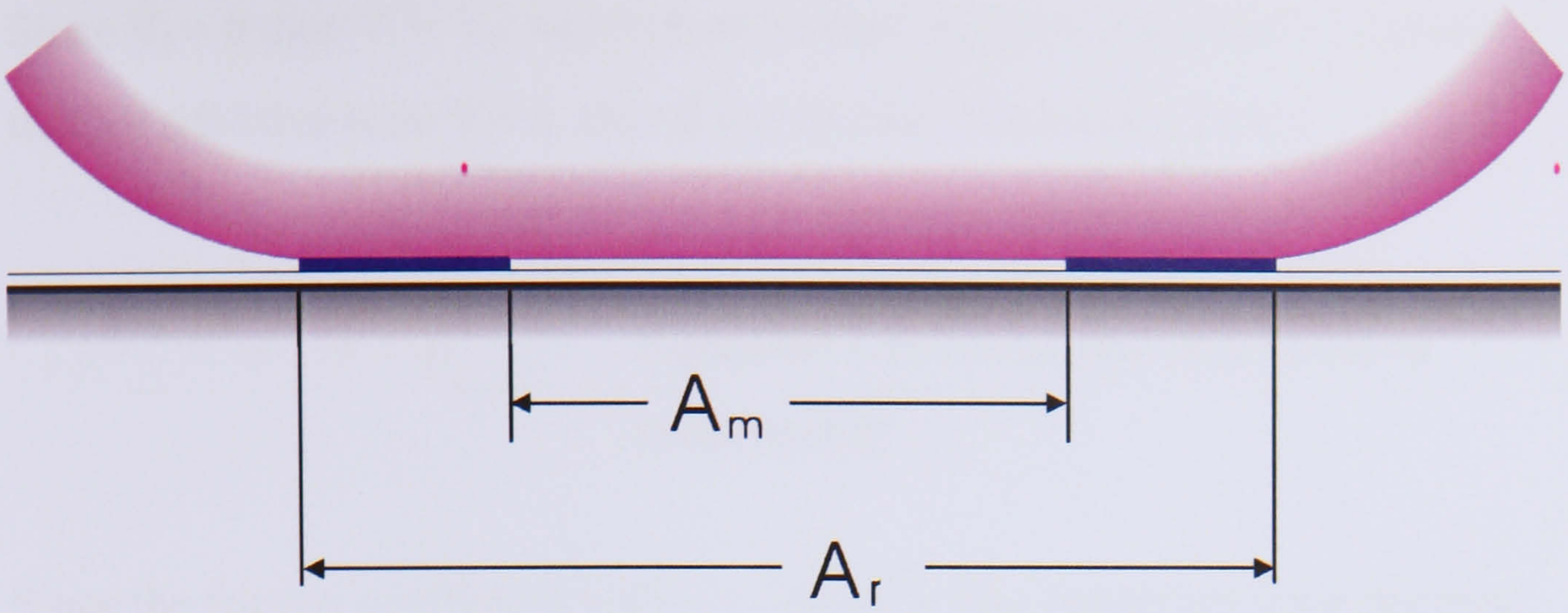

Figure 1.5 Fractional film defect at asperity contact

Between these values for β the resultant wear volume will be the sum of that contributed by the area of metallic contact and the area of contact separated by boundary film (Equation 1.14):

$$V_t = V_m + V_f$$ **Equation 1.14 Total wear volume in a contact**

where: V_t = Total wear volume (mm^3); V_m = Volume of material removed due to metallic contact (mm^3); V_f = Volume of material removed from the area of contact separated by boundary film through fatigue, subsurface cracking and hydraulic action (mm^3).

V_m and V_f can be expressed in terms of the fractional film defect β:

$$V_m = \beta V_{mf}$$ **Equation 1.15 Metallic contact wear fraction**

$$V_f = (1-\beta)V_{ff}$$ **Equation 1.16 Boundary film wear fraction**

where: V_{mf} = Wear volume for unlubricated contacts; V_{ff} = wear volume when boundary film separation is complete.

The wear volume can be expressed in terms of the fractional film defect:

$$V_t = \beta V_{mf} + (1-\beta)V_{ff}$$ **Equation 1.17 Wear volume relationship**

Since $V_f \approx 0$ then $V_t = V_m$ and Archards wear equation (Equation 1.2) shows that for adhesive wear $V \propto A_r$ then β can be found (Equation 1.18):

$$V_t = \beta V_{mf} \therefore \beta = \frac{V_t}{V_{mf}}$$

Equation 1.18 Simplified wear volume relationship

Since the friction coefficient within a contact is also dependant upon the area of metallic contact and that of film separation the fractional film defect can be expressed in terms of friction:

$$f_t = \beta f_{mf} + (1 - \beta) f_{ff}$$

Equation 1.19 friction coefficient relationship

where: f_t = total friction coefficient; f_{mf} = friction coefficient for unlubricated contacts; f_{ff} = friction coefficient when boundary film separation is complete.

1.2.2 Hydrocarbon Refrigerants

1.2.2.1 Design Implications for the Hermetic Compressor

The similar thermodynamic properties of R134a to R12 are the main reason for its selection as a zero ODP replacement refrigerant (Na, Chun et al. 1998), however the reduction in Coefficient of Performance (COP) is well documented (Granryd 2000) (Meurer and Law 1998). R600a on the other hand has quite different thermodynamic properties, it has a greatly reduced vapour saturation pressure and volumetric refrigerating capacity (45%) compared to R134a and R12, this leads to the requirement for a larger compressor swept volume to achieve the same cooling capacity (80% larger than R12). Since the R600a has a lower pressure drop than either R134a or R12 piston pressure is reduced, increasing COP relative to both R134a and R12 (Granryd 2000) (Meurer and Law 1998) (Paul 1996) (Meyer 1996). The improved COP for R600a over R134a is borne out in the compressor manufacturer data tables (Danfoss, Electrolux). The manufacturers group equivalent compressor technologies together as standard, efficient and high efficiency compressors.

For this study, compressors in the 155-165W range have been compared (Figure 1.6). For efficient Danfoss compressors the improvement in ranges from 8-13% and high efficiency models range from 5-9%. For Electrolux compressors the improvements are from 4-10% for efficient and 2-6% for high efficiency models. The actual swept volume for the R600a compressors is 66% greater than that of similarly rated R134a compressors.

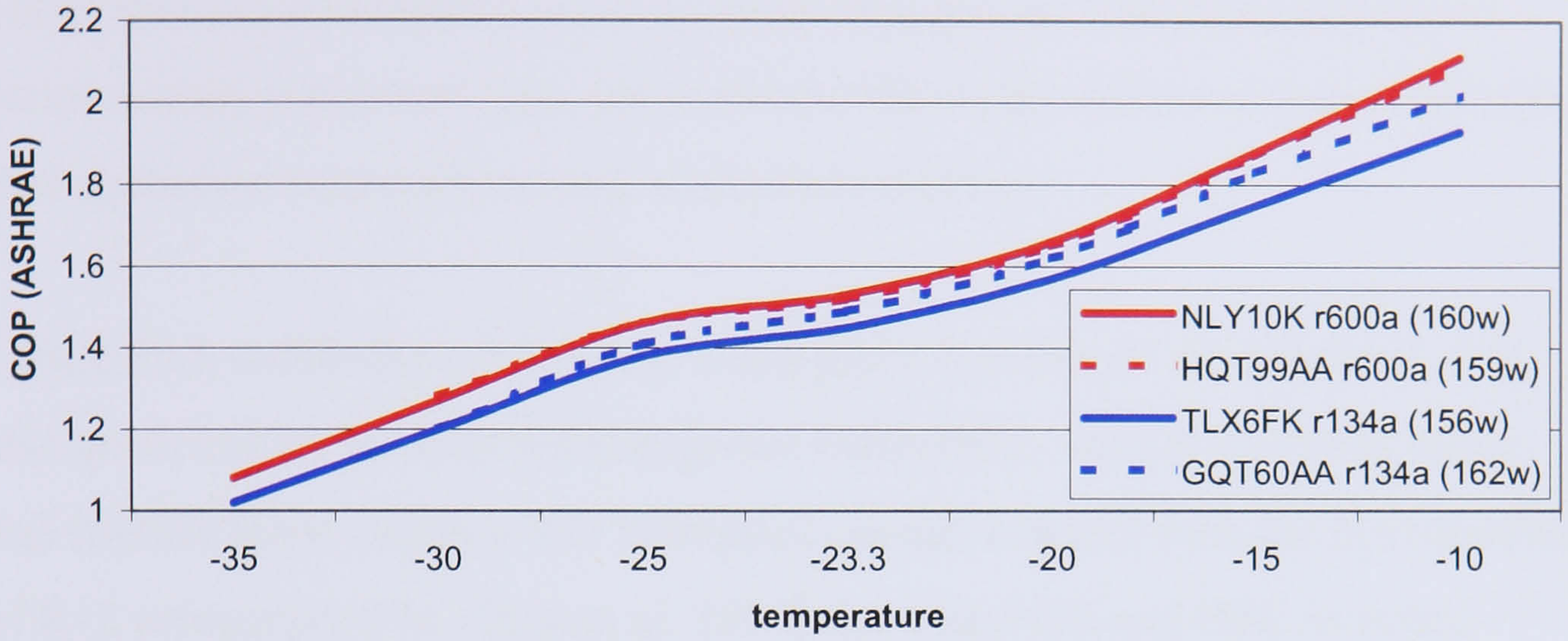

Figure 1.6 Comparison of COP, R134 and R600a 160W compressors

1.2.2.2 Design Implications for the Lubricant

The Lubricant used in hermetic compressors has a number of tasks to perform other than lubrication to bearings, journals and piston. It must also provide electrical insulation between the motor windings and compressor shell, cool the motor and compressor mechanism and provide sealing for the piston, cylinder and valve mechanisms (Reyes-Gavilan, Eckard et al. 1996). To provide adequate lubricant return and to prevent fouling of the capillary tube and evaporator, the refrigerant and lubricant should be miscible. Although experiments have shown excellent oil return of immiscible combinations using R134a (Reyes-Gavilan, Eckard et al. 1996) the range of experimentation is limited and not in agreement with consensus. For CFC refrigerants the lubricant of choice has been mineral oil (MO), for HFCs synthetic lubricant poly-ol-ester (POE) are preferred (Na, Chun et al. 1998) while for HCs MO's are again in favour, although POE's and polyalkylene glycol (PAG) are also compatible (Granryd 2000).

Since the lubricant film thickness is a product of lubricant viscosity, sliding velocity, contact pressure and surface roughness, changing any one of these will have an effect on the lubrication regime. For the hermetic compressor,

there are a number of areas at which wear can occur. The main motor/crankshaft bearings and journals, the crank pin/connecting rod (big-end) bearing and journal, the piston pin/connecting (small-end) bearing and journal, the piston/cylinder sliding interface and the inlet/exhaust flapper (reed) valves are all subject to varying degrees of wear. Previous studies (Na, Chun et al. 1998; Ciantar, Hadfield et al. 1999; Ciantar 2000) have shown the piston pin/connecting rod bearing to be the most susceptible. The contact is of the reciprocating conformal type, the surfaces effectively endure constant start/stop sliding motion hence alternating lubrication regimes.

Lubrication within the compressor is not just a function of the lubricant, it is also governed by the selected refrigerant (Mizuhara, Akei et al. 1994). Wear and friction force within a MO lubricated contact reduces with the introduction of R12 refrigerant (Na, Chun et al. 1998) but with POE and HFC in actual compressors the wear characteristics increase (Mizuhara, Akei et al. 1994). Experiments have shown that chlorine within the CFC refrigerant creates an Extreme Pressure (EP) film to reduce wear when boundary lubrication exists at the contact. With HFCs this same phenomenon occurs with the fluorine, only at higher loads (Ciantar, Hadfield et al. 2000). The higher wear in HFC compressors is due to the fact that they never reach the same contact temperatures or pressures seen during experimentation to create the boundary EP layer (Mizuhara, Akei et al. 1994).

With HCs the range of lubricants available is somewhat broader, MO, POE and PAG all being miscible with the refrigerant. The refrigerant, however, may be too readily adsorbed into MO's, significantly reducing its viscosity, thereby increasing the required refrigerant charge (Granryd 2000). The use of PAG lubricants, less miscible than MO's, with HCs results in less reduction of viscosity and a reduced refrigerant charge compared with MO's although at very high pressures (100bar) the viscosity of PAG is reduced by 80% (Jonsson 1998).

1.2.3 Sustainable Development

Sustainable development can be defined as "*..development that meets the needs of the present without compromising the ability of future generations to meet their own needs"* (WCED 1987). To follow this ethos, every aspect of a product's lifecycle must be examined to evaluate its impact on current and future generations. For a product to be sustainable one should examine and question all aspects of its life cycle, even its very existence. In adopting this approach one should consider the socio-economic and environmental implications of recycling, servicing, reuse, dismantling and their implications on materials, production processes, in-use power consumption and longevity. To this end, it is useful to employ life-cycle assessment (LCA) to weigh alternative scenarios for their true impact.

1.2.3.1 Environmental Considerations

For the refrigeration industry, ozone depletion has historical importance due to the reliance on CFCs for both the refrigerant and insulation foam-blowing agent. The Montreal protocol has eliminated the use of these compounds and O.D.P. therefore no longer holds the environmental importance it once did. Much more significant for the refrigeration industry are the GWP of both the refrigerant and the in-use phase of its life cycle Whilst the refrigerants direct GWP contribution is only impacted by refrigerant leakage through failures in assembly, servicing or disposal procedures, the indirect contributions of a change in refrigerant can be much more significant. These include durability through compressor wear and in-use energy consumption (CO_2 emissions of power generation plants).

The UK is currently obliged under the Kyoto agreement to reduce CO_2 emissions by 12½% compared to 1990 levels and has a domestic goal of 20% (Royal Commission on Environmental Pollution 2001). The report by the Royal Commission recommends a reduction in CO_2 emissions of 60% by 2050, a target mirrored by a cabinet office report and one that may influence future energy policy (Performance and Innovation Unit 2002).

The use of hydrocarbon refrigerants has the direct environmental advantage of a greatly reduced GWP when compared to HFC refrigerants, however, the

unseen or external environmental consequences are also relevant though somewhat harder to ascertain. Although HFCs have a much lower GWP and ODP compared to CFCs, the reduced Coefficient of Performance (COP) and inferior wear characteristics lead to a higher environmental burden during the products in use phase (Ciantar and Hadfield 2000). For HC R600a the COP is superior to both R134a and R12 (Meyer 1996; Paul 1996; Meurer and Law 1998; Granryd 2000), however the long term wear and durability of equipment using this refrigerant is unknown.

To gauge the true cost to the environment, life cycle analysis tools (LCA) and cost benefit analysis (CBA) can be used evaluate alternative scenarios for the deployment of hydrocarbon refrigerants.

1.2.3.2 Life Cycle Assessment

To fully evaluate the environmental implications of using HC refrigerants one must consider cradle to grave interactions and implications. These should cover the whole life cycle from material extraction, processing, manufacturing, transportation, use and final disposal. The interactions at each phase include material inputs, energy use, direct and indirect emissions (Pira International 1997). To enable the comparison alternative systems and scenarios a formal methodology is employed, one such technique being lifecycle assessment (LCA) developed from methodology defined by SETAC (Society of Environmental Toxicology and Chemistry 1993). The LCA comprises four principle phases: defining the goal and scope, inventory analysis, impact assessment and interpretation of results (ISO-14040 1997). Guidelines for the implementation of LCA can be found in the relevant international standards (ISO-14040 1997; ISO-14041 1998; ISO-14042 2000; ISO-14043 2000). Previous studies (Mayerhofer, Krewitt et al. 1997; Ciantar 2000; Ciantar and Hadfield 2000) have shown that the in-use phase of domestic refrigeration products accounts for the most significant emissions during the products life cycle. For a standard refrigerator, energy consumption over 15 years is estimated at 1600-8200 kWh with a comparable production value of 1100 kWh per appliance (Mayerhofer, Krewitt et al. 1997). Electrolux, in an environmental product declaration for the highly efficient ER8199B fridge-freezer, states 1058 kWh for manufacturing with 219 kWh/year or 3720 kWh

energy use over a 17-year life span. The GWP impact of a domestic refrigerator related to energy use can be as high as 97% implying the irrelevance of HFCs GWP (Hugeut 2000). However, whilst this may be true of older, less efficient models, the Electrolux model mentioned previously has a GWP in use of less than 1500kg CO_2-eq (1995 UK fuel mix over 15 years operation (European Commission 1998). The refrigerant and blowing agent alone for an equivalent HFC unit would be 715kg CO_2-eq (0.25 kg refrigerant, 0.3 kg blowing agent, R134a).

Whilst the in-use contribution to the over all environmental impact has been reduced over the past five years it is still the most significant contribution to the products total equivalent warming impact (TEWI). The TEWI for the production of refrigerants has also been shown to be insignificant in comparison with the other stages within an LCA (Campbell and McCulloch 1998).

1.2.4 Environmental Indicators

Although GWP is of great importance, damages caused by other key pollutants can be as, if not more, significant (European Commission 1998). The potential effects of the most significant indicators are described below (Environment Agency 2004).

1.2.4.1 Global warming potential

The global warming potential is measured in tonnes of CO_2 emitted. The impact of other green house gases is also included by multiplying the quantities by their CO_2 equivalence to provide a final value for the lifecycle GWP.

1.2.4.2 SO_2 emissions

Sulphur dioxide (SO_2) emissions effects both the environment and human health. SO_2 can directly affect breathing, especially those with existing lung condition. SO_2 can also combine with water to produce sulphuric acid (H_2SO_4) hence acid rain. The deposition of acid rain can affect forestry, water supply, fish stocks and cause damage to buildings.

1.2.4.3 NO_x emissions

As with SO_2, nitrous oxide (NO_x) emissions can contribute to acid rain but also contribute to the formation of ground level ozone and nitrogen dioxide. Nitrous oxide can cause respiratory illness in children and reduces the natural resistance to infection.

1.2.4.4 PM10 emissions

Particulates with a diameter less than 10 microns (PM10) can also cause serious respiratory illness. The particulates are small enough to enter deep into the lung and cause premature death among those with existing conditions.

1.2.5 Economic Valuation

Within the normal course of business, an organisation and indeed the consumer can be aware of the direct (or internal) economic costs of product ownership. These traditional costs would be reflected in the purchase price, servicing costs and utility bills. The cost of using the environment as a source of raw material and receptor of waste products (including pollutants) is borne by society as a whole. These external costs can be incurred locally (soil and water contamination, particulates, noise), regionally (acid rain, air quality, deforestation), or global (climate change, ozone depletion) (Antheaume and Labouze 1998). The economic costs of the damage caused can vary according to the local or regional source of the contamination (European Commission 1998). Environmental costs for particulates, SO_2 and NO_x pollution can be more than ten times as great per ton of emissions in land locked Central European states where the contamination plumes extend across populated regions. Peripheral countries, that are more coastal, will have their contamination plumes falling into the sea or generally less populated areas (European Commission 1998; European Commission 1998). Within the private sector there has been more emphasis upon comparative weightings between impact categories, often with little regard to scientific values. Often these weights may vary within the same organisation depending upon the context of the operation and audience (Gameson 1998).

1.2.6 Cost Benefit Analysis

By assigning monetary value to environmental exchanges we can begin to assess a product or service's true lifecycle cost. The cost of avoiding damages to the environment should be considered against the value of any benefits brought by their avoidance (Sturges 2001). Cost Benefit Analysis (CBA) allows us to assign monetary values to environmental exchanges and compare them with the economic activities required for their abatement (Sturges 2001). The primary difficulties in implementing CBA arise from double counting costs that have already been internalised through national or international environmental policy and taxation (RDC-Environment and Pira International 2001) and the lack of consensus in damage valuation.

1.2.6.1 Emissions costs, Global Warming

The values assigned to global warming damages can vary from as little as €3.8/tC to as much as €139/tC within the same project (Tol and Downing 2000). The difficulty of valuing long-term damages such as global warming is further exacerbated by the application of a discount rate (Rao 2000). The theory is that a dollar invested today will grow faster than inflation, therefore damage at todays cost can be funded by a lesser amount invested for remediation in the future (Tol, Fankhauser et al. 2000). With a time frame stretching over a hundred years, minor variations of discount rates can have a dramatic effect on valuation (Tol and Downing 2000). For a central estimate using EU values a 0% discount rate over a 200 year time horizon gives a $244.8/tC. With a 1% discount rate the value drops to $71 whilst for 3% it falls to $16.8 (Tol and Downing 2000). Conversely, the costs of damages can rise over time if the atmospheric sink for CO_2 is regarded as a finite resource, following the principles of the Hotelling rule for non renewable resources, offsetting the effects of discounting (Nadal and Girardin 2001). The pro's and cons of discounting for the European Commissions ExternE project are discussed at length in Appendix VII of the Methodology Annexes of the ExternE report (European Commission 1998).

GWP costs can be calculated through the valuation of a wide range of damage scenarios such as loss of habitation and agicultural land caused by rising sea levels or changes to agricultural yields through climate change. However, these

lead to the wide range of valuations described previously, therefore the costs of carbon reduction and mitigation projects can be used instead.

Schemes can vary from low or negative cost impact (energy efficient light bulbs) to high cost impact (photovoltaic solar power schemes) (Markandya and Halsnaes 2002). For energy efficient lighting the purchase costs are outweighed by the energy savings, therefore the cost of any carbon abatement will be negative. For photovoltaic cells, the manufacturing costs are high when compared to the energy savings, therefore carbon abatement costs for this scheme will be high. The costs of greenhouse gas emissions can be calculated from the cost of avoiding those emissions through forestation, efficient power generation, and carbon sequestration projects. Typically, "good housekeeping" schemes are associated with low or negative costs (<€5/tCO_2), mitigation schemes with medium costs (€5-€15/tCO_2) whilst sequestration and transport schemes are associated with high costs (>€15/tCO_2) (Nadal and Girardin 2001).

A third source of global warming costs comes from carbon trading schemes. Here CO_2 emission limits are allocated to industry according to GWP reduction targets, those under cutting their limits can sell the un-used allocation to those exceeding. Industries may choose to improve their energy efficiency or mitigate through afforestation schemes in order to reduce emissions, alternatively they may buy unused emissions through the carbon trading scheme. This process should, in theory, balance the cost of mitigation with the traded price, therefore the traded price would be representative of the cost of CO_2 emissions. In order to meet the requirements of the Kyoto Protocol an EU-wide emissions trading scheme would need to allocate a price of €32.60/tCO_2 (Capros and Mantzos 2000), although this depends upon the willingness of participant nations to embrace the scheme.

1.2.6.2 Emissions Costs, SO_2, NO_x and PM_{10}

The emissions damages costs for the remaining key indicators (1.2.4) can be taken directly from the ExternE project as detailed (Table 1.3).

Emission	Units	Valuation (Euros)
Acidification	Kg SO_2 equiv.	7.4
Nitrogen oxides	Kg NO_x	2.3
Particulates	Kg PM10	17

Table 1.3 Emissions valuation, key indicators

1.2.7 State of the Art

Previous works on the tribological performance of refrigerants under pressure have been concentrated on HFCs. Whilst some testing has been carried out using actual compressors on test stands (Reyes-Gavilan, Eckard et al. 1996; Ciantar and Hadfield 2000) others have used pressurised test machines. A variety of test machines have been used: Pressurised pin on disk (Na, Chun et al. 1998); Ring on disk operating up to, but not beyond, atmospheric pressure (Mizuhara, Akei et al. 1994); Optical fluid film thickness measuring apparatus (Akei, Mizuhara et al. 1996); Pressurised pin on oscillating disk (Yoon, Poppe et al. 1996). Although all of these machines work in a pressurised environment, only the pin on oscillating disk can simulate something close to a reciprocating motion. All of the previous works have concentrated on HFCs and CFCs. Whilst the sustainability and environmental issues surrounding refrigerator systems have been addressed (Ciantar 2000; Ciantar and Hadfield 2000), the conclusions are drawn from compressors on test stands and again, only for HFCs and CFCs. For the compressor's end of life phase, a non-invasive method of wear assessment has been developed (Hurst and Kelly 1998) and a system of automated recycling centres proposed (Uhlmann, Spur et al. 2001).

The contributions to knowledge from this project are:

- The development of the novel pressurised reciprocating test machine;
- The tribological evaluation of HC refrigerants under a pressurised atmosphere;
- The evaluation of lubricants under a pressurised HC environment;
- The environmental implications of the use of HC refrigerants.

2 Compressor operational analysis

2.1 Background

The physical and theoretical attributes of the compressor were required for the derivation of test methodologies and subsequent interpretation. At the component level, material and dimensional attributes provide the core data for the operational, contact, lubrication and wear regimes. The physical production methods and material quantities of the device were required for input into the LCA. To obtain the attributes, a standard refrigeration compressor was dismantled and the component dimensions measured, weighed and assessed for material type and manufacturing technique.

2.2 Refrigerants

The refrigerants selected are those most commonly used in domestic refrigeration, namely R134a and R600a. Hydrofluorocarbon refrigerant R134a is a direct replacement for chlorofluorocarbon refrigerant R12. The thermodynamic properties are very similar to R12 but with zero ODP and a lower GWP. R600a is high purity isobutane which, unlike R134a or R12, is highly flammable. R600a does however possess excellent thermodynamic properties, zero ODP and near zero GWP. Further details on both R600a and R134a can be found in the appendices (Appendix A).

2.3 Lubricants

The lubricants are those that the refrigeration industry found to be most compatible for the selected refrigerants. In the case of R134a the selected lubricant was additised polyolester (POE) whilst for R600a additised and plain mineral oil (MO) was evaluated alongside the additised POE. The POE lubricant is based on Pentaerythritol whilst the MO is naphthanic. Further details of both lubricant types can be found in the appendices (Appendix B).

2.4 Compressor Physical Attributes

2.4.1 Dismantling Procedure

The compressor was first weighed to provide a baseline value prior to subsequent dismantling. The main casing was first cut around the circumferencial welded band to allow access to the main internal components (Appendix C). The compressor was dismantled to component level for weight and dimensional measurement. The components were further dismantled and subsequently weighed to separate material and manufacturing processes. The dismantling process provides two sets of physical data for assessment:

- Manufacturing data, the compressors materials and processes that were used for the production of the device which can be used within the LCA.
- Mechanical data, the compressor's component dimensions for calculating the operational regimes.

2.4.2 Manufacturing Data

A physical material inventory was compiled from the compressor (Table C.1) and are categorised by material process:

- Raw material and process, as supplied to the manufacturer.
- Production process, as carried out by the manufacturer, i.e. piston casting.
- Production post process, as carried out by the manufacturer, i.e. piston machining.
- Assembly process, as carried out by the manufacturer, i.e. welding, wire winding.

A summary of the data (Table 2.1) shows that the most predominant material is steel sheet although a significant quantity of copper wire is used for the motor windings. The steel sheet mass includes the compressor casing, motor field coil winding cage and the motor core plates.

Material	Mass (g)
Aluminium	200
Copper (wire)	738
Polyethylene	154
Steel (casting)	2043
Steel (forged)	95
Steel (sheet)	6160
Steel (tube)	28
Steel (wire)	29
Total	9447

Table 2.1 Material Inventory summary

2.4.3 Mechanical Data

Subsequent to dismantling of the R134a hermetic compressor, the component dimensions were measured or calculated and recorded as either operationally or contact geometry related (Table 2.2).

Component Parameter	R134a (measured)	R600a (derived)
Cylinder bore diameter (mm)	20.88	25
Piston stroke (mm)	17.48	20
Connecting rod length (mm)	37.96	43
Motor speed (rpm)	2900	2900
Piston mass (g)	34.8	52.2
Gudgeon pin and fastener mass (g)	6.2	9.2
Gudgeon pin diameter (mm)	8.0	9.58
Gudgeon pin surface roughness Ra, (μm)	0.085	0.085
Small end bearing (mm)	8.12	9.7
Small end surface roughness Ra, (μm)	0.173	0.173
Gudgeon pin contact width (mm)	7.44	9.5

Table 2.2 Compressor component parameters

The data can be used to project mechanical operating characteristics (Table 2.3). These can then be used in conjunction with the operational conditions to project lubrication regimes and in conjunction with material rates, forecast long-term performance.

Parameter	R134a	R600a
Swept volume (mm^3)	5985	9817
Volume above piston (mm^3)	231	332
Starting volume (mm^3)	6216	10150
Final (compressed) volume (mm^3)	231	332
Compression ratio (max)	26.9	30.5
Small end sliding distance (mm)	1.86	2.25
Small end sliding speed (ms^{-1})	0.28	0.34

Table 2.3 Mechanical operating characteristics

2.5 Theoretical attributes

To model the operational characteristics of the compressor, the component parameters (Table 2.2 & Table 2.3) need to be combined with the in-use operating conditions, namely pressure and temperature.

2.5.1 Refrigeration cycle

At start-up the compressor hermetic chamber will be at room temperature and pressurised to the corresponding refrigerant saturation pressure. During operation the pressure in the compressor chamber drops to match the evaporator pressure, whilst the vapour temperature is superheated above the evaporator temperature. The compressor raises the pressure of this superheated vapour to match the condenser pressure, itself a match for the saturation pressure of the refrigerant at the condenser temperature. The operational conditions can be determined by overlaying the requisite refrigeration cycle (Table 2.4) onto the refrigerants pressure-enthalpy chart for R134a (Figure A.4) and R600a (Figure A.2). The data points from the resultant cycle plot (Figure 2.1) are presented in tabular format (Table 2.5).

Parameter	Value
Evaporator Temperature (°C)	-25
Super heating (°K)	20
Condenser Temperature (°C)	40
Sub Cooling (°K)	10

Table 2.4 Refrigeration cycle parameters

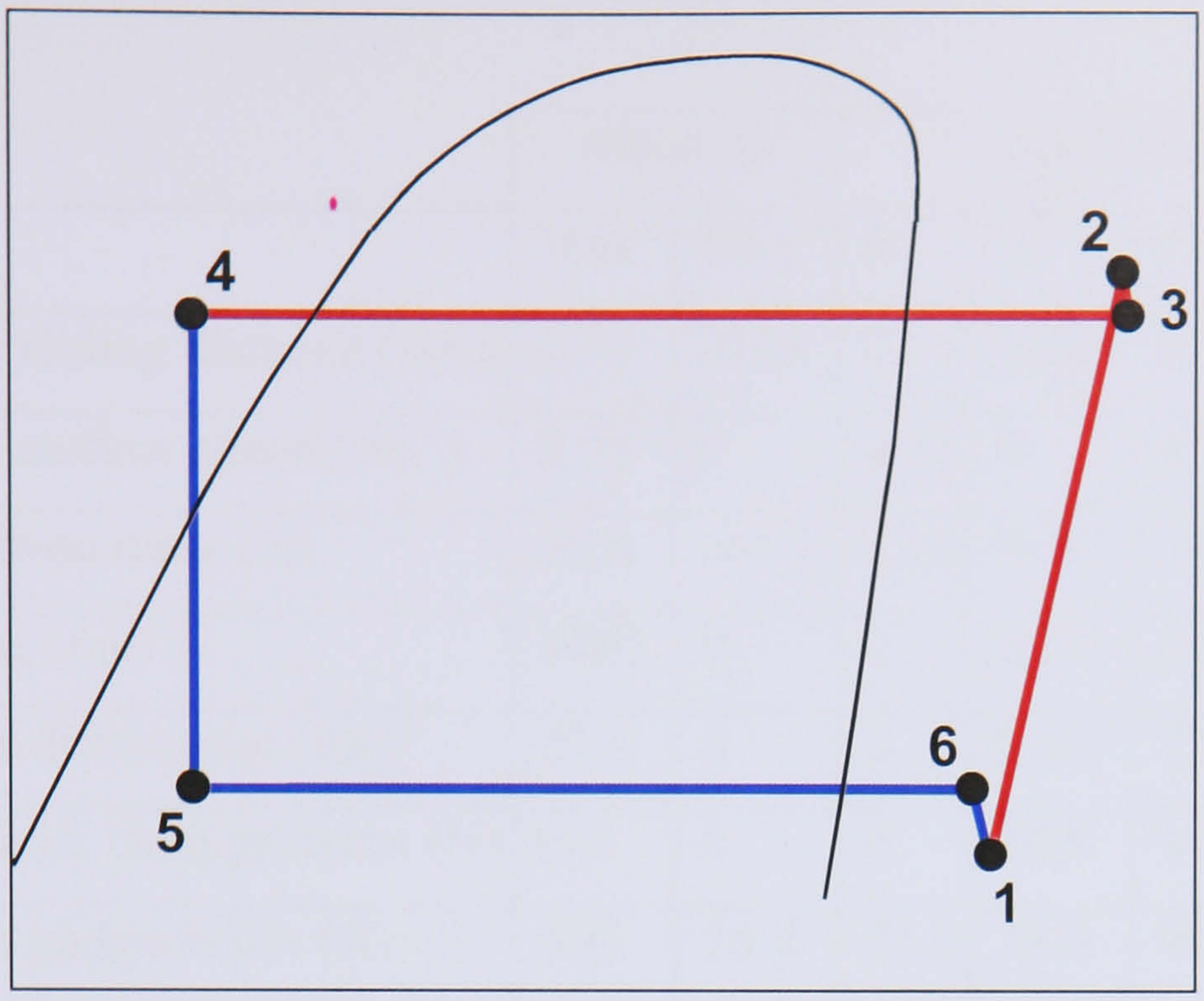

Figure 2.1 Typical refrigeration cycle

	R134a cycle		R600a cycle	
Data Point	*Temp. (°C)*	*Pressure (bar)*	*Temp. (°C)*	*Pressure (bar)*
1. Compressor inlet	-5	1.06	-5	0.58
2. Compressor outlet	68	10.17	57	5.28
3. Condenser inlet	68	10.17	57	5.28
4. Expansion valve inlet	30	10.17	30	5.28
5. Evaporator inlet	-25	1.06	-25	0.58
6. Evaporator outlet	-5	1.06	-5	0.58

Table 2.5 Refrigeration cycle operational conditions

2.5.2 Gudgeon pin surface velocity

The mechanical operation of the compressor provides fluctuating contact speeds and loads at the gudgeon pin bearing. A spreadsheet solution was derived for the whole cycle to provide the required contact data. Beginning with the piston at the bottom of the stroke (bdc), the solution is advanced in increments of one degree until the full cycle is complete. A short list of derived data values is shown for both R134a (Table 2.6) and R600a (Table 2.7).

	Absolute		Angle after bdc			
Parameter	Max	Min	0°	90°	180°	270°
Gudgeon pin sliding distance (mm)	0.93	-0.93	0	0.93	0	-0.93
Gudgeon pin surface speed (ms^{-1})	0.28	0	0.28	0	0.28	0
Piston load, from mass (N)	25.4	-40.7	25.4	8.95	-40.7	6.64
Swept volume (mm^3)	5985	0	0	2643	5985	2643
Max pressure differential (bar)	27.5	0	0	0.78	27.5	0.78
Max piston load, from pressure (N)	941	0	0	26.8	941	26.8
Total load on gudgeon pin (N)	900	25.4	25.4	35.8	900	33.5

Table 2.6 Derived mechanical values, R134a

	Absolute		Angle after bdc			
Parameter	Max	Min	0°	90°	180°	270°
Gudgeon pin sliding distance (mm)	1.12	-1.12	0	1.12	0	-1.12
Gudgeon pin surface speed (ms^{-1})	0.34	0	0.34	0	0.34	0
Piston load, from mass (N)	43.2	-69.3	43.2	15.37	-69.3	11.5
Swept volume (mm^3)	9817	0	0	4330	9817	4330
Max pressure differential (bar)	17.14	0	0	0.43	17.14	0.43
Max piston load, from pressure (N)	841	0	0	21.2	841	21.2
Total load on gudgeon pin (N)	772	30.2	43.2	36.6	772	32.6

Table 2.7 Derived mechanical values, R600a

It is clear that the R134a compressor's gudgeon pin to small end contact has a shorter sliding distance and lower sliding speed than that of the R600a. Both compressor types have similar sliding characteristics, with directional reversals (velocity drops to zero) at 90° and 270° (Figure 2.2).

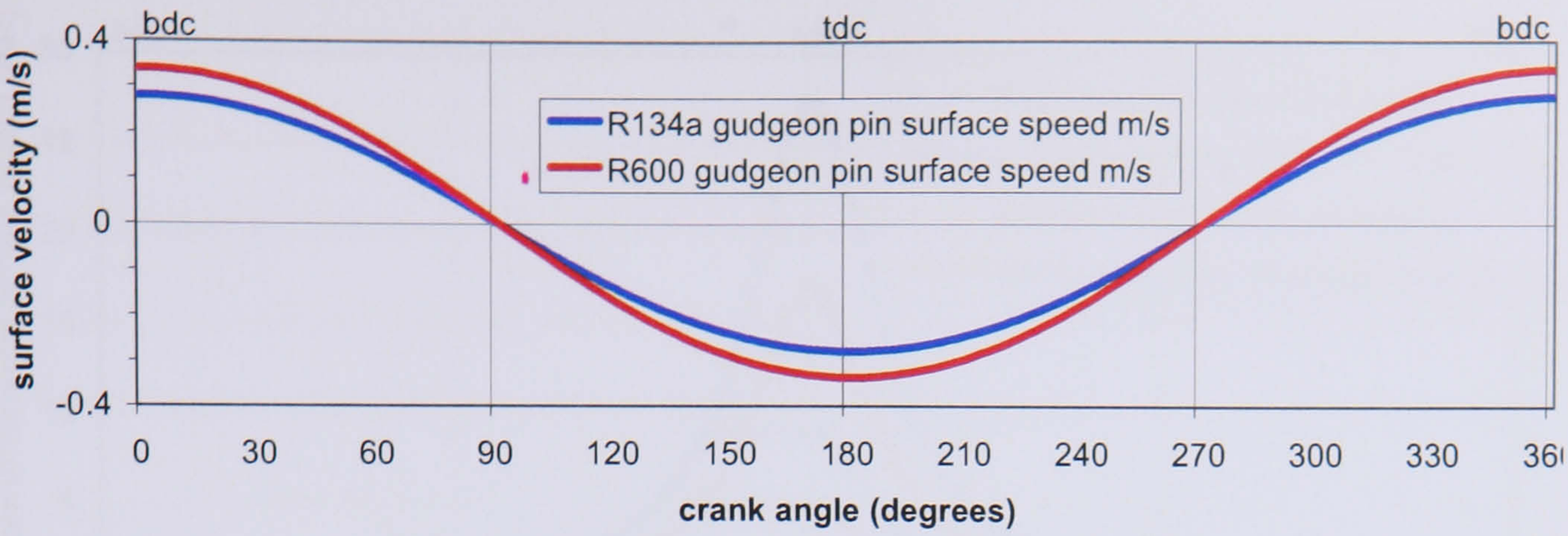

Figure 2.2 R134a and R600a gudgeon pin surface speeds

2.5.3 Compressor operating pressures

From the derived mechanical values (Table 2.6 & Table 2.7) it appears that the compressors can achieve considerable operating pressures, however, the compressor discharges its refrigerant charge at the same pressure as that found at the condenser. The discharge pressure is data point 2 in the refrigeration cycle (Figure 2.1 & Table 2.5) and limits the maximum pressure differential across the piston for both R134a and R600a (Table 2.8 & Figure 2.3). The pressure differential chart also depicts the pumping action of the compressor. The regions 0°-150° represent compression of the refrigerant to discharge pressure, 150°-180° the discharging of compressed refrigerant into the condenser, 180°-240° the return stroke and 240°-360° suction of a fresh refrigerant charge into the cylinder.

	at crank angle			
R134a compressor	0°	90°	180°	270°
Pressure differential (bar)	0	0.784	9.11	0
Max piston load, from pressure (N)	0	26.9	312	0
Total load on gudgeon pin (N)	25.4	35.8	271	6.64
R600a compressor	-	-	-	-
Pressure differential (bar)	0	0.43	4.7	0
Max piston load, from pressure (N)	0	21.2	231	0
Total load on gudgeon pin (N)	43.17	36.6	161	11.45

Table 2.8 Revised pressure and load, set to data point 2

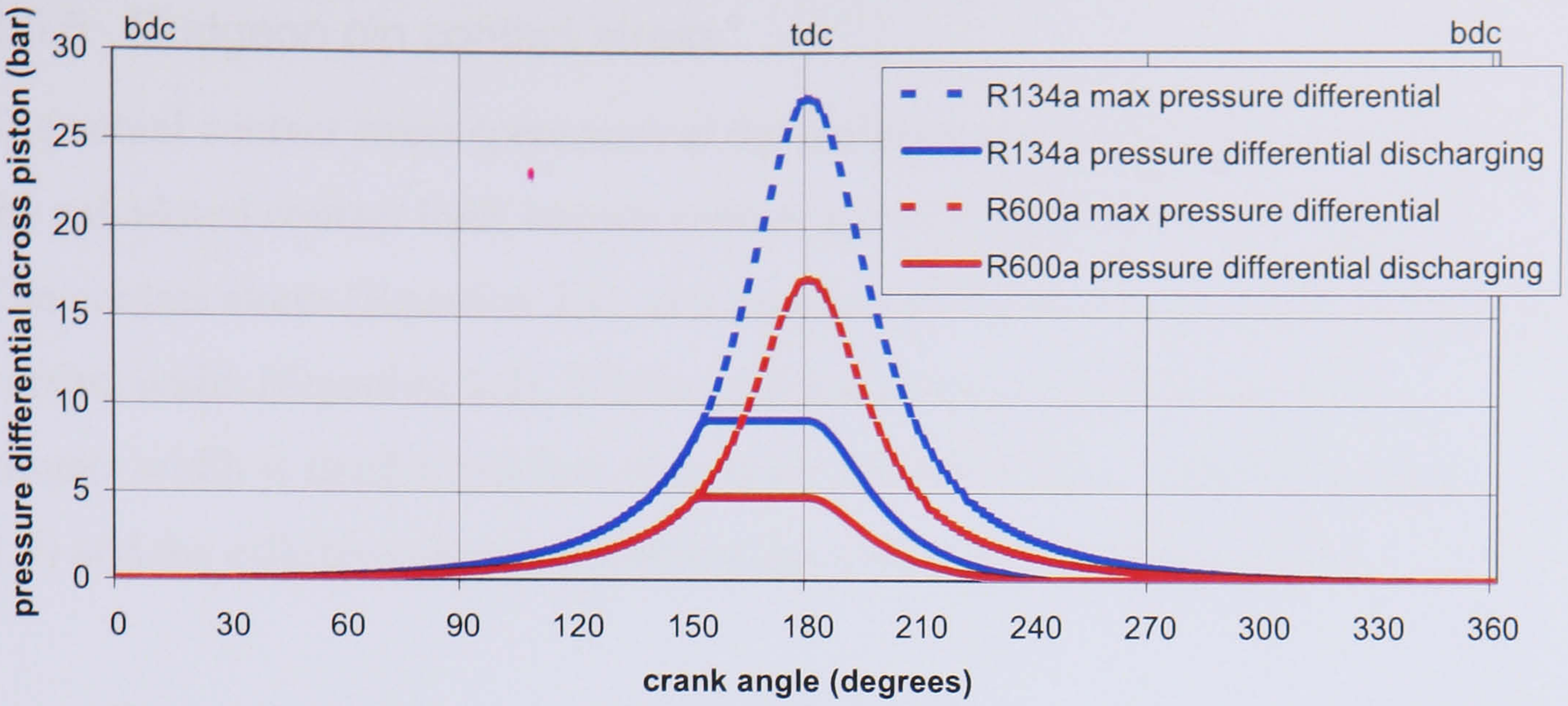

Figure 2.3 Revised piston pressure differential

2.5.4 Gudgeon pin load

The gudgeon pin load depends on both the pressure acting upon the piston by the refrigerant under compression and mass of the piston and pin being accelerated and decelerated by the action of the crankshaft and connecting rod. The pressure component is the pressure differential between the compressed gas side and the hermetic chamber side of the piston. The revised total load takes account of the discharge pressure of the compressed refrigerant (Table 2.8) and can be displayed in chart form (Figure 2.4).

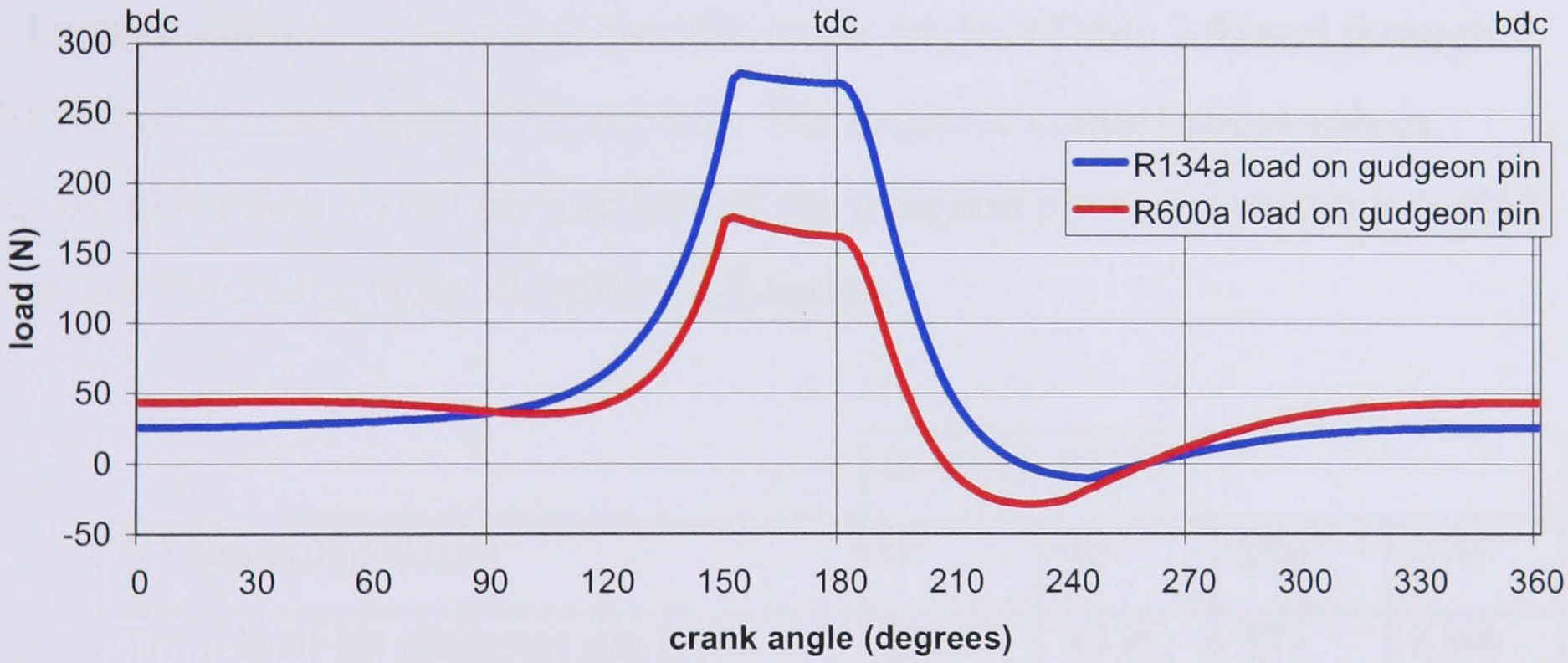

Figure 2.4 Revised load on gudgeon pin

The gudgeon pin loads for both compressor types are very similar at both 90° and 270° although the maximum load on the R600a compressor is 175N at 152° compared with 278N at 154°. The reversal in gudgeon pin load at 208°-260° for the R600a and 228°-258° for the R134a compressors can be attributed to acceleration during the return stroke of the piston.

2.5.5 Gudgeon pin contact stress

The actual contact stress (pressure) at the gudgeon pin can be calculated from the calculated contact load, known contact geometry and material properties. The contact stress (Equation 2.1), is a function of the load, contact length and contact width (Equation 2.2). Whilst load and contact length are known, contact width is itself a function of th load, contact relative radius (Equation 1.9) and the effective elastic modulus (Equation 1.11) (Williams 1994).

$$P = \frac{W}{4 l_h b_h}$$

Equation 2.1 Contact stress

where: P = contact stress (Pa); b_h = half the contact width (m); l_h = half the contact length (m); W = contact load (N);

$$b_h = \sqrt{\frac{4WR_e}{\pi E' l_h}}$$

Equation 2.2 Contact width

where: R_e = contact relative radius; E' = effective elastic modulus.

The contact width can be substituted into the spreadsheet solution to provide calculated contact pressures at specific crank angles (Table 2.9) and through the full compressor cycle (Figure 2.5). The negative contact stress values represent loading on the reverse face of the gudgeon pin as the piston is pulled back by the connecting rod small end bearing.

	at crank angle			
R134a compressor	0°	90°	180°	270°
Total load on gudgeon pin (N)	25.4	35.8	271	6.64
Contact area (mm^2)	2.1	2.5	6.9	1.1
Contact stress (MPa)	12.1	14.4	39.5	6.2
R600a compressor				
Total load on gudgeon pin (N)	43.17	36.6	161	11.45
Contact area (mm^2)	3.7	3.4	7.2	1.9
Contact stress (MPa)	11.7	10.7	22.6	6.0

Table 2.9 Gudgeon pin contact area and pressure

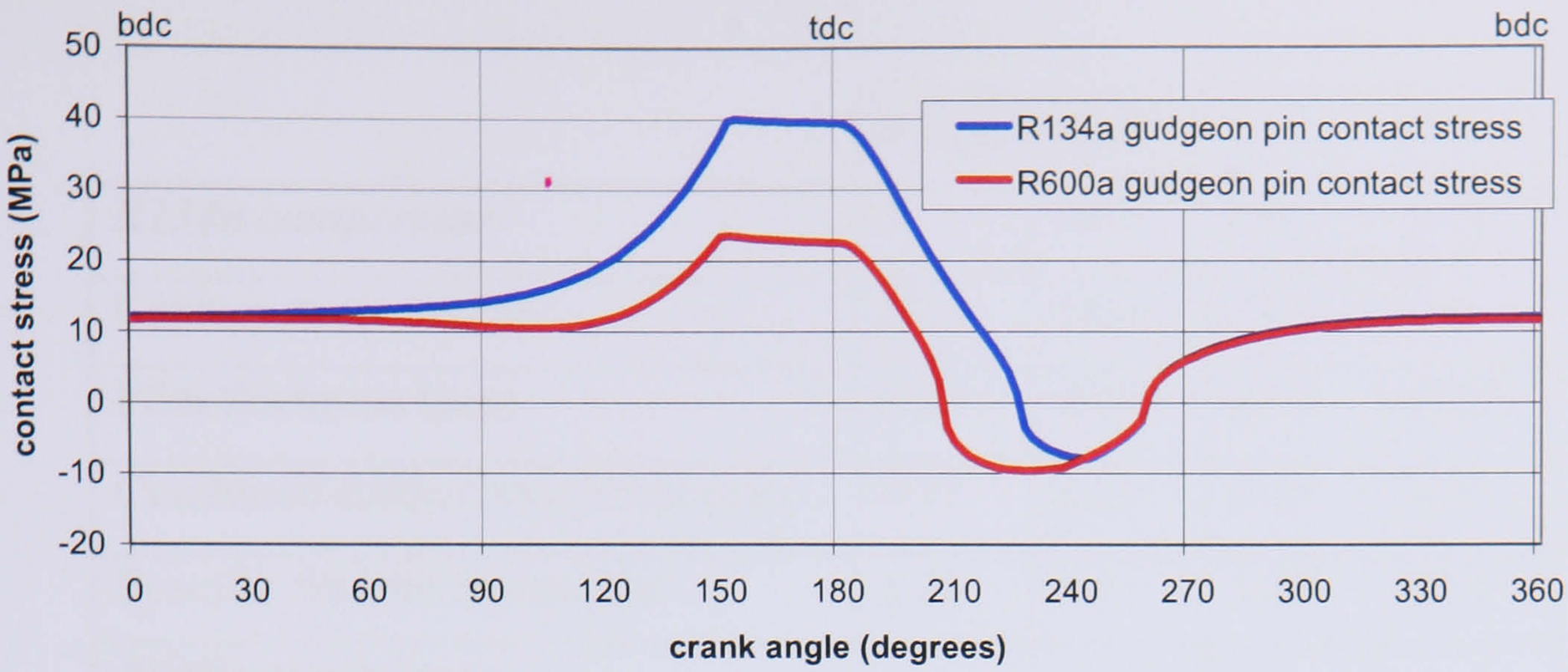

Figure 2.5 Gudgeon pin contact stress

The maximum contact stress for the R134a compressor can be almost twice that of the R600a equivalent. The contact stress when the crank angle is 90° and 270° is similar for both compressor types. At this angle the contact speed is at a minimum and the sliding direction is reversing.

2.5.6 Lubrication film thickness

The lubricant film thickness is the separation of the contacting surfaces by elastohydrodynamic action. As the surfaces slide relative to each other a lubricant film is generated causing the surfaces to separate. The film thickness is dependant upon the lubricant viscosity, pressure-viscosity coefficient, contact load, relative radius and effective elastic modulus (Equation 1.10). The film thickness can be further compared to the combined surface roughness' of the contacting surfaces to provide the specific film thickness ration, hence an indication of the lubrication regime (Equation 1.12). The equations were utilised within the spreadsheet solution to project values at specific crank angles (Table 2.10) and for the complete cycle (Figure 2.6). The chart also depicts the film thickness required to achieve the upper limits of boundary lubrication (λ=1) through mixed mode lubrication and into full elastohydrodynamic lubrication (λ=3). From the chart it is clear that EHD lubrication is never achieved and although mixed mode lubrication is predominant, the reversal in sliding direction causes the film thickness to collapse.

	at crank angle			
R134a compressor	0°	90°	180°	270°
Contact stress (MPa)	12.1	14.4	39.5	6.2
Film thickness (μm)	0.39	0.025	0.33	0.028
Combined surface roughness (μm)	0.21	0.21	0.21	0.21
Specific film thickness ratio	1.86	0.11	1.56	0.13
R600a compressor				
Contact stress (MPa)	11.7	10.7	22.6	6.0
Film thickness (μm)	0.51	0.03	0.46	0.036
Combined surface roughness (μm)	0.21	0.21	0.21	0.21
Specific film thickness ratio	2.4	0.16	2.18	0.17

Table 2.10 Lubricant film thickness and specific film thickness ratio

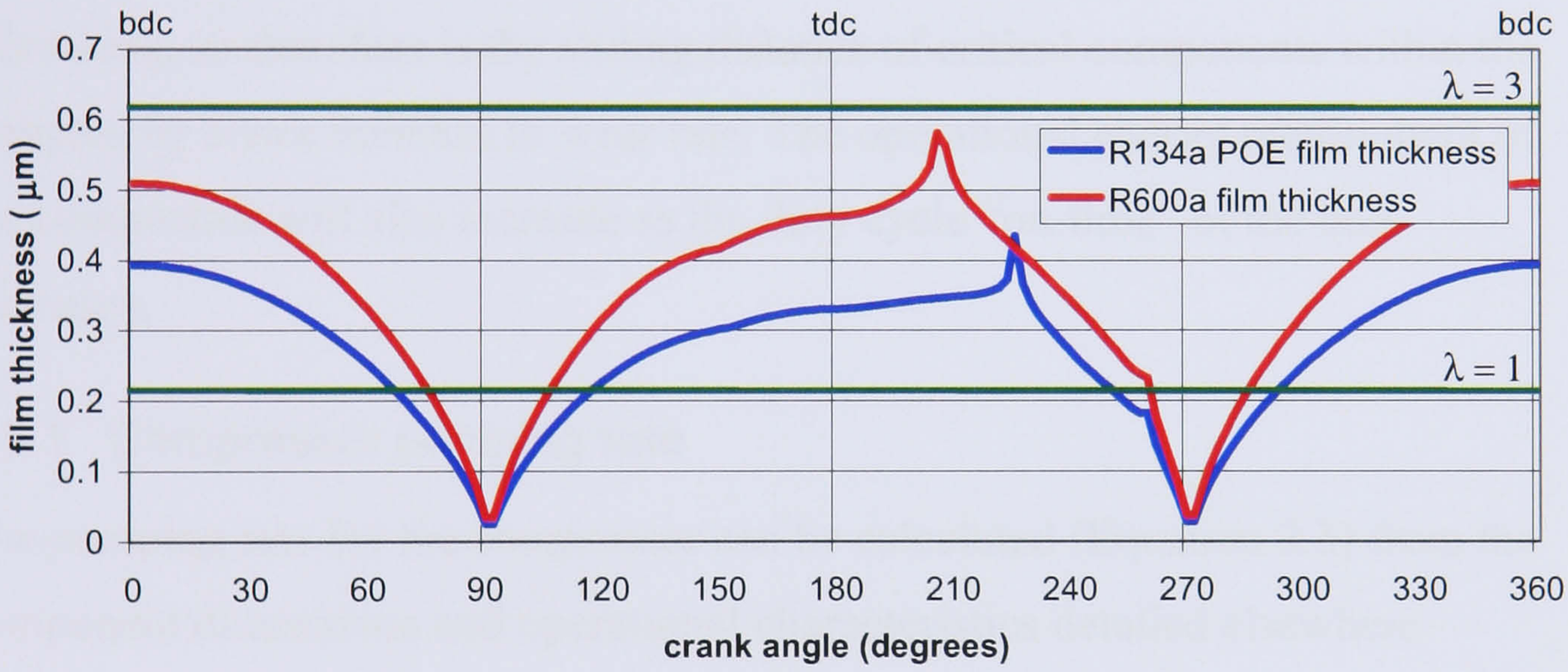

Figure 2.6 Film thickness and lubrication regime

The reduced film thickness at the reversal of sliding direction more dramatic for the R134a compressor than the R600a. The peaks at 220° and 260° (200° and 260° for R600a) represents the transfer of gudgeon pin load from the upper to lower face as the piston force becomes negative. If the film thickness chart (Figure 2.6) is compared with that for the gudgeon pin contact stress (Figure 2.5) it is clear that the boundary-lubricated regime for both compressors coincides with similar levels of contact stress. These details are important for the development of the experimental test programme (4.3-4.4).

2.6 Compressor longevity

The compressor longevity is dependant upon the rated duty cycle, wear rate of critical components and technical obsolescence. The compressor should remain operational for the lifetime of the appliance, in the case of domestic refrigeration this is typically 15-17 years (1.2.3.2). The hermetic compressor has a typical duty cycle (run duration per operational cycle) of 30% under normal operating conditions. This allows the compressor to run a longer cycle for increased cooling performance when required, for example if a warm body is introduced to the storage compartment, or freezer. During the life of the device wear may take place significantly reducing the available compression hence pumping efficiency. Any reduction in pumping efficiency will be countered by longer duty cycles until the compressor runs at 100%. At this point the compressor can no longer pump enough refrigerant at the required pressure to maintain cooling within the refrigerator. Whilst the duty cycle is increasing, so therefore is the sliding distance of critical components within the compressor hence increase in wear rate. The operational energy requirement of the compressor will also increase as the duty cycle "on-time" of the unit increases.

2.6.1 Compressor pumping rate

The pumping rate for the compressor can be calculated (Equation 2.3) from the component dimensions and operational characteristics detailed elsewhere (Table 2.3 & Table 2.5).

$$\left(\frac{V_1 P_1}{P_2}\right) - V_2 = V_d$$

Equation 2.3 Refrigerant discharge rate

Where: V_1 = volume at bottom of stroke, crank angle 0° (mm^3); P_1 = pressure at beginning of cycle (Bar); P_2 = pressure at discharge (Bar); V_2 = volume at top of stroke, crank angle 180°(mm^3); V_d = volume of refrigerant discharged (mm^3).

2.6.2 Compressor pumping cycle

The equation for pumping rate can be modified to provide pressure volume charts for both compressor types (Figure 2.7 & Figure 2.8). The equation

consists of two parts, discharge (0°-180° crank angle) (Equation 2.4) and suction (180°-360° crank angle) (Equation 2.5). The maximum compression pressure is limited to the discharge pressure value P_2. The minimum suction pressure is limited to the pressure at the beginning of the cycle P_1.

$$\left(\frac{V_1 P_1}{V_c}\right) = P_3$$

Equation 2.4 Refrigerant pressure during discharge stroke

$$\left(\frac{V_2 P_d}{V_c}\right) = P_3$$

Equation 2.5 Refrigerant pressure during suction stroke

Where: V_c = Volume within compression chamber, refrigerant volume (mm^3);

P_3 = Pressure within compression chamber, refrigerant pressure (Bar);

$P_1 \leq P_3 \leq P_2$.

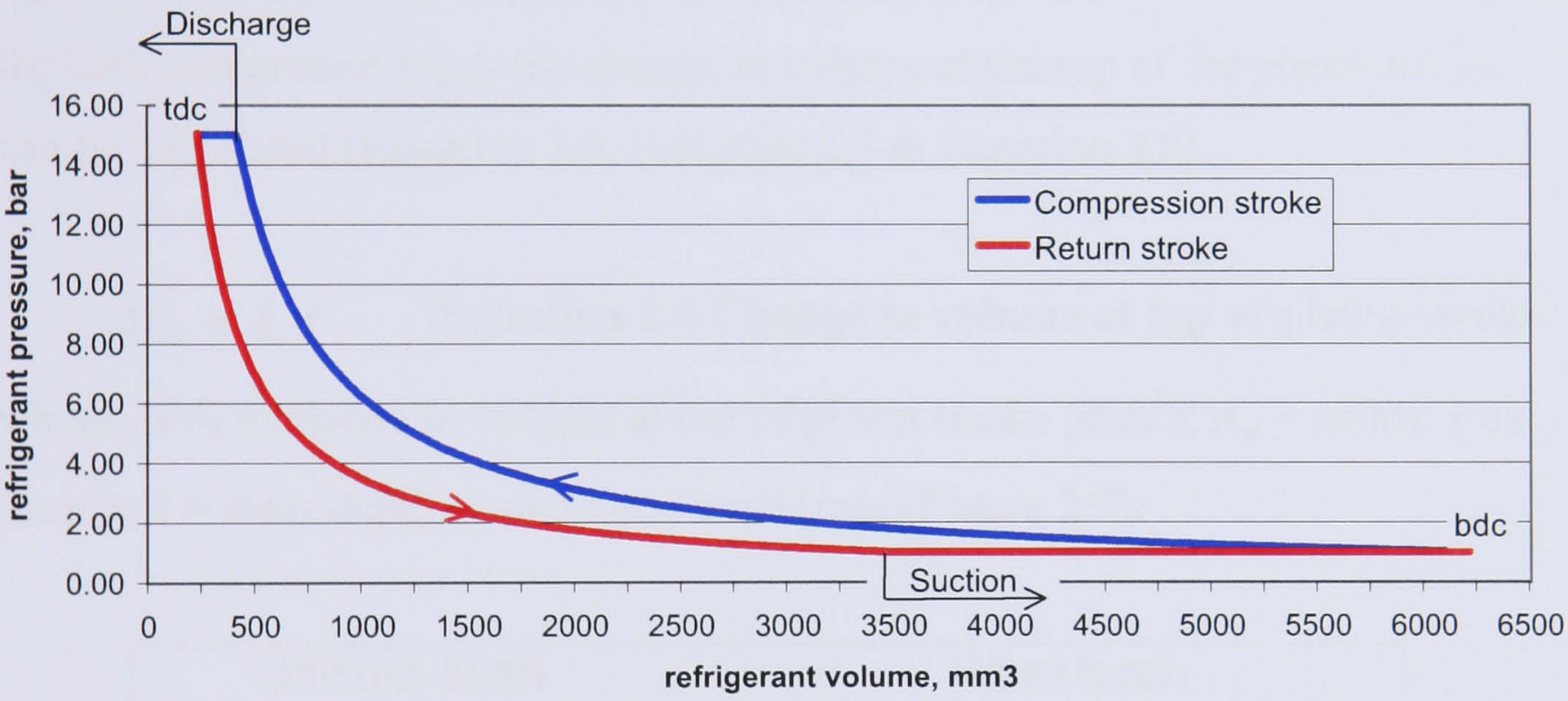

Figure 2.7 Pressure volume diagram, R134a compressor

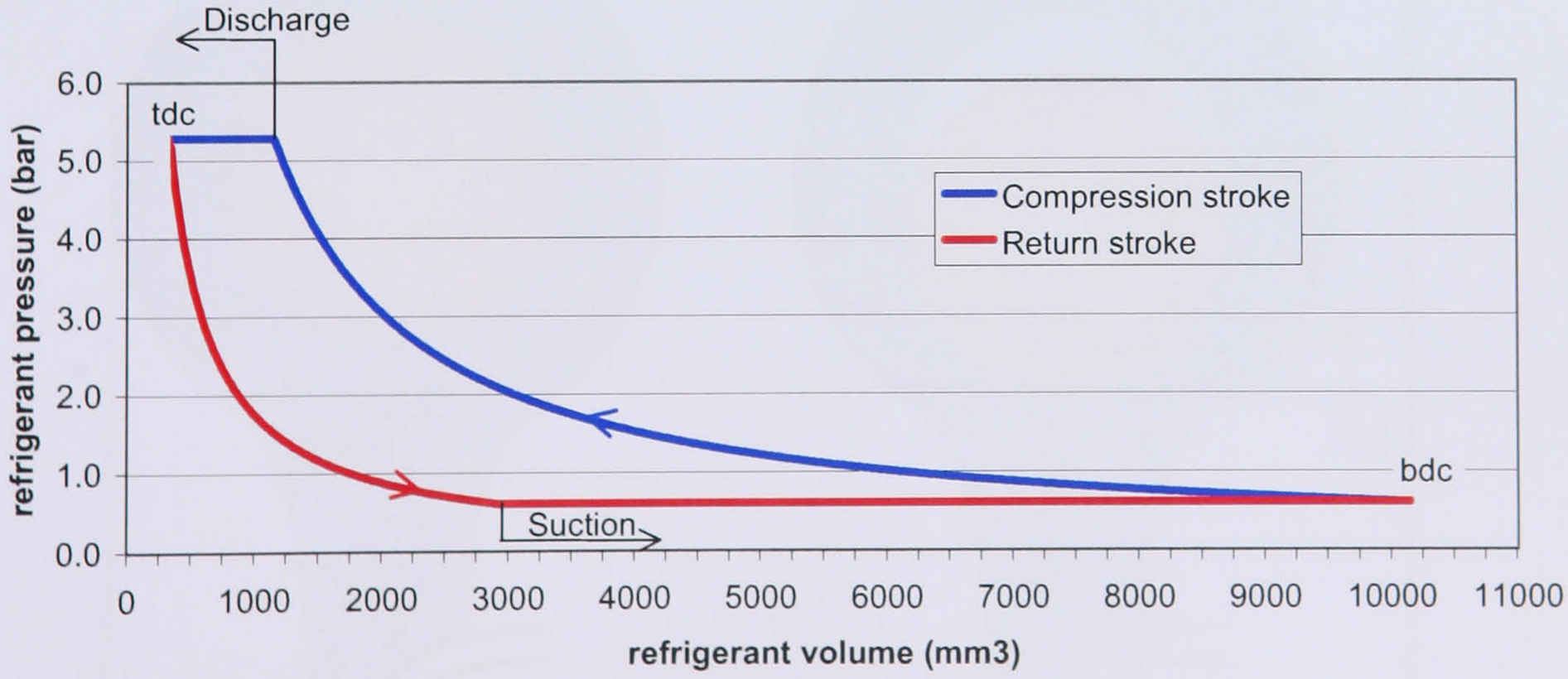

Figure 2.8 Pressure volume diagram, R600a compressor

The flat portion of the compression stroke represents V_d the volume of gas at the discharge pressure P_2 discharged from the compressor whilst the flat portion of the return stroke represents the volume of gas V_1 drawn into the compressor at the suction pressure P_1.

2.6.3 Effects of wear on compressor performance

The refrigerant volume for the pressure volume diagram is inversely proportional to the piston sliding distance therefore any wear at the gudgeon pin/small end bearing will have an effect on the compressor performance. As the gudgeon pin wears the transition point (A) from discharge to suction will occur at ever increasing volumes, reducing the refrigerant discharge volume for each cycle. The operating characteristics and gudgeon pin dimensions vary between the two compressors therefore wear at the small end/gudgeon pin will effect each compressor differently. If a nominal wear coefficient, *k*, is selected for both compressor types the change in volume at the top of the piston stroke can be calculated (Equation 2.6, Equation 2.7 & Equation 2.8).

$$\Delta V_2 = A_p d$$ **Equation 2.6 Change in volume at top of piston stroke**

where: ΔV_2 = change in volume at top of piston stroke (mm^3); A_p = piston area (mm^3); d = wear depth at small end bush (mm)(Figure 2.9).

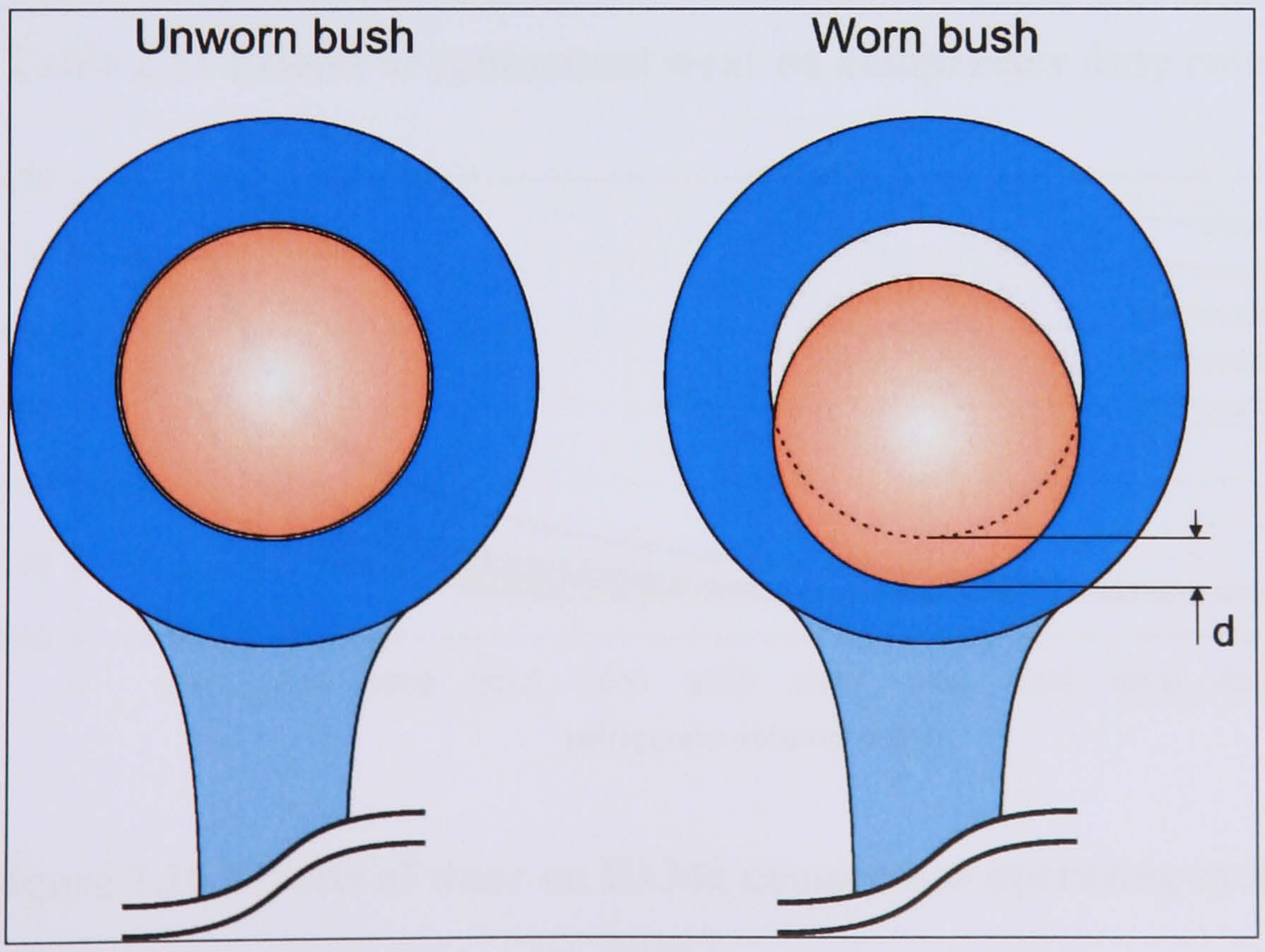

Figure 2.9 small end bush wear depth

$$\frac{M_r}{A_b} = d$$ **Equation 2.7 Wear depth at small end bush**

where: M_r = material removed from small end bearing (mm^3); A_b = Axial cross sectional area of compressor small end/gudgeon pin bearing (mm^2).

$$klW_p = M_r$$ **Equation 2.8 Material removed from small end bush**

Where: k = dimensional wear coefficient ($mm^3/N/m$); l = small end/gudgeon pin sliding distance (m); W_p = load on piston (N).

As the compressor wears, the pumping rate reduces, necessitating an increase in the duty rate of the compressor, hence energy consumption. An increase in duty rate will also lead to an increase in sliding distance, hence bearing wear rate. If the spreadsheet is modified to incorporate the equations, it can demonstrate the effects of wear over time for both compressor types (Table 2.11, Figure 2.10, Figure 2.11).

	R134a compressor	R600a compressor
Nominal wear coefficient (k)	$2X10^{-8}$	$2X10^{-8}$
V_2 after year 2 as % of year 0	111%	107%
V_d after year 2 as % of year 0	94%	97%
Years until duty rate > 50%	11 years (53%)	25 years (52%)

Table 2.11 Effects of component wear on compressor duty rate

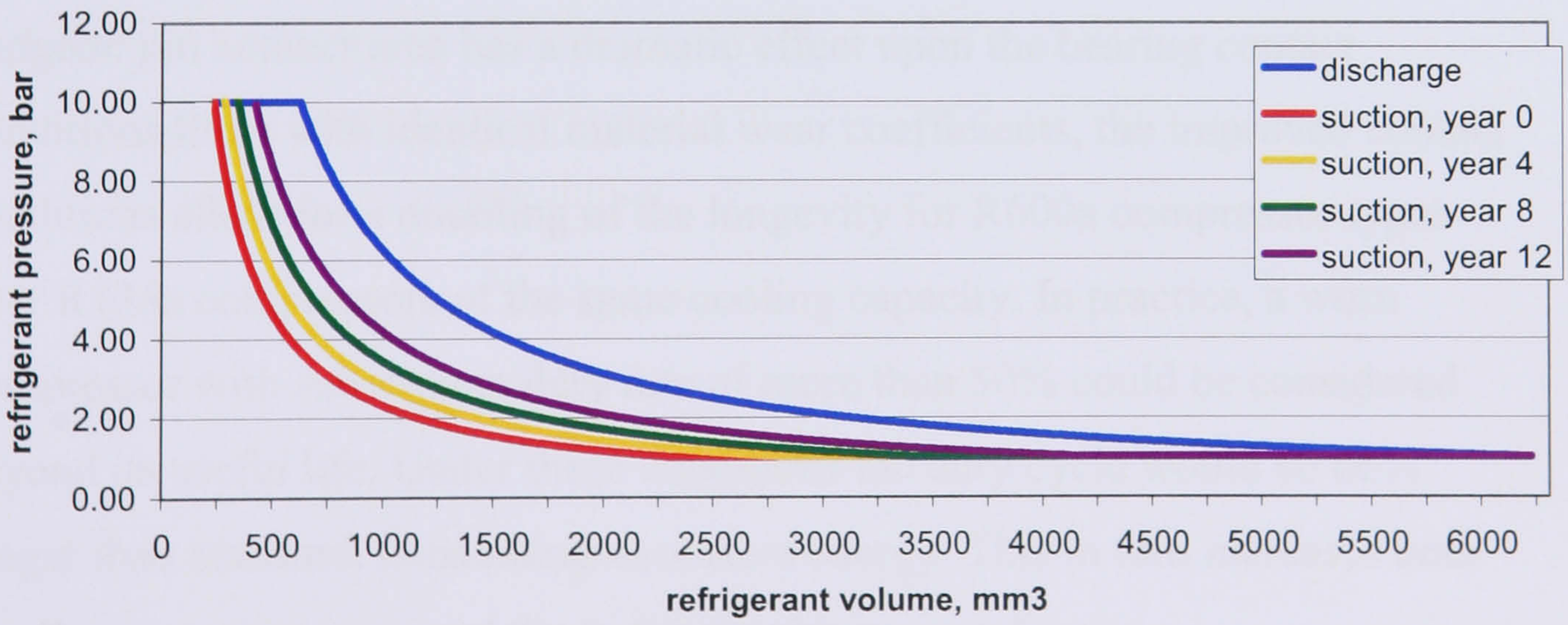

Figure 2.10 Effects of wear on R134a compressor operating cycle

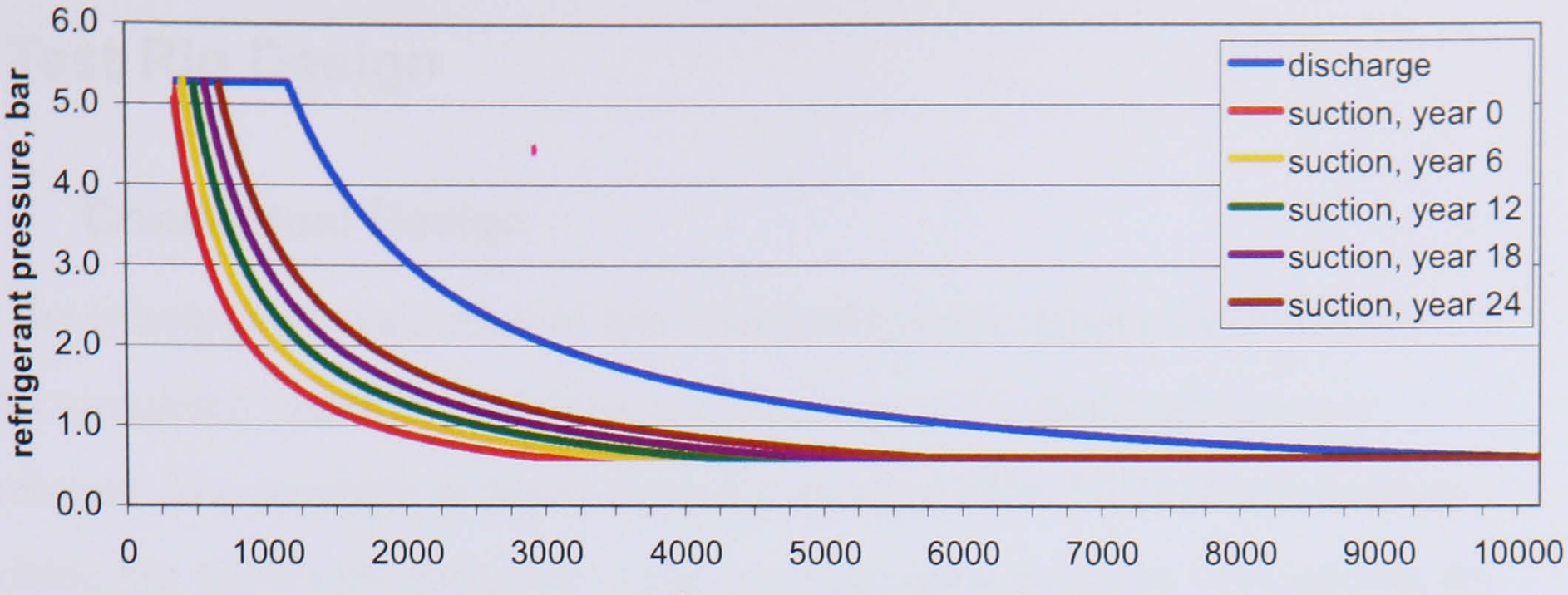

Figure 2.11 Effects of wear on R600a compressor operating cycle

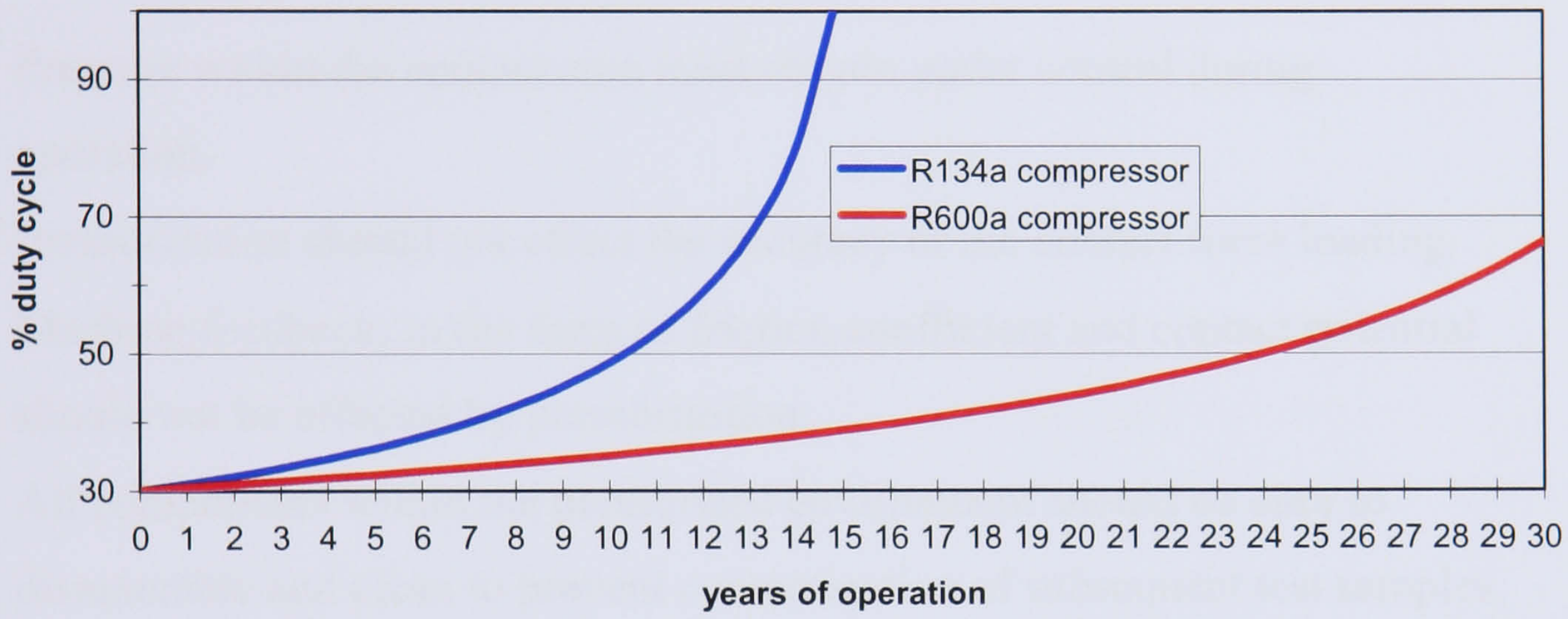

Figure 2.12 Effects of wear on compressor duty cycle over time

The selected wear coefficient is nominal, being chosen only to demonstrate its effect on the performance of the compressor types. From the table and charts it is clear that the reduced effective piston pressure combined with the larger gudgeon pin contact area has a dramatic effect upon the bearing contact conditions.Even with identical material wear coefficients, the improved contact conditions allow for a doubling of the longevity for R600a compressor types over R134a compressors of the same cooling capacity. In practice, a worn compressor with subsequent duty rate of more than 50% could be considered beyond its useful life. Under these conditions the duty cycle would be 66% longer than standard, consuming excessive energy. This in turn increases both the direct running costs and the indirect environmental costs.

3 Test Rig Design

3.1 Conceptual Design

For the tribological evaluation of lubricant-refrigerant charge combinations under simulated operation conditions a novel micro friction machine was developed. The machine is based upon the existing Plint TE70 micro-friction machine but allows for variation in the environmental pressure surrounding the contact to simulate operating conditions found within the hermetic compressor. To provide this pressurisation a number of key design criteria have to be met.

- Pressure within the contact area must remain under control during operation.
- Pressurisation should not effect the accuracy of the contact force loading.
- Machine feedback, in the form of friction coefficient and contact potential should not be effected by pressurisation.
- All components within the pressurised environment should be easy to disassemble and clean to prevent contamination of subsequent test samples.

The existing TE70 micro-friction machine operates by sliding a ball or pin sample in a reciprocating motion over a fixed sample plate. The plate is mounted in a bath to hold the lubricant (if required) and is connected to a transducer to provide friction force feedback, hence friction co-efficient. The pin or ball sample and the fixed plate can be electrically isolated therefore a potential divider may be used to measure lubricant film formation and contact gap. Wear at the contact is evaluated by post-test sample analysis.

3.2 Design Outline

To pressurise the hydrocarbon atmosphere surrounding the contact it is necessary to construct a pressure chamber around the oil bath, samples and mechanism. The chamber could envelop the whole apparatus or just the samples and oil bath.

The advantages of the all-enveloping chamber are that only static sealing is required and the micro-friction machine can remain identical to the standard

model. The disadvantages of this strategy are the pressurisation of a large volume of hydrocarbon atmosphere with subsequent risk and the difficulty of cleaning any contaminated components between testing.

The advantages of the smaller chamber are the reduced volume of hydrocarbon required and the reduced component count requiring cleaning between testing. The disadvantages are that reciprocating motion must be transmitted into the chamber and force feedback transmitted back out to the sensor, both require dynamic sealing. The design of the micro-friction machine therefore requires extensive modification.

Since it would be considered extremely dangerous to pressurise a large chamber (approximately 24 litres) containing electronic equipment with a hydrocarbon gas, the smaller chamber was selected as the most suitable option.

3.3 Design Concepts

The design problems that need to be addressed are transferral of reciprocating motion into the chamber, transferral of force feedback out of the chamber, sealing of transfer mechanisms, prevention of pressure variance due to transfer and the prevention force feedback due to pressure variance.

3.3.1 Motion and Force Transfer

If the transfer of force into the chamber is by reciprocating piston this can lead to variances in the internal volume hence pressure. The volume can be maintained constant by continuing the piston (rod) through the chamber, this also ensures that pressure acting on the piston is balanced and not trying to drive it from the chamber.

The same arguments apply to the force feedback transfer mechanism, if the connection is by piston the pressure in the chamber will exert a force. If the piston is continued through the chamber the pressure will exert a force in both directions and cancel out.

3.3.2 Transfer Mechanism Sealing

The sealing arrangements for the transfer mechanisms are the most critical aspect of the micro-friction machine design and must meet the following criteria:

- Provide 100% sealing at low absolute pressure differentials (0.5-4.0 bar).
- Perform under non lubricated conditions.
- Material compatibility with proposed lubricants, refrigerants and test samples.
- Life expectancy should be relative to the cost of the seal but at least 16 hours (99% M.T.B.F.) or 2.88M cycles.
- Maximum cost of seal replacement should be £5UK per hour of operation.

To seal a short stroke reciprocating mechanism there are two possible types of sealing arrangement, sliding wiper type seals and fixed conformable seals. The former would include "V" type packing, O-ring seals and sprung lip seals, whilst the later includes diaphragms, roll seals and bellows.

The problem with the O-ring and sprung lip type of seals is that they rely on transfer of the operating medium to provide a lubricating film between the sealing edge and the operating surface. Friction will also increase under pressure as the seal tightens against the sliding surfaces. Seals of this type also tend to provide a degree of self-centring which, in this case, is undesirable. Any sealing should allow for radial misalignment in order to maintain contact loading. These types of seals would prove unreliable under long duration test programmes resulting in gradual loss of operating medium and test pressure.

The "V" type packing would prove more reliable for sustained pressure operation, however these seals are not designed for operating at the speeds required (5mm reciprocation at 50Hz) and may wear rapidly, they also exhibit poor frictional qualities and would therefore prove unsatisfactory (Busak and Shamban 2001). Again, these seals also have only limited radial compliance and would be unable to provide sufficient loading accuracy.

The fixed conformable seals consisting of bellows, flat and convoluted (roll seal or top hat) diaphragms and are fixed at both the rod and housing and do not require dynamic sealing. This non-sliding interface negates the need for lubrication at the seal, hence no potential for leakage or sliding friction. These non-sliding conformable seals have distinct operating, material and manufacturing characteristics.

3.3.2.1 Flat diaphragm

The flat diaphragm can be manufactured from sheet materials such as steels and copper alloys or from reinforced elastomers. The seal has a flat profile, possibly including a number of shallow convolutions and is inexpensive to produce in a wide range of standard sizes. The low cost and material compatibility would appear to provide an excellent choice, however the design characteristic of this type of seal restricts the available stroke for a given diametric clearance (DiaCom 2001).

3.3.2.2 Convoluted diaphragm

The convoluted diaphragm can be manufactured from a variety of pure or fabric reinforced elostomer giving a wide selection compatible materials. The seal exhibits friction free characteristics and is inexpensive to produce in a wide range of standard sizes. The seal can be used for relatively long strokes without sacrificing longevity. The seals can operate in the range -50°C to +315°C and at pressures up to 410 bar. Whilst the materials available appear compatible, reverse compatibility may be a problem, the elastomer may leach into the lubricant affecting its tribological performance. Additionally, the nature of the convoluted diaphragm means that it can only support pressure on one side. Back pressure results in the convolution folding back on itself, the result is a locked diaphragm, elastomer to elastomer friction and rapid seal failure (DiaCom 2001).

3.3.2.3 Bellows

The bellows can come in two distinct styles: the hydro-formed, which resembles the hose for a vacuum cleaner; the edge welded, which resembles a camera bellows.

The hydro-formed bellows is cheaper to produce than the edge welded but is less flexible, therefore requiring a longer section for the same overall stiffness and life expectancy (Palatine Precision 1998).

The edge welded bellows is more complicated and is effectively a stack of pre convoluted diaphragms welded together, this is much more expensive than hydro-forming but results in a much more flexible package, hence smaller with enhanced longevity (Palatine Precision 1998).

Manufacturers such as Advanced Products guarantee their bellows for 5,000,000 cycles at their full deflection (Advanced Products 2001), this equates to 28 hrs of operation at 50Hz (3x8hr tests or 28x1hr tests). Reducing the deflection to 50% can increase the life of the bellows dramatically, typically by a factor of 100 (Caradon Hydroflex 2001), this would equate to 500,000,000 cycles or 2800hrs of operation at 50Hz (350x8hr tests or 2800x1 hr tests).

For the prototype pressurised micro friction machine bellows were selected as the most suitable sealing mechanism. They require no lubrication to maintain their sealing performance, the test medium will have no effect upon the stiffness or friction feedback potential, materials used in construction are unlikely to effect the test medium characteristics and seal failure is unlikely to be catastrophic.

3.4 Prototype Design

The prototype detail design was carried out by Plint and Partners and is, essentially, the standard TE77 machine with the addition of the described pressurised chamber in place of the conventional oil-bath arrangement. The load is applied by means of a spring balance attached to a cantilever arrangement. The cantilever exerts a force upon the force feedback transfer mechanism, hence contact. The reciprocating input mechanism and the force feedback transfer mechanism are electrically isolated to allow for film thickness measurements via contact potential. A piezo transducer attached to a yoke measures force feedback, the yoke is connected to the force feedback rod mounted upon which is a ball housing that carries the ball sample. The plate sample is mounted on the reciprocating motion rod, supported at each end by linear bearing blocks.

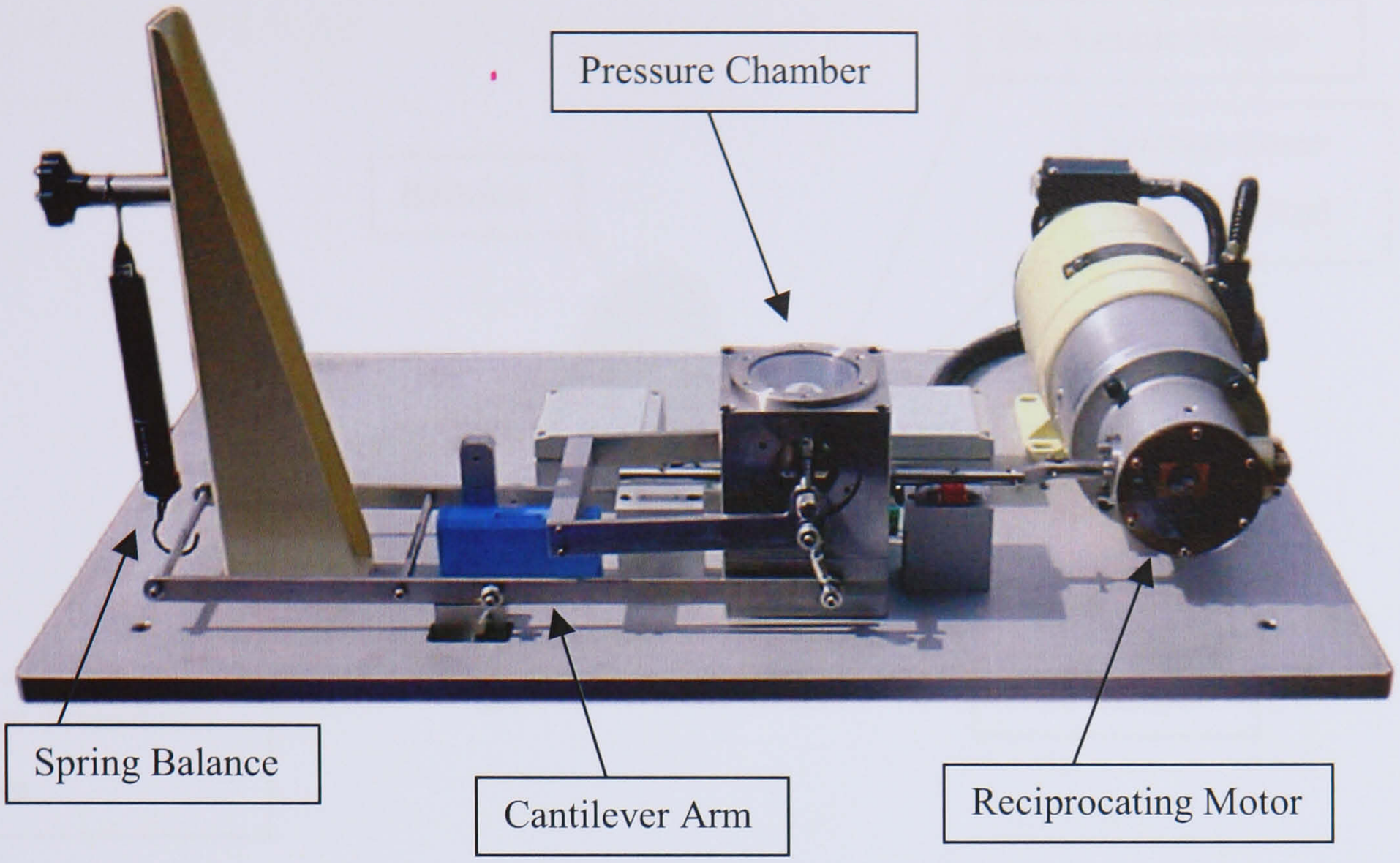

Figure 3.1 Pressurised micro-friction machine

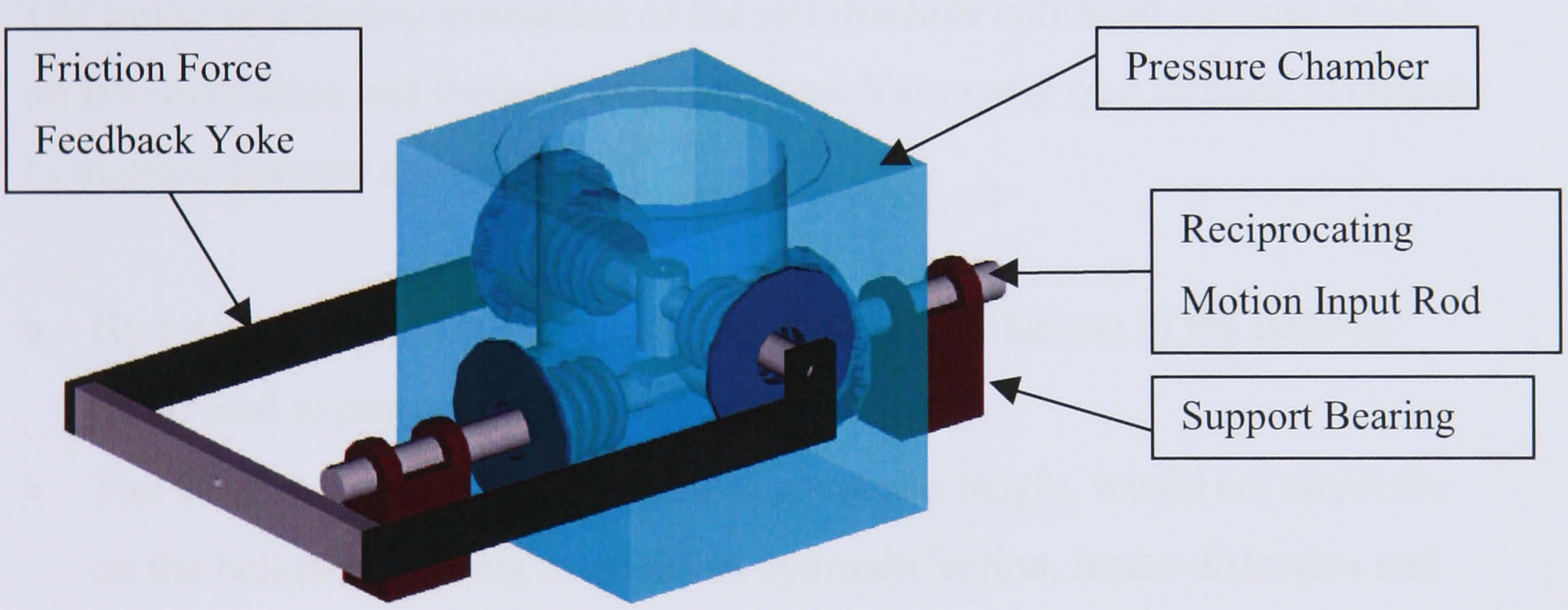

Figure 3.2 Pressure Chamber Detailed View

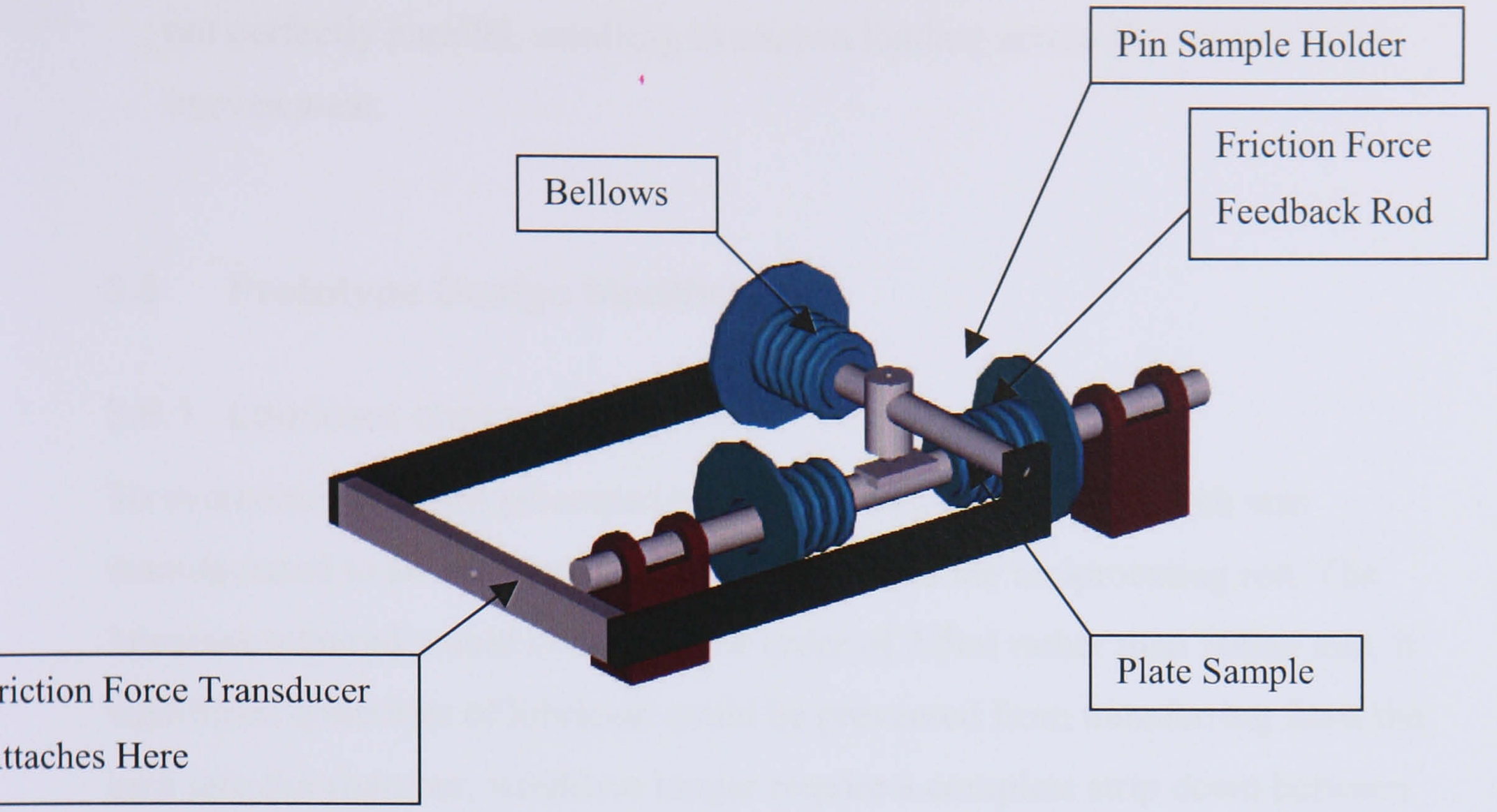

Figure 3.3 Force transfer mechanism

3.5 Prototype Evaluation

The initial operational evaluation of the test machine consisted of basic hands-on familiarisation and theoretical projections. Very early on a number of design limitations became apparent.

- Hydraulic action of the lubricant within the convolutions of the bellows could lead to potential weld failure.
- The Lubricant level, being limited to specimen height, would act unevenly on the bellows resulting in an offset hydraulic action, hence distortion and potential failure.
- Uneven hydraulic action and distortion may introduce vibration and uneven force loading at the sample contact.
- Each test would require in the order of 500ml of lubricant.
- The machine would require a complete strip-down and clean between each test therefore downtime would be in the order of three hours.
- To measure contact potential, hence boundary film formation, the test samples need to be electrically isolated and connection provided to the controller.

- Tested with Pin on Plate samples, it became apparent that the samples were not perfectly parallel, resulting in uneven loading across the contact hence uneven wear.

3.6 Prototype Design Modifications

3.6.1 Lubricant charge bath

To overcome problems presented by the lubricant charge an oil bath was manufactured to sit between the sample plates and the reciprocating rod. The lubricant required would now be in the order of 2.5ml rather than 500ml and, if significant quantities of lubricant could be prevented from transferring from the bath into the chamber, would no longer require a complete strip down between tests. The oil bath required a sample plate of 0.8mm thickness, however the sample plates supplied were not perfectly flat and thicker plates of 2.5mm were proposed along with modification of the oil bath to suit.

3.6.2 Contact potential measurement

To solve the electrical isolation problem, an upper holder was produced from Tufnol, however it proved difficult to provide a reliable electrical connection to the sample. This shortcoming was overcome by using the original sample holder and isolating the plate by way of a non-conductive shim beneath the bath. This design provides a more suitable method of completing the circuit via the sample plate. To provide the connection from the samples back to the controller a screened cable is used, terminated with BNC connection at the controller, crocodile clip and 4mm pin at the other. The crocodile clip is used to connect as close as possible to the upper, non-isolated, sample at the force feedback yoke. The pin connects via a socket to a second flexible wire run through the chamber charging pipework, into the chamber itself terminating with a single pole socket connector. The socket connects to the bath and plate via modified ring terminal and screw. The terminal enables easy connection and disconnection from the wiring hence reducing the chance of cable damage.

3.7 Investigation of uneven contact loading

The problems of uneven contact loading became apparent after first use of preliminary pin on plate samples, taking place after the installation of the oil bath. The extent of the uneven loading is clear from the image (Figure 3.4) and depicts a triangular wear contact rather than rectangular.

Figure 3.4 Uneven contact wear at pin sample

To investigate the uneven contact, measurements were taken for the height differentials of the oil bath and feedback rod from the reference top face of the pressure chamber. The pin sample holder was checked to ensure correct clamping and parallel alignment of the sample with the feedback rod. The feedback rod was also investigated for compliance; the ability of the rod to self adjust small differentials hence provide an evenly loaded contact.

3.7.1 Results of the investigation

3.7.1.1 Oil bath measurements

Measurement taken from the top face of the chamber to the edge of the oil bath showed that the bath (and plate sample) was running at an angle to the reference top face and, by implication, the pin sample. The angle of offset from the reference was calculated as 0.65°, enough to provide a height differential across the 10mm pin and plate contact of 0.11mm.

3.7.1.2 Feedback rod measurements

Measurements of the feedback rod indicated a variable differential of 0.2mm across the length of the measure (50mm) which calculated to a differential at the pin and plate of 0.04mm. When compared to the offset at the oil bath, the feedback rod measurements were initially deemed insignificant. Further

investigation indicated that the feedback yoke and rod were being pulled out of true by misalignment of the friction transducer mounting. Although the alignment was only adrift by 0.5mm this was enough to pull the mechanism off centre.

3.7.1.3 Feedback mechanism compliance

Although the bellows of the feedback mechanism are compliant, the bell crank loading mechanism was found to be very rigid, preventing the rod from self-adjusting to suit the angular offset of the plate. Removing the central tie-rod and slackening the assembly bolts made the mechanism more compliant than standard. This improved compliance had a beneficial effect on the wear at the contact however, such was the degree of offset at the plate, this was not enough to overcome the self-centring nature of the bellows and wear offset occurred albeit at a reduced level.

3.7.1.4 Plate offset test

To check that levelling of the plate sample would indeed provide an even wear rate the sample was shimmed on one side using a 0.5mm thick washer. The resultant wear on the surface of the pin was uniform, indicating that modification to the oil bath (or input rod) geometry would correct the uneven wear at the contact.

3.7.2 Modifications resulting from the investigation

The oil bath already required modification to suit thicker plate samples therefore any modifications carried out to correct the contact offset could take this into consideration. Three solutions were proposed:

- Machining the back face of the bath to provide the correct depth and angle.
- Milling a pocket into the bath to take account of the new plate thickness and angular offset.
- Machining the bath in a lathe to take account of the new plate thickness and angular offset.
- Shimming the input rod in conjunction with machining the bath.

3.7.2.1 *Machining the back face*

Although this appears the most obvious solution it would leave the side-wall of the bath somewhat lower with reference to the top of the plate sample, hence possibility of lubricant spilling out into the chamber under operation.

3.7.2.2 *Milling a pocket*

The milling of a pocket into the bath to take the plate and correct its offset is the most technically suitable solution. The pocket would provide the added benefit of acting as a lowest-point oil sink to aid the removal of lubricant after each test.

3.7.2.3 *Machining the bath*

Machining the inside of the bath to take the extra thickness of the plate sample is relatively simple and can be carried out in a lathe. To allow for the offset requires the production of a support tool that can hold the bath securely in the lathe at the desired angle.

3.7.2.4 *Shimming the input rod and machining the bath*

Eventually, the proposals were rejected in favour of a simpler solution to shim the force input rod at the support bearings. This route was deemed simpler and allowed the rod to be levelled more precisely to the reference top face of the pressure chamber and didn't require any complicated jigs to achieve the desired result. In conjunction the cantilever mechanism was loosened to provide increased flexibility and self-alignment of the samples at their contact. To enable the use of thicker plates the inside of the bath was also machined.

3.8 Pressure chamber charging equipment

The test chamber also required the design of mechanisms for charging and discharging and for charge condition monitoring. The pressure chamber was supplied with three $\frac{1}{8}$ B.S.P. access ports as standard. The three ports were adapted for charging, discharging and monitoring functions as described. One port has been adapted to provide the charge temperature feedback via a K-type thermocouple. The second port was equipped as the charging port, utilising a Danfoss refrigerant valve, $\frac{1}{4}$" S.A.E. Flare fittings and a Schraeder type valve

at the hose connection (Figure 3.5). The charging port also incorporates a Danfoss refrigerant pressure transmitter to provide charge pressure feedback hence, in conjunction with the temperature feedback, charge condition monitoring. The third port has been equipped as the discharge port, again utilising a Danfoss refrigerant valve, $\frac{1}{4}$" S.A.E. Flare fittings and a Schraeder type valve at the hose connection. The discharge port also incorporates a tee branch to provide routing for the contact potential connection. To Facilitate the additional input of charge pressure and temperature, the Machine controller hardware required reconfiguring and the Compendex software required the set-up and calibration of supplementary inputs.

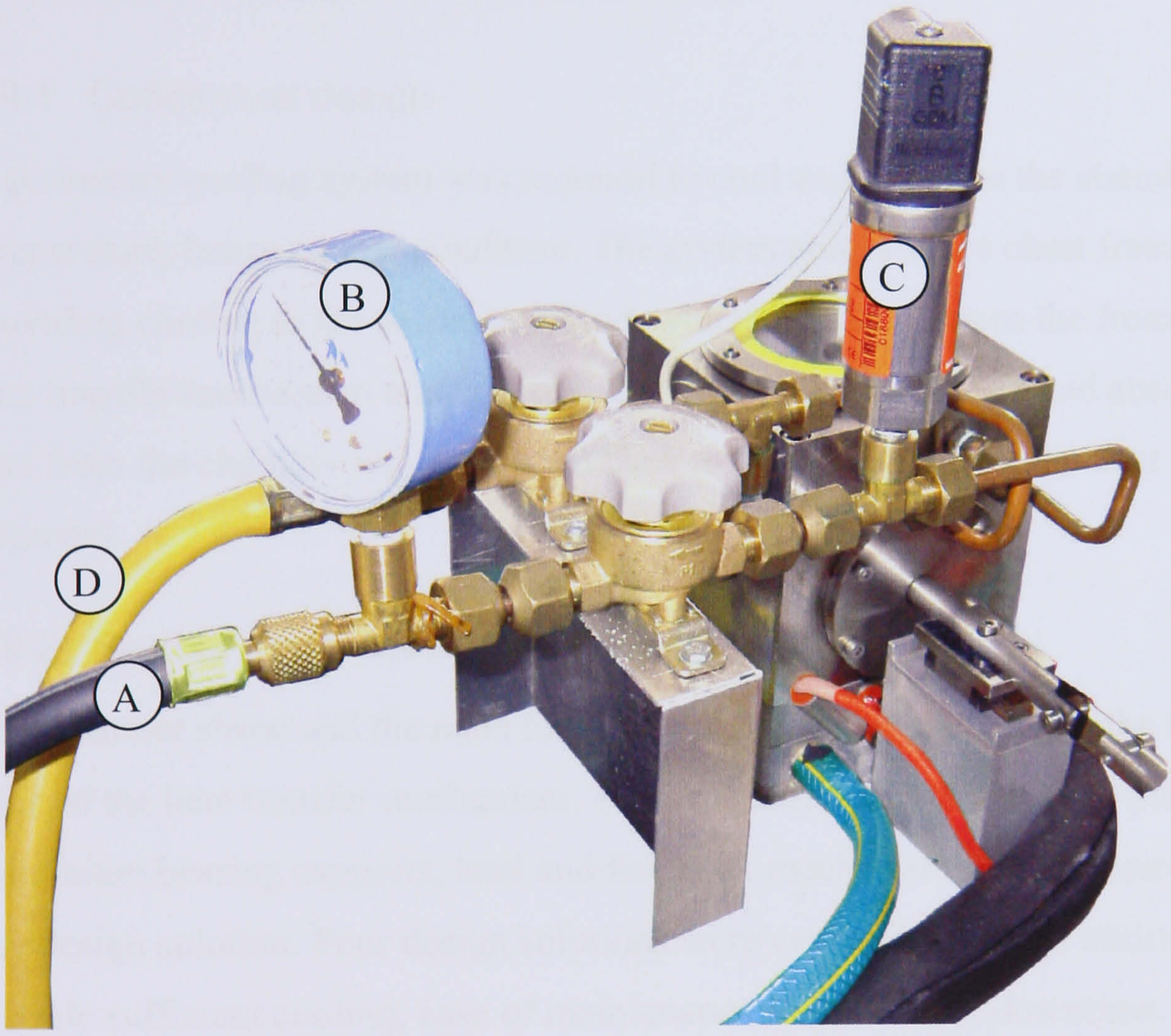

Where: Refrigerant charging is via the charging hose (A) supply pressure measured at the pressure gauge (B) chamber pressure recorded via the sender unit (C) with evacuation via the vacuum hose (D).

Figure 3.5 Chamber charging apparatus

3.9 Pressure chamber cooling equipment

The experiments (4.4) require the refrigerant to be held in a saturated state. For R600a saturation requires a pressure of approximately 3.5bar absolute at 25°C whilst R134a requires a pressure of approximately 6.7bar absolute at 25°C. The R134a condition is outside of the machine operating specification therefore the temperature needed to be reduced to allow saturation at a lower pressure. For saturation of R134a within the machines operating limit the temperature should be reduced to 8°C, providing a saturation pressure of approximately 3.9bar absolute. To provide this temperature reduction a secondary cooling system was designed to cool the chamber hence charge.

3.9.1 Conceptual design

A secondary cooling system was required to cool and maintain the chamber temperature, hence charge condition. The system consists of a chest freezer, providing cooling to the secondary fluid, which is pumped from the freezer to a heat transfer mechanism attached to the pressure chamber. The fluid absorbs heat from the chamber and is pumped back to the freezer where the heat is removed.

3.9.2 System design overview

The chamber shape and the need for maintenance access complicate the final form of the heat transfer mechanism. The substantial aluminium base-plate, aluminium bearing supports, load and feedback mechanisms further complicate any design solution. Four design solutions were evaluated for their ability to provide sufficient cooling, ease of maintenance and inter-test downtime. The design was further enhanced by switching the pump through a relay triggered by an analogue output from the machine controller. This provides more accurate temperature control during extended test programmes.

3.9.2.1 Indirect clip-on solution

An aluminium hood was designed to contact a large surface area of the chamber, the hood supporting a heatsink, itself retaining the coil of copper tubing (Figure 3.6). Areas of the mechanism not contacting the chamber were

insulated using foam rubber and pipe lagging materials. This solution (designated HS1) provided only moderate cooling performance, achieving a drop in charge temperature of approximately 8-12°C over 4 hours. This particular design was ineffective due a low flow rate when used with low temperature coolant and poor thermal conductivity to the chamber.

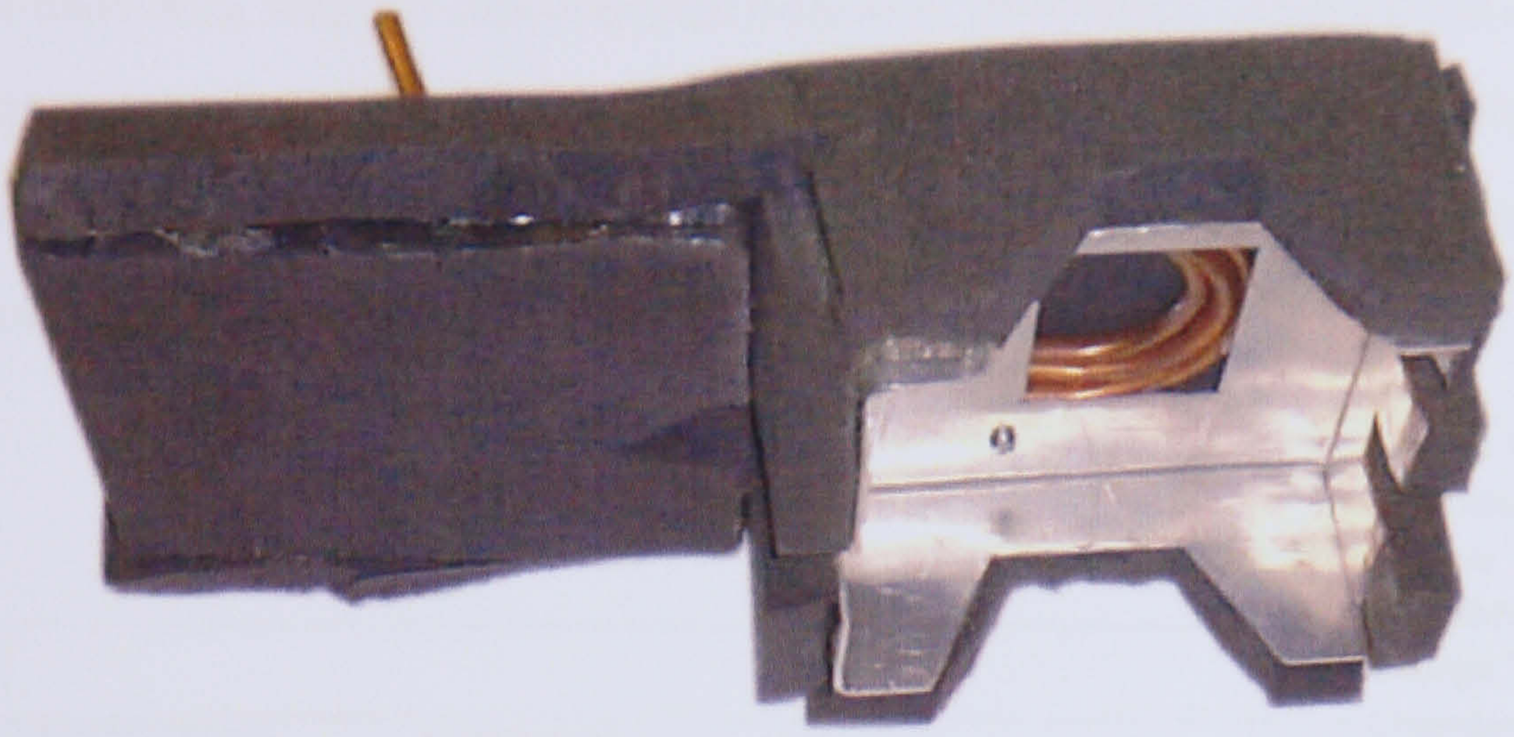

Figure 3.6 Indirect clip-on cooling hood

3.9.2.2 Direct heatsink solutions

A heatsink was designed to cool the chamber charge directly. The first iteration of this heatsink (designated HS2) replaced the existing chamber window and drew heat from the inside of the chamber to fluid circulating through a coil of copper tubing wrapped tightly around the heatsink (Figure 3.7). The results from the first direct heatsink proved promising, therefore a second iteration (HS3) was evaluated whereby the external copper tubing was replaced with larger bore internal passageways to improve coolant flow.

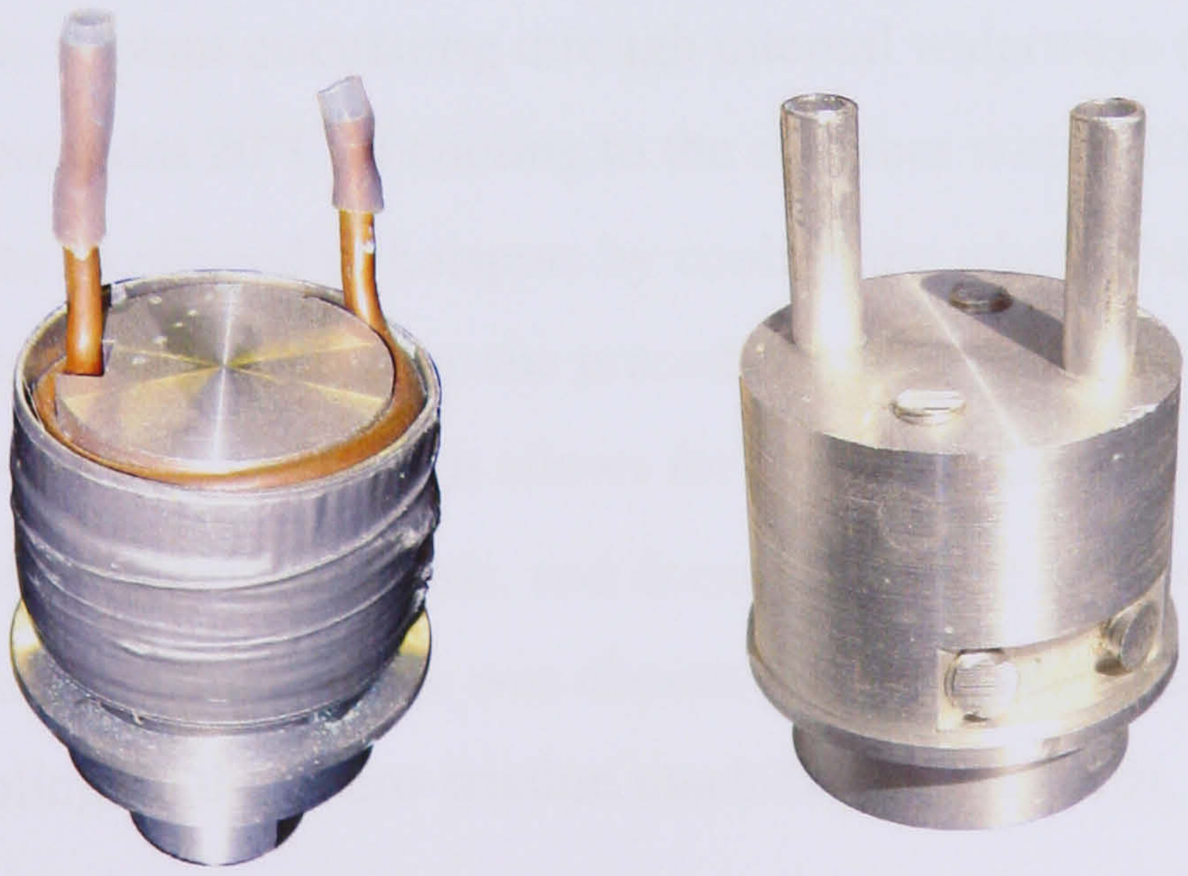

Figure 3.7 Direct cooling heatsink (left: HS2; right: HS3)

The solution provided rapid cooling of the charge with a drop in temperature of 14°C in less than 10 minutes. However, the chamber itself is not cooled as rapidly with the temperature falling by 9°C in 70 minutes. This technique would therefore be likely to maintain warm areas within the chamber and an unstable or inconsistent charge condition. The design also required removal between tests and, since it replaces the window, prevented observation during tests. The outer parts of the mechanism and chamber were further insulated with foam rubber and lagging material. The heat transfer for this variant are compared with subsequent designs in chart format (Figure 3.8).

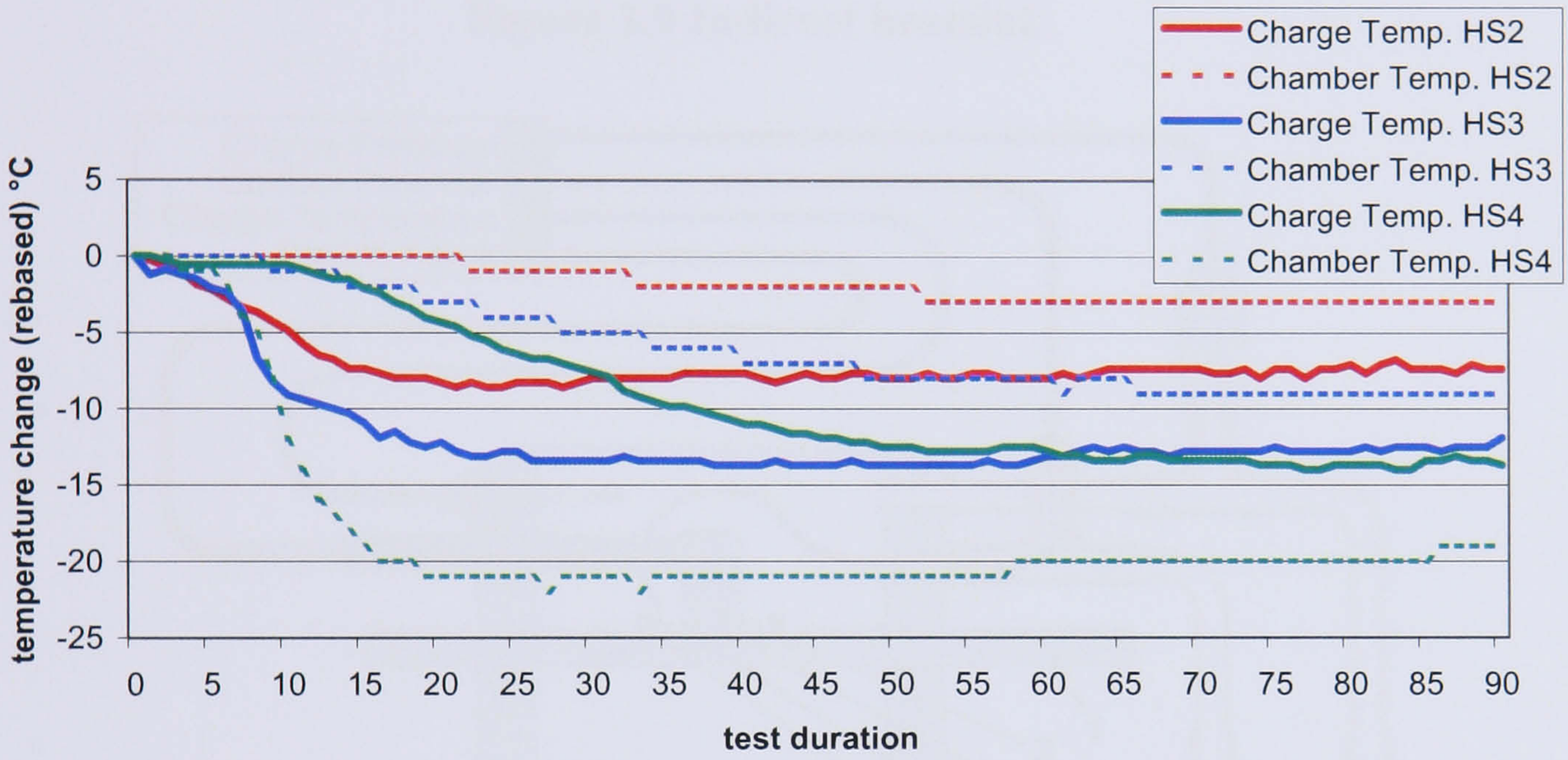

Figure 3.8 Change in temperature for alternative cooling solutions

3.9.2.3 Indirect heatsink solution

A heatsink block (designated HS4) was designed to mount between the heater block and the base of the chamber. The block draws heat through the base of the chamber, to coolant circulating through internal waterways (Figure 3.9). The solution provides 20°C of cooling to the chamber within 20 minutes and also reduces the likelihood of hotspots by cooling the whole chamber. The charge is cooled less quickly than the preceding method, taking 60 minutes to register a fall of 13°C. The design allows for a permanent mounting, negating the need for removal between tests, and doesn't interfere with normal operation of the machine. This final device was chosen for employment as the preferred method of cooling on the micro-friction machine (Figure 3.10).

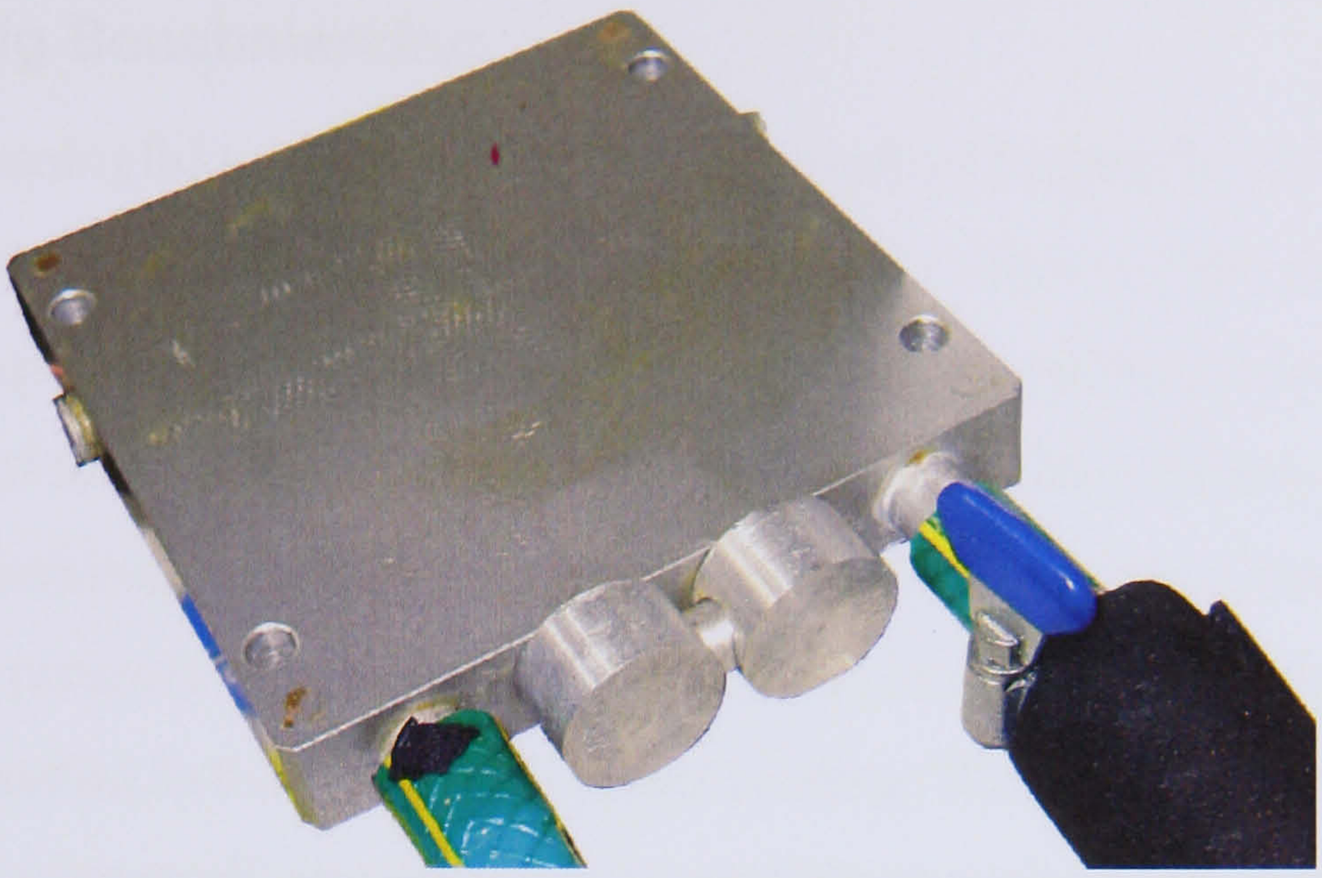

Figure 3.9 Indirect heatsink

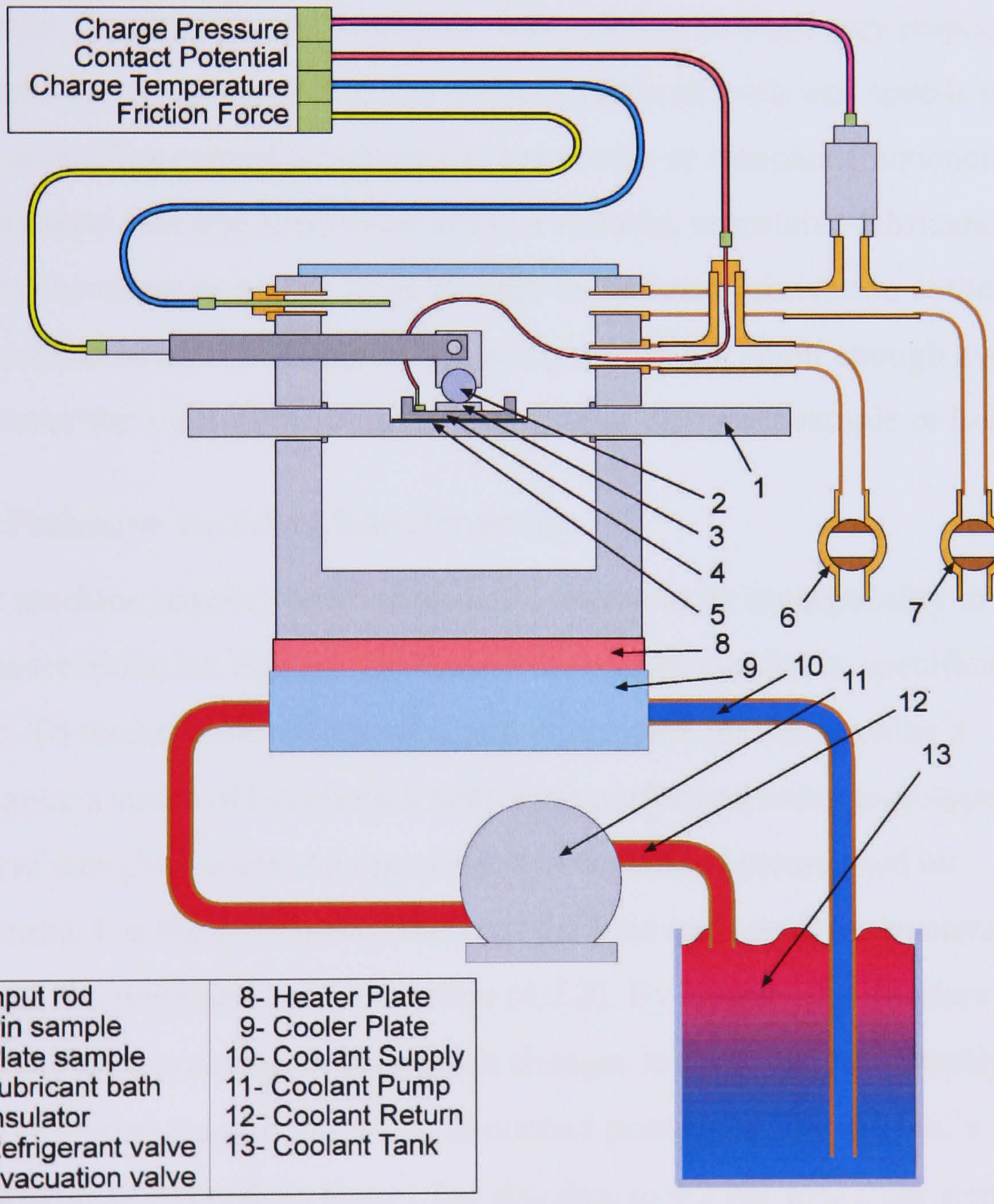

1- Input rod	8- Heater Plate
2- Pin sample	9- Cooler Plate
3- Plate sample	10- Coolant Supply
4- Lubricant bath	11- Coolant Pump
5- Insulator	12- Coolant Return
6- Refrigerant valve	13- Coolant Tank
7- Evacuation valve	

Figure 3.10 Final schematic overview

3.10 Test Rig Benchmarking

Prior to any meaningful testing the machine required calibrating to provide a benchmark for subsequent works. Areas of potential concern include a change in stiffness or squirming of bellows and the machines natural resonance. Pressurisation of the chamber may cause the bellows to stiffen thereby reducing the sensitivity of the friction force feedback mechanism. Changes in the operational pressure may also cause the bellows to squirm or deform, resulting in variation in the simulated contact loading. By operating the machine under a "control" atmosphere it is possible to evaluate changes in sensitivity and contact conditions hence account for these during the test programme. To ascertain the machines susceptibility to frequency response variations a test programme was run across a range of loads and speeds to identify anomalies caused by its natural harmonics or resonant frequencies. A similar method was also used to ascertain a suitable, repeatable lubricant measure. The measure had be large enough to maintain lubrication at the sample contact across the range of operating speeds but small enough avoiding spillage over the sides of the bath or drag against the upper sample or holder.

3.10.1 Pressure Variation Benchmarking

The test machine requires benchmarking to ascertain its susceptibility to performance variation through changes in the charge condition, specifically pressure. To measure the effects of chamber pressure on the machine's performance a series of benchmark tests were performed using prototype test pieces and straight mineral oil operating in a controlled pressurised air environment. For the purposes of the tests the load and speed parameters are taken from the proposed test parameters (4.2.2). By varying the pressure in steps it should be possible to distinguish changes in response due directly to machine performance and those due to contact parameters. In test No.'s 1 and 2 the pressure was stepped up from 1 bar absolute to 4.2 bar in 0.2 bar steps at 2-minute intervals. The test parameters are summarised (Table 3.1).

Test No.	Load (N)	Speed (Hz)	Start Pressure (Bar)	Finish Pressure (Bar)	Step (Bar)	Step Duration (s)
1	20	27	1	4.2	0.2	120
2	20	27	1	4.2	0.2	120
3	20	27	1	1.4	0.05	30

Table 3.1 Pressure variation benchmark parameters

With the indicated friction force and pressure plotted against time it is possible to distinguish between variances in friction feedback caused directly by changes in the machines dynamics and those due to changes in the contact parameters. Any fluctuations due to machine dynamics occur in parallel with changes in pressure, where as those caused by contact parameters will be more gradual and random. Changes in machine dynamics can be seen in the graph (Figure 3.11) by sudden changes in friction force at 120 seconds and 240 seconds.

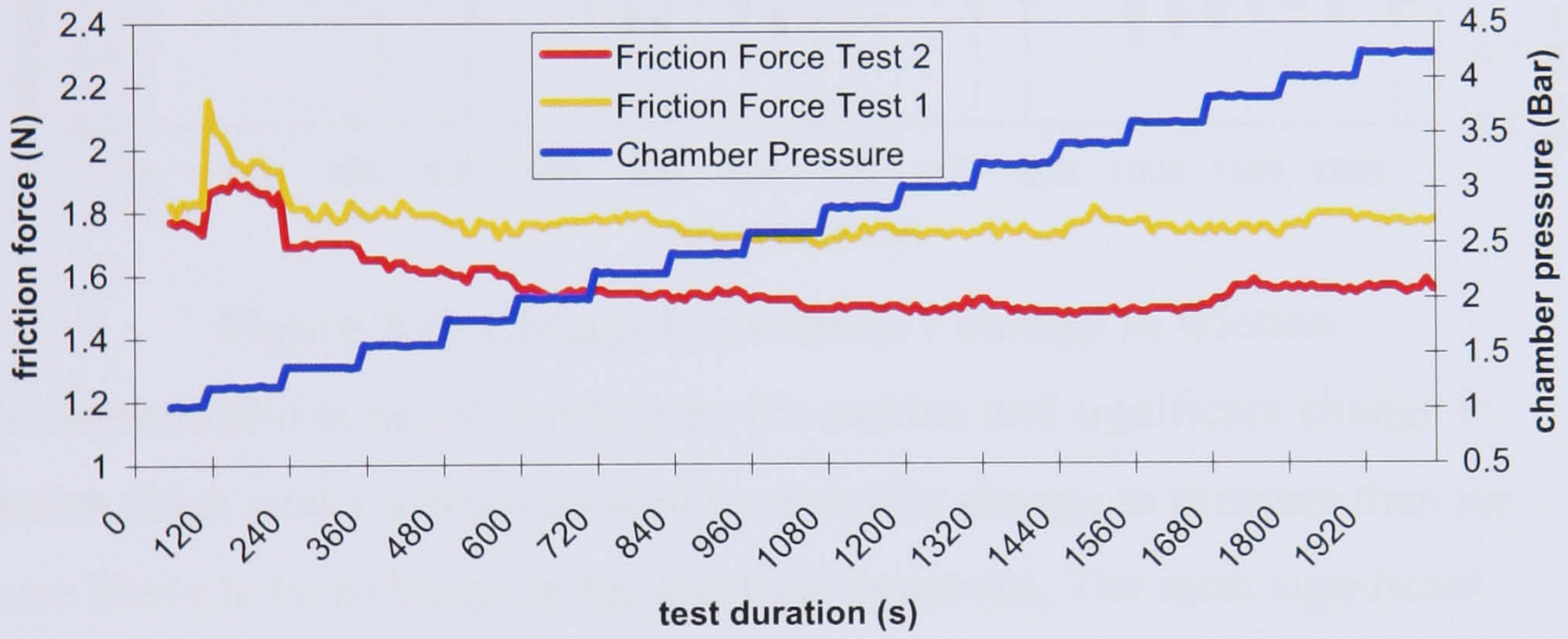

Figure 3.11 Effect of change in pressure on machine performance

These times correspond to pressure changes of 1.0 bar to 1.2 and 1.2 to 1.4 bar. The random and gradual changes in contact parameters can be seen in the fluctuating nature of the data plot and do not correlate with sudden changes in pressure. To investigate the 1-1.4 bar pressure band further, a third test was conducted (Table 3.1). The pressure was stepped from 1 bar to 1.4 bar and back in 0.05 bar steps at 30-second intervals. The results from the test (Figure 3.12) are difficult to Interpret and a further graph is required to plot the change in pressure and change in friction force reading against time (Figure 3.13).

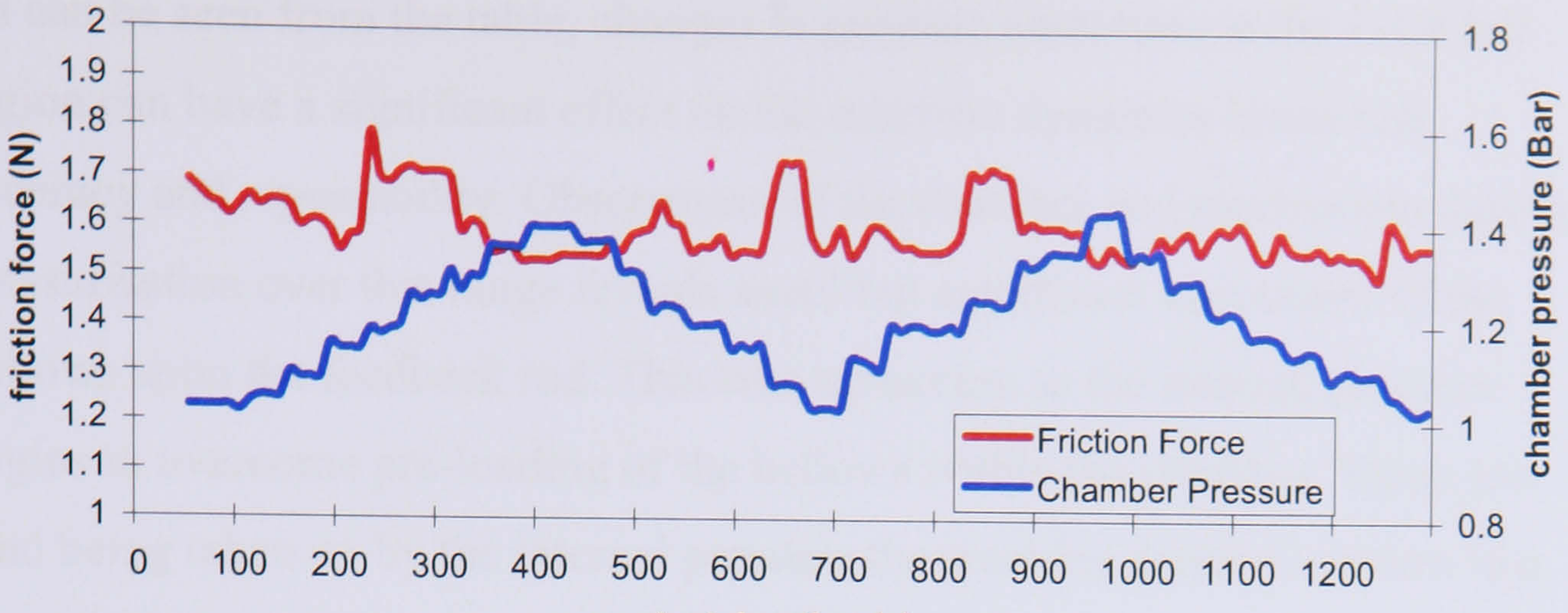

Figure 3.12 Focussed pressure response test

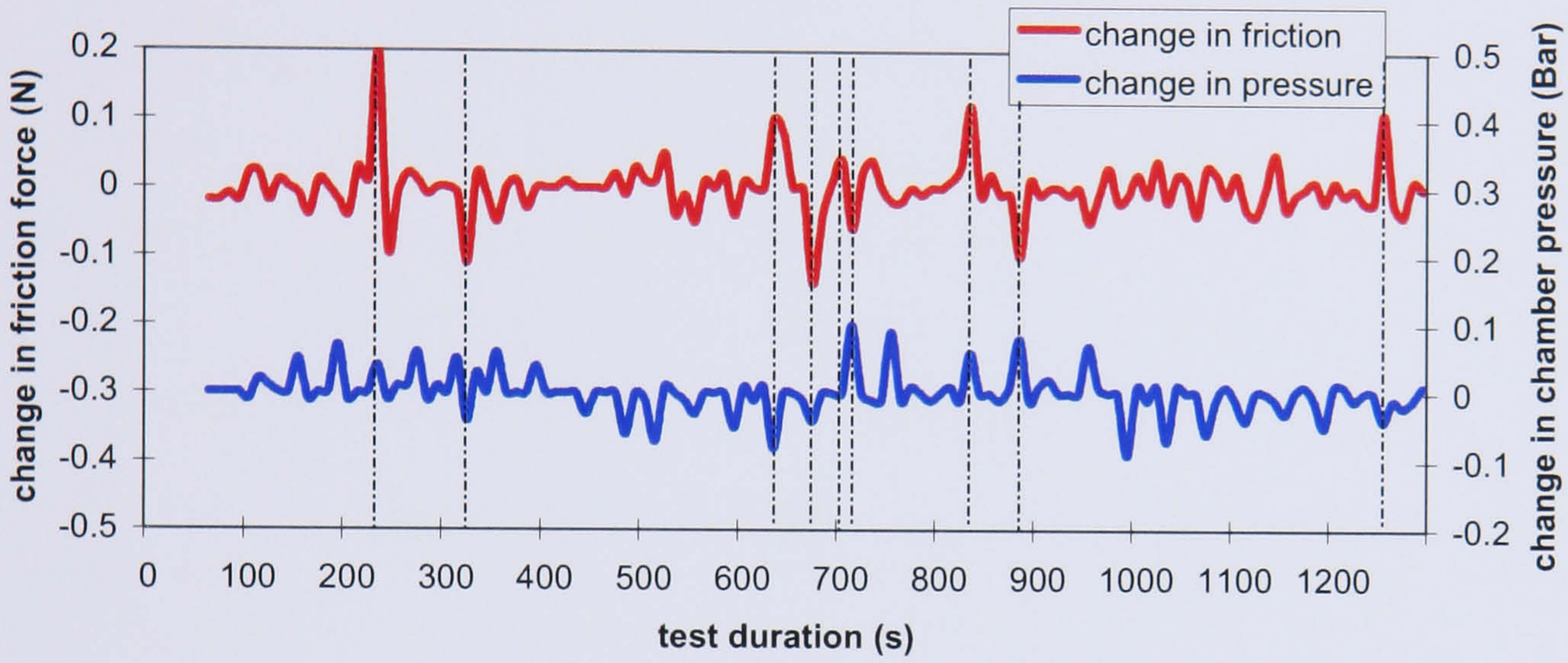

Figure 3.13 Change in pressure v change in friction

This second plot is easier to interpret, if a sudden and significant change in friction (high peak) is accompanied by a similar change in pressure then the cause likely to be a change in the machine dynamics. The most significant fluctuations in the friction force and their corresponding pressure step are shown (Table 3.2).

Time step (s)	220-230	230-240	310-320	510-520	620-630
Δ Friction (N)	+0.2	-0.09	-0.11	+0.05	+0.1
Pressure step (Bar)	1.15-1.19	1.19-1.18	1.26-1.31	1.3-1.23	1.16-1.08
Time step	660-670	700-710	820-830	870-880	1240-1250
Δ Friction (N)	-0.14	-0.06	+0.12	-0.1	+0.11
Pressure step (Bar)	1.07-1.03	1.03-1.13	1.19-1.25	1.25-1.33	1.1-1.06

Table 3.2 Pressure steps corresponding to significant friction changes

As can be seen from the table, changes in pressure anywhere in the 1-1.4 bar region can have a significant effect on the machine dynamics hence test accuracy and repeatability. Observation of the chamber and mechanism during pressurisation over this range reveals small but significant movement of the bellows upon the feedback rod. This take-up occurs as the internal pressure begins to overcome pre-loading of the bellows within the chamber. Upon pre-load being taken up by the internal pressure the machine dynamics return to a predictable nature.

4 Experimental Methodology

4.1 Mechanical Design

For the micro-friction machine to provide meaningful results, the test regime should follow that of the hermetic compressor as closely as possible. Whilst it would be impossible to completely mimic the operating conditions, the contact pressure (load), temperature, operating pressure and surface velocities should closely match those of the compressor. To ascertain the contact conditions present in the actual compressor a unit was dismantled and measurements taken or calculated (Table 2.2 & Table 2.3). From the measurements detailed, along with refrigerant and lubricant specifications, it is possible to create a spreadsheet (2.5) and derive contact parameters relative to crank angle (Table 2.4-Table 2.10) and projected in chart format (Figure 2.2-Figure 2.6). These derived contact parameters can be used to formulate the test piece contact parameters and to benchmark against them.

4.1.1 Small End Bearing Contact Parameters

The spreadsheet solution indicates that the maximum load at the contact is $55MNm^2$ for the HFC134a compressor and $32.6MNm^2$ for the R600a achieved at 160°-180° abdc. The surface speed of the small end to gudgeon pin contact however, is at a maximum across this range and at a minimum at 90° and 270°. It is these reductions in surface speeds to zero during the reversal of sliding direction that cause the film thickness to collapse at these crank angles (Figure 2.6). The film thickness is compared to the combined surface roughness, and indicates that boundary lubrication occurs (specific film thickness ratio below 1) between 66° and 118° for the HFC134a compressor and 74° and 108° for the R600a.

4.1.2 Contact Parameter Overview

To truly follow the contact at the small end of the actual compressor the test pieces would need to have identical contact conditions. For the contact parameters to match the upper test specimen would need an equivalent radius of 390mm for the R600a and 270mm for the R134a simulations. Contact

parameters such as these would provide a wear regime similar to the actual compressor, however the run time of the actual compressor over its 15-year life is in the order of 22,000 hours. The machine is designed to accept either a 10mm ball sample or 10mm diameter pin sample therefore a pin sample of material equivalent to the small end bearing was selected (4.1.1.3).

4.2 Test Specimens

Material test specimens were produced to match the contact parameters described utilising materials and processes of a similar nature to those used in the actual compressor. In the case of the gudgeon pin, flat steel plate of an appropriate composition, hardness and surface finish was selected (4.2.3). In the case of the connecting rod, an aluminium alloy was selected for the pin sample.

4.2.1 Test Specimen Contact Parameters

The cyclic loading of the actual contact complicates the task of matching the contact parameters. However, the load at the region surrounding the area of boundary lubrication (specific film thickness <1) is relatively constant with a pressure of 14-21MNm^2 from 66° to 118° for the HFC134a compressor and remaining constant at 11.5 MNm^2 from 74° to 108° for the R600a. The load for the test specimens can therefore remain constant through each cycle, with the level selected providing correlation to the actual compressors film thickness. By expanding the spreadsheet solution it is possible overlay the derived small end contact parameters with those of the test specimens. Using this technique, parameter combinations can be selected that will lead to a similar regime to that found at the small end bearing of the actual compressor (Table 4.1).

4.2.2 Accelerated Wear Test Parameters

To carry out a full test program using matched parameters would be beyond the time constraints of this project, therefore a combination of tests has been used. Matched parameter tests were used as a benchmark for accelerated wear tests using standard geometry test pieces. The standard test pieces are 10mm x 10mm diameter pins manufactured from materials described.

	Compressor		Test Samples
	R134a	R600a	
Equivalent radius (m)	0.27	0.39	0.005
abdc	70/110	70/110	70/110
Load (N)	35/63	43	20
Contact area ($\times 10^{-6}$ m^2)	2.5/3.3	3.7	0.28
Contact stress (MPa)	14.2/19	11.6	70.3
Surface speed (ms^{-1})	0.098	0.12	0.13
Combined r.m.s. surface roughness (μm)	0.21	0.21	-
Film thickness (μm)	0.19/0.17	0.26	-
Specific film thickness ratio	0.92/0.82	1.2	-

Table 4.1 Parameter selection

4.2.3 Material Composition

The material composition of the test pieces should closely match those of the typical gudgeon pin and small end bearing. For the test pieces previous works have identified the material compositions using Energy Dispersive X-ray (EDX) (Safari and Hadfield 1998; Ciantar, Hadfield et al. 1999) or industrial collaboration (Yoon, Poppe et al. 1996). For these works materials close to the material specifications have been identified as LM13AE109, with a Vickers hardness of 1.31 GPa, for the connecting rod small end and 52100 bearing steel, Vickers hardness 7.36 GPa, for the gudgeon pin. A comparison of material composition for these works has been made (Table 4.2, Table 4.3). 100/102Cr6 has identical composition to 52100 and due to its availability in flat sheet form, this material was selected for the wear plate.

Material	Fe	C	Cr	Mn	Ni
by EDX[1]	97.791	Inc. in Fe	0.99	0.89	0.33
1018 steel[2]	98.81-99.26	0.14-0.2	-	0.6-0.9	-
52100 steel	96.77	0.98	1.5	0.35	0.15

[1] from (Safari and Hadfield 1998), [2] from (Yoon, Poppe et al. 1996).

Table 4.2 Plate sample material composition

Material	Al	Cu	Mg	Ni	Si
by EDX[1]	80.7	3	-	0.167	13.54
380[2]	80-89.5	3-4	0.1	0.5	7.5-9.5
LM13AE109	80-86.4	0.8-1.3	0.8-1.5	1-1.5	11-13

[1] from (Safari and Hadfield 1998), [2] from (Yoon, Poppe et al. 1996).

Table 4.3 Pin sample material composition

4.2.4 Test Piece Manufacturing

For the test pieces to correctly simulate the operational conditions in the actual compressor they require similar manufacturing processes to those of the actual components. F. J. Engineering Ltd produced the test pieces for these works.

4.2.4.1 Pin sample production

The material selected for the pin sample was matched for the compressor connecting rod. The material was supplied as casting billet and therefore required processing with manufacturing techniques employed in the production of the con-rod. The aluminium alloy was first cast into 13mm diameter rods prior to turning and surface finishing to 0.1μ Ra. All samples were produced from the same material billet, processing and finishing of all components taking place at the same time to ensure consistency between samples, hence test parameters.

4.2.4.2 Plate sample production

The material selected for the plate was matched to the gudgeon pin. The material was supplied as flat sheet form and requires cutting, hole forming, hardening and finishing to meet the required plate specification. For these samples the sheet was hardened and tempered to the correct level prior to laser cutting of the plates to size including hole forming. The plates were surface ground to remove scratches, burrs and surface anomalies providing the required surface finish. All samples were produced from a single sheet, finishing processes carried out at the same time on the same machine to ensure consistency between samples, hence test parameters. The plate samples in "as supplied" condition were finished to 0.15μ Ra and have been classified as "A

type" plates. For testing with a smoother contact surface a number of the plates were subsequently re-finished to 0.05μ Ra and classified as "B type" plates.

4.2.5 Test piece Benchmarking

For the results of the experimentation to be useful they must relate to the actual lubrication, material and contact regime as the actual compressor. The test piece contact parameters (section 4.1.2) and material composition (section 4.1.3) are not a perfect match for the actual compressor. To address these issues, additional test piece types were produced to act as benchmarks for the material selection and the contact parameters.

4.3 Experimental Test Conditions

For the experimental testing procedure to yield comparable results a broad spectrum of operational conditions should be considered. The start-up and run phases each have different operational temperature and pressure conditions and should be factored into any test regime. To understand the tribological friction and wear regimes present and the effects of alternative refrigerant and lubricant combinations, the surface and load characteristics should be modified for extended testing at the compressors run phase operational conditions.

4.3.1 Operational Environment

The operational contact environment within the test chamber should match the conditions found with the hermetic compressor at the gudgeon pin/small end contact. For these works the compressor operating parameter values (Table 2.4) are plotted onto refrigerant pressure-enthalpy charts (Appendix Figure A.2 & Figure A.4) to provide data plots (Figure 2.1) for determining the operating environments (Table 2.5 & Table 4.4).

Refrigerant	**R600a**	**R134a**
Typical compressor operating temperature at start up (°C)	25	25
Typical operating pressure at start up (bar)	3.5	6.7
Typ. Compressor in-use temperature (discharge temp) (°C)	57	68
Saturation pressure at -25°C (evaporator pressure) (bar)	0.6	1.1
Compressor chamber operating pressure in-use (bar)	0.8	1.5

Table 4.4 Compressor operating environment

4.3.1.1 R134a Test Environment

The R134a test regime operational environment was derived from the data table (Table 4.4). For simulating the start up conditions the chamber should be held at 25°C with the pressure at 6.7 bar absolute to ensure refrigerant in the liquid condition. This would, however, exceed the test rig's design specification, therefore the pressure should be limited to 4 bar absolute. In this case the saturation pressure is 7°C (approximately 3.7 bar abs) and if the temperature is raised to 25°C the pressure will rise to 4.0 bar absolute. This does not allow for saturation at 25°C and requires an equivalent test with R600a. Saturation of R134a can be reached within the test rig design constraint if the chamber temperature is reduced to 5°C, pressurised to 3.5 bar absolute. This required further adaptation of the test rig. For simulating the in-use environment the temperature was raised to 68°C and the pressure dropped from 6.7bar absolute to a calculated level of 1.5 bar absolute. Referring back to section 3.10.1 the test machine can prove unpredictable within the 1-1.2 bar abs operating range. Although the test pressure is to the upper end of this range, consideration should be given to ensuring the mechanism has taken up any "slack" before testing is commenced. An additional "extreme" raised temperature test was devised to simulate heat build up in extreme operational conditions, in this case the temperature was raised to 110°C with a subsequent rise in chamber pressure to 1.7 bar. The in use chamber pressure was derived, using Charles' law, from the pressure of the refrigerant arriving in the compressor from the evaporator (1.0 bar) and the rise in temperature from -25°C to the compressor temperature of 68°C. The test environments are summarised in tabular format (Table 4.5).

Simulated Environment	**Temperature (°C)**	**Pressure (bar)**
R134a reduced temperature, saturated start up	5	3.5
R134a pressure limited start up test	25	4.0
R134a in use test	68	1.5
R134a extreme in use test	110	1.7

Table 4.5 R134a test environment

4.3.1.2 *R600a Test Environment*

The R600a test regime operational environment is derived from the data table (Table 4.4). For simulating the start up conditions the chamber should be held at 25°C with the pressure at 3.5 bar absolute to ensure refrigerant in the liquid condition condition. However, since the test rig is unable to provide an equivalent test for R134a alternative start up environments are required to match those achievable for the R134a. For R600a we can take the saturation pressure at 7°C (2.0 bar abs) and raise the temperature to 25°C to give an environment pressure of 2.1 bar. To match the achievable R134a saturated test, a similar test should also be carried out with the chamber temperature reduced to 5°C and the refrigerant pressure at 1.9 bar.

For simulating the in-use environment the temperature should be raised to 57°C and the pressure dropped from 3.5 bar absolute to a calculated level of 0.8 bar. As with the R134a tests an extreme temperature test was carried out at 110°C with a subsequent rise in chamber pressure to 0.9 bar. The in use chamber pressure is derived, using Charles' law, from the pressure of the refrigerant arriving in the compressor from the evaporator (0.6 bar) and the rise in temperature from -25°C to the compressor temperature of 57°C. The test environments are summarised in tabular format (Table 4.6).

Simulated Environment	**Temperature (°C)**	**Pressure (bar)**
R600a reduced temperature, saturated start up	5	1.9
R600a pressure limited start up test equivalent	25	2.1
R600a in use test	57	0.8
R600a extreme in use test	110	0.9

Table 4.6 R600a test environment

4.3.2 Extended Testing

To provide data for the tribological investigation into friction and wear regimes present at the contact extended testing should be carried out using alternative loading and plate surface finish. The "B type" plates should be utilised under under the same environmental conditions as the run phase tests (Table 4.7).

Simulated Environment	Duration (s)	Temperature (°C)	Pressure (bar)
R134a in use test	7200	68	1.5
R600a in use test	7200	57	0.8
R134a in use test	14400	68	1.5
R600a in use test	14400	57	0.8
R134a in use test	86400	68	1.5
R600a in use test	86400	57	0.8

Table 4.7 Extended testing parameters

The first batch of extended test experiments should have identical load and duration as the operational tests, the only variation being the plate surface finish. Subsequent experiments should extend the duration of the test to provide frictional data over time and to allow comparison of wear rates at test termination. A final set tests with reduced load should be used to ascertain the effects of load on the friction and wear regimes over a range of durations (Table 4.8).

Simulated Environment	Load (N)	Duration (s)	Temperature (°C)	Pressure (bar)
R134a in use test	15	86400	68	1.5
R600a in use test	15	86400	57	0.8
R134a in use test	15	237600	68	1.5
R600a in use test	15	237600	57	0.8

Table 4.8 Reduced load extended test parameters

4.4 Test Regime

To obtain meaningful and comparable data a repeatable test regime was required to satisfy both the mechanical and environmental criteria discussed in sections 4.1 through 4.3.

- Test with R134a and R600a
- Test with MO and POE lubricants
- Test with additised and un-additised lubricants
- Test with mechanical conditions described in 4.1
- Test at range of environmental conditions described in section 4.3

To satisfy these requirements tables of proposed tests can be compiled representing the initial accelerated wear (Table 4.9), extended (Table 4.10) and reduced load tests (Table 4.11). From these tables the number of tests, test material requirements, time allocations and scheduling can be derived. From the tables we can derive twenty-eight alternative test configurations, if each test is conducted three times this will provide for a total of eighty-four tests.

Test	Lubricant	Refrigerant	Pressure (bar)	Condition	Temp. (°C)
1	MO	R600a	1.9	Liquid	5
2	MO	R600a	2.1	Vapour	25
3	MO	R600a	0.8	Vapour	57
4	MO	R600a	0.9	Vapour	110
5	MO+Ad	R600a	1.9	Liquid	5
6	MO+Ad	R600a	2.1	Vapour	25
7	MO+Ad	R600a	0.8	Vapour	57
8	MO+Ad	R600a	0.9	Vapour	110
9	POE+Ad	R600a	1.9	Liquid	5
10	POE+Ad	R600a	2.1	Vapour	25
11	POE+Ad	R600a	0.8	Vapour	57
12	POE+Ad	R600a	0.9	Vapour	110
13	POE+Ad	R134a	3.5	Liquid	5
14	POE+Ad	R134a	4.0	Vapour	25
15	POE+Ad	R134a	1.5	Vapour	68
16	POE+Ad	R134a	1.7	Vapour	110

Table 4.9 Initial accelerated wear tests (A plates, 20N)

Test	Lubricant	Refrigerant	Pressure (bar)	Temp. (°C)	Duration (s)
17	MO	R600a	0.8	57	14400
18	MO+Ad	R600a	0.8	57	14400
19	POE+Ad	R600a	0.8	57	14400
20	POE+Ad	R134a	1.7	68	14400
21	MO	R600a	0.8	57	86400
22	MO+Ad	R600a	0.8	57	86400
23	POE+Ad	R600a	0.8	57	86400
24	POE+Ad	R134a	1.7	68	86400

Table 4.10 Extended test conditions, (B type plates, 20N)

Test	Lubricant	Refrigerant	Pressure (bar)	Temp. (°C)	Duration (s)
25	MO+Ad	R600a	0.8	57	86400
26	POE+Ad	R134a	1.7	68	86400
27	MO+Ad	R600a	0.8	57	237600
28	POE+Ad	R134a	1.7	68	237600

Table 4.11 Reduced load test conditions, (B type plates, 15N)

4.4.1.1 Test Rationalisation

The requirement for eighty-four tests was compounded by the need for dismantling, cleaning and re-assembly of the test equipment between tests. Since this process takes several hours to complete three months of test time could be taken-up just with this process. Therefore testing was conducted in batches, grouped according to lubricant type and refrigerant. Cleaning between individual tests limited to the bath, sample holders and assembly screws. Full disassembly and cleaning regime only being required if the refrigerant or lubricant type was changed. Under these circumstances it was possible to conduct three tests per day.

4.5 Test Programme

For the implementation of the described test regime (4.4) a test programme was developed. The programme covered the following key procedures:

- Sample height calibration
- Pre-test preparation
- Charging procedure
- Conducting the test
- De-charging and sample recovery

4.5.1 Sample height calibration

To obtain reliable hence comparable results, the contact loading of all tests needed to be identical. To this end, ensuring the bellows were perfectly centred eliminated any pre-load tension in the mechanism. To eliminate the pre-loading the operating height of the plate surface relative to the pin was critical and needed shimming for each test. Using a simple calculation (Equation 4.1) the correct shim can be selected for placing between the bath and the input rod.

$$T_s = D_b - \left(D_p + H_p + T_{pl}\right) \qquad \textbf{Equation 4.1 Shim thickness}$$

Where: Ts = Thickness of shim required; Db = Distance to inside of bath (no shims fitted); Dp = Distance to top of pin holder (bellows centred); Hp = Distance top of pin holder to bottom of pin; Tpl = Plate thickness.

4.5.2 Pre-test preparation procedure

For a first off test where the lubricant specification or refrigerant had changed from the previous test, the chamber, bellows, bath and components exposed to the charge required cleaning. This was carried out using an ultrasonic bath with acetone cleaning fluid. For tests where the refrigerant and lubricant specification was the same as the previous test, only the bath, pin holder and mounting screws required cleaning.

Upon reassembly, a new sample pin was fitted to the pin sample holder and mounted onto the feedback rod followed by a new plate to the lubricant bath and subsequent mounting to the force input rod utilising the correct shim. The chamber lid was replaced and the whole pressurised at 4bar absolute to check for leakage. Where no leakage was found the refrigerant hose valve was closed and fitted to the refrigerant can, the other end fitted to the chamber inlet valve, which was open. The vacuum hose was fitted to the vac pump, the other end fitted to the chamber outlet valve, which was also be open. At this point the pump evacuated the chamber and hoses for a duration of ten seconds, subsequently the outlet valve was closed followed by the inlet. The refrigerant hose valve (at the can end) was then opened to fill the hose up to the inlet valve then closed off to retain the refrigerant in the line for the subsequent charging procedure. The chamber was de-pressurised and the chamber temperature raised (or reduced) to that required for the test.

4.5.3 Charging procedure

The chamber lid was removed and lubricant measured into the bath using a fresh 5ml syringe prior to refitting. With the can on weighing scales and delivery line full with refrigerant, any change in weight represents refrigerant delivered to the chamber. The refrigerant was then delivered to the chamber via the inlet valve until either the correct pressure had been achieved or the correct gas mass had been delivered. The chamber temperature was allowed to settle to to the required level and with the target charge condition achieved, the refrigerant can isolated.

4.5.4 Test procedure

The machine was pre-loaded to 5 Newtons and the contact "settled" to provide and even loading across the pin. With the temperature/pressure already set during charging the machine was run up to target speed prior to applying increasing loads in 5 Newton, 2 minute steps up to the target load. The target load was run for the required duration prior to test termination.

The test provided information on friction and contact potential over time, any wear at the contact being observed during post-test analysis. Data generated during the test was be recorded using the machines control software and

represented charge temperature, charge pressure, reciprocation frequency, contact potential and friction coefficient.

4.5.5 De-charging procedure

The charge was allowed to cool, if necessary, to below 30°C. A manually operated pressure pump was connected to the inlet valve whilst a length of hosing leading to a ventilation point is attached to the outlet. The outlet valve was opened to allow the internal pressure to equalise with the ambient, any remaining refrigerant gas being flushed from the system by the manual pump. The lid was then removed, lubricant drawn off using a syringe and samples removed for post-test analysis.

5 Test Results

The results generated from the micro friction machine can be grouped together according to their test configuration. The first batch of tests comprise those with "A" type plates and a duration of two hours (7200s), the variables within these tests are the refrigerant/lubricant charge and the test temperature. The second batch of tests comprises those with "B" type plates. The variables within these tests are the refrigerant/lubricant charge and the test duration whilst the variation from previous tests would be surface roughness. The third batch of tests comprises those with "B" type plates and reduced load. The variables within these tests are the refrigerant/lubricant charge and the test duration whilst the variation from previous tests would be the contact load. The results can be further divided into two distinct groups, frictional data and wear data. The frictional data is gathered from the test machine during its normal operation and can therefore be plotted against time for each test run. The wear data, however, can only be measured after the test has completed and therefore cannot be plotted against time. The wear data can be plotted against the individual or grouped test variables only, either the refrigerant/lubricant charge, temperature, load, surface finish or overall test duration.

5.1 Initial Tests

The first batch of tests (tests 1 – 16) was carried out according to the described procedures. Measurements generated from data acquisition have been used to plot friction coefficient and contact potential against time for each test. At the conclusion of the test, the samples were cleaned and wear scars measured for calculation of the wear rate. By averaging the test results for each charge combination at each temperature range we can rate and rank their relative frictional and wear performance over the duration of test.

5.1.1 Reduced temperature saturated tests

The reduced temperature saturated tests were carried out at 5°C with each charge combination pressurised to the relevant refrigerant saturation point. Any increase in refrigerant quantity over and above the saturation point would not result in an increase in pressure, rather a liquid state would develop within the test chamber. The development of any liquid refrigerant would be proportional to the mass of delivered refrigerant, not the pressure, therefore overcharging is possible and would introduce inconsistencies. To maintain consistency for the saturated tests the refrigerant was weighed into the chamber. Each of the four charge combinations were tested at least three times and the results for friction and contact potential collated plotted to charts (Appendix Figure D.1 - Figure D.8). The results were then averaged to provide comparisons between each charge for both friction (Figure 5.1) and contact potential (Figure 5.2). The samples were measured after each experiment to calculate the material wear coefficient (Appendix Table D.1), an average being taken for each charge (Figure 5.3).

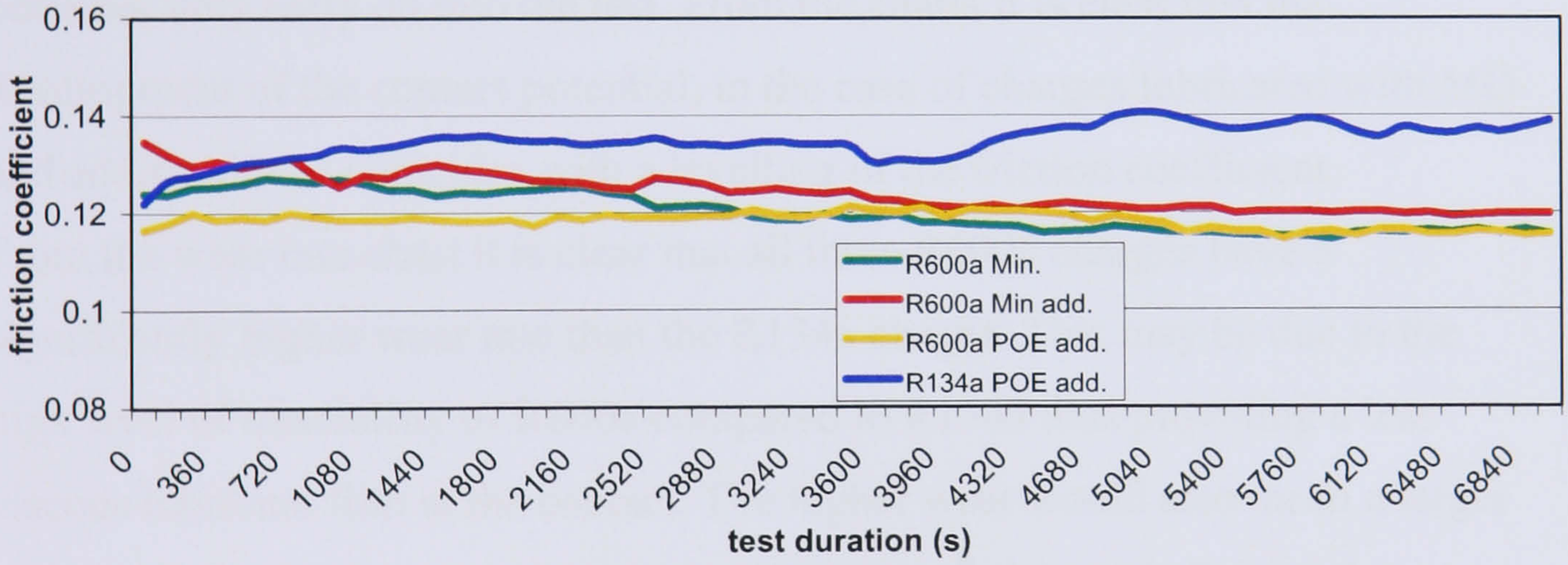

Figure 5.1 Saturated test friction coefficient, 7200s, 20N, A plates

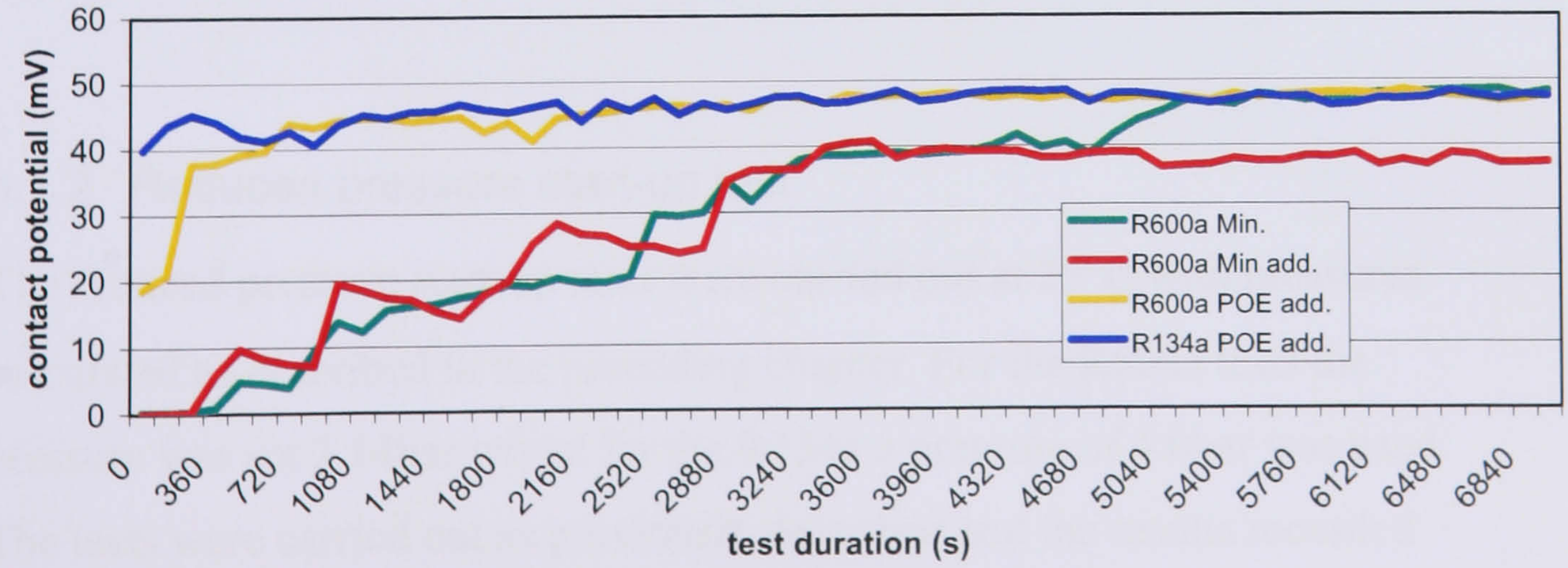

Figure 5.2 Saturated test contact potential, 7200s, 20N, A plates

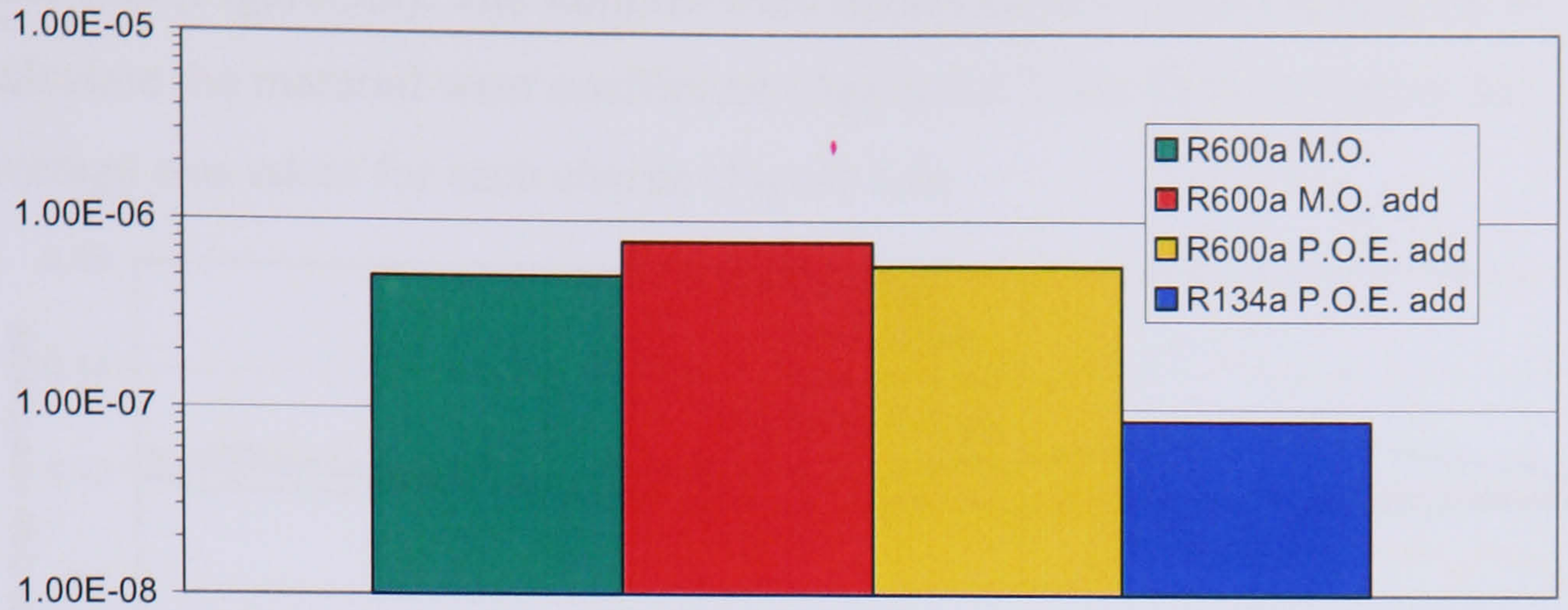

Figure 5.3 Saturated test wear coefficient (k), 7200s, 20N, A plates

From the friction coefficient chart it can be observed that both the R600a MO and additised MO charges have a declining friction coefficient until 3960s, where upon the coefficient levels off. The R600a POE charge has a steady friction coefficient whilst the R134a POE charge has a rising but erratic trend. From the contact potential chart it can be observed that both the R600a MO and additised MO charges have a slowly increasing contact potential, reaching a level of 40mV at 3960s. The two POE charges achieve a high contact potential very early on into the test. From the charts it is clear that the development of the contact potential, in the case of charges lubricated with MO and additised MO coincides with a levelling of the friction coefficient.

From the wear rate chart it is clear that all three R600a charges have a significantly higher wear rate than the R134a charge. This may be due to the high level of miscibility of R600a compared to R134a thus providing a less viscous lubricant film at the contact. The higher wear would also mean a larger contact area hence lower contact pressure. This may in turn influence the friction coefficient as recorded in the chart.

5.1.2 Reduced pressure start-up test

The reduced pressure start-up tests were carried out at 25°C with pressures calculated as described in the preceding chapter. For the R600a tests the pressure was set 2.14bar whilst for the R134a a pressure of 4.0bar was used. The tests were carried out as previously described and the results recorded collated and plotted to charts. The results were then averaged to provide comparisons between each charge for both friction (Figure 5.4) and contact

potential (Figure 5.5). The samples were measured after each experiment to calculate the material wear coefficient (Appendix Table D.1), as before an average was taken for each charge (Figure 5.6).

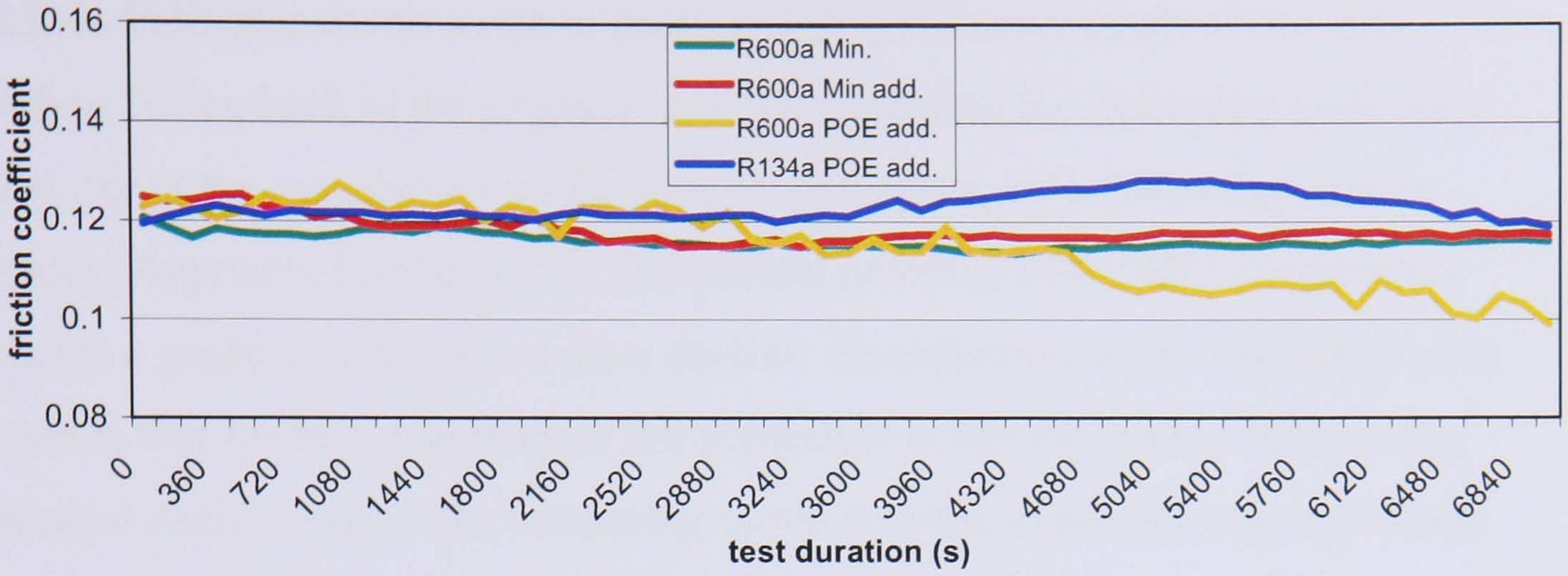

Figure 5.4 reduced pressure friction coefficient, 7200s, 20N, A plates

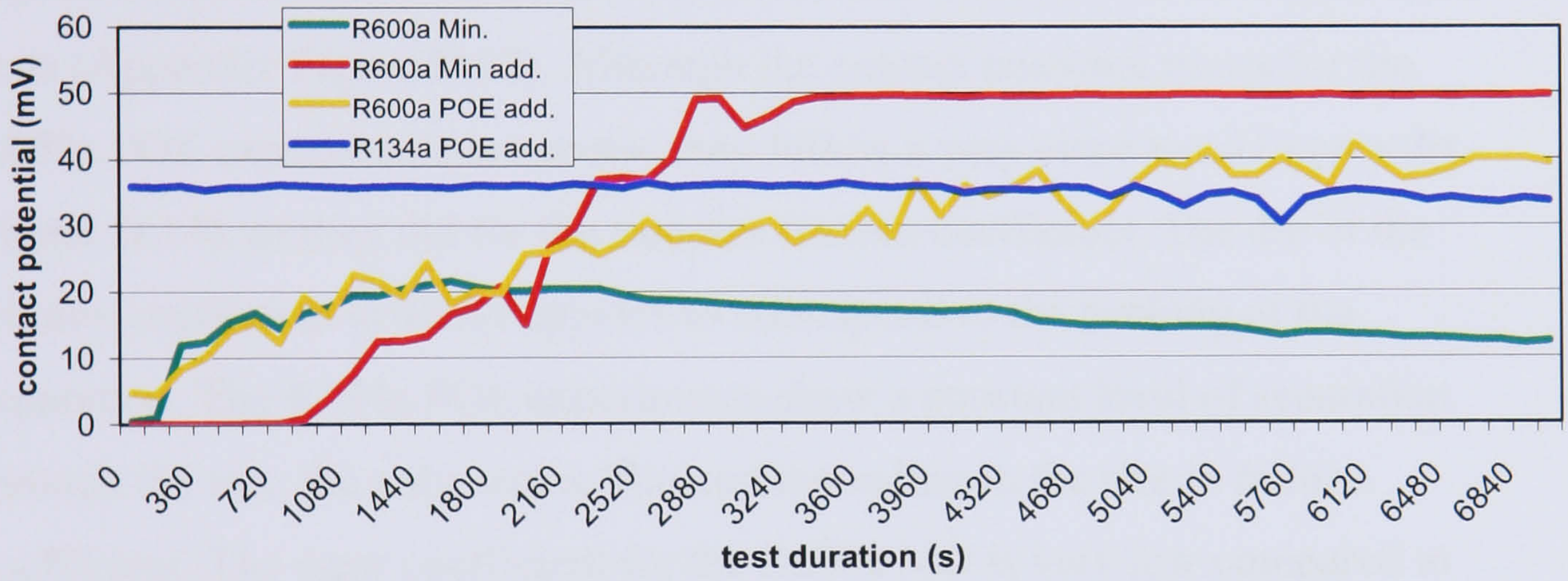

Figure 5.5 Reduced pressure contact potential, 7200s, 20N, A plates

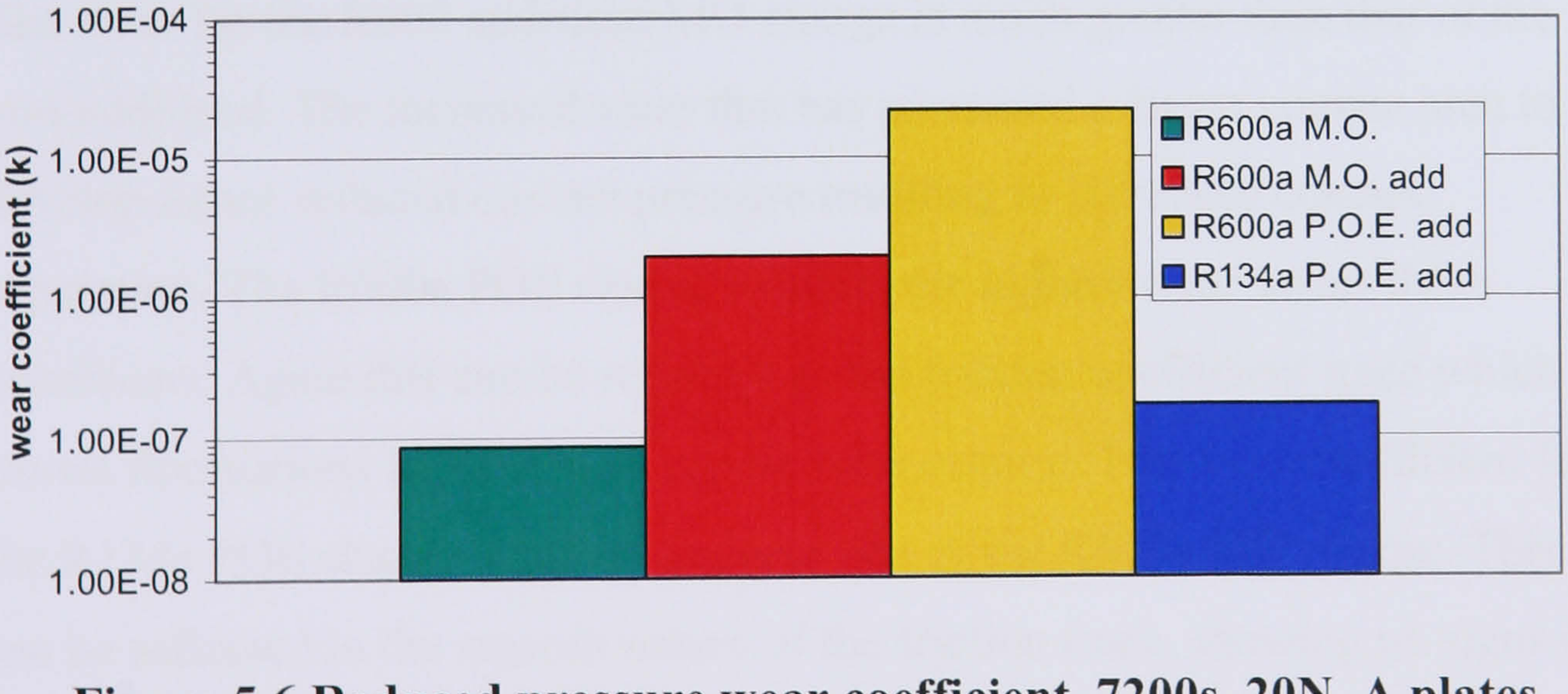

Figure 5.6 Reduced pressure wear coefficient, 7200s, 20N, A plates

The MO and additised MO friction plots appear to follow each other very closely. They both exhibit a declining trend for the first half of the test before levelling off. The individual sample plots, however, show a wide variation in results for the MO compared to the additised MO and R600a POE charges (Appendix Figure D.9, Figure D.11, Figure D.13). The R600a POE plot shows

a distinct reduction in friction over time throughout the duration of the test. The reduction in friction for this combination is significantly greater than for the other charges, the most pronounced change in friction occurring at 4680s. The R134a POE plot shows a rise in friction during the second half of the test before falling back to the original level. Examination the individual plots show that this is the case for two of the three experiments, both following similar traces (Appendix Figure D.15). The contact potential of the MO experiments shows a gradual build up and slow decline. Examination of the individual plots reveals that for two experiments full separation occurred quickly followed by gradual decline, whilst the remaining samples failed to provide any significant gap (Appendix Figure D.10). The additised MO built and maintained a strong separation with, like the friction coefficient, little variation between individual tests (Appendix Figure D.12). Although the contact potential traces for the R600a POE experiments are erratic they follow a very close trend (Appendix Figure D.14), as they did for the samples friction coefficient. The dip in the friction coefficient at 4680s appears to correspond to the peaking of the separation. The R134a POE experiments show a constant level of separation through the test, the only erratic blip corresponding to the rise in friction coefficient. The wear coefficient for the R600a MO is very low compared to the other charges and reflects the smooth nature of the friction coefficient trace. The wear for the R600 additised MO charge is much greater than that of the non-additised. The increased wear that has promoted a larger contact area to develop hence reduced contact pressure resulting in increased contact separation. The R600a POE charge exhibits the highest wear under these conditions. Again this can be reflected in the friction coefficient trace which shows fluctuations indicating an erratic wear regime. The wear coefficient for the R134a POE charge is much closer to that of the R600a MO charge. This can be reflected in the smooth nature of the friction trace, showing no signs of an erratic nature. The contact separation takes place very early and may be a result of chemical action from the refrigerant lubricant combination.

5.1.3 In use test

The in-use tests were carried out under the compressors typical operating conditions as described in the preceding chapter. For the R600a tests the pressure was set 0.78bar with the temperature at 57°C, for the R134a a pressure of 1.47bar and temperature of 68°C was used. The tests were carried out as previously described and the results recorded collated and plotted to charts. The results were then averaged to provide comparisons between each charge for both friction (Figure 5.7) and contact potential (Figure 5.8). The samples were measured after each experiment to calculate the material wear coefficient (Appendix Table D.1) and an average taken for each charge condition (Figure 5.9).

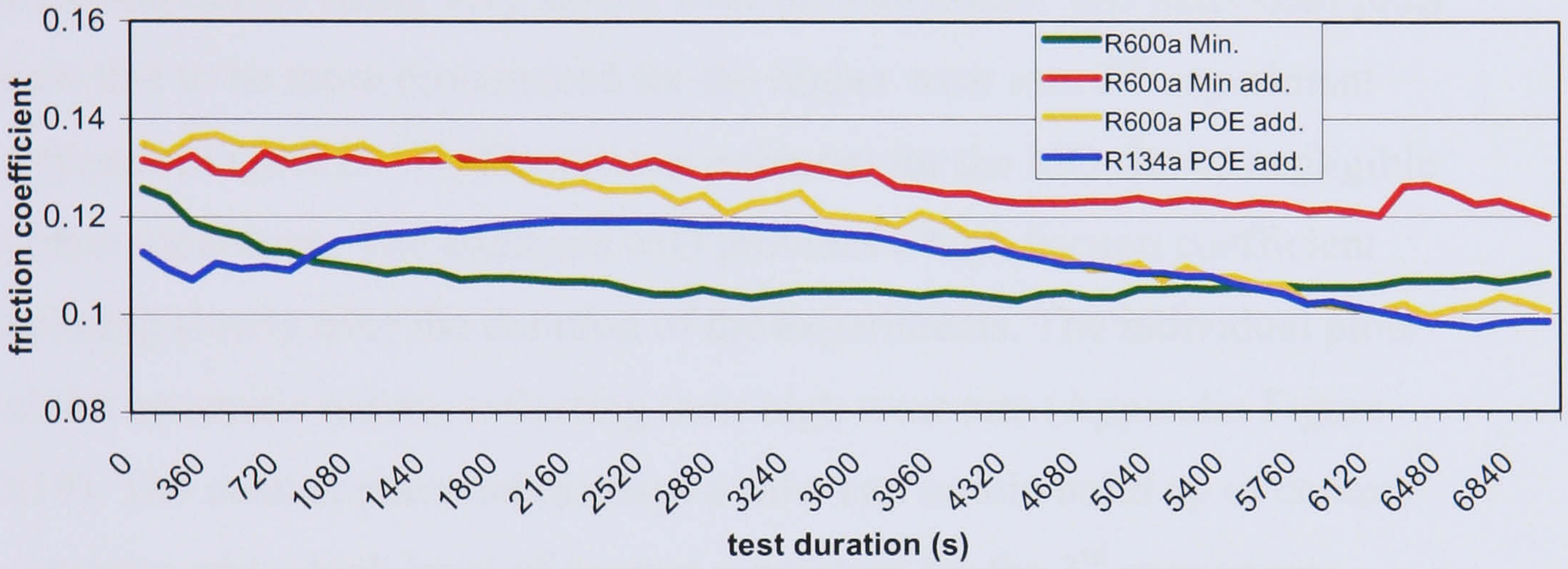

Figure 5.7 In-use test, friction coefficient 7200s, 20N, A plates

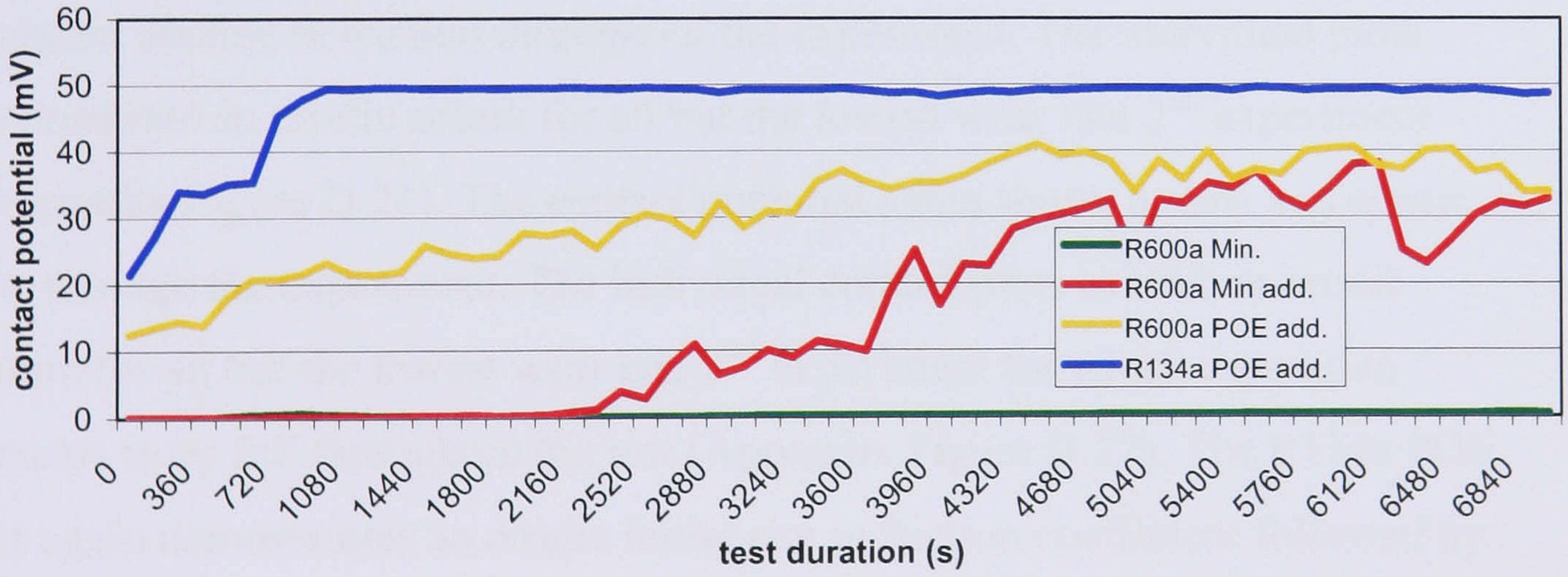

Figure 5.8 In-use test, contact potential 7200s, 20N, A plates

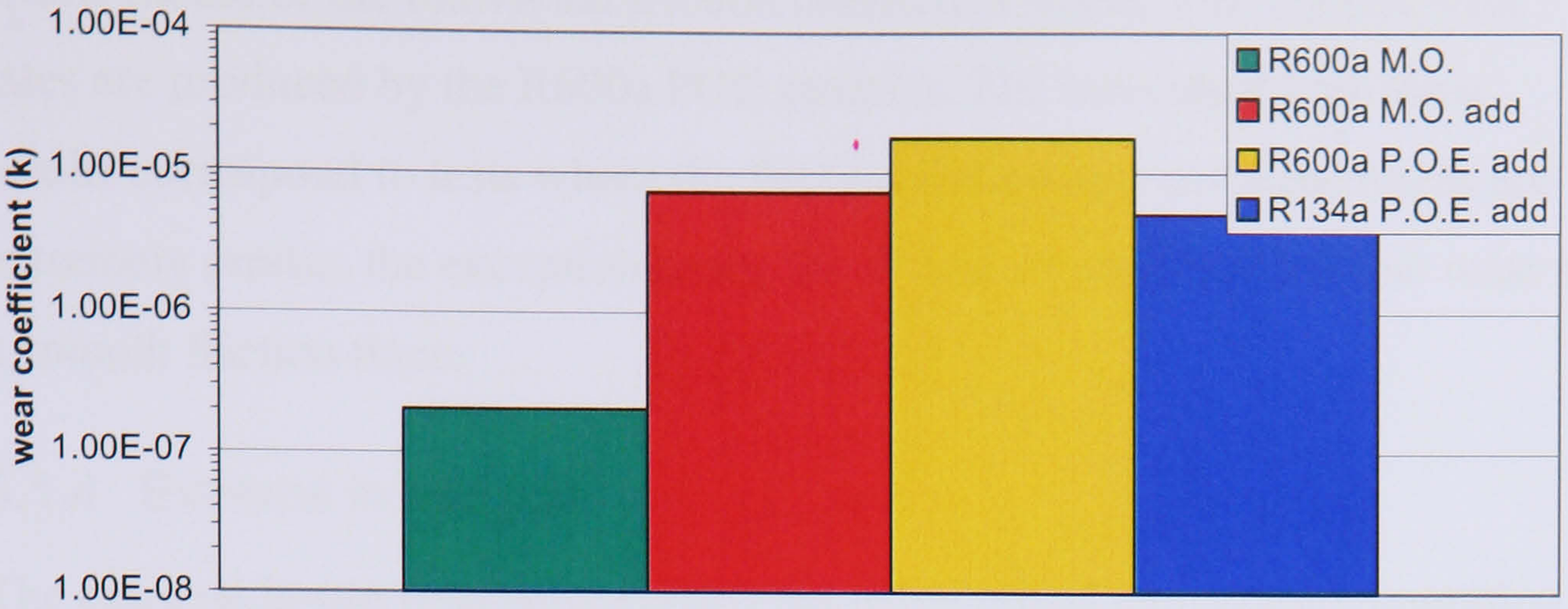

Figure 5.9 In-use test, wear coefficient 7200s 20N, A plates

The MO plot no longer corresponds to the additised MO under the in-use experimental conditions. The friction coefficient declines rapidly at the outset of the test before rising very slowly over the remainder. The individual plots show this to be more pronounced for the higher wear rate 2nd experiment (Appendix Figure D.17). The contact potential for the MO shows negligible contact separation. The additised MO provides a high friction coefficient declining slowly over the duration of the experiments. The individual plots exhibit an erratic nature, reflecting their high wear rate (Appendix Figure D.19). The contact potential displays a slow and erratic build up of contact separation and a high level of contact separation for the 3rd experiment corresponds to a dip in the friction for its plot. The R600a POE again shows a constant decline in friction throughout the experiment. The individual plots demonstrate an erratic nature for all but the lowest wear rate 2nd experiment (Appendix Figure D.21). The contact potential again shows a slow and erratic rise through the experiment. The individual contact plots exhibit an erratic nature for all but the lowest wear rate 2nd experiment for which separation appears to be full throughout the test (Appendix Figure D.22). The R134a POE test again demonstrates an erratic initial rise in friction coefficient followed by a gradual reduction. The individual plots (Appendix Figure D.23) show this to be the case for all but the higher wear rate 2nd test run where the friction stayed constant. The contact potential shows a rapid rise at the outset, corresponding to the erratic rise in friction, followed by constant separation. The wear rate of the MO samples is much lower than for the other charge combinations and is again reflected by the smooth friction and contact potential trace. The additised MO wear rate is significantly higher (by a factor of 100) and is reflected by the

erratic nature of the individual friction coefficient traces. The highest wear rates are produced by the R600a POE samples. The individual high wear results correspond to tests where the friction and contact potential traces are extremely erratic, the exception being the 3rd test which exhibited low wear and a smooth friction trace.

5.1.4 Extreme in use test

The extreme in-use tests were carried out using raised temperature operating conditions as described in the preceding chapter. For the R600a tests the pressure was set 0.91bar with the temperature at 110°C, for the R134a a pressure of 1.65bar and temperature of 110°C was used. The tests were carried out as previously described and the results recorded collated and plotted to charts. The results were then averaged to provide comparisons between each charge for both friction (Figure 5.10) and contact potential (Figure 5.11). As before, the samples were measured after each experiment to calculate the material wear coefficient (Appendix Table D.1), with an average being taken for each charge (Figure 5.12).

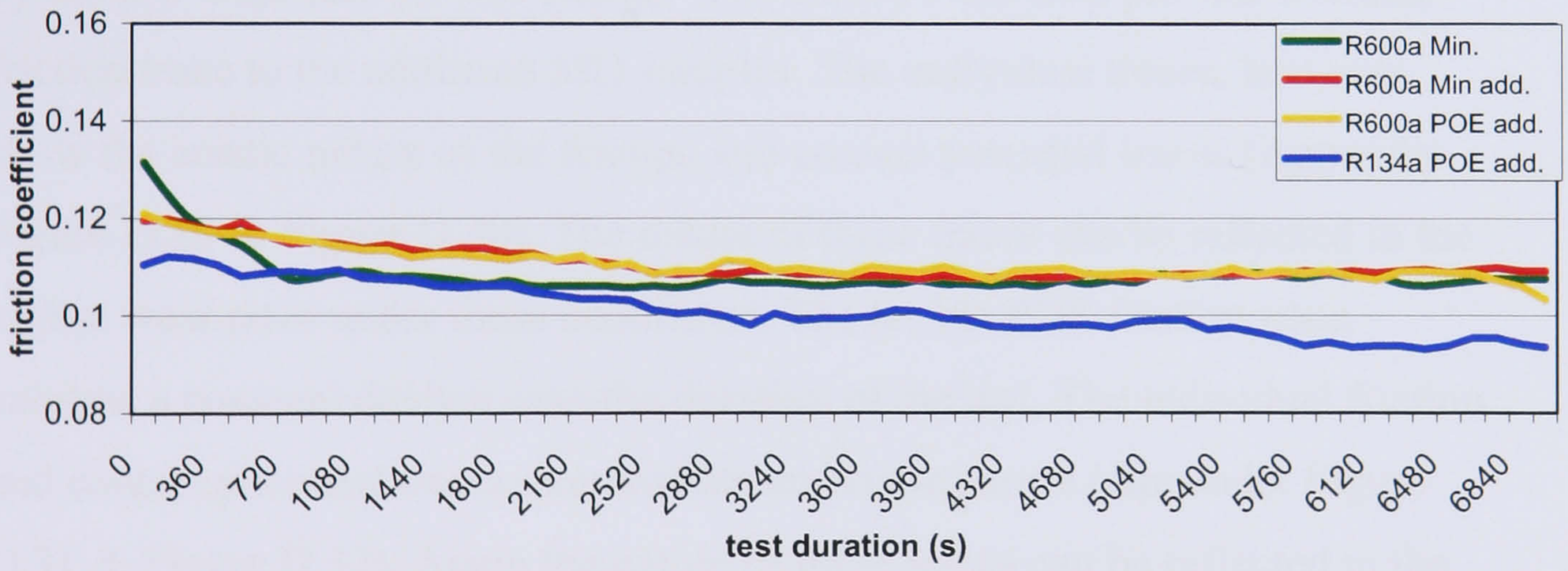

Figure 5.10 Extreme in-use test, friction coefficient 7200s, 20N, A plates

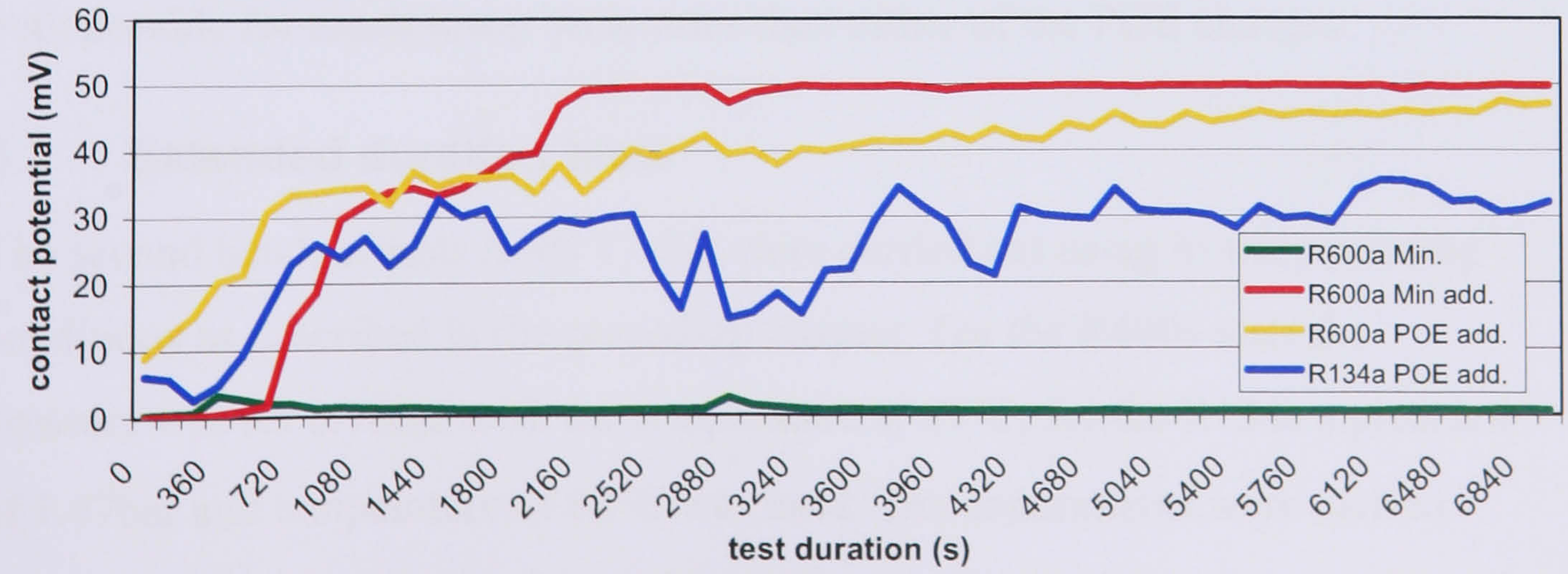

Figure 5.11 Extreme in-use test, contact potential 7200s, 20N, A plates

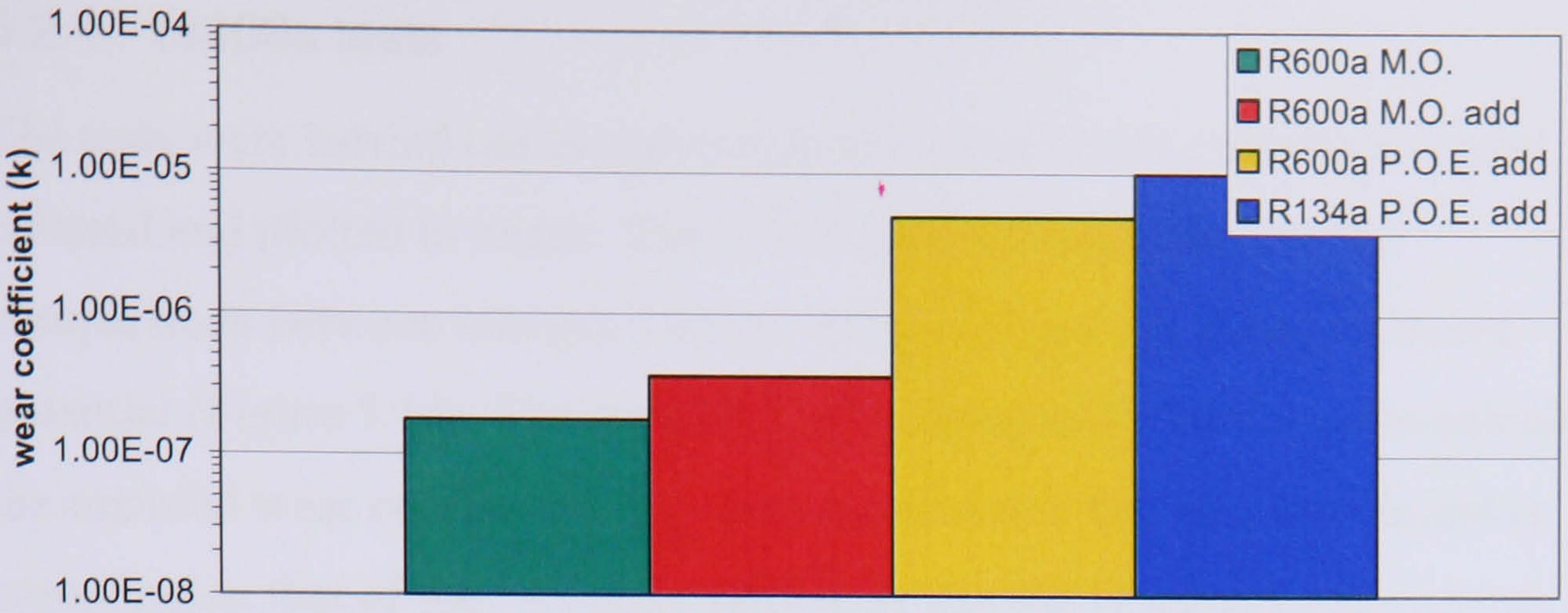

Figure 5.12 Extreme in-use test, wear coefficient, 7200s, 20N, A plates

The MO friction trace is very similar to that produced by the in-use test, the only appreciable difference is that the initial decline is more rapid. The individual friction traces are constant and non-erratic in nature, reflecting the low wear rate for this charge (Appendix Figure D.25). Again, the contact potential trace shows little separation under these conditions. The additised MO provides an initial erratic but declining trace followed by a more constant and consistent period. The individual friction traces shows this more consistent period correlates to the sudden and sustained contact potential and is reflected by the low wear rate for this charge. The R600a POE tests provide a similar friction trace to the additised MO samples. The individual traces, however, show the erratic nature of the friction and contact potential traces (Appendix Figure D.29 & Figure D.30). The nature of these traces can be reflected in the higher wear rates under these conditions. The R134a POE friction trace exhibits a constant decline over the duration of the test. The individual friction and contact potential traces demonstrate an erratic nature (Appendix Figure D.31 & Figure D.32). Again the nature of these traces can be reflected in the higher wear rates for these conditions. The MO and additised MO experiments both provide for much lower wear rates than either of the POE charges.

5.2 Extended duration tests

The second batch of tests (tests 17-24) were carried out using in-use operating conditions as described in the preceding chapter. For the R600a tests the pressure was set 0.78bar with the temperature at 57°C, for the R134a a pressure of 1.47bar and temperature of 68°C was used. The experiments were carried out over two duration's, 14400s and 86400s using the smoother B type plates.

5.2.1 14400s tests

The tests were carried out as previously described and the results recorded collated and plotted to charts. The results were averaged to provide comparisons between charges for both friction (Figure 5.13) and contact potential (Figure 5.14). The samples were subsequently measured to calculate the material wear coefficient, for these experiments the wear coefficient is compared to that of the "A" plate sample in-use test (Figure 5.15).

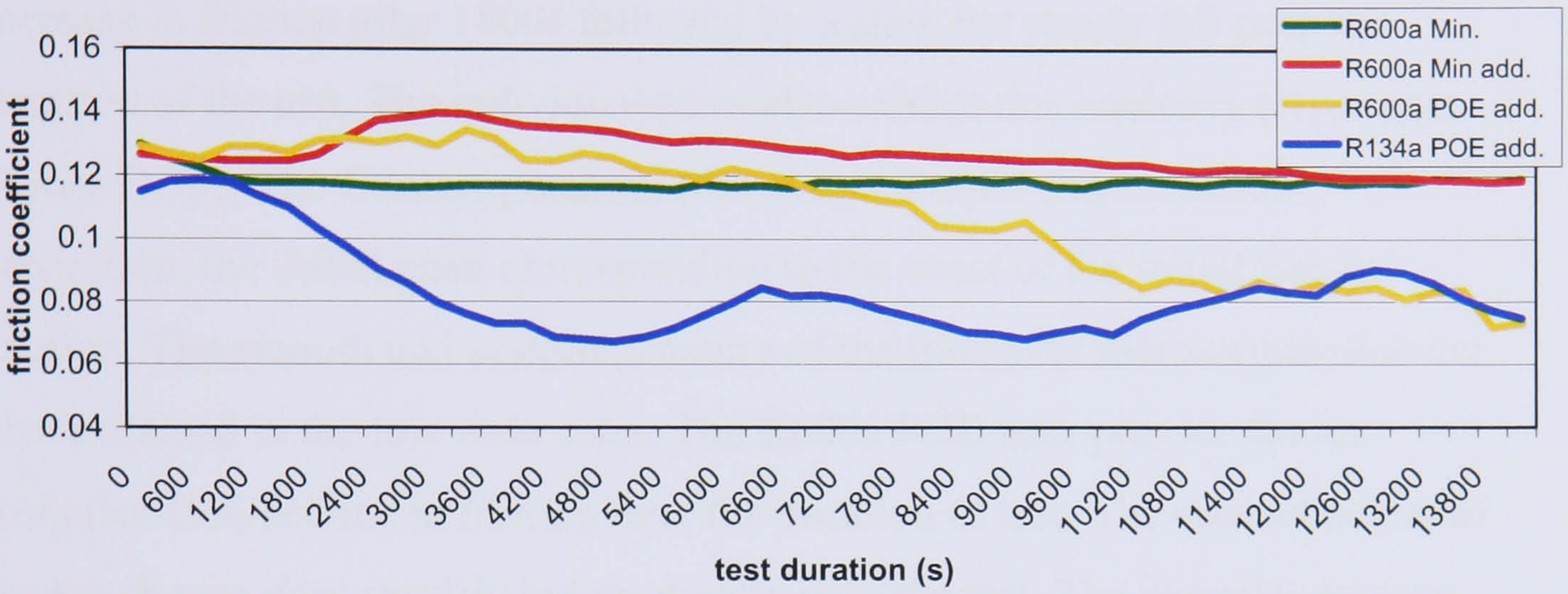

Figure 5.13 Extended in-use test, friction coefficient 14400s, 20N, B plates

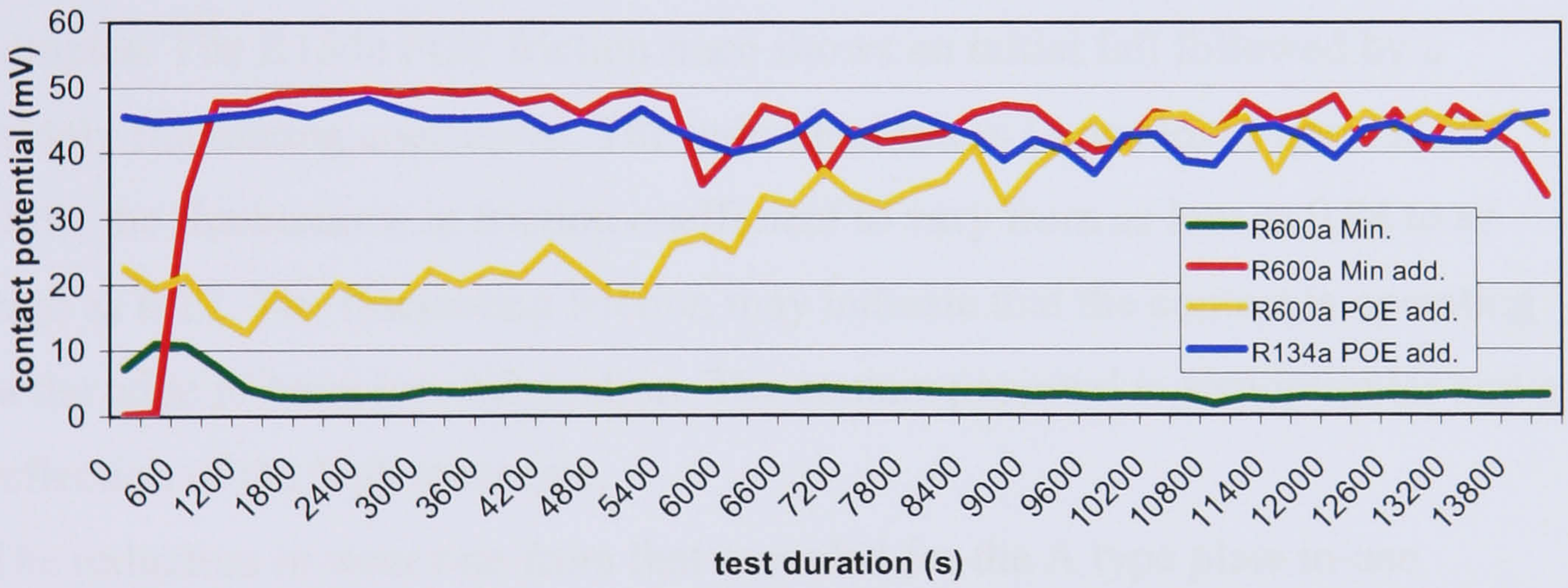

Figure 5.14 Extended in-use test, contact potential 14400s, 20N, B plates

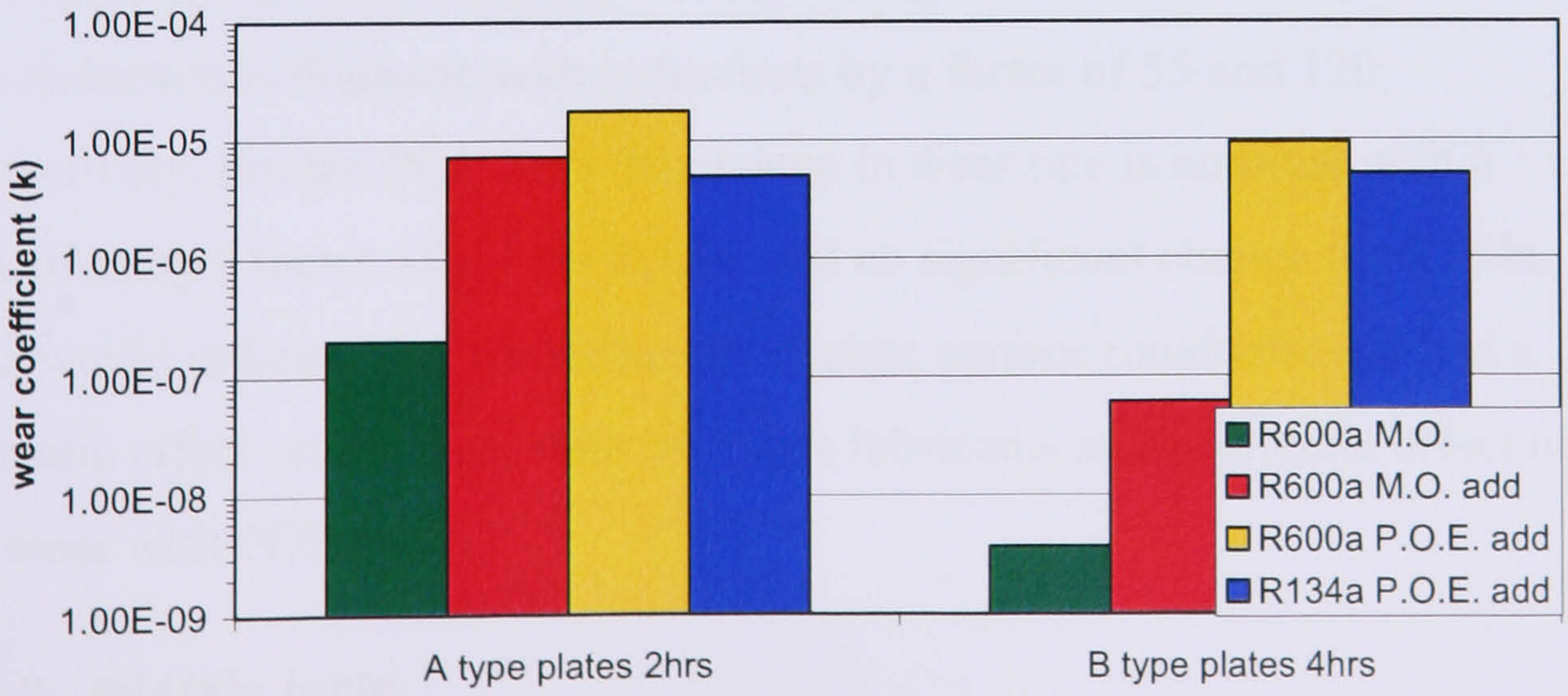

Figure 5.15 Extended in-use test, wear coefficient 14400s, 20N, B plates

The MO friction trace was, once more, very similar to the in-use test result. The trace has an initial decline followed by a constant friction coefficient throughout the duration of the test, the smooth nature of the trace is reflected in the low wear rate for this combination. The individual friction and contact potential (Appendix Figure D.33, Figure D.34) traces are also similar in nature and show that, for friction at least, the charge combination is relatively unaffected by the reduction in surface roughness. The additised MO shows an increase in friction after 1800s followed by a slow but steady fall over the duration of the test. The individual plots also exhibit this tendency (Appendix Figure D.35). The Contact potential plot shows a rapid and sustained separation, the initial peak corresponding to the onset of the initial rise in friction. The smooth and sustained nature of the traces for this combination are also reflected in the low wear rates. The R600a POE tests provide for an irregular 45% decline in friction over the duration of test. The contact potential for the charge rises steadily but erratically over the test. The irregular friction and contact potential traces are consummate with the high wear rate for these samples. The R134a POE friction trace shows an initial fall followed by a widely fluctuating coefficient. The individual traces (Appendix Figure D.39) show the fluctuations in friction coefficient to vary from as low as 0.04 to as high as 0.12. The fluctuating friction may indicate that the contact is operating at the edge of boundary lubrication. The contact potential is also irregular and a reflection of the high wear rate.

The reduction in wear rate from that recorded for the A type plate in-use experiments can reveal much about the nature of the lubrication regime of the individual charge combinations. For the MO and additised MO tests the wear rate reduction is dramatic with reductions by a factor of 55 and 120 respectively. For the POE tests the change in wear rate is nominal with a reduction by a factor of 1.9 for R600a and no significant change for R134a. This would indicate that the reduction in plate surface roughness has had a dramatic effect on the wear with MO type lubricants and negligible effect on the wear with POE types.

5.2.2 86400s tests

The tests were carried out as previously described and the results recorded, collated and plotted to charts. The results were then averaged to provide comparisons between each charge for both friction (Figure 5.16) and contact potential (Figure 5.17). The samples were measured after each experiment to calculate the material wear coefficient. For these experiments the wear coefficient is compared to that of the "A" plate in-use and "B" plate 14400s duration tests (Figure 5.18). The MO test friction coefficient was again very similar to the preceding results. The trace has an initial decline followed by a constant and regular trace, reflecting the low wear rate for this charge combination. The contact potential remains low through the test until 36000s where upon it gradually rises to provide separation over the second half of the experimental duration. The individual contact traces (Appendix Figure D.42) show that for two of the three experiments the maximum contact potential was achieved whilst the other remained low throughout.

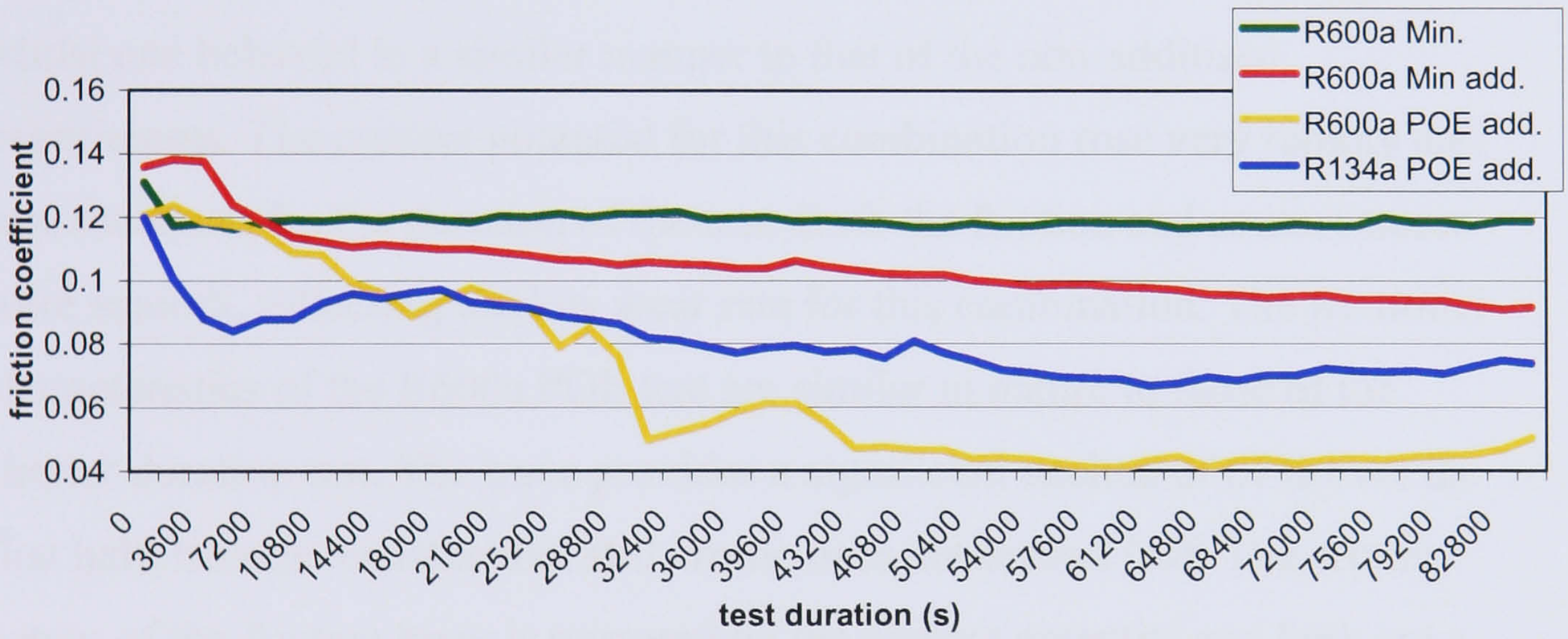

Figure 5.16 Extended in-use test, friction coefficient 86400s, 20N, B plates

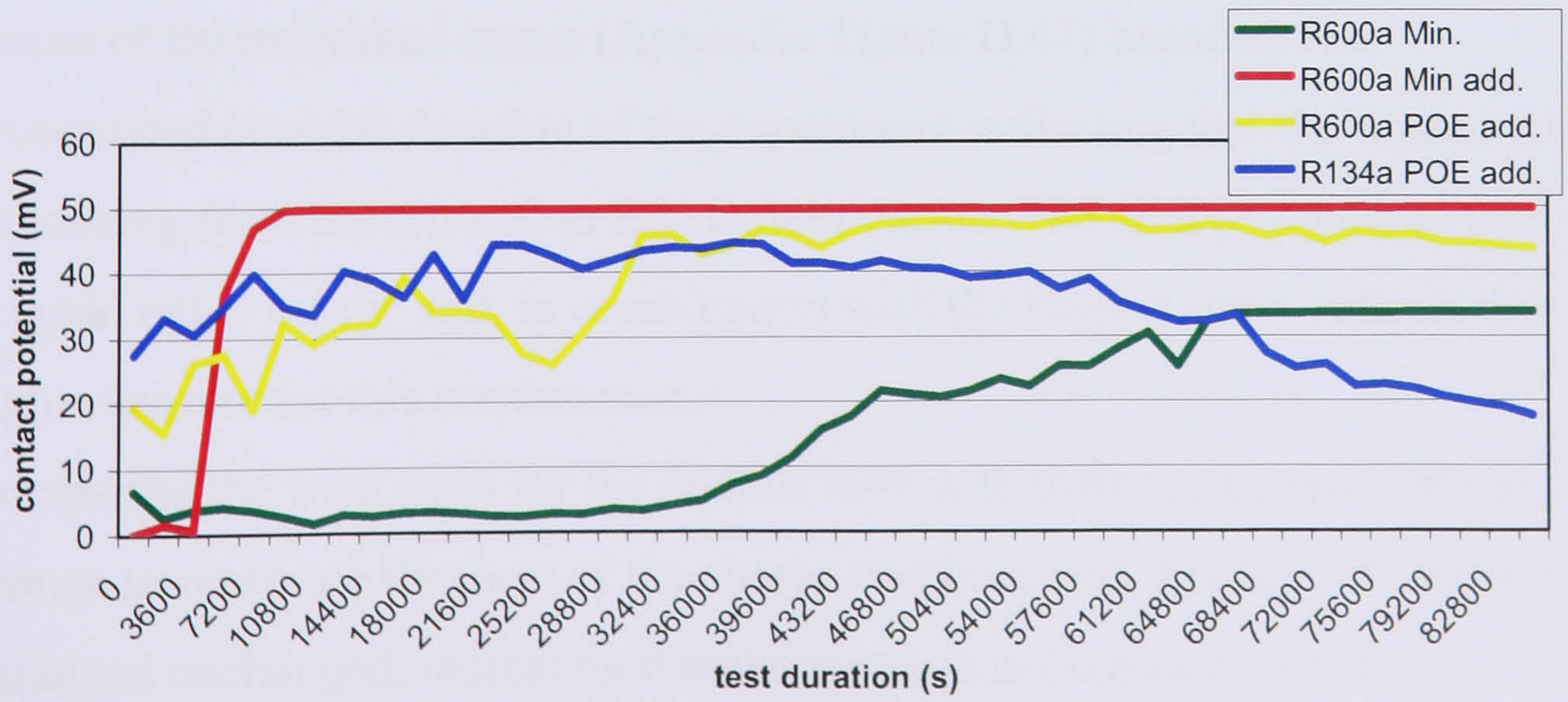

Figure 5.17 Extended in-use test, contact potential 86400s, 20N, B plates

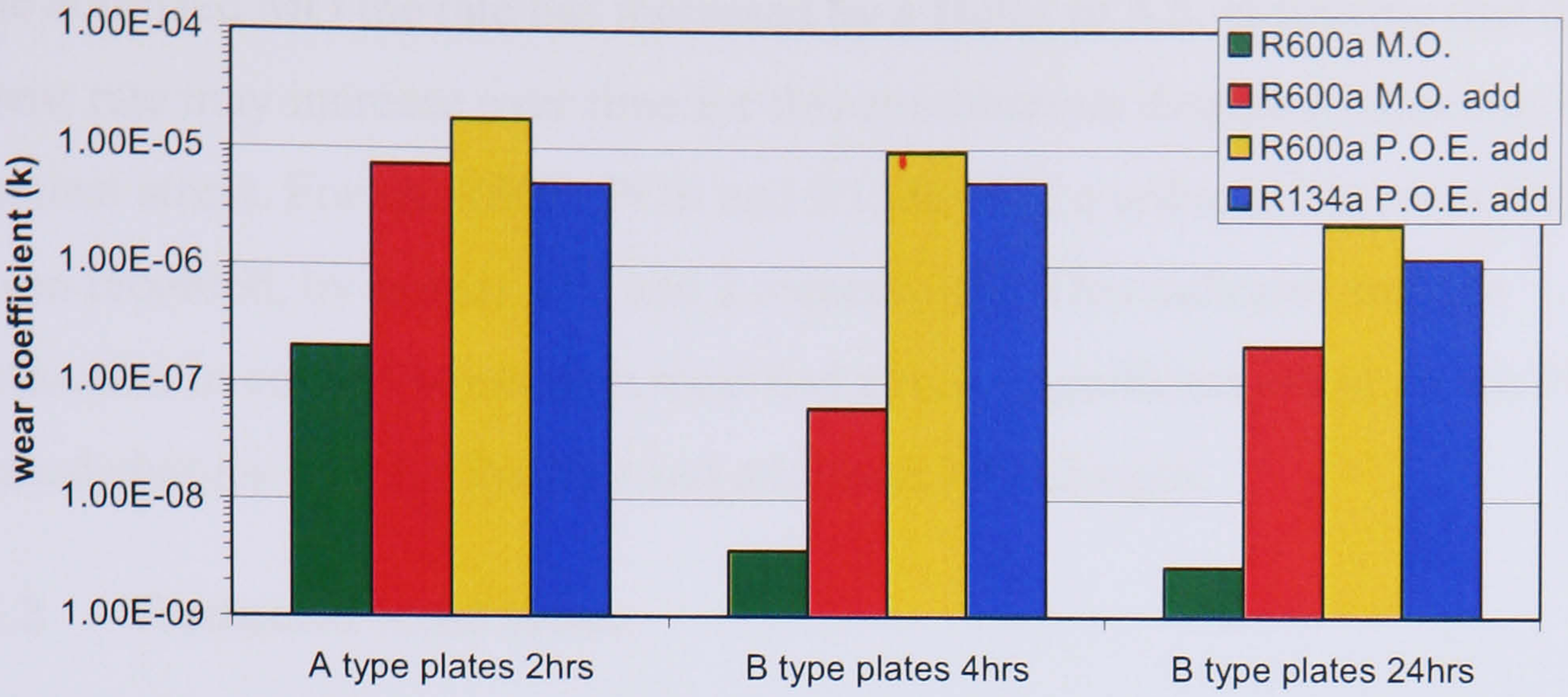

Figure 5.18 Extended in-use test, wear coefficient 86400s, 20N, B plates

This may indicate that the regime is in transition from boundary to E.H.D. lubrication as the contact area increases with sample wear. The additised MO shows a rapid decline in friction between 3600s and 7200s followed by a sustained gradual fall over the duration of the test. The individual traces (Appendix Figure D.43) show that two of three tests followed this pattern whilst one behaved in a similar manner to that of the non-additised experiments. The contact potential for this combination rose very rapidly and was sustained for the duration of the test. Both the friction and contact traces were smooth, reflecting the low wear rate for this combination. The frictional characteristics of the R600a POE test are similar in nature to those of the shorter duration test. The trace provides a significant decline of 67% over the first half, become constant but still erratic over the second half. The erratic nature of the friction trace is mirrored by the contact potential and both are a reflection of the high wear rate for this combination. The R134a POE friction trace is again very similar to that provided over the shorter duration. The erratic nature of the individual traces (Appendix Figure D.47) becomes less pronounced over the duration of the experiment indicating that the regime may be moving from transitional to E.H.D. lubrication. The contact potential trace is again rather erratic and, in combination with the friction trace, reflects the high wear rate for this combination.

Comparing the wear rates for the 86400s tests with their predecessors shows a change in wear rate for most of the charge combinations. For the MO the rate remained unchanged, indicating that the increase in contact area and subsequent reduction contact stress has had little effect on the wear regime. For

the additised MO the rate has increased by a factor of 3.5, indicating that the wear rate may increase over time for this combination despite a reduction in contact stress. For the R600a POE and R134a POE a reduction in wear rate has been recorded, by factors of 4 and 2 respectively. This indicates that the reduction in contact stress with wear had a more significant effect on the POE based charges than for the MO and additised MO charges.

5.3 Reduced load tests

The third batch of tests (tests 25-28) were carried out using in-use operating conditions as described in the preceding chapter. Due to the duration of the experiments, they were only conducted for the R600a additised MO and R134a additised POE charge combinations. For the R600a tests the pressure was set 0.78bar with the temperature at 57°C whilst for the R134a a pressure of 1.47bar and temperature of 68°C was used. The experiments were carried out over durations of 86400s and 237600s using the smoother B type plates and a test loading of 15N.

5.3.1 86400s tests

The tests were carried out as previously described and the results recorded collated and plotted to charts. The results were then averaged to provide comparisons between each charge and the 20N extended tests for both friction (Figure 5.19) and contact potential (Figure 5.20). The samples were measured after each experiment to calculate and compare the material wear coefficient (Figure 5.21).

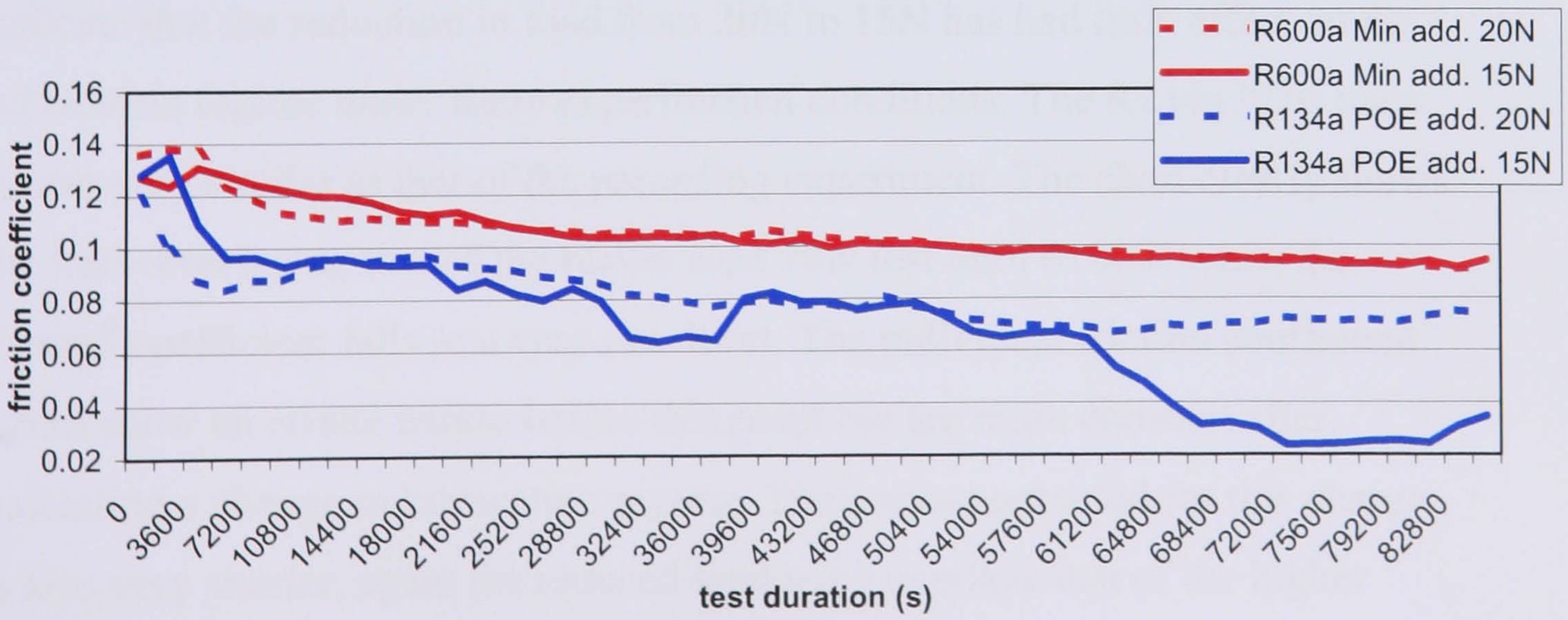

Figure 5.19 Reduced load test, friction coefficient 86400s, 15N, B plates

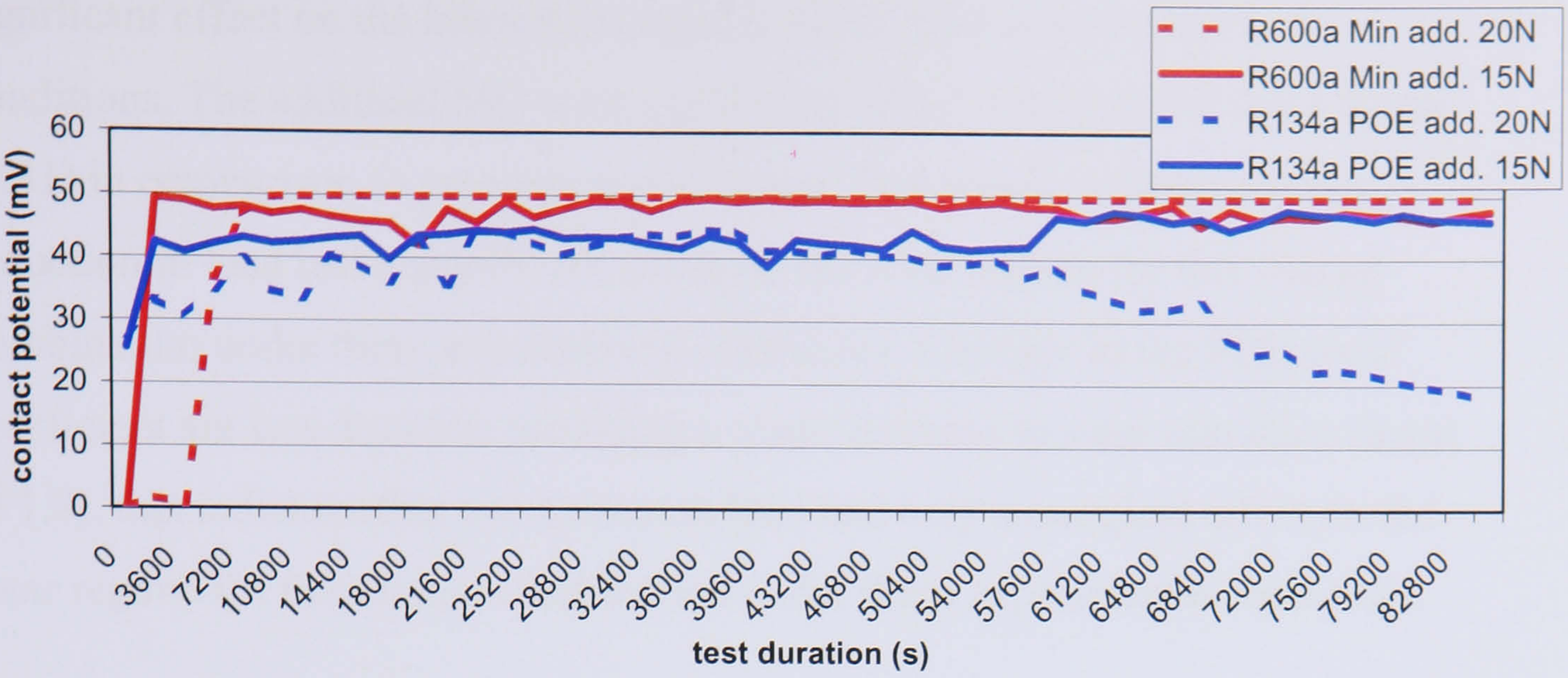

Figure 5.20 Reduced load test, contact potential 86400s, 15N, B plates

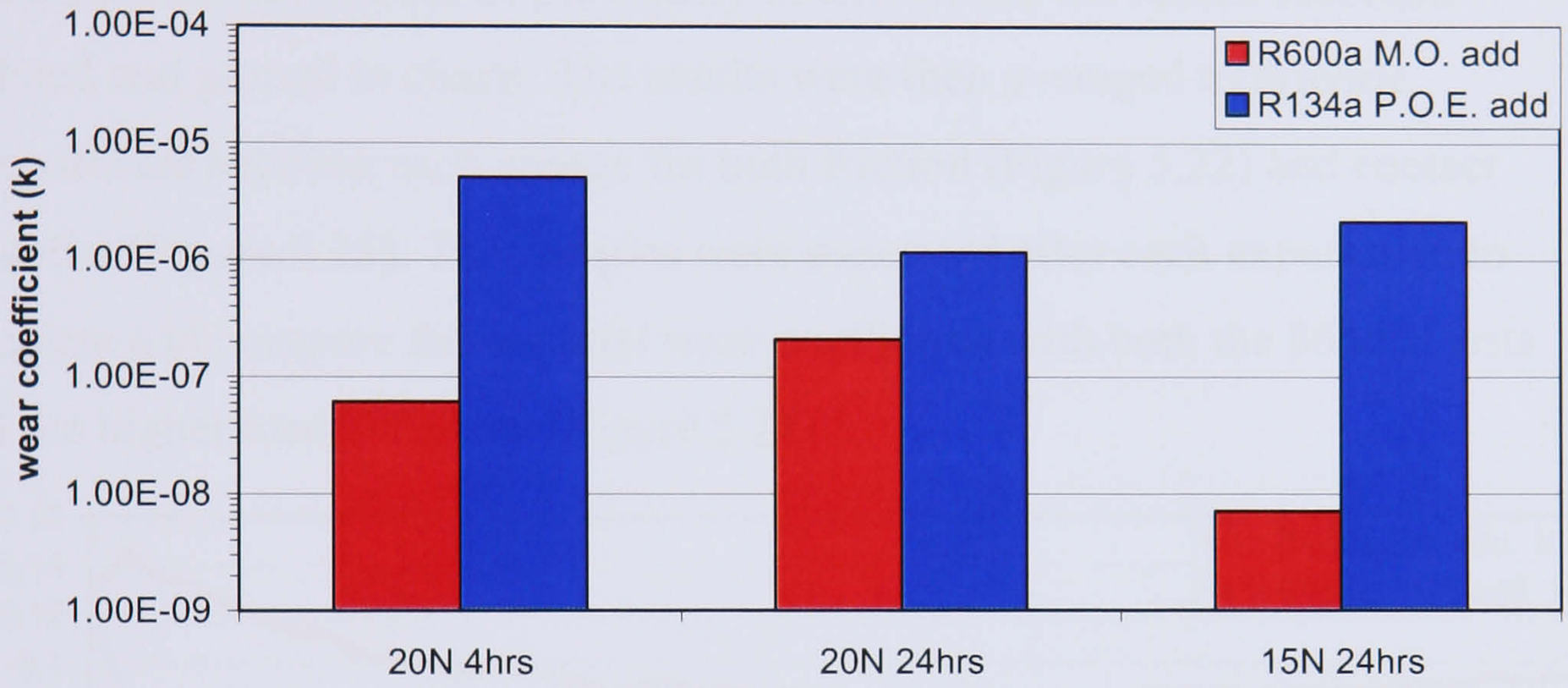

Figure 5.21 Reduced load test, wear coefficient 86400s, 15N, B plates

The R600a additised MO trace is again very similar to that of the preceding experiment. The chart clearly shows the trace overlaying that of the higher load 20N test. The contact potential for this charge is also very similar, again the reduced load trace overlays that of the higher load 20N test. This would indicate that the reduction in load from 20N to 15N has had little effect on the lubrication regime under these experimental conditions. The R134a POE trace is also very similar to that of the preceding experiment. The chart clearly shows the trace overlaying that of the higher load 20N test until 61000s when the friction coefficient falls to a very low level. The individual friction coefficient traces show an erratic nature before this point but are more constant after, indicating a change in lubrication regime. The contact potential for this charge is also very similar, again the reduced load trace overlays that of the higher load 20N test until 61000s when the contact potential rises to the maximum. This would indicate that the reduction in load from 20N to 15N has had a

significant effect on the lubrication regime under these experimental conditions. The additised MO wear coefficient shows a further fall (by a factor of 31) in comparison to previous experiments. This would indicate that the reduction in load had a significant effect on the wear regime for this charge combination under these experimental conditions. Changes to the POE wear coefficient are less dramatic recording a slight increase in wear rate (by a factor of 1.8), this indicates that a reduction in load had only a marginal effect on the wear regime for this charge combination under these experimental conditions.

5.3.2 237600s tests

The tests were carried out as previously described and the results recorded collated and plotted to charts. The results were then averaged to provide comparisons between each charge for both friction (Figure 5.22) and contact potential (Figure 5.23). The samples were measured after each experiment to calculate and compare the material wear coefficient with both the 86400s tests and the higher load 20N tests (Figure 5.24).

Figure 5.22 Reduced load test, friction coefficient 237600s, 15N, B plates

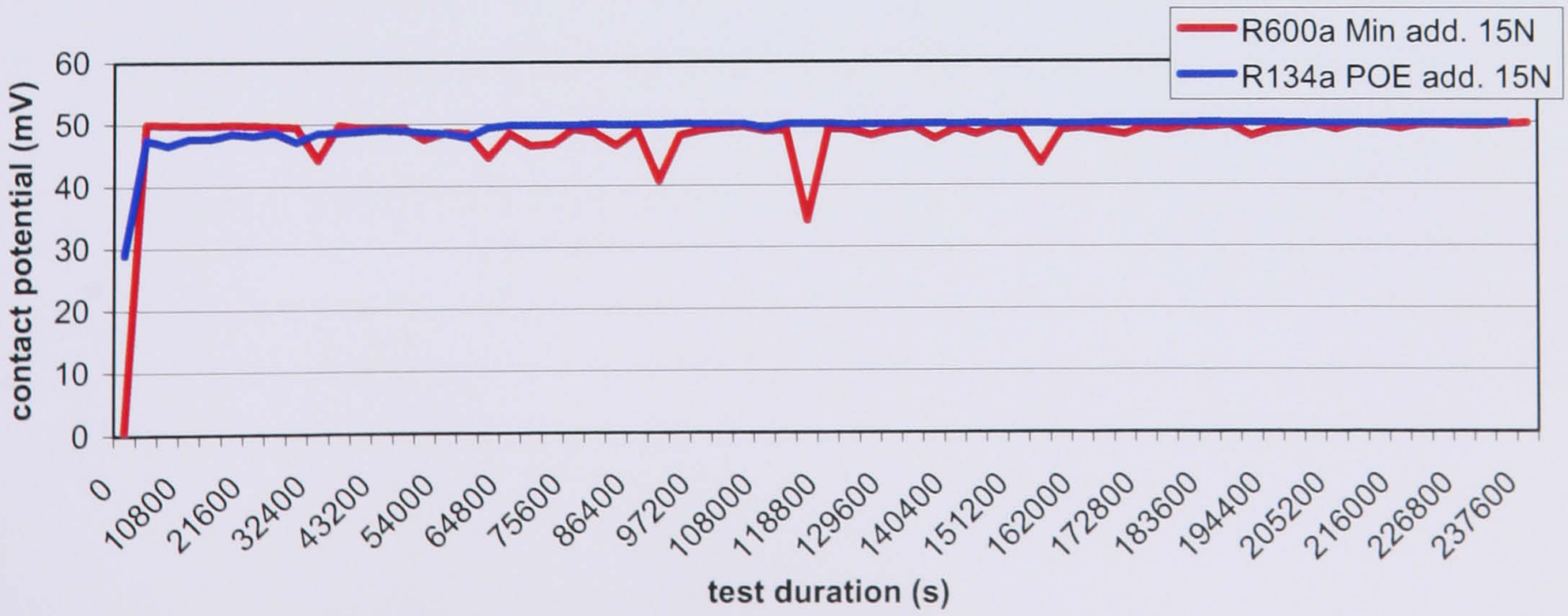

Figure 5.23 Reduced load test, contact potential 237600s, 15N, B plates

Figure 5.24 Reduced load test, wear coefficient 237600s, 15N, B plates

The R600a additised MO friction trace shows a steady continuation of the coefficient over time. This is also the case for the contact potential and indicates that the lubrication regime remains stable for this charge combination under these experimental conditions. The R134a additised POE friction trace shows the previously recorded decline to a very low coefficient continues for the duration of the test. This is also the case for the contact potential and indicates that, for the period after 61000s, the lubrication regime remains stable for this charge combination under these experimental conditions. The additised MO wear coefficient increased slightly over the longer test but only by a factor of 2.8. The reduction in recorded wear coefficient for the POE, however, may indicate that the wear regime has changed beyond 61000s.

6 Characterisation and interpretation

6.1 Post test observations

After testing the lubricant remaining in the bath was observed. In the case of experiments conducted with MO and additised MO, the lubricant remained clean, and free of significant contamination. In the case of experiments conducted using POE the lubricant was black with contamination from wear particles or reacted products. The POE pin and plate samples had also accumulated a gel type product in the areas beyond the extent of sliding contact (Figure 6.1).

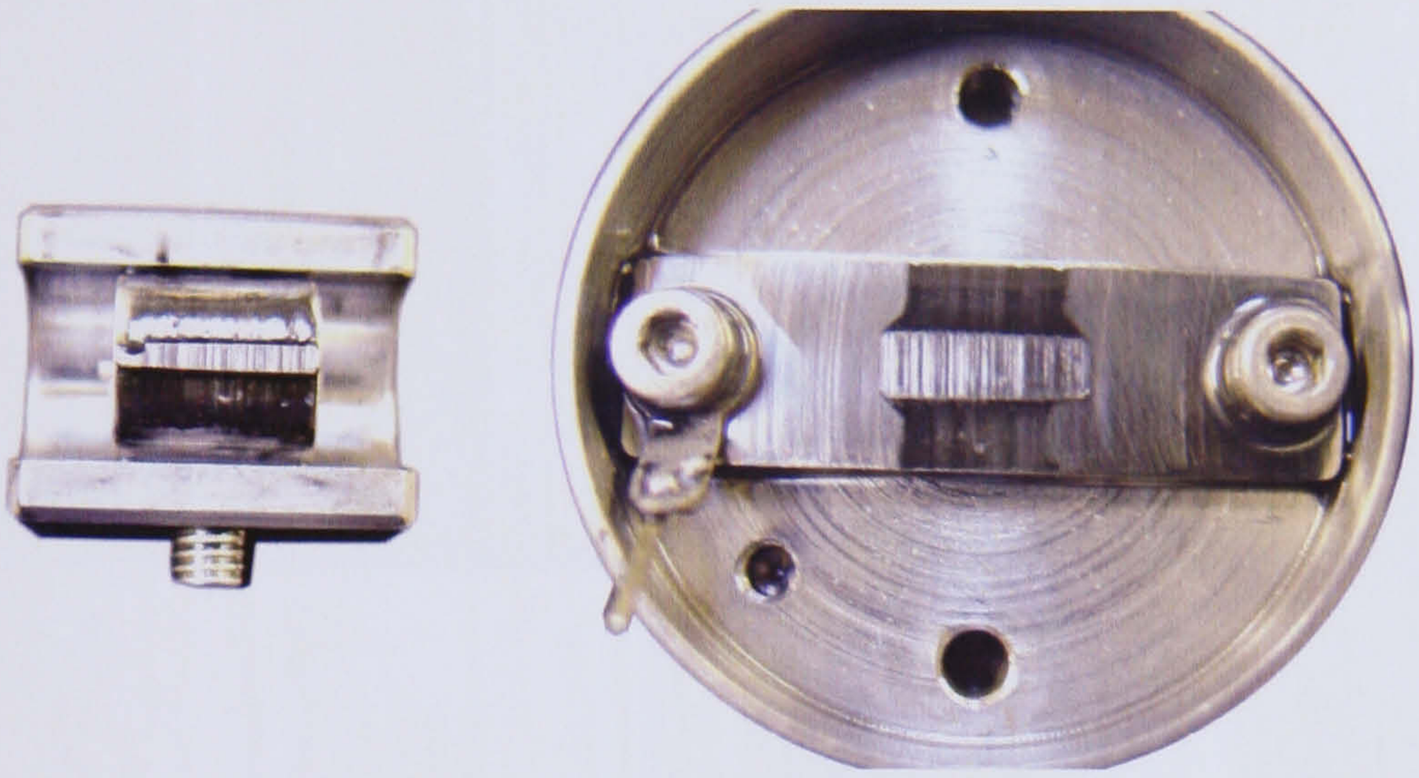

Figure 6.1 Gel type deposition, pin and plate samples

6.2 Surface characterisation

Pin and plate samples from each of the experimental configurations were cleaned in acetone using an ultrasonic bath prior to examination using an Olympus BX microscope. Images were recorded for both the pin and plate contact surfaces and collated according to experimental regime.

6.2.1 Initial experimental samples

6.2.1.1 Reduced temperature saturated test

The reduced temperature sample images are compared (Figure 6.2) and depict the surface conditions for each refrigerant/lubricant charge. The R600a MO charge appears to show material deposition on the worn surface of the pin sample. The steel plate counter-face shows no significant tribolayer but a

smearing of the surface. The smearing appears to be the flattening of high points on the ground surface. The R600a additised MO pin image depicts a tribolayer on both the pin face and (to a lesser degree) the plate. The R600a POE pin and plate samples shows much less deposition on either wearing surface. The pin sample shows no significant build up of tribolayers, whilst the plate sample have only a thin film of deposition. The lower wear rate R134a POE pin shows a more significant tribolayer build up whilst the plate surface also shows signs of a thin film deposition. The pin and plate samples for the reduced pressure start-up tests were very similar to those of the reduced temperature tests shown here.

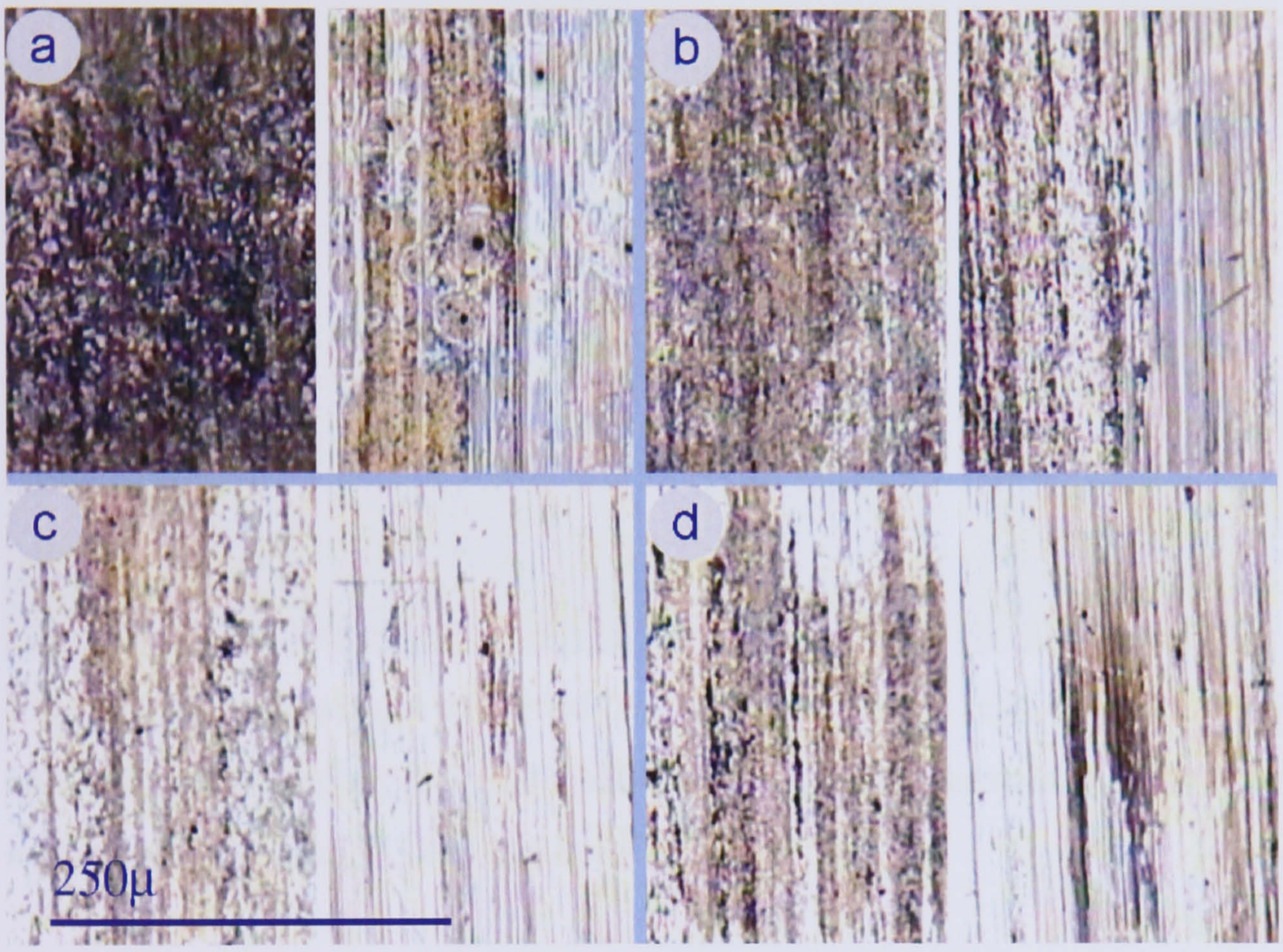

Figure 6.2 Comparison of initial test samples, saturated test. (pin left, plate right); a: R600a MO; b: R600a additised MO; c: R600a additised POE; d: R134a additised POE

6.2.1.2 In-use test

The pin and plate wear surfaces for the in-use test programme are compared (Figure 6.3) and show the surface conditions present at the contact surfaces. The lowest wear rate R600a MO again exhibit significant deposition of tribolayers on the wearing face of the pin sample. The plate, once more, shows little sign of tribolayer deposition but does show signs of surface wear. The

higher wearing R600a additised MO pin sample has a lower level of deposition at the pin but higher level at the plate than the R600a MO test samples. The R600a POE and R134a POE samples both exhibit similar surface conditions of little or no significant deposits at the pin contact but slight deposition on the worn surfaces of the plate. The pin and plate surfaces for the extreme (110°C) in-use tests were similar to those of the in-use test detailed here.

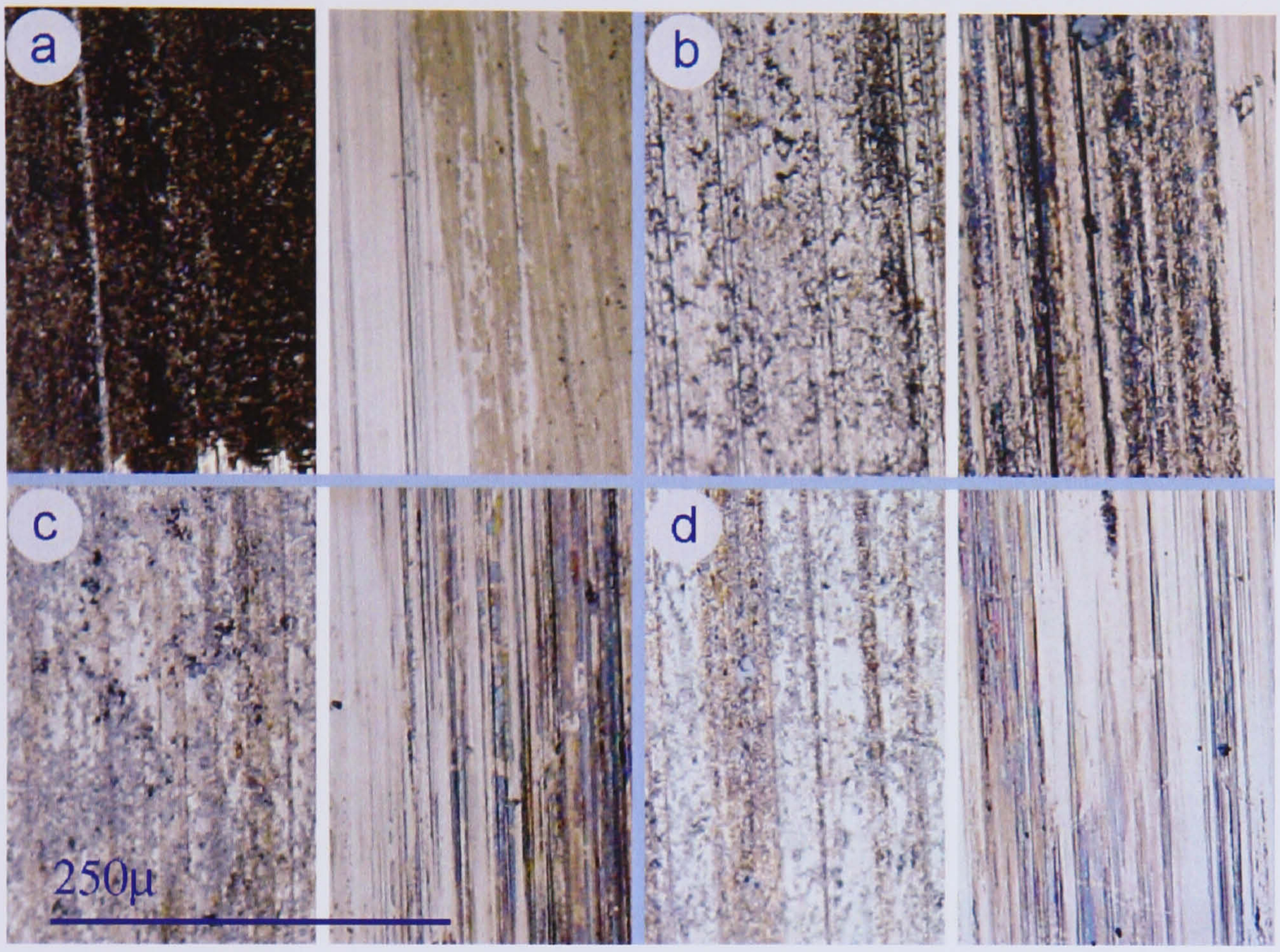

Figure 6.3 Comparison of initial test samples, in-use test.
(pin left, plate right); a: R600a MO; b: R600a additised MO; c: R600a additised POE; d: R134a additised POE

6.2.2 Extended duration tests

6.2.2.1 14400s duration tests

The 14400s tests were carried out using the smoother "B" type plates under the same conditions as the in-use tests. The pin and plate wear surfaces are compared (Figure 6.4) and show the surface conditions present at the contact surfaces. The Lowest wear rate R600a MO samples show significant tribo-layer formation at the pin wear face. The plate counter-face shows no sign of deposition but does exhibit signs of surface wear at the contact surface. The low wear rate R600a additised MO samples show tribo-layer deposition on both the worn surface of the pin sample and the plate counter-face. The higher

wear rate R600a POE pin samples exhibit no tribo-layer formation, rather the contact surface appears polished or etched. The plate counter-face, however, shows significant surface deposition. The high wear rate R134a POE shows similar surface conditions to those observed for the R600a POE at both pin and plate wear surfaces.

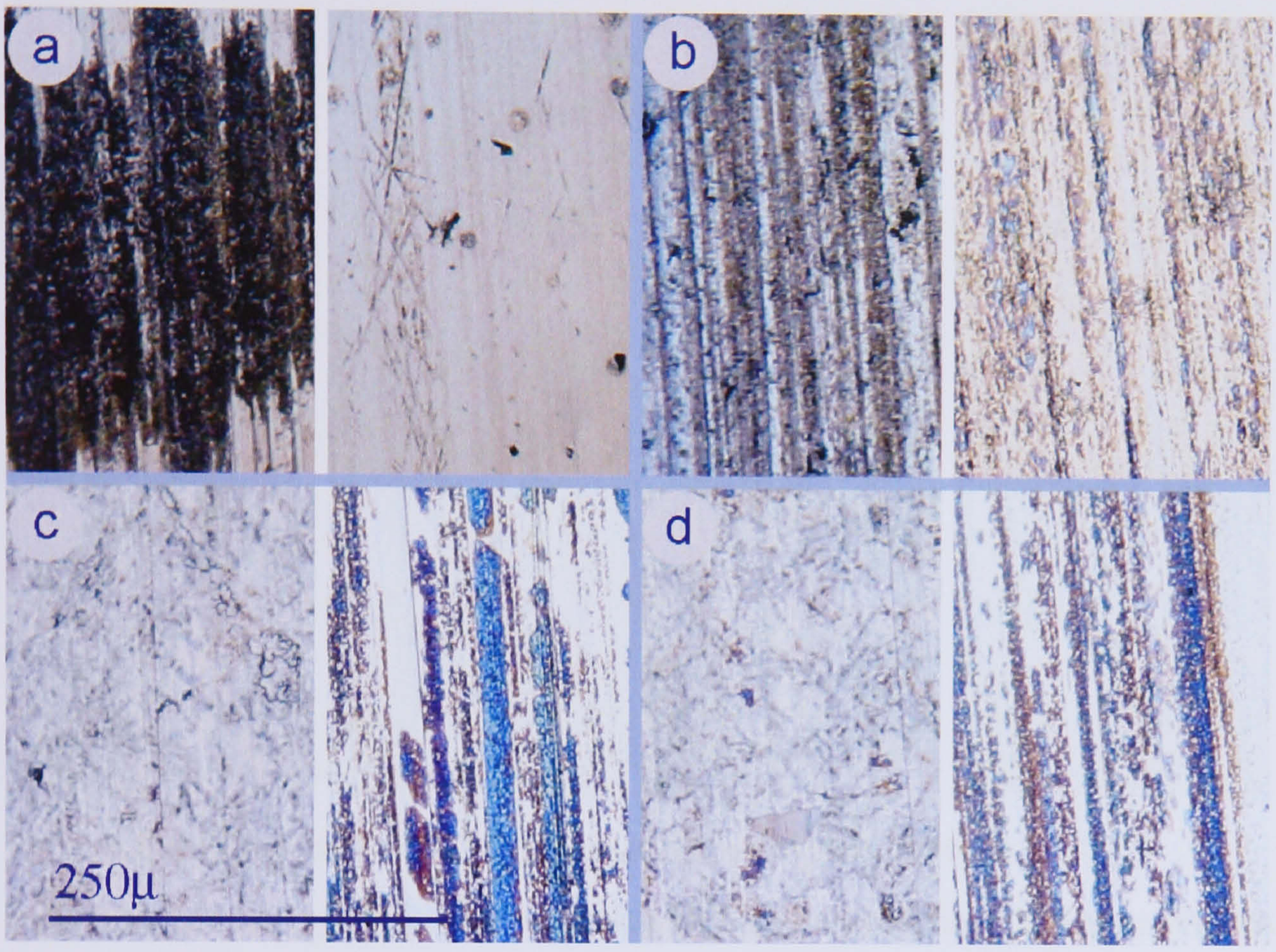

Figure 6.4 Comparison of extended test samples, 14400s tests. (pin left, plate right); a: R600a MO; b: R600a additised MO; c: R600a additised POE; d: R134a additised POE

6.2.2.2 86400s duration tests

The 86400s tests were carried out using the smoother "B" type plates under the same conditions as the in-use tests. The pin and plate wear surfaces are compared (Figure 6.5) and show the surface conditions present at the contact surfaces. The R600a MO pin sample exhibits similar tribo-layer deposition at the pin sample to that of the shorter duration 14400s test. The plate sample counter-face shows no sign of deposition but does exhibit much more significant surface wear than that found on the previous tests. The R600a additised MO pin and plate samples both show equal levels of surface deposition and are very similar to those observed for the charge combination's previous tests. Both the R600a POE and R134a POE samples show similar surface conditions. The pin wear surfaces exhibit no surface depositions but do

show signs of polishing or etching. The plate sample counter-faces have a lower level of surface deposition than the shorter duration 14400s tests. Both the pin and plate samples do, however, show signs of surface scoring.

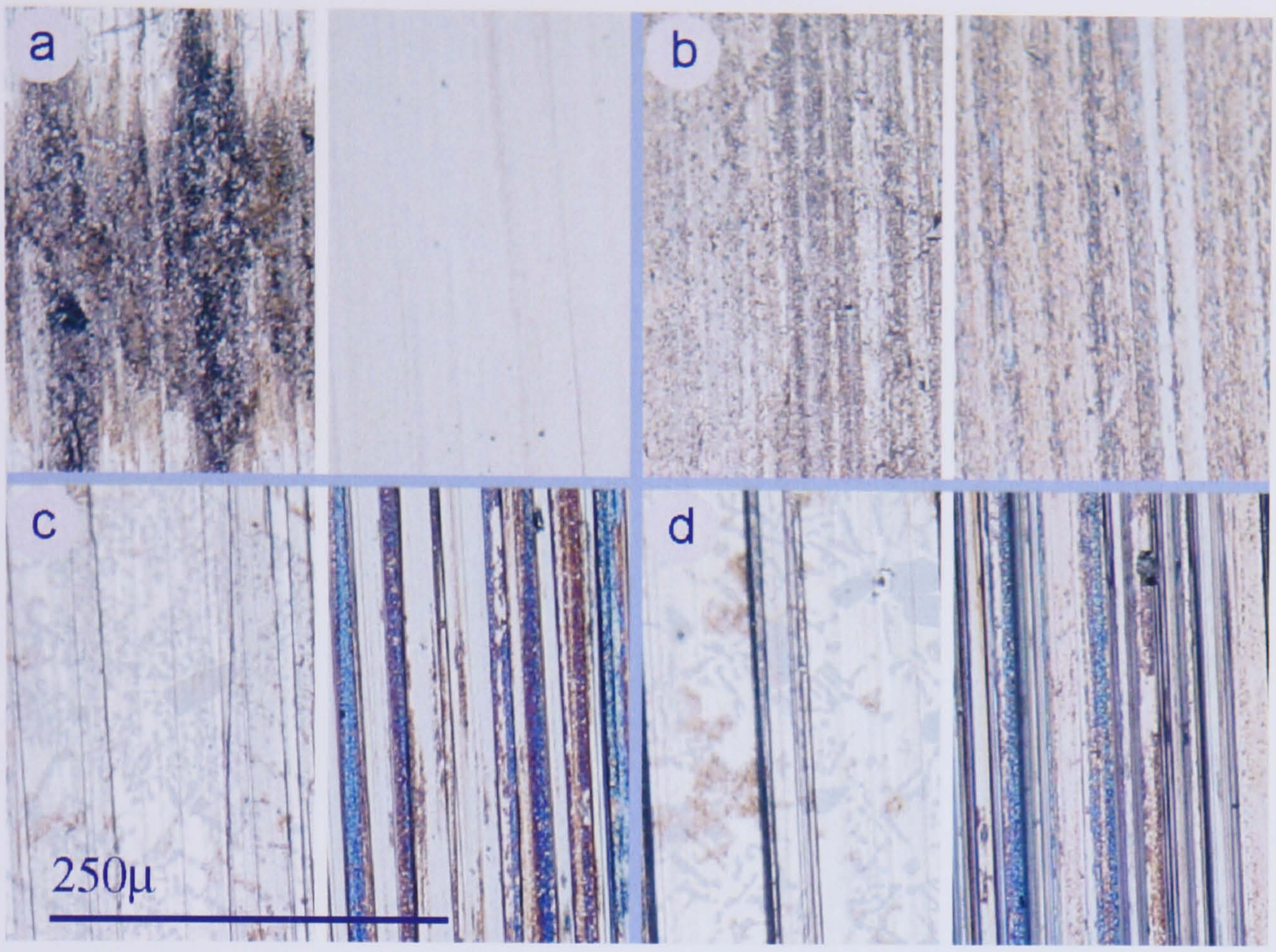

Figure 6.5 Comparison of extended test samples, 86400s tests. (pin left, plate right); a: R600a MO; b: R600a additised MO; c: R600a additised POE; d: R134a additised POE

6.2.3 Reduced load tests

6.2.3.1 86400s tests

The 86400s reduced load tests were carried out using the same "B" type plates as the extended tests and under the same conditions except for the applied load, which was reduced to 15N. The pin and plate samples are compared (Figure 6.6) and show the surface conditions present at the test conclusion. The R600a additised MO test shows heavier deposition at the pin than the equivalent 20N test. The plate counter-face exhibits less deposition than the 20N test and have visible surface wear. The surface conditions present for the pin and plate samples show more resemblance to the 20N 86400s non-additised R600a MO wear faces than those of the 20N 86400s R600a additised MO surfaces. The R134a additised POE pin and plate samples are very similar to those of the equivalent 20N test. The pin wear surface exhibits no surface deposition but

again shows signs of polishing or etching. The plate sample counter-face has a lower level of surface deposition than the equivalent 20N test and the pin and plate samples also show signs of surface scoring.

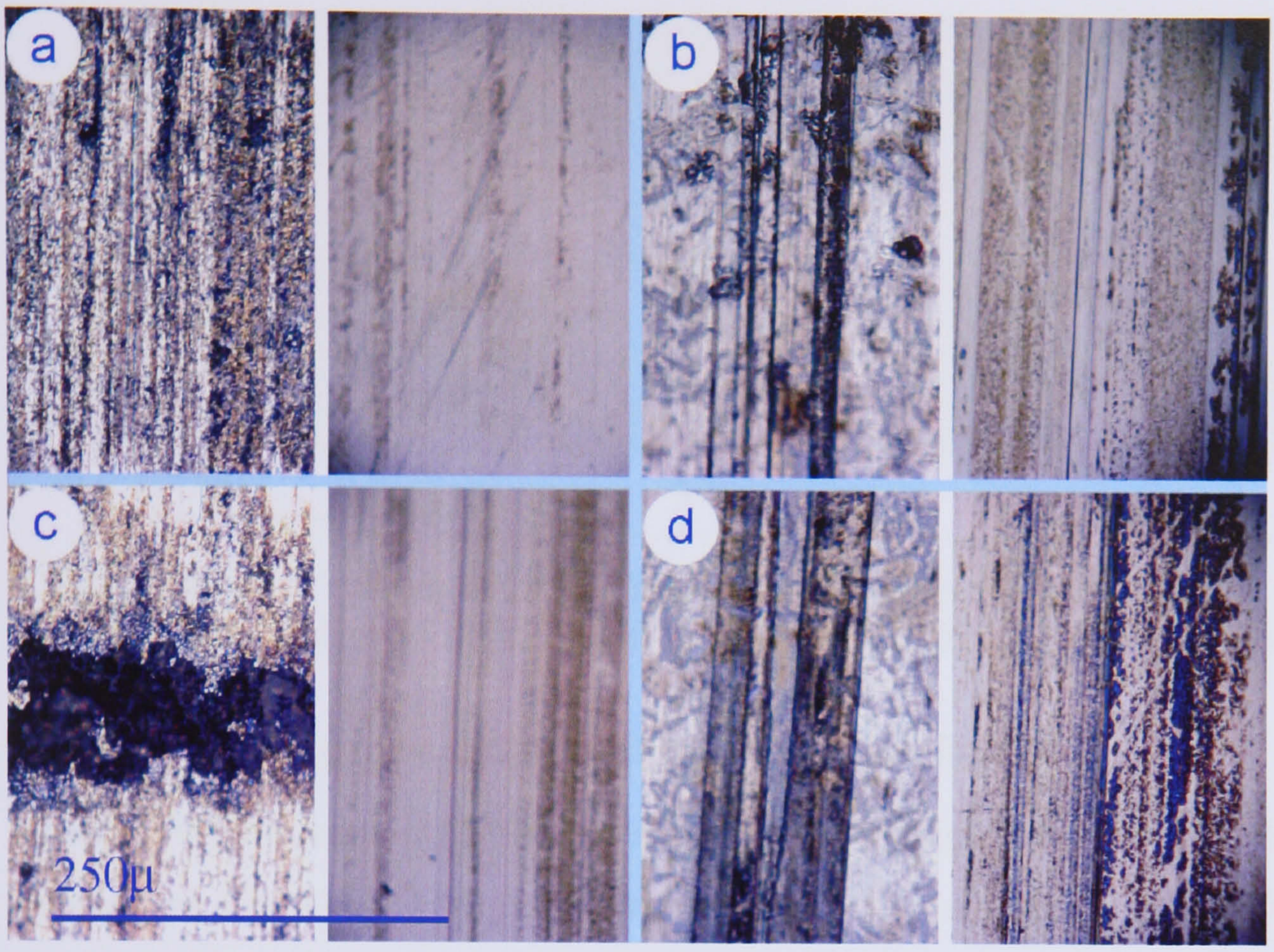

Figure 6.6 Comparison of reduced load samples, 86400s and 237600s tests. (pin left, plate right); a: R600a additised MO 86400s; b: R134a additised POE 86400s; c: R600a additised MO 237600s; d: R134a additised POE 237600s;

6.2.3.2 237600s tests

The 237600s tests were carried out under the same conditions as the 86400s tests. The pin and plate samples are compared (Figure 6.6) and show the surface conditions present at the test conclusion. The R600a additised MO test shows similar deposition at the wearing surface of the pin to that found with the 86400s test. The pin also shows a very dense band of deposition concentrated at the centre of the wear surface. The plate counter-face has some light deposition but, like the 86400s test, also shows signs of surface wear. The R134a additised POE pin and plate samples appear very similar to those of the 86400s test. The pin exhibits signs surface scoring and the plate sample a similar level of surface deposition to the 86400s test. The additised MO plate exhibits less deposition than the equivalent POE sample plate at the region adjoining the wear scar (Figure 6.7). The additised MO plate also shows much

more significant wear at the plate, demonstrated by the removal of the original cross hatching marks still present beyond the extent of the scar and still present within the POE wear scar.

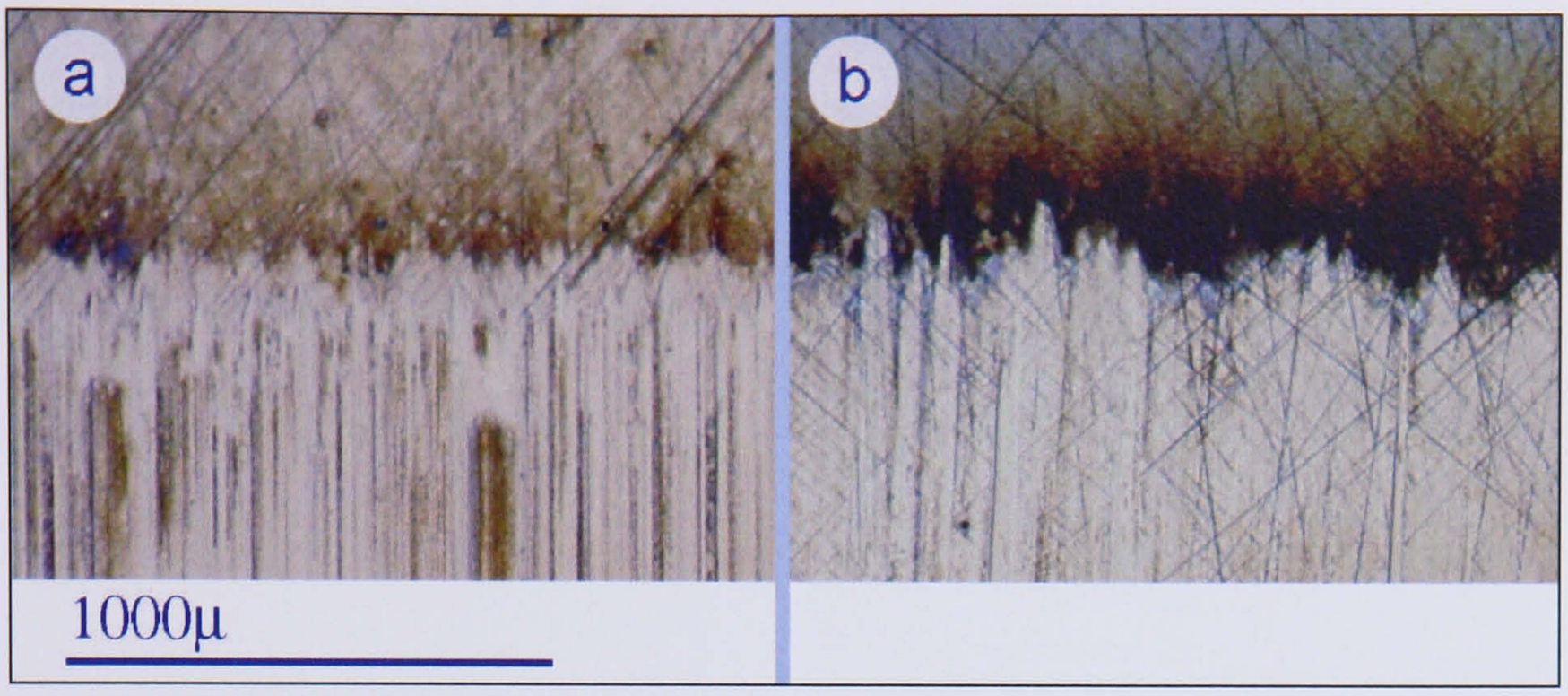

Figure 6.7 Comparison of plate samples, edge of wear scar.
a: R600a additised MO 237600s; b: R134a additised POE 237600s

6.3 Electron probe examination of wear surfaces

The 237600s test samples were subjected to examination by scanning electron microscope (SEM) and energy dispersive x-ray (EDX) using a Jeol JXA-840A electron probe micro-analyser.

6.3.1 Electron probe surface condition

The SEM images for the contact areas of the pin and plate samples (Figure 6.8) illustrate the extent of the wear area for both R600a MO and R134a POE combinations. Surface scoring is more evident on the POE pin and plate surfaces than for those of the additised MO. There also appears to be significant deposition beyond the extent of the wear scars on both POE pin and plate samples. The localised effects of wear can be illustrated by SEM (Figure 6.9) and EDX (Figure 6.10) for the central wear areas of the pin and plate samples. The wear area for the R134a POE plate sample appears to show more frequent, though shallower, surface scoring than the equivalent R600a MO plate. The images also show a degree of deposition within the wear scars, more so within those of the R134a POE plate. EDX spectra for the plates show a significant level of both aluminium and silicon, indicating material deposition from the pins to the plates. The R134a POE pin image shows a relatively smooth wear surface when compared to the R600a MO pin which has a granular surface deposition. The EDX spectra for the R600a MO pin shows a

much higher level of silicon present at the surface than might be expected from the material stock. The areas adjacent to the wear scars were also examined by SEM (Figure 6.11) and EDX (Figure 6.12).

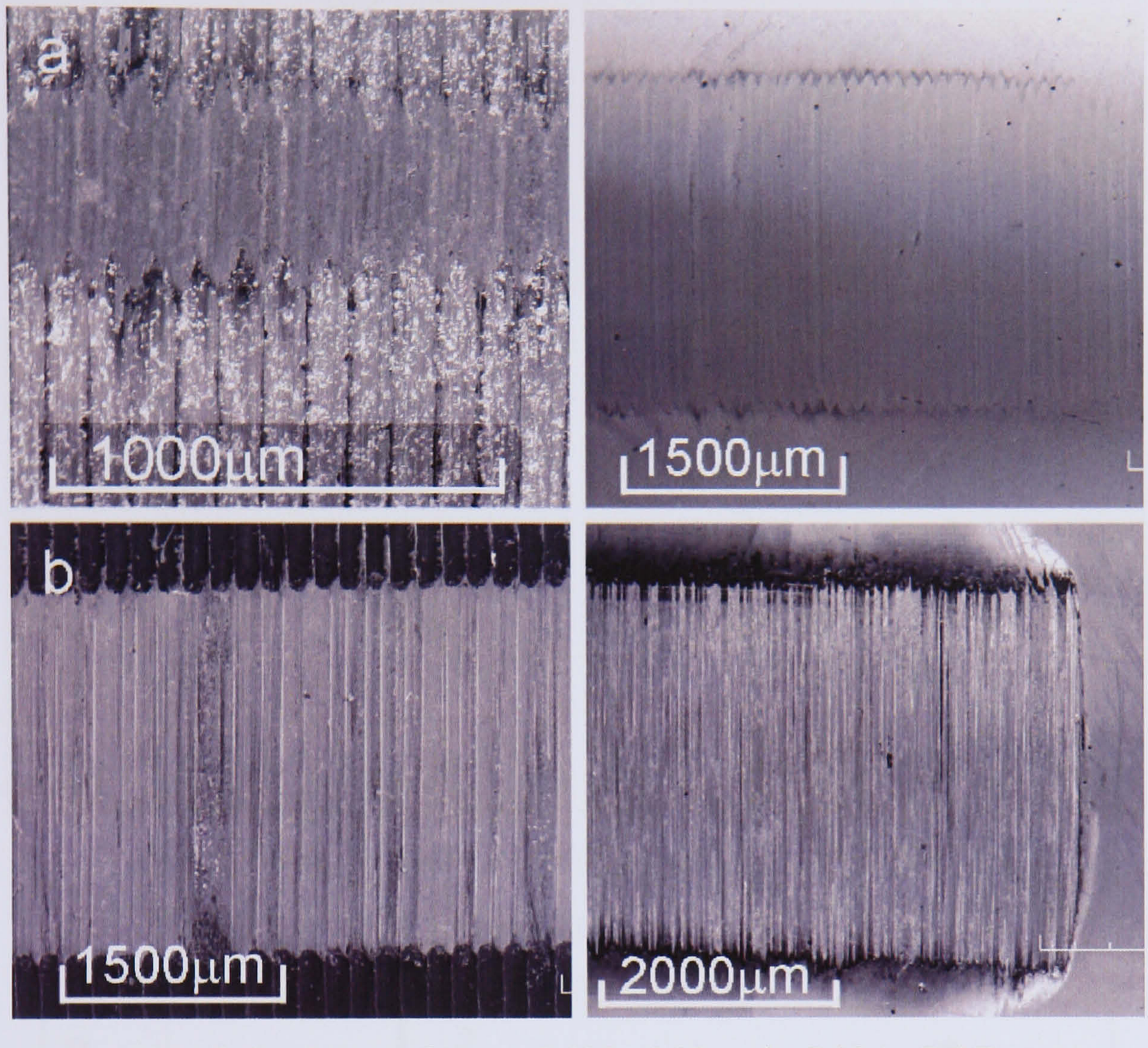

(pin left, plate right); a: R600a MO+; b: R134a POE+

Figure 6.8 SEM images of pin and plate contacts

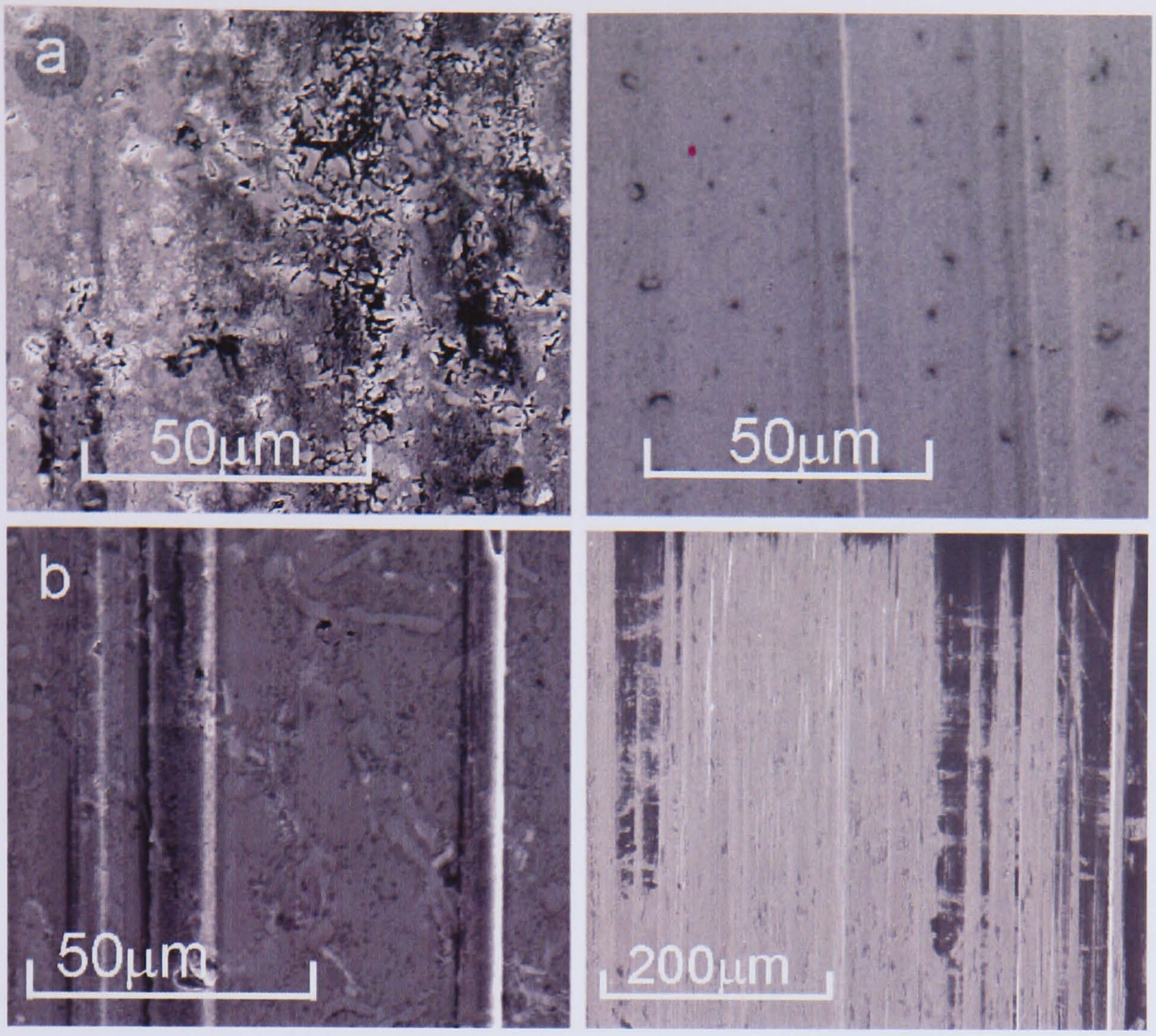

(pin left, plate right); a: R600a MO+; b: R134a POE+

Figure 6.9 SEM images of pin and plate wear areas

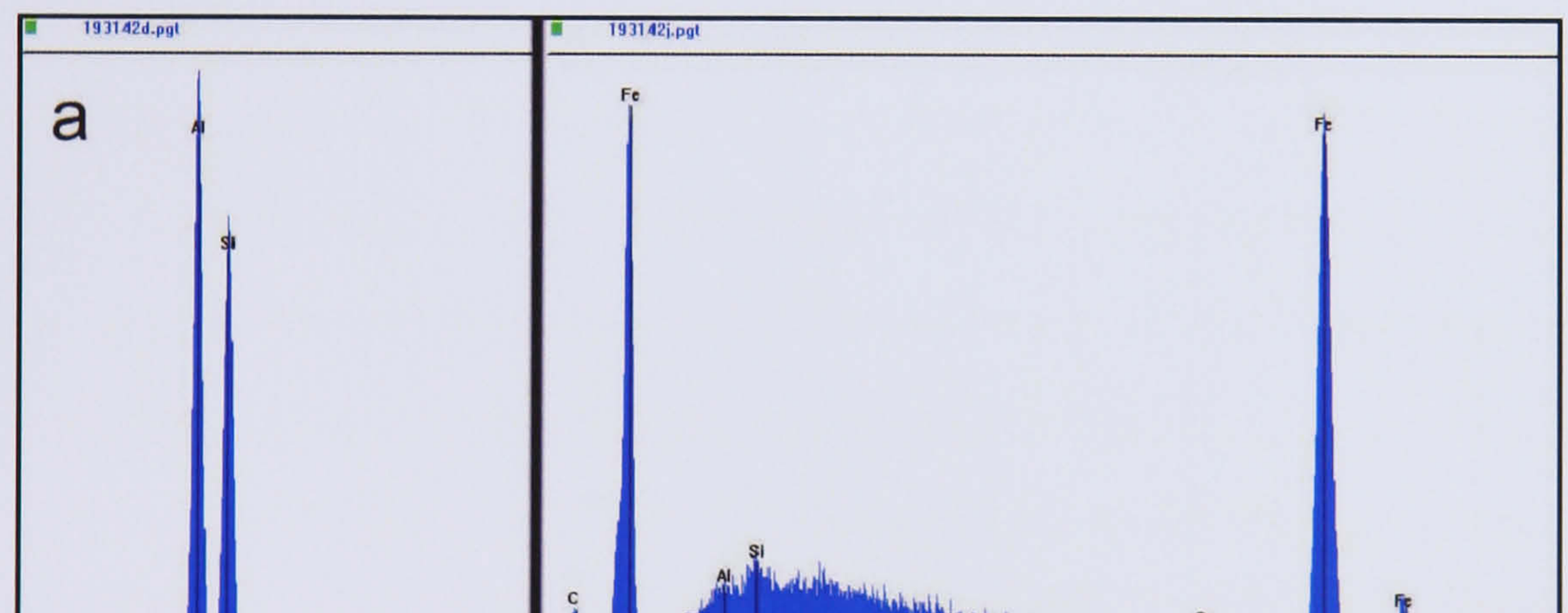

(pin left, plate right); a: R600a MO+; b: R134a POE+

Figure 6.10 EDX spectra, worn area of pin and plate samples

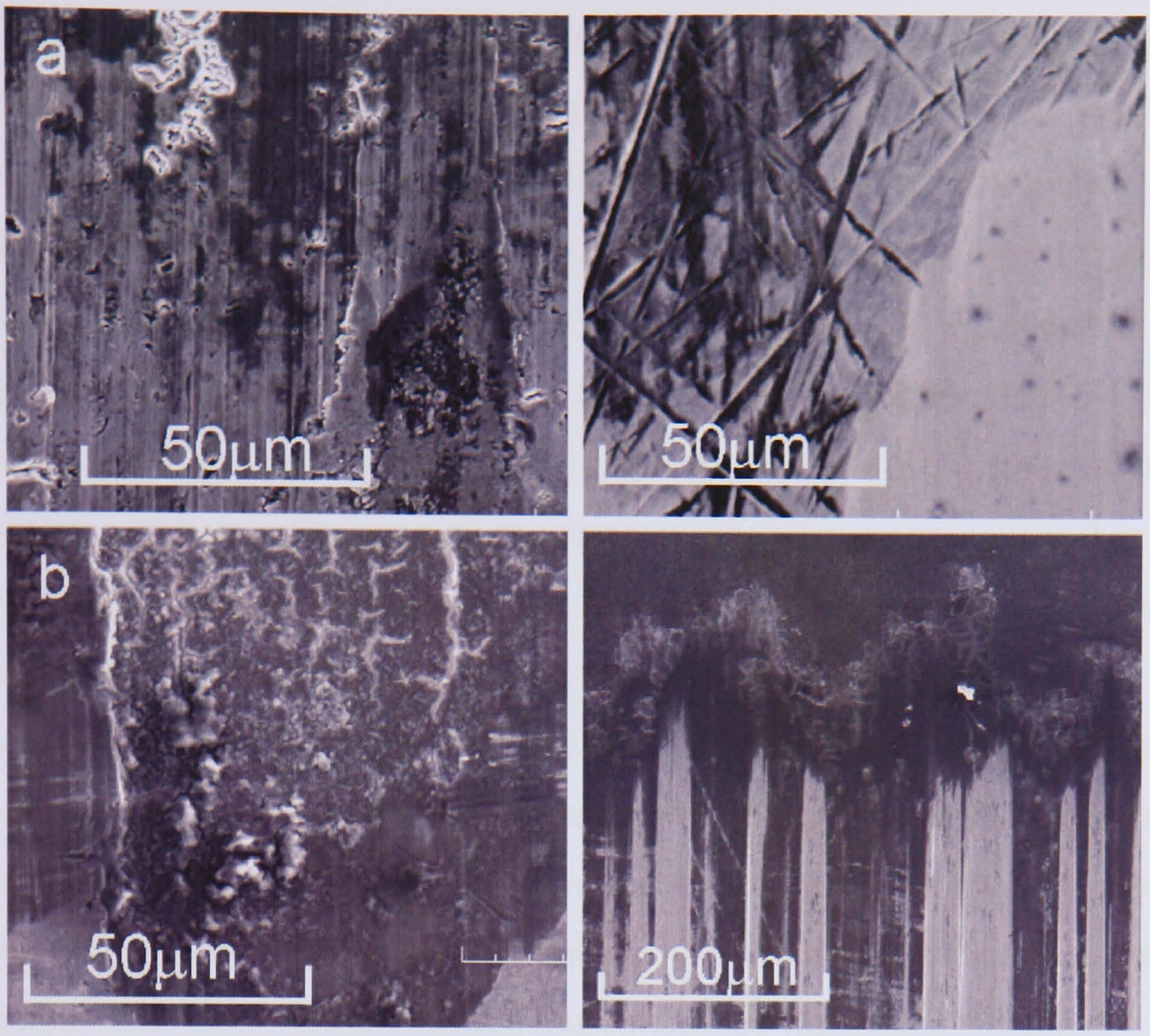

(pin left, plate right); a: R600a MO+; b: R134a POE+

Figure 6.11 SEM images, areas adjacent to wear scar

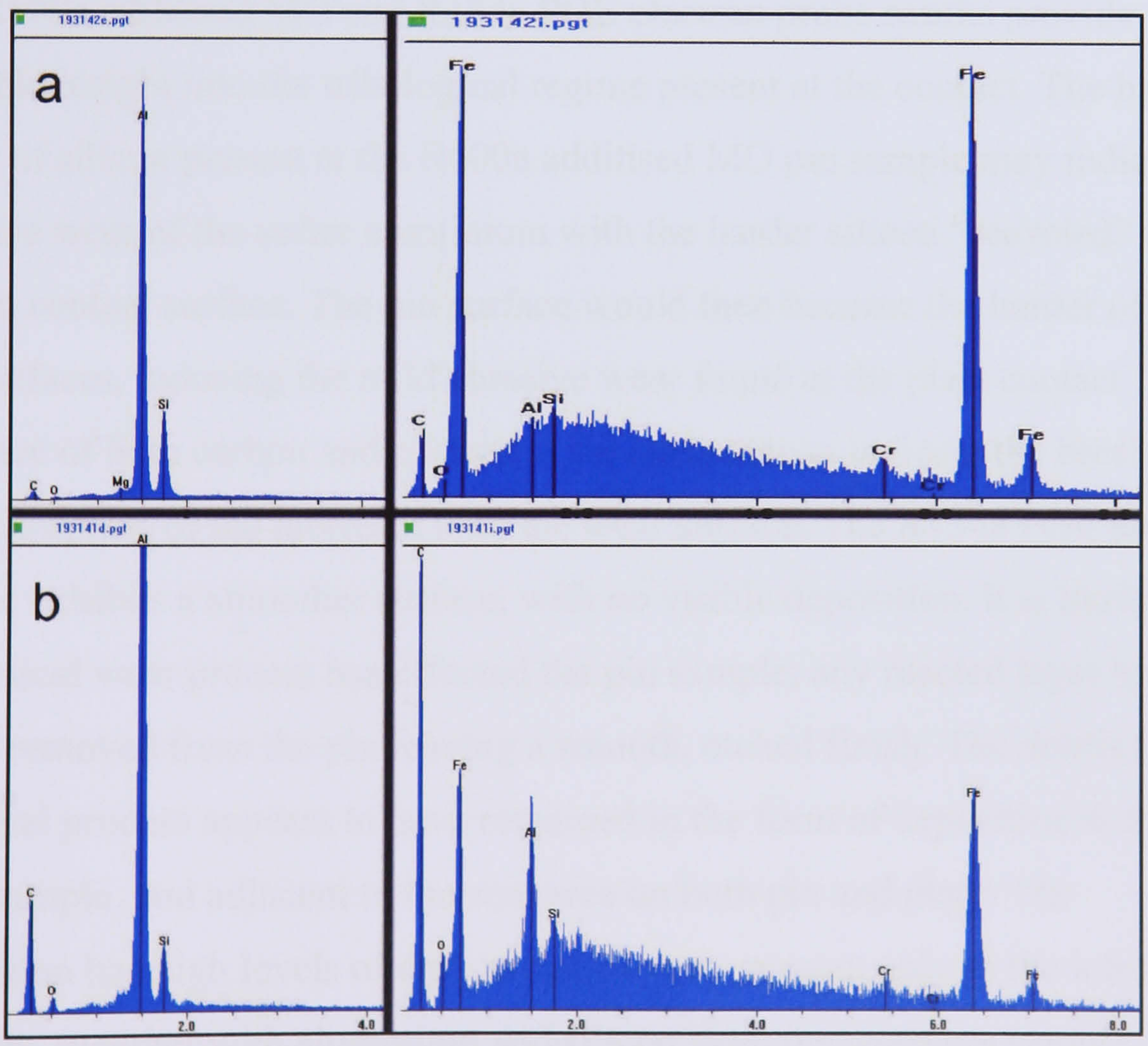

(pin left, plate right); a: R600a MO+; b: R134a POE+

Figure 6.12 EDX spectra, unworn area of pin and plate samples

The R600a MO plate sample exhibits only light deposition, primarily around the fringe of the wear scar. The wear scar itself is significantly deeper than that of the R134a POE plate, evident from the removal of the original surface hatching still present on the R134a POE plate. The R134a plate has extensive deposition both surrounding the contact and extending into it. EDX spectra for these surfaces again show the presence of aluminium and silicon material from the pin samples, however the R134a POE spectra exhibits very high levels of aluminium, carbon and oxygen on the plate surface when compared to the R600a MO plate. Both the pin samples show signs of deposition around the wear scar area although this is again more significant for the R134a POE sample. The EDX spectra show the R134a POE deposition to be elevated in carbon and oxygen compared to the substrate whilst the R600a MO pin shows lower levels of carbon and oxygen but raised levels silicon compared to the R134a POE pin. The carbon and oxygen are likely to be a result of lubricant decomposition whilst the silicon and aluminium are from the pin sample.

6.3.2 Interpretation of results from electron probe examination

The R600a additised MO and R134a POE electron probe results provide valuable insight into the tribological regime present at the contact. The higher levels of silicon present at the R600a additised MO pin sample may indicate abrasive wear of the softer aluminium with the harder silicon "recycled" into the pin contact surface. The pin surface would then become the harder of the two surfaces, inducing the mild abrasive wear found at the plate contact. The presence of both carbon and oxygen at the surface may indicate the breakdown and adsorption of the lubricant onto the wear surface. The R134a POE pin sample exhibits a smoother surface, with no visible deposition. It is likely that a chemical wear process has effected the pin sample, any reacted layer being easily removed from the pin leaving a smooth, etched finish. The debris from chemical process appears to have remained in the form of deposition at the plate sample, and adjacent to the scar area on both pin and plate. The deposition has high levels of carbon and oxygen, present only in the lubricant package, together with aluminium and silicon from the worn pin sample.

6.4 Tribological Interpretation

The tribological conditions at the wear contact can be influenced by a number of factors. The surface velocity, contact load, contact pressure, lubricant viscosity and material surface roughness all contribute to the formation of E.H.D.L. films and subsequent surface degradation through abrasive and adhesive wear mechanisms. The lubricant and its additive package may also be reactive with the material contact surfaces and contribute to increased wear through chemical wear mechanisms or, under certain conditions, reduced friction and wear through the formation of sacrificial boundary films. The introduction of the refrigerant to the package can further complicate the tribological mechanisms since it can reduce the lubricant viscosity and performance to varying degrees dependant on temperature, pressure, refrigerant type and lubricant composition.

6.4.1 Tribological results overview

To assist with the interpretation of both the experimental test machine data and the surface characterisation a table was constructed comprising the results from each charge combination over a number of key conditions (Table 6.1). The friction coefficient and contact potential values are the average for the final 10% of each experimental duration. The shorter duration pin wear volume can be subtracted from the extended duration to calculate the effective wear coefficient during the extended test period (Appendix D.4).

6.4.2 Key factors

The summary highlights a number of key factors influencing the tribological regime for each charge combination. Altering the surface finish of the plate samples from the “A” type to “B” type plates, extending the duration and reducing the load all significantly reduces affect the performance and surface conditions of the samples. The effect of these changes in operating conditions on the performance of the charge combinations can be summarised for each combination.

	Condition	In use	Extended		Reduced load	
	Experimental Duration	7200s	14400s	86400s	86400s	237600s
R600a MO	Friction coef.	0.108	0.118	0.119	-	-
	Contact potential (mV)	0.4	2.9	34	-	-
	Wear volume (mm^3)	$3.0x10^{-3}$	$1.1x10^{-4}$	$5.0x10^{-4}$	-	-
	Wear coef.	$2.0x10^{-7}$	$3.7x10^{-9}$	$2.7x10^{-9}$	-	-
	Effective wear coef.	-	-	$2.5x10^{-9}$	-	-
	Apparent contact area (mm^2)	1.6	0.4	0.8		
	Apparent Contact stress (MPa)	12.3	47	27	-	-
	Pin tribo-layer	High	High	High	-	-
	Plate tribo-layer	Low	Low	Low	-	-
R600a addit MO	Friction coef.	0.122	0.119	0.092	0.093	0.093
	Contact potential (mV)	31	41	50	47	49
	Wear volume (mm^3)	$1.1x10^{-1}$	$1.9x10^{-3}$	$3.9x10^{-2}$	$9.9x10^{-4}$	$5.9x10^{-3}$
	Wear coef.	$7.3x10^{-6}$	$6.1x10^{-8}$	$2.1x10^{-7}$	$7.1x10^{-9}$	$1.5x10^{-8}$
	Effective wear coef.	-	-	$2.4x10^{-7}$	-	$2.0x10^{-8}$
	Apparent contact area (mm^2)	8.3	1.4	6.3	1.1	2.4
	Apparent Contact stress (MPa)	2.4	14	3.8	13	6.2
	Pin tribo-layer	Medium	Medium	Medium	High	High
	Plate tribo-layer	Medium	Medium	Medium	Low	Low
R600a addit POE	Friction coef.	0.101	0.078	0.047	-	-
	Contact potential (mV)	36	45	43	-	-
	Wear volume (mm^3)	$2.8x10^{-1}$	$2.9x10^{-1}$	$4.3x10^{-1}$	-	-
	Wear coef.	$1.8x10^{-5}$	$9.5x10^{-6}$	$2.3x10^{-6}$	-	-
	Effective wear coef.	-	-	$8.4x10^{-7}$	-	-
	Apparent contact area (mm^2)	10.5	12.5	13		
	Apparent Contact stress (MPa)	1.9	1.6	1.5	-	-
	Pin tribo-layer	Low	Low	Low	-	-
	Plate tribo-layer	Medium	Medium	Medium	-	-
R134a addit POE	Friction coef.	0.098	0.081	0.073	0.03	0.018
	Contact potential (mV)	49	43	19	47	50
	Wear volume (mm^3)	$7.9x10^{-2}$	$1.6x10^{-1}$	$2.2x10^{-1}$	$3.0x10^{-1}$	$3.0x10^{-1}$
	Wear coef.	$5.1x10^{-6}$	$5.1x10^{-6}$	$1.2x10^{-6}$	$2.1x10^{-6}$	$7.9x10^{-7}$
	Effective wear coef.	-	-	$3.8x10^{-7}$	-	$1.2x10^{-8}$
	Apparent contact area (mm^2)	7.1	9.3	10.3	12.2	12.2
	Apparent Contact stress (MPa)	2.8	2.2	1.9	1.24	1.23
	Pin tribo-layer	Low	Low	Low	Low	Low
	Plate tribo-layer	Medium	Medium	Medium	Medium	Medium

Table 6.1 Tribological summary for in-use temperature range

6.4.2.1 *R600a lubricated with mineral oil*

The resultant effect of changes to the key experimental parameters of surface roughness, duration and contact load can be summarised for R600a MO test conditions (Table 6.2).

	change to test parameter	
Resultant condition	**Plate Surface Roughness**	**Extend Duration**
Friction coefficient (factor)	-1.1	0
Contact potential (factor)	+7.25	+11.7
Wear coefficient (factor)	-51	-1.4
Effective wear coefficient (factor)	-	-1.4

Table 6.2 Effect of changes to key parameters, R600a MO

Changing the surface conditions by substituting the "A" type plates for the "B" type plates significantly reduces the wear coefficient of the R600a MO charge combination but slightly increases the terminal friction coefficient. The reduction in wear rate for the "B" samples also means the terminal contact pressure is maintained. The higher contact pressure may well contribute to the higher friction coefficient, even so the coefficient only changes by a factor of 1.1 from the "A" plate samples. The reduction in wear coefficient in response to surface condition is much more dramatic and indicates that, for this combination, abrasive wear is the dominant regime. The effective wear rate also reduces over the extended duration test, though not significantly. This charge combination also differs from the other combinations by having significant tribo-layer build up at the pin but very little at the plate sample. This Tribo-layer appears to protect the softer pin material from abrasive wear at the contact with the harder plate sample but contributes to visible wear at the plate sample.

6.4.2.2 *R600a lubricated with additised MO*

The resultant effect of changes to the key experimental parameters of surface roughness, duration and contact load can be summarised for R600a additised MO test conditions (Table 6.3). Changing the surface conditions by replacing the "A" type plates with the "B" type plates significantly reduces the wear coefficient of the R600a additised MO charge combination but has a neglible effect on the terminal friction coefficient.

	Test parameter changed			
Resultant condition	**Plate Surface Roughness**	**Extend Duration**	**Reduce Load**	**Extend Duration**
Friction coef. (factor)	0	-1.3	0	0
Contact potential (factor)	+1.3	+1.25	0	0
Wear coef. (factor)	-120	+3.4	-30	+2.1
Effective wear coef. (factor)	-	+3.9	-	+2.8

Table 6.3 Effect of changes to key parameters, R600a additised MO

The change in surface roughness reduced the wear by a factor of 120, a greater reduction than recorded for the R600a non-additised MO combination. The reduction in load from 20N to 15N also effects the wear coefficient, resulting in a reduction by a factor of 30. The influence of both load and surface finish indicates that for this combination, abrasive wear is dominant. The effective extended wear coefficient shows an increase, however, by a factor of 3.9, indicating that the wear rate increases over the duration of the experiment. The surface observations show the presence of tribo-layers at both the pin and plate counter-faces, the latter causing wear at the pin sample whilst protecting the plate from wear. SEM and EDX examination of the surfaces (6.3) has shown the pin deposition to be higher in silicon than the base material stock, indicating adhesive wear of the softer aluminium material whilst recycling the silicon back into the contact. The plate sample shows deposition of aluminium and silicon from the pin sample. Since the only difference between this combination and the R600a MO is the presence of the additive package, the additive package has induced the material transfer to the plate.

6.4.2.3 R600a lubricated with additised POE

The effect of changes to the key experimental parameters of surface roughness, duration and contact load can be summarised for R600a additised POE test conditions (Table 6.4). Changing the surface conditions by replacing the "A" type plates with the "B" type plates reduces the wear coefficient and terminal friction coefficient of the R600a additised POE charge combination. The change in surface roughness has only a small effect on the wear coefficient, reducing the wear by a factor of 1.9, a much smaller reduction than recorded for either of the MO combinations.

	Test parameter changed	
Resultant condition	**Plate Surface Roughness**	**Extend Duration**
Friction coefficient (factor)	-1.3	-1.7
Contact potential (factor)	+1.25	0
Wear coefficient (factor)	-1.9	-4.1
Effective wear coefficient (factor)	-	-11.3

Table 6.4 Effect of changes to key parameters, R600a additised POE

The reduction in surface is therefore much less significant for wear with this charge combination, and abrasive wear is therefore unlikely to be the dominant regime. The reduction in friction coefficient is significant, however, recording reductions by a factor of 1.3 for the change in surface roughness and by a factor of 1.7 for the extended test. The effective extended wear coefficient also shows a very significant reduction by a factor of 11.3, indicating that the wear rate decreases over the duration of the test. The surface observations typically show the pin surface polished or etched, with tribo-layers present only at the plate. These factors would indicate that for this charge combination chemical wear is dominant.

6.4.2.4 R134a lubricated with additised POE

The effect of changes to the key experimental parameters of surface roughness, duration and contact load can be summarised for R134a additised POE test conditions (Table 6.5). Changing the surface conditions by replacing the "A" type plates with the "B" type plates reduces the wear coefficient and terminal friction coefficient of the R134a additised POE charge combination.

	Test parameter changed			
Resultant condition	**Plate Surface Roughness**	**Extend Duration**	**Reduce Load**	**Extend Duration**
Friction coef. (factor)	-1.1	-1.24	-2.4	-1.7
Contact potential (factor)	0	-2.5	+2.5	0
Wear coef. (factor)	0	-4.3	+1.8	-2.7
Effective wear coef. (factor)	-	-13.4	-	-116

Table 6.5 Effect of changes to key parameters, R134a additised POE

The change in surface roughness has no effect on the wear coefficient unlike the reductions recorded for either of the MO combinations but similar in nature to that recorded for the R600a POE experiments. The reduction in surface is therefore much less significant for wear with this charge combination, and abrasive wear is therefore unlikely to be the dominant regime. The reduction in friction coefficient is also less significant for the change in surface roughness, recording reduction by a factor of 1.1, than for the extended test, recording a further reduction by a factor of 1.24. The effective extended wear coefficient also shows a reduction by a factor of 4.3, indicating that the wear rate decreases gradually over the duration of the test. The reduction in load from 20N to 15N has a much more significant effect on the friction coefficient, recording a reduction by a factor of 2.4 and, extending the test, by a further factor of 1.7. Although the reduction in load indicates an increase in wear coefficient over the 20N tests, the extended duration wear records a significant reduction, the effective wear rate reducing by a factor of 116. The reduction in wear rate accompanies the reduction in friction coefficient as the contact area increases. The contact stress can be used indicate the maximum stress for the low friction low wear rate regime. For this charge combination the maximum stress is 1.23MPa. The surface observations typically show the pin surface polished or etched, with tribo-layers present at the plate. The SEM and EDX examination (6.3) reveals a smooth, etched pin surface with deposition at the plate sample. The EDX reveals the debris composition to be high in carbon and oxygen, likely to be the result of decomposition of the lubricant package. These factors would indicate that for this charge combination chemical wear is dominant.

6.4.3 Effective wear and friction coefficients

The MO combinations appear to operate under a conventional boundary lubrication regime whilst for the POE combinations chemical wear may be the dominant regime (Table 6.6). For the MO charges, the friction and wear rates stay relatively constant throughout the duration of the tests. For the POE charges, the friction and wear rates decline over time (in line with apparent contact stress) until a low wear rate, low friction regime is established at a lower apparent contact stress.

Charge condition	Apparent contact stress (MPa)	Friction coefficient (μ)	Wear coefficient (k)
R600a MO, 20N, 86400s	25	0.12	$2.5x10^{-9}$
R600a additised MO, 20N, 86400s	3.8	0.092	$2.4x10^{-7}$
R600a additised MO, 15N, 237600s	6.2	0.093	$2.0x10^{-8}$
R600a POE, 20N, 14400s	1.6	0.078	$9.5x10^{-6}$
R600a POE, 20N, 86400s	1.5	0.047	$8.4x10^{-7}$
R134a POE, 20N, 86400s	1.9	0.073	$3.8x10^{-7}$
R134a POE, 15N, 237600s	1.23	0.018	$1.2x10^{-8}$

Table 6.6 Effective friction and wear coefficients

The apparent contact stress is calculated from the apparent (measured) contact area rather than the real area of contact described previously (Equation 1.4). The apparent contact stress can also be compared to the real contact stress (Equation 6.1).

$$P_r = \frac{W}{A_r}$$

$$\because A_r = \frac{W}{Y_s}$$

$$\therefore P_r = Y_s$$

Equation 6.1 Real contact stress

where: P_r = real contact stress (Pa); W = contact load; A_r = real area of contact; Y_s = material yield strength of the softer material.

dividing the real contact stress by the apparent contact stress provides a ratio of real to apparent contact area (Equation 6.2).

$$Q_r = \frac{P_r}{P_a}$$

$$\therefore Q_r = \frac{A_r}{A_a}$$

Equation 6.2 Real contact stress ratio

where: Q_r = real contact stress ratio; P_a = apparent contact stress (Pa); A_a = apparent area of contact (m^2).

When the real contact stress ratio approaches unity, the real contact area will be large and most of the apparent contact area will be under stress. Under these conditions the opportunity for film re-growth will be limited, therefore wear rates may be high. A lower ratio provides for a reduced contact duration at any site, hence promote film re-growth under chemically active regimes. For the effective wear coefficients described previously, the real contact stress ratio can be calculated (Table 6.7).

Charge condition	**P_a**	**Q_r**	**Friction (μ)**	**Wear (k)**
R600a MO, 20N, 86400s	25	$1.9x10^{-2}$	0.12	$2.5x10^{-9}$
R600a additised MO, 20N, 86400s	3.8	$2.9x10^{-3}$	0.092	$2.4x10^{-7}$
R600a additised MO, 15N, 237600s	6.2	$4.7x10^{-3}$	0.093	$2.0x10^{-8}$
R600a POE, 20N, 14400s	1.6	$1.2x10^{-3}$	0.078	$9.5x10^{-6}$
R600a POE, 20N, 86400s	1.5	$1.1x10^{-3}$	0.047	$8.4x10^{-7}$
R134a POE, 20N, 86400s	1.9	$1.5x10^{-3}$	0.073	$3.8x10^{-7}$
R134a POE, 15N, 237600s	1.23	$9.4x10^{-4}$	0.018	$1.2x10^{-8}$

Table 6.7 Real contact stress ratios

For POE lubricant charges, chemical wear is suspected to be the dominant regime. For these combinations a transition to a low wear, low friction regime occurs as the real contact stress ratio falls below $1x10^{-3}$.

6.5 Tribological effects on the actual compressor

The effective friction and wear data (Table 6.6) can be transposed into the model for the actual compressors. For the R134a compressor the higher friction and wear rates can be used to simulate conditions prior to the reduction in contact stress and subsequent lower friction and wear rates. The increased contact area will also influence the EHD film forming capability of the bearing, the film thickness increasing as the contact area increases. For the R600a compressor the additised MO rates are used to simulate the operational scenario. The additised MO rates can be taken from the higher 20N load to simulate the initial contact conditions until wear reduces the contact stress to a threshold level of 3.8 MPa.

6.5.1 R600a additised MO compressor

6.5.1.1 Effect of wear coefficient on compressor performance

For the R600a additised MO compressor, the initial contact conditions (Table 6.8) of change in performance and contact stress threshold are used to calculate wear. Subsequently, the revised wear conditions are used to calculate compressor performance and longevity.

	Initial	Threshold	Max wear
Contact load, max (N)	175	175	175
Contact load, average (N)	49.6	49.6	49.6
Contact width (m)	0.0095	0.0095	0.0095
Contact length (m)	0.000785	0.00137	0.0096
Contact stress, max (MPa)	23.5	13.4	1.92
Contact stress, average (MPa)	10.9	3.8	0.55
Boundary condition range (λ<1)	74°-108°	86°-96°	89°-91°
Mixed lubrication range (λ<3)	0°-360°	72°-110°	88°-92°
Contact stress, boundary, max (MPa)	10.8	3.8	0.54
Contact stress, max (MPa)	23.5	3.8	0.54

Table 6.8 R600a additised MO gudgeon pin contact geometry during use

For an unworn compressor, the small end contact width can be calculated as previously described (Equation 2.2). However, wear at the small end bush increases the contact width, therefore the contact stress will reduce until the contact width is equal to the gudgeon pin diameter (Figure 6.13) where b is the contact width. The primary contact regime changes from mixed lubrication, when the compressor is new and unworn, to elasto-hydrodynamic for a compressor with reduced contact stress (Figure 6.14). The region of mixed mode lubrication is restricted to 72°-110°, whilst the boundary condition is reduced to a much narrower band of 86°-96°. The maximum contact stress within these bands is similar to the average for the full cycle. The volume and depth of material removed to reach the threshold contact stress can be calculated using simple equations (Equation 6.3, Equation 6.4). For this charge combination, the variable is contact length and the depth and volume of material removed is shown in table format (Table 6.9). The point in time at which the required volume is removed can be calculated using the wear equation described previously (Equation 2.8).

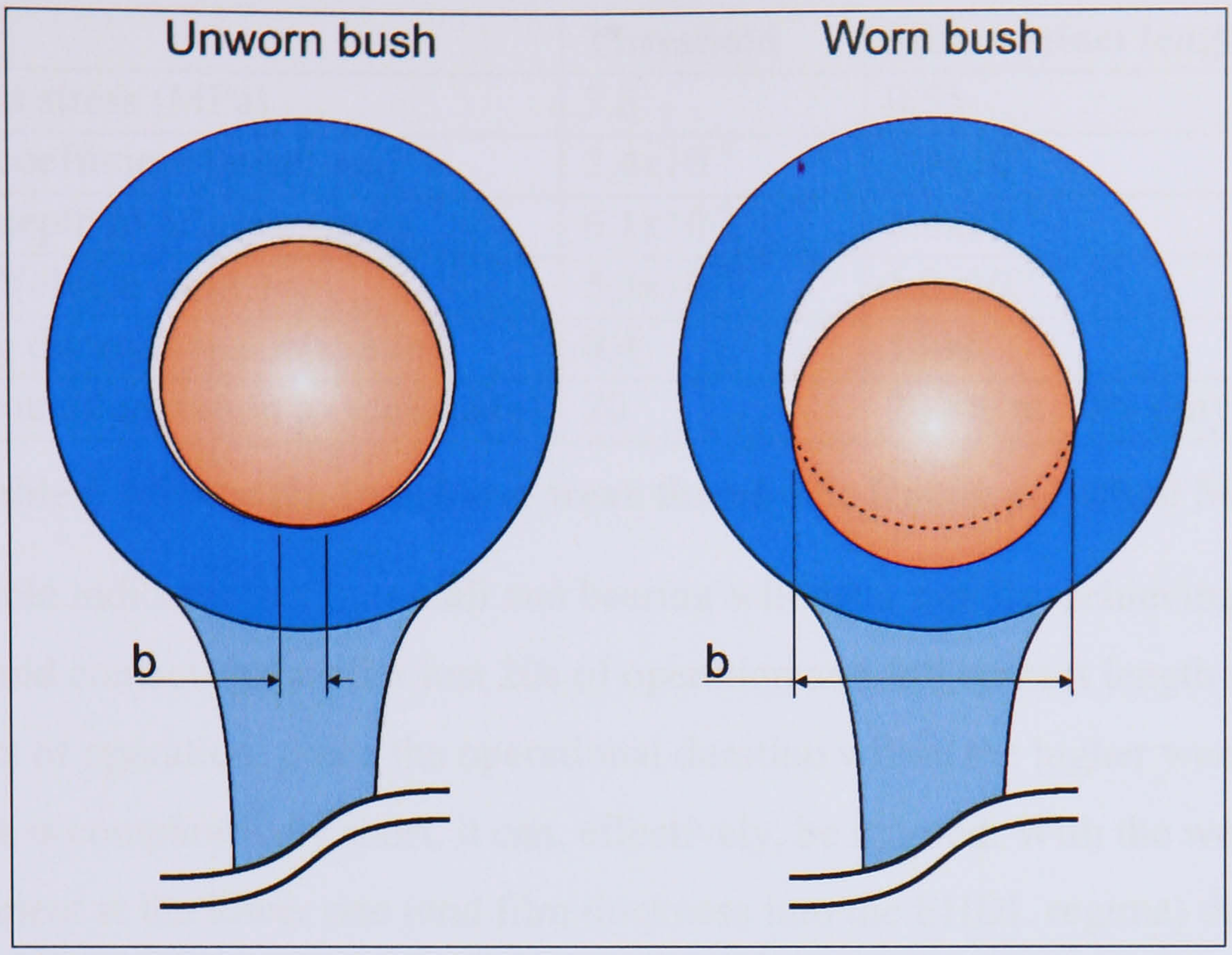

Figure 6.13 Small end bush contact width

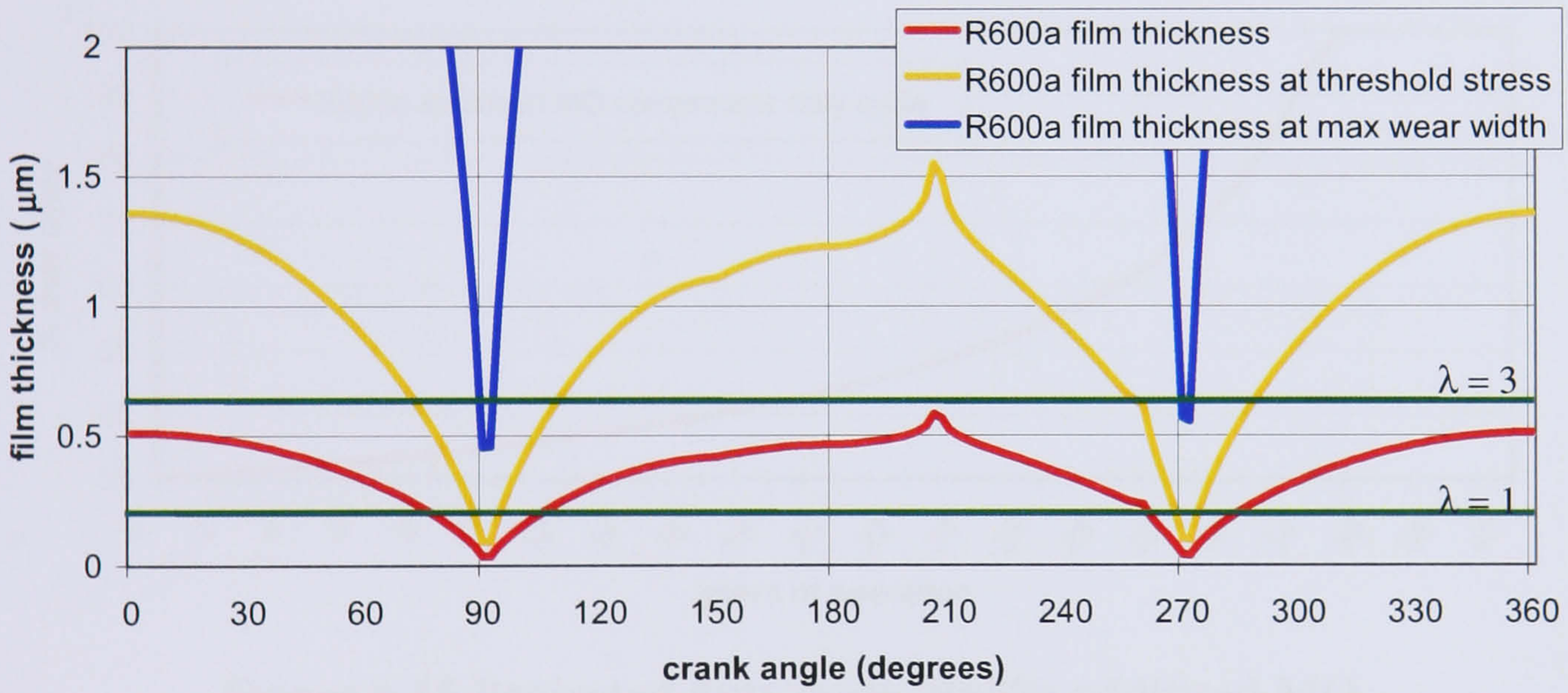

Figure 6.14 Film thickness relative to small end wear, R600a additised MO

$$V_r = \frac{b l_b^{\,3}}{12}\left(\frac{1}{R_1} - \frac{1}{R_2}\right)$$

Equation 6.3 Volume of material removed from small end bush

$$h = \frac{l_b^{\,2}}{8}\left(\frac{1}{R_1} - \frac{1}{R_2}\right)$$

Equation 6.4 Depth of material removed from small end bush

Where: V_r = volume removed (m^3); h = depth of material removed (m); b = contact width (m); l_b = contact length (m); R_1 = gudgeon pin radius (m); R_2 = small end radius (m).

	Threshold	Max contact length
Contact stress (MPa)	3.8	0.55
Wear coefficient (mm/N/m)	$2.4x10^{-7}$	$2.0x10^{-8}$
Wear depth to achieve (mm)	$6.1x10^{-4}$	$3.0x10^{-2}$
Wear Volume (mm^3)	$5.3x10^{-6}$	$1.8x10^{-3}$
Sliding distance to achieve (m)	0.4	1300
Duration of operation to achieve (s)	20	20000 at 30% duty

Table 6.9 Duration to achieve wear thresholds R600a additised MO

The table indicates that the small end bearing will wear rapidly, achieving the threshold contact stress after just 20s of operation and full contact length within $5^1/_2$ hrs of operation. Since the operational duration within the higher wear rate regime is comparatively short, it can, effectively, be ignored. With the wear coefficient at the lower rate (and film thickness into the EHDL regime) the longevity can be plotted to a chart (Figure 6.15) as previously described (2.6.3).

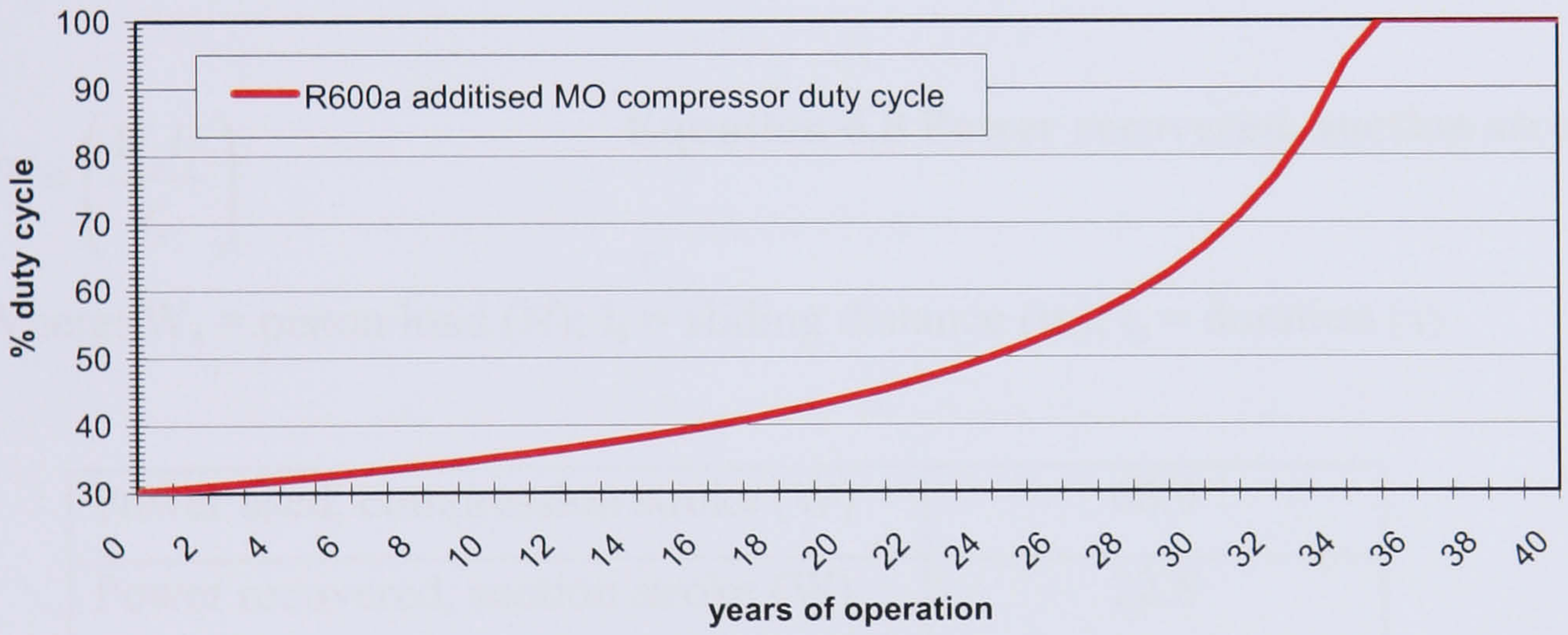

Figure 6.15 Projected duty cycle, R600a additised MO

The expected useable life of the compressor (duty cycle below 50%) operating under these conditions is 24 years. More significantly, the duty cycle at the end of the refrigerators expected life of 15years is 38.7%.

The power consumption for the compressor when new is 100W and can be divided into useful power, used in the pumping operation of the compressor, and dissipated power, lost through friction and heat (Equation 6.5) (Table 6.10).

$$P_t = P_u + P_d$$

Equation 6.5 Compressor power consumption

where: P_t = total power (W); P_u = useful power (W); P_d = dissipated power (W).

Consumption of useful power will always be the same, since the duty cycle is extended to discharge the same refrigerant volume. The dissipated power will, however, increase inline with the duty cycle, as the energy lost is relative to the operational duration. Useful power by the compressor can be calculated (Equation 6.6) from energy required to compress and discharge the refrigerant (Equation 6.7) and energy recovered from the suction cycle (Equation 6.8).

$$P_u = P_c - P_s$$

Equation 6.6 Compressor useful power

Where: P_c = power used during compression stroke (W); P_s = power recovered during suction stroke (W).

$$P_c = \left(\frac{W_c l_c}{t_c} \right)$$

Equation 6.7 Power used, compression stroke

Where: W_c = piston load (N); l_c = sliding distance (m); t_c = duration (s)

$$P_s = \left(\frac{W_s l_s}{t_s} \right)$$

Equation 6.8 Power recovered, suction stroke

Where: W_s = piston load (N); l_s = sliding distance (m); t_s = duration (s)

Power used, compression stroke (W)	66.9
Power recovered, suction stroke (W)	22.8
Useful power (W)	44.1
Total power when new, (W)	100
Power dissipated, (W)	55.9

Table 6.10 Useful and dissipated power, R600a additised MO

The change in duty cycle over time can be used to project energy consumption over the useful life of the compressor (Table 6.11). For the compressor consuming 100W of power during operation the annual consumption would be 263kWh, rising to 301kWh by year 15. The total energy consumption over this lifetime would be 4200kWh compared to 3942kWh if no wear took place at the gudgeon pin/small end bearing. 258 kWh of energy loss is therefore attributable to wear at the bearing. Extending the operational lifetime of the

compressor to 25 years would result in a significant rise in the duty cycle, hence energy consumption. Annual energy consumption would increase to 360 kWh, a rise of 38% over consumption when new.

	Year 0	Year 15	Year 25
Duty cycle (%)	30	38.7	50
Useful energy consumption (kWh)	116	116	116
Dissipated energy consumption	147	186	244
Annual energy consumption (kWh)	263	301	360
Lifetime energy consumption (kWh)	-	4200	7497
Lifetime energy (no wear) (kWh)	-	3942	6570
Energy lost due to wear (kWh)	-	258	927

Table 6.11 Duty cycle and energy consumption, R600a additised MO

6.5.1.2 Effect of friction coefficient on compressor performance

Frictional losses within the compressor can be attributed to the piston on cylinder bore, gudgeon pin/small end bush, the crank pin/big end bearing and the crankshaft main bearings. Since the big end and main bearings are journal bearings with higher surface velocities and larger contact geometries they operate under hydrodynamic conditions. frictional losses are a function of the lubricant viscosity, since no surface contact is expected during normal operation. For the piston and bore sealing between the surfaces is through the lubricant, not piston rings, therefore contact is limited. The gudgeon pin/small end bearing is the only bearing within the compressor where surface contact occurs during normal operation, therefore energy loss through friction can be calculated from piston load, duration and distance slid (Table 6.12). From the table it is clear that the energy lost due to friction at the gudgeon pin/small end bearing, whilst significant, is much less than that attributable to wear. The energy lost energy over the lifetime of the compressor being 44kWh compared with 301kWh due to wear at the bearing contact.

	R600a additised MO
Load at small end bearing (N)	49.6
Friction coefficient	0.093
Friction force (N)	4.61
Distance slid per second (m)	0.217
Energy lost (kWh) over 15 years	44

Table 6.12 Energy lost due to friction, R600a additised MO

6.5.2 R134a additised POE compressor

6.5.2.1 Effect of wear coefficient on compressor performance

For the R134a additised POE compressor, the initial contact conditions (Table 6.13) of change in performance and contact stress threshold are used to calculate wear. Subsequently, the revised wear conditions are used to calculate compressor performance and longevity. As with the R600a compressors, wear at the small end bearing increases the contact length, the stress value will continue to fall until the contact width length is equal to the gudgeon pin diameter. Again, the primary contact regime changes from mixed lubrication, when the compressor is new and unworn, to elasto-hydrodynamic for a compressor with reduced contact stress (Figure 6.16).

	Initial	Threshold	Max wear
Contact load, max (N)	278	278	278
Contact load, average (N)	63.5	63.5	63.5
Contact width (m)	0.0074	0.0074	0.0074
Contact length (m)	0.000935	0.00684	0.008
Contact stress, max (MPa)	40	5.47	4.67
Contact stress, average (MPa)	15.75	1.25	1.07
Boundary condition range (λ<1)	68°-116°	89°-91°	89°-91°
Mixed lubrication range (λ<3)	0°-360°	86°-96°	86°-96°
Contact stress, boundary, max (MPa)	18.3	1.14	0.97
Contact stress, mixed, max (MPa)	40	5.47	4.67

Table 6.13 R134a additised POE gudgeon pin contact geometry during use

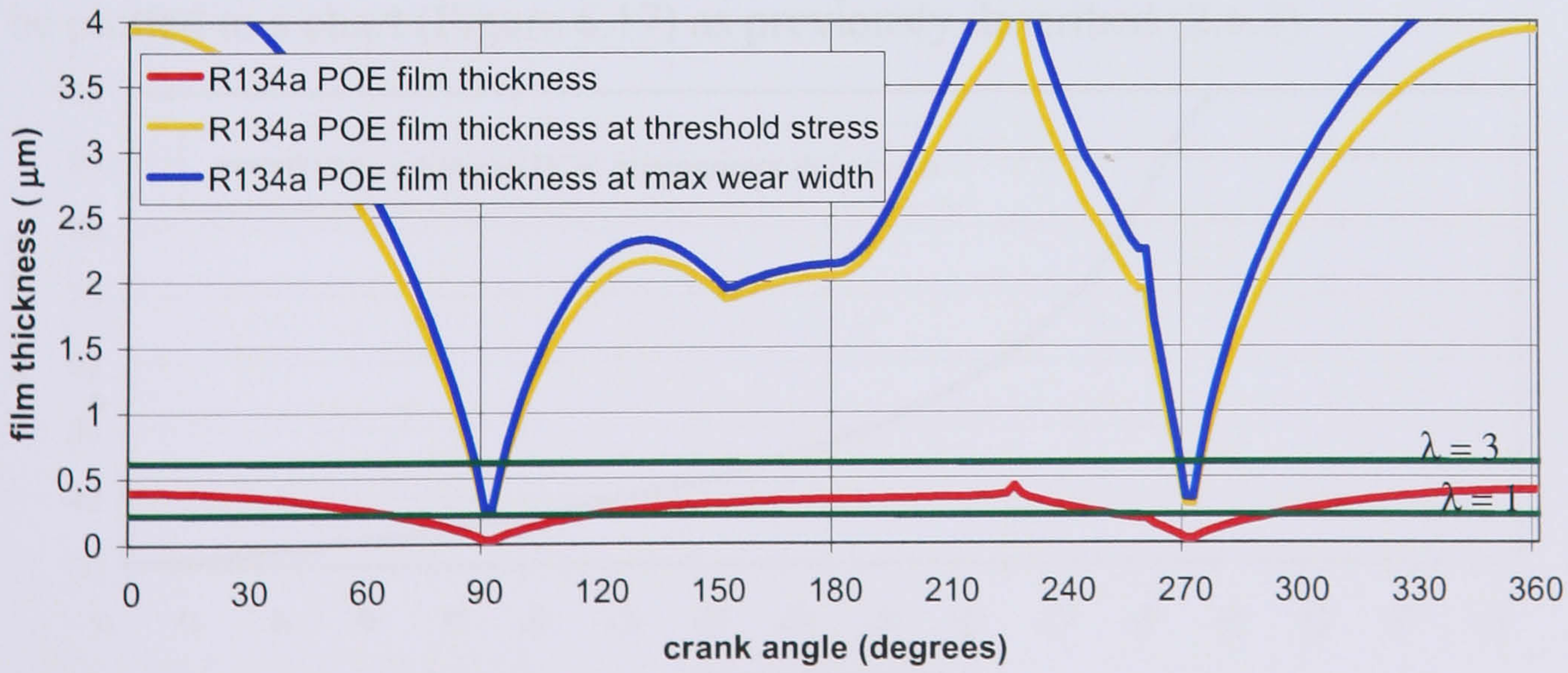

Figure 6.16 Film thickness relative to wear, R134a additised POE

The region of mixed mode lubrication is restricted to 86°-96°, whilst the boundary condition is reduced to a much narrower band of 89°-91°. The maximum contact stress within these bands is similar to the average for the full cycle. The volume and depth of material removed to reach the threshold contact stress can be calculated using the equations previously described (Equation 6.3, Equation 6.4). For this charge combination, the variable is contact length and the depth and volume of material removed shown in table format (Table 6.14).

	Threshold	Max contact length
Contact stress (MPa)	1.25	1.07
Wear coefficient (mm/N/m)	$3.8x10^{-7}$	$1.2x10^{-8}$
Wear depth to achieve (mm)	$2.2x10^{-2}$	$2.9x10^{-2}$
Wear Volume (mm^3)	$7.3x10^{-4}$	$1.2x10^{-3}$
Sliding distance to achieve (m)	30	683
Duration of operation to achieve (s)	170	12633 at 30% duty

Table 6.14 Duration to achieve wear thresholds, R134a additised POE

The point in time at which the required volume is removed can be calculated using the wear equation described previously (**Equation 2.8**). The table indicates that the small end bearing will wear rapidly, achieving the threshold contact stress after just 170s of operation and full contact length within $3^1/_2$ hrs of operation. As before, the operational duration within the higher wear rate regime is comparatively short and can, effectively, be ignored. With the wear coefficient at the lower rate (and film thickness into EHDL) the longevity can be plotted to a chart (Figure 6.17) as previously described (2.6.3).

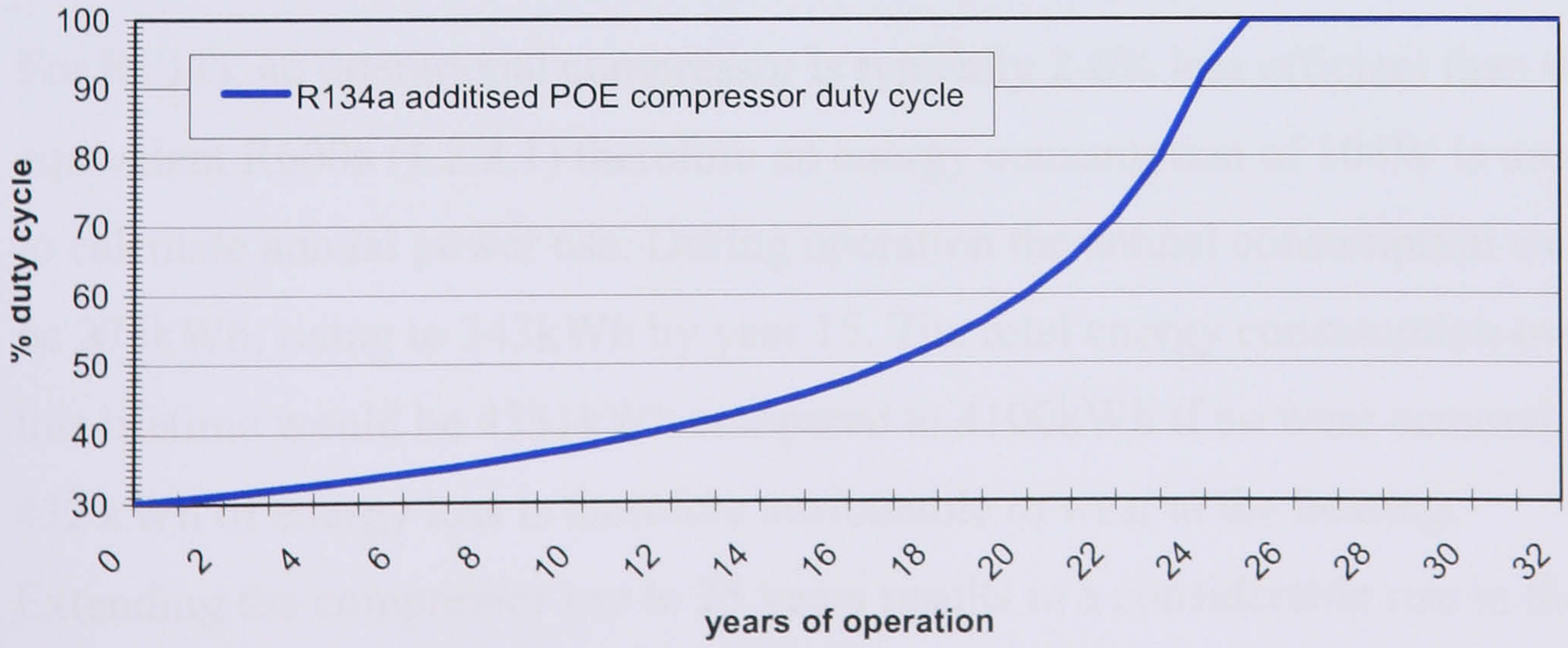

Figure 6.17 Projected duty cycle, R134a additised POE

The expected life of a compressor (duty cycle below 50%) operating under these conditions is 17 years. More significantly, the duty cycle at the end of the refrigerators expected life of 15years is 45.4%.

The useful and dissipated power can be calculated (Table 6.15) using the equations described previously (Equation 6.5, Equation 6.6, Equation 6.7 & Equation 6.8) and the change in duty cycle over time used to project energy consumption over the useful life of the compressor (Table 6.16).

Power used, compression stroke (W)	75.7
Power recovered, suction stroke (W)	29.8
Useful power (W)	45.8
Total power when new, (W)	104
Power dissipated, (W)	58.2

Table 6.15 Useful and dissipated power, R134a additised POE

	Year 0	Year 15	Year 25
Duty cycle (%)	30	45.4	100
Useful energy consumption (kWh)	120	120	120
Dissipated energy consumption (kWh)	153	222	470
Annual energy consumption (kWh)	273	343	590
Lifetime energy consumption (kWh)	-	4531	8892
Lifetime energy (no wear) (kWh)	-	4100	6833
Energy lost due to wear (kWh)	-	432	2060

Table 6.16 Duty cycle and energy consumption, R134a additised POE

For R134a, an operational compressor is typically 2-6% less efficient than the equivalent R600a (1.2.2.1) therefore an energy consumption of 104W is used to calculate annual power use. During operation the annual consumption would be 273kWh, rising to 343kWh by year 15. The total energy consumption over this lifetime would be 4531kWh compared to 4100kWh if no wear occured. 432 kWh of energy loss is therefore attributable to wear at the bearing. Extending the compressor use to 25 years results in a considerable rise in the duty cycle, hence energy consumption. Annual energy consumption would increase to 590 kWh, more than double the consumption when new.

6.5.2.2 *Effect of friction coefficient on compressor performance*

The same methodology applies to the R134a additised POE compressor as discussed previously (6.5.1.2) and the results presented (Table 6.17). From the table it is clear that the energy lost due to friction at the gudgeon pin/small end bearing is again much less than that attributable to wear and can be considered insignificant. The energy lost over the lifetime of the compressor being 9.2kWh compared with 335kWh due to wear at the bearing contact.

	R134a additised MO
Load at small end bearing (N)	63
Friction coefficient	0.018
Friction force (N)	1.13
Distance slid per second (m)	0.18
Energy lost (kWh) over 15 years	9.4

Table 6.17 Energy lost due to friction, R134a additised POE

6.6 Compressor energy requirement summary

The results from the power calculations can be presented in tabular format for comparison (Table 6.18).

	Compressor type	
Power consumption (kWh)	R600a add MO	R134a POE
No wear	3942	4100
Due to wear	258	432
Due to friction	44	9.4
With wear	4200	4531
With friction and wear	4244	4541

Table 6.18 Summary of compressor's energy consumption

From the data presented it is clear that effect of wear on the power consumption of the hermetic compressor is much more significant than that of friction. The larger gudgeon pin contact area and reduced contact load of the R600a compressor greatly enhance the longevity and energy consumption over the equivalent R134a compressor.

7 Conclusions and future work

The experimental research undertaken has shown that compressor longevity can be enhanced through the use of hydrocarbon refrigerant R600a in comparison to hydrofluorocarbon refrigerant R134a. The improvements are primarily, but not limited to, component dimensional requirements dictated by the thermo-dynamic properties of the refrigerants. The reduced piston pressure and the increased gudgeon pin contact area combining to provide a reduced bearing contact stress when compared to the equivalent R134a scenario. The lower operating pressure of the R600a compressor also requires a lower proportion of its piston stroke to achieve, resulting in enhanced wear tolerance over the R134a type.

7.1 Conclusions

An experimental pressurised micro-friction machine was developed for the evaluation of alternative refrigerant charge combinations over a range of tribological conditions.

Experimental wear tests on material samples have shown that, the R600a Additised MO charge resulted in consistently higher wear rates than those conducted with equivalent R600a non-additised MO charge.

At the outset of the experiments, the R134a POE charge provides much higher wear rates than either of the equivalent R600a MO charges. Over the duration of longer experiments, wear at the pin sample led to an increase in contact area hence reduced apparent contact stress producing very low friction and reduced wear characteristics for the R134a POE charge.

The reduction of surface roughness for the steel plate sample led to reduced pin wear in the case of both the R600a MO and additised MO conditions. For the POE charges, the reduction in surface roughness had no effect on the wear of the aluminium pin counter-face.

SEM and EDX analysis of the surfaces for R600a additised MO samples shows adhesive wear of the softer aluminium in the pin sample resulting in higher levels of harder silicon at the surface than the original material base stock. The plate samples shows material transfer from the pin sample to the plate surface whilst light microscopy shows no evidence of material transfer for the R600a non-additised MO charge. Results suggest that adhesive wear is the dominant regime for both R600a additised and non additised MO charges.

SEM and EDX analysis of the surfaces for the R134a POE pin sample show etching of the pin surface whilst carbon and oxygen suggest a breakdown of the lubricant package. Again there is material transfer from the pin to plate sample but also deposition of carbon and oxygen but reduced surface wear compared to the R600a additised MO plate. Light microscopy exhibits near identical surface conditions for both the R134a and R600a POE samples indicating the refrigerant had little effect on the wear regime. Results suggest chemical wear is the dominant regime with any chemical film deposition at the pin sample unable to sustain separation until the apparent stress falls below a critical value.

For this thesis, experimental friction and wear coefficients were used to calculate efficiency and durability of compressors operating with both R600a additised MO and R134a POE charges. The comparison of these charges showed duty cycles rose, over time, much more rapidly for the R134a type compressor than the R600a, even when assuming a lower friction and wear rate.

7.2 Future Work

The experimental pressurised micro-friction machine, whilst performing well in the evaluation of friction, requires refinement in order to provide more accurate wear analysis. The machine should either provide real-time wear data

or a more accurate pin mounting system to allow precise re-alignment of samples if measured during the experiment.

The sample materials presented for evaluation during the course of these works represent those found in one domestic refrigeration compressor type at the outset of the project. The material combinations may not be those most suitable for the refrigerant charge combinations, therefore further testing is required to evaluate current and proposed material combinations and to ascertain those most suitable.

References

Advanced Products (2001). "Advanced Products website."

Akei, M., K. Mizuhara, et al. (1996). "Evaluation of film forming capability of refrigeration lubricants in pressurized refrigerant atmosphere." Wear(196): 180-187.

Antheaume, N. and E. Labouze (1998). "The External Cost Assessment of the Dataset from a Life Cycle Inventory." SAE Special Publications **1342**: 81-86.

Archard, J. F. (1953). "Contact and Rubbing of Flat Surfaces." Journal of Applied Physics **24**(8): 981-988.

Archard, J. F. and M. T. Kirk (1960). "Lubrication at point contacts." Proceedings of the Royal Society: 532-549.

Bodensiek, E. J. (1965). "Specific film thickness -an index to gear tooth surface determination." Proceedings of the AGMA Aerospace Gearing Symposium: 32-37.

Boustead, I. (1993). Ecoprofiles of the European plastics industry Report 3: Polyethylene and polypropolene, APME.

Busak and Shamban (2001). Rod Seals Product Catalogue, Busak and Shamban.

Campbell, N. J. and A. McCulloch (1998). "The Climate Change Implications of Manufacturing Refrigerants: A calulation of "production" energy contents of some common refrigerants." Trans IChemE **76**(B): 239-244.

Capros, P. and L. Mantzos (2000). The Economic Effects of EU-Wide Industry-Level Emissions Trading to Reduce Greenhouse Gases. Athens, Institute of Communication and Computer Systems of National Technical University of Athens.

Caradon Hydroflex (2001). Bellows Life Prediction, Caradon Hydroflex. **2001**.

Ciantar, C. (2000). Sustainable Development of Refrigerator Systems using Replacement Environmentally Acceptable Refrigerants. School of Design, Engineering & Computing. Bournemouth, Bournemouth University: 234.

Ciantar, C. and M. Hadfield (2000). "An environmental Evaluation of mechanical systems using environmentally acceptable refrigerants." International Journal of Life Cycle Assessment **5**(4): 209-220.

Ciantar, C., M. Hadfield, et al. (1999). "The Influences of lubricant viscosity on the wear of hermetic compressor components in HFC-134a environments." Wear **236**: 1-8.

Ciantar, C., M. Hadfield, et al. (2000). "The Influence of POE and PVE lubricant blends within hermetic refrigerating compressors operating with HFC-134a refrigerant." Wear **241**(1): 53-64.

Cranvey, D. (1997). "Replacement refrigerants -environment based fluid selection." Mechanical Incorporated Engineer: 129-133.

DETR (1999). Fridge-freezers in the United Kingdom. London, Department of Environment, Transport and the Regions.

DiaCom (2001). DiaCom Product Website.

DTI (2004). Estimates of primary energy demand and electricity generation. London, Department of Trade and Industry: 2.
Environment Agency (2004). Environmental Indicators, Department for Environment
Food and Rural Affairs. **2004**.
ETH-ENET (1995). okoinventare fur energiesysteme.
European Commission (1998). ExternE- Externalities of Energy, All-EU Summary. **2002**.
European Commission (1998). ExternE- Externalities of Energy, Methodology Annexes, European Commission
Directorate General XII
Science, Research and Development.
European Commission (1998). ExternE- Externalities of Energy, UK Introduction. **2002**.
Fuks, G. J. (1962). The Properties of Solutions of Organic Acids in Liquid Hydrocarbons at Solid Surfaces. Research in Surface Forces. B. V. Derjagin. Moscow, Trans-Consultants Bureau, New York: 79-88.
Gameson, T. (1998). Private Sector Methods for Weighting Environmental Indicators, European Commission.
Granryd, E. (2000). "Hydrocarbons as refrigerants." International journal of refrigeration **24**: 15-24.
Hamrock, B. J. and D. Dowson (1979). "Minimum film thickness in eliptical contacts for different regimes of fluidfilm lubrication." Proc. 5th Leeds-Lyon Symp. on Tribology, Elastohydrodynamics and Related Topics: 22-27.
Hugeut, J.-P. (2000). Stationary Refrigeration and Air Conditioning: Proposals to Reduce the Emission of Greenhouse Gases. Brussels, EUCRAR.
Hurst, C. J. and A. D. Kelly (1998). Non-destructive assessment of wrist journal bearings in hermetic reciprocating compressors. International compressor engineering conference, Purdue University.
Hutchings, I. M. (1992). Tribology, Friction and wear of engineering materials. London, Edward Arnold.
ISO-14040 (1997). Environmental management-Life cycle assessment-Principles and framework.
ISO-14041 (1998). Environmental management-Life cycle assessment-Goal and scope definition and inventory analysis.
ISO-14042 (2000). Environmental management-Life cycle assessment-Life cycle impact assessment.
ISO-14043 (2000). Environmental management-Life cycle assessment-Life cycle interpretation.
Jonsson, U. (1998). Elastohydrodynamic lubrication and lubricant rheology in refrigeration compressors. Department of Mechanical Engineering. Lulea, Lulea University of Technology, Sweden.
Kassfeldt, E., T. Norrby, et al. (2000). Wear and friction in boundary lubricated contacts. Tribology in Environmental Design 2000, Bournemouth, Professional Engineering Publishing.
Markandya, A. and K. Halsnaes (2002). Climate Change and Sustainable Development. London, Earthscan.

Mayerhofer, P., W. Krewitt, et al. (1997). Extension of the Accounting Framework, Final Report. Stuttgart, Institute of Energy Economics and the Rational Use of Energy (IER).
Meurer, C. and J. Law (1998). R12 Replacements for the Appliance Industry. CHINA Refrigeration 1998, Solkane Refrigerant Seminar, Shanghai, China.
Meyer, A. (1996). "Hydrocarbon Blends in Small Scale Refrigeration Appliances." GTZ Yearbook 1996: 87-92.
Mizuhara, K., M. Akei, et al. (1994). "The Friction and Wear Behaviour in Controlled Alternative Refrigerant Atmosphere." STLE tribology transactions **37**(1): 120-128.
Montgomery, R. S. (1965). "Chemical Effects on Wear in the Lubrication of Aluminium." Wear **8**(4): 289-302.
Na, B. C., K. J. Chun, et al. (1998). "A tribological study of refrigeration oils under HFC-134a environment." Tribology International **30**(9): 707-716.
Nadal, G. and O. L. Girardin (2001). "Economic impact of the valuation of life cycle CO2 emissions from renewable and fossil energy systems." International Journal of Global Energy Issues **15**(1/2): 84-96.
Nichols and Sturges (1996). Environmental benefits of offset energy, ETSU/DTI.
Oki Institute GEMIS.
Palatine Precision (1998). Welded Diaphragm Bellows Catalogue, Paltine Precision Ltd.
Paul, J. (1996). "A Fresh Look at Hydrocarbon Refrigeration -Experience and Outlook." GTZ Yearbook 1996: 73-84.
Performance and Innovation Unit (2002). The Energy Review. London, UK Government Cabinet Office.
Pira International (1997). PEMS.4 User Manual.
Plint, G. (2000). Specification and Design of Tribological Tests. Cambridge University Tribology Course, Plint and Partners Ltd.
Pre-Consultants (2001). SimaPro. Amersfoort, NL, Pre Consultants.
Rao, P. K. (2000). Sustainable Development, Economics and Policy, Blackwell.
RDC-Environment and Pira International (2001). Evaluation of costs and benefits for the achievement of reuse and recycling targets for the different packaging materials in the frame of the packaging and packaging waste directive 94/62/EC.
Reyes-Gavilan, J., A. Eckard, et al. (1996). "A Review of Lubrication and Performance Issues in Refrigeration Systems Using an HFC (R-134a) Refrigerant." Journal of the Society of Tribologists and Lubrication Engineers **52**(4): 317-322.
Royal Commission on Environmental Pollution (2001). Energy - The Changing Climate. London, Royal Commission.
Safari, S. and M. Hadfield (1998). "Wear behaviour of the piston/gudgeon pin in a hermetic compressor with replacement CFC refrigerants." Wear **219**: 8-15.
Society of Environmental Toxicology and Chemistry (1993). Guidelnes for Life-cycle Assesment: "A Code of Practice".

Stachowiak, G. W. and A. W. Batchelor (2001). Boundary and Extreme Pressure Lubrication. Engineering Tribology, Butterworth-Heinemann: 389-390.

Stachowiak, G. W. and A. W. Batchelor (2001). Corrosive and oxidative wear. Engineering Tribology, Butterworth-Heinemann: 553-570.

Stolarski, T. A. (1989). "Probability of scuffing in lubricated contacts." Proceedings of the Institution of Mechanical Engineers **203**: 361-369.

Stolarski, T. A. (1996). "A system for wear prediction in lubricated sliding contacts." Lubrication Science **8**(4): 315-350.

Sturges, M. (2001). Evaluating the Environmental Effectiveness and Economic Efficiency of Extended Producer Responsibility (EPR), Pira International.

Tol, R. S. J. and T. E. Downing (2000). The marginal cost of climate changing emissions. Amsterdam, Institute for environmental studies, Vrije Universiteit: 68.

Tol, R. S. J., S. Fankhauser, et al. (2000). "How Much Damage Will Climate Change Do?" World Economics **1**(4): 179- 206.

Uhlmann, E., G. Spur, et al. (2001). Developement of flexible automatic disassembly processes and cleaning technologies for the recycling of consumer goods. Proceedings of the IEEE International Symposium on Assembly and Task Planning, Fukuoka, Japan.

Wan Yong and X. Qunji (1995). "Friction and wear characteristics of P-containing antiwear and extreme pressure additives in the sliding of steel against aluminium alloy." Wear **188**(1/2): 27-32.

WCED (1987). Our Common Future. UK, World Commission on Environment and Development.

Williams, J. A. (1994). Boundary Lubrication and Friction. Engineering Tribology. Oxford, Oxford University Press: pp348-380.

Williams, J. A. (1994). Engineering Tribology. Oxford, Oxford University Press.

Yoon, H. K., C. H. Poppe, et al. (1996). "Predicting Lubricant Performance in Refrigerant Compressors: A Comparison Between Component Testing and Benchtesting." ASHRAE Transactions **102**(1): 86-95.

Appendices

Appendix A Refrigerant Data

A.1 R600a

Hydrocarbon refrigerant, high purity Isobutane, $(CH3)_3CH$.

Trade name: Care 10 (Calor)

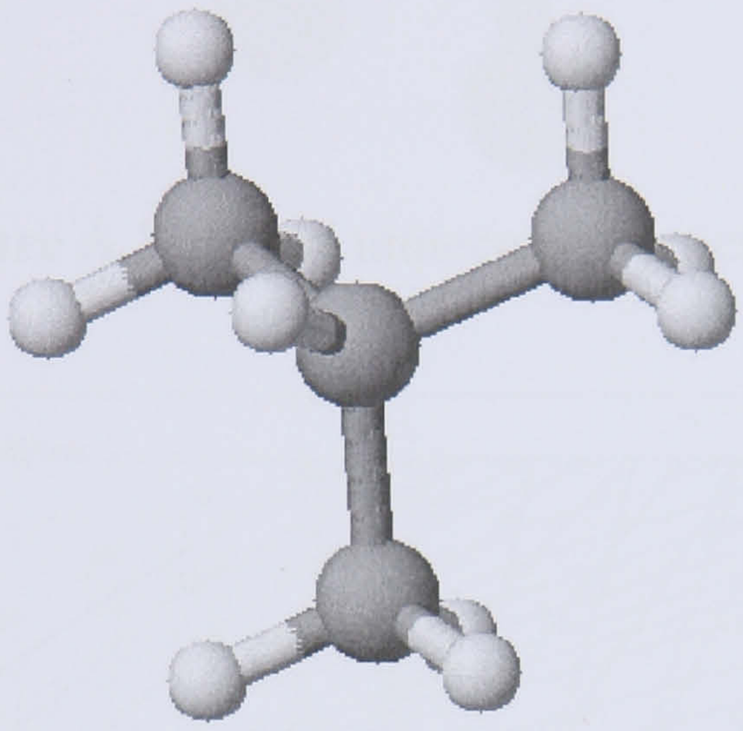

Figure A.1 R600a molecular structure

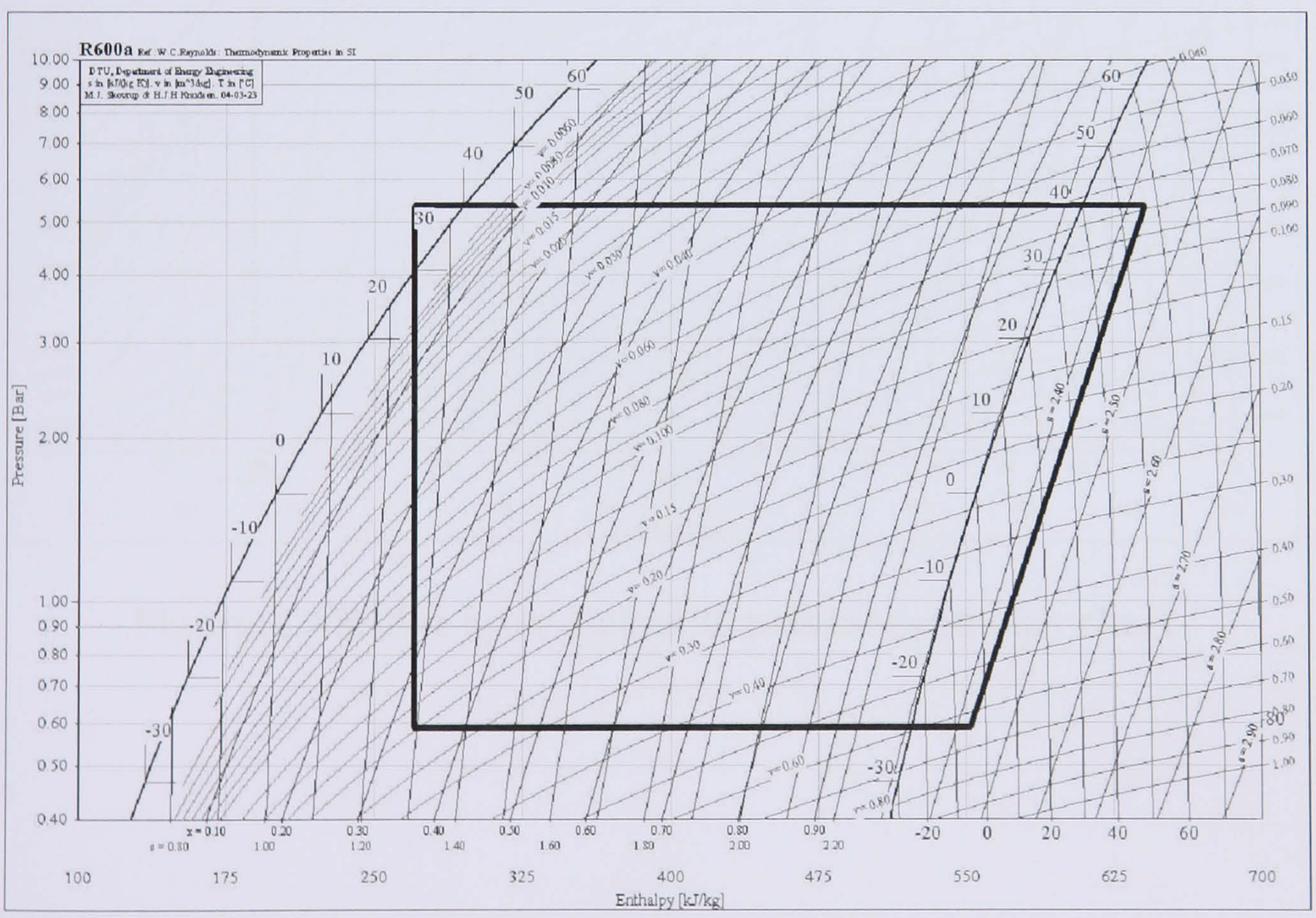

Figure A.2 R600a cycle plotted to pressure enthalpy chart

A.2 R134a

Hydrofluorcarbon refrigerant, 1,1,1,2-tetrafluorethane CF_3CH_2F

Trade name: Suva (Dupont)

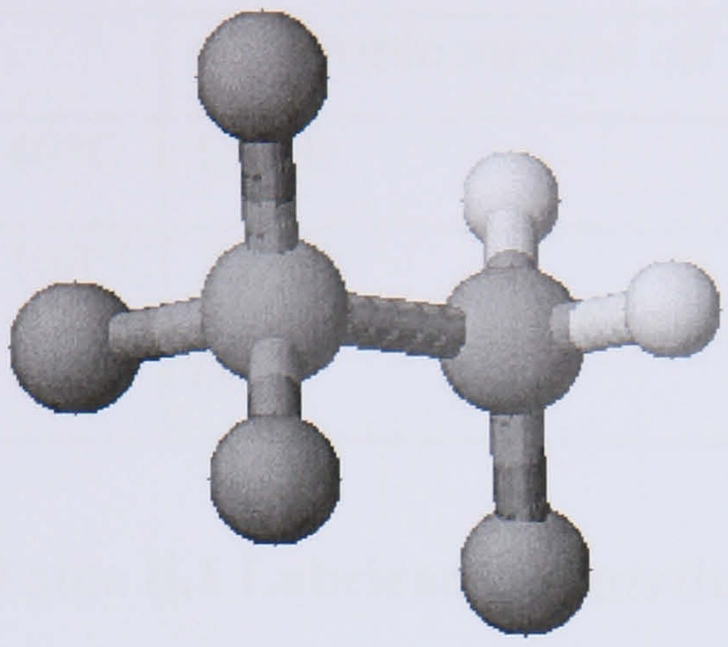

Figure A.3 R134a molecular structure

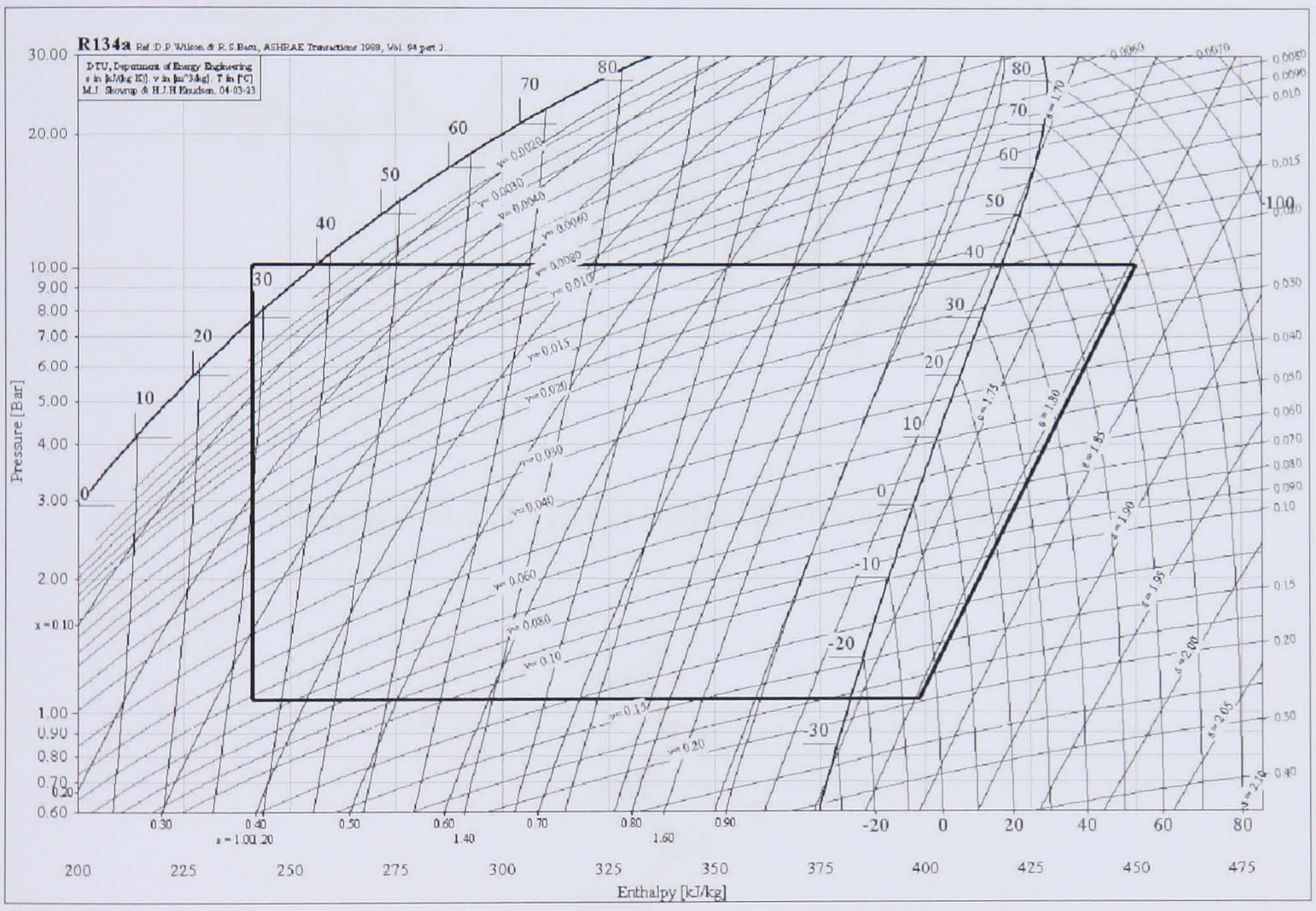

Figure A.4 R134a cycle plotted to pressure enthalpy chart

Appendix B Lubricant Data

Lubricant type	Mineral Oil	Polyolester
Trade name (Castrol)	Icematic AW15	Icematic SW15
Base	naphthenic mineral oil	pentaerythritol
Kinematic viscosity at 40°C	15 cSt	15 cSt
Kinematic viscosity at 100°C	3.2 cSt	3.6 cSt
Viscosity Index	60	130

Table B.1 Lubricant properties

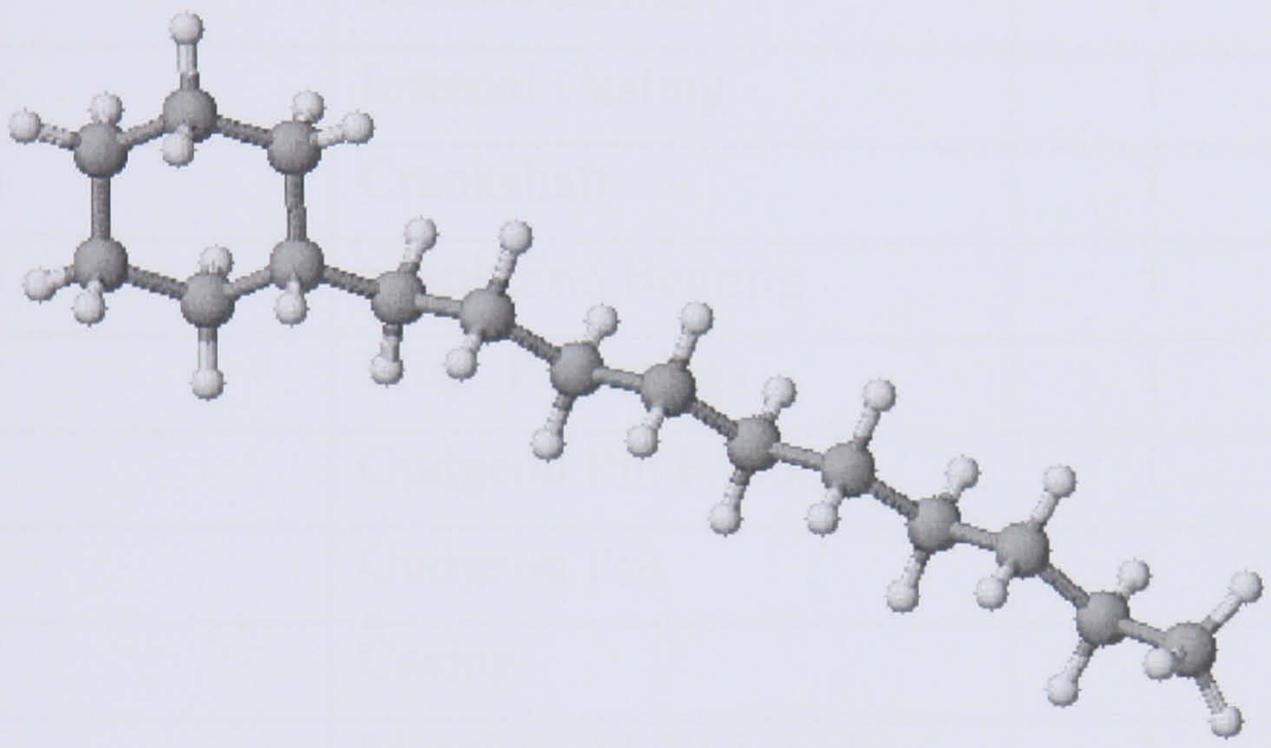

Figure B.1 Typical naphthenic structure

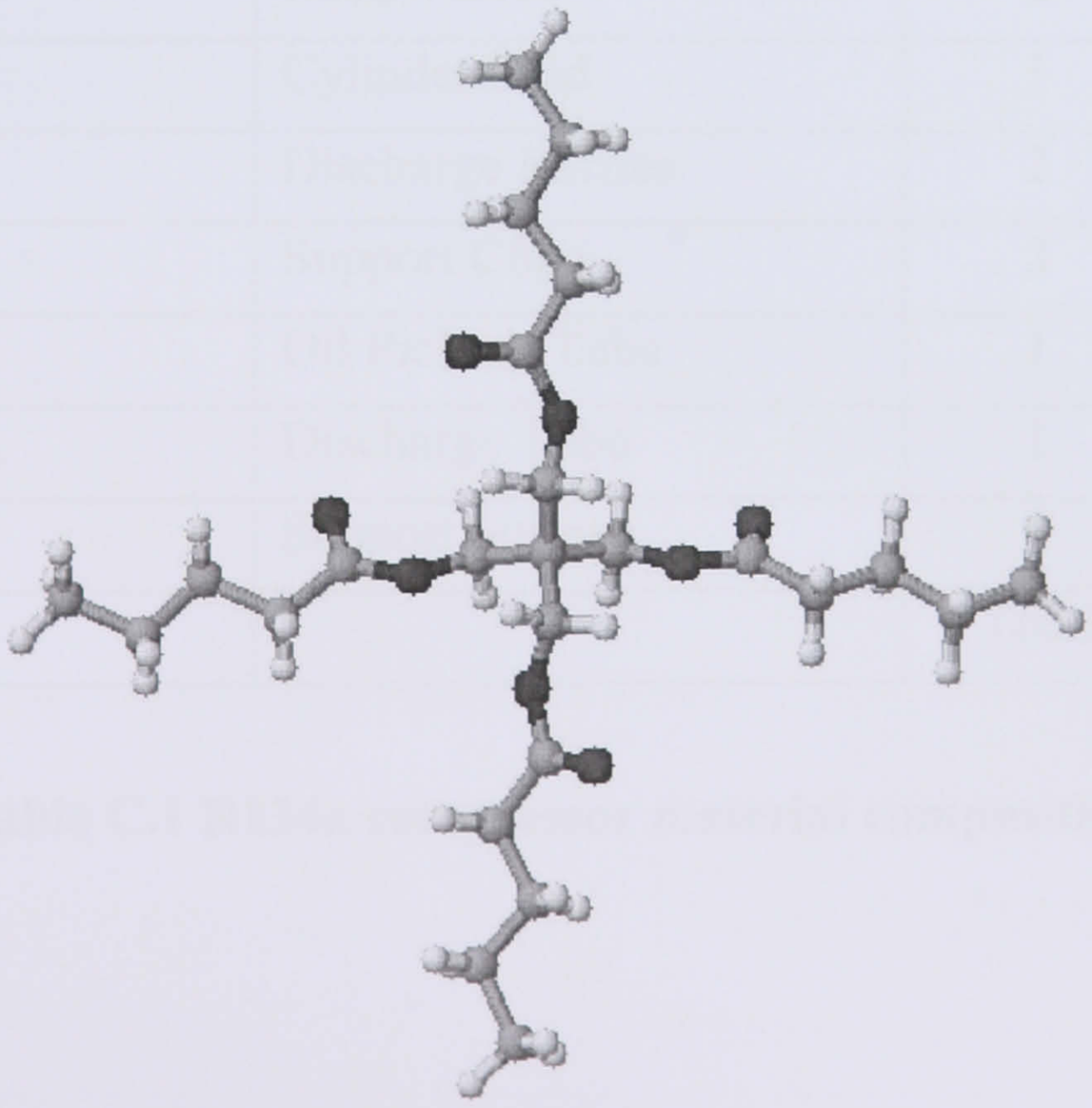

Figure B.2 Typical POE structure (pentaerythritol tetra-pentanoate)

Appendix C Hermetic Compressor Disassembly

Material	Component	No Off	Mass g.
Aluminium	Motor Core Ends	1	104.4
Aluminium	Connecting Rod	1	11.74
Aluminium	Big End Bearing Cap	1	5.6
Aluminium	Piston	1	34.8
Aluminium	Valve cover	1	43.9
Copper (wire)	Motor Windings	1	737.9
Polyethylene	Misc. Plastic Parts	1	100
Polyethylene	Winding Insulators	1	28
Polyethylene	Suction Baffle	1	26.4
Steel (casting)	Internal Casting	1	1723
Steel (casting)	Crankshaft	1	240.5
Steel (casting)	Crank End Bearing	1	79.79
Steel (forged)	Misc. Fastenings	1	88.58
Steel (forged)	Gudgeon Pin Fastener	1	0.13
Steel (forged)	Gudgeon Pin	1	6.04
Steel (sheet)	Casing	1	3100
Steel (sheet)	Motor Field Coil Body	1	2196.2
Steel (sheet)	Motor Core Plates	1	750
Steel (sheet)	Reed Valves	2	4.2
Steel (sheet)	Cylinder head	1	46.5
Steel (sheet)	Discharge Baffles	2	15.8
Steel (sheet)	Support Clips	3	9.1
Steel (tube)	Oil Pick-up Tube	1	12.65
Steel (tube)	Discharge Tube	1	15.5
Steel (wire)	Support Springs	3	9.5
		Total	9390

Table C.1 R134a compressor material composition

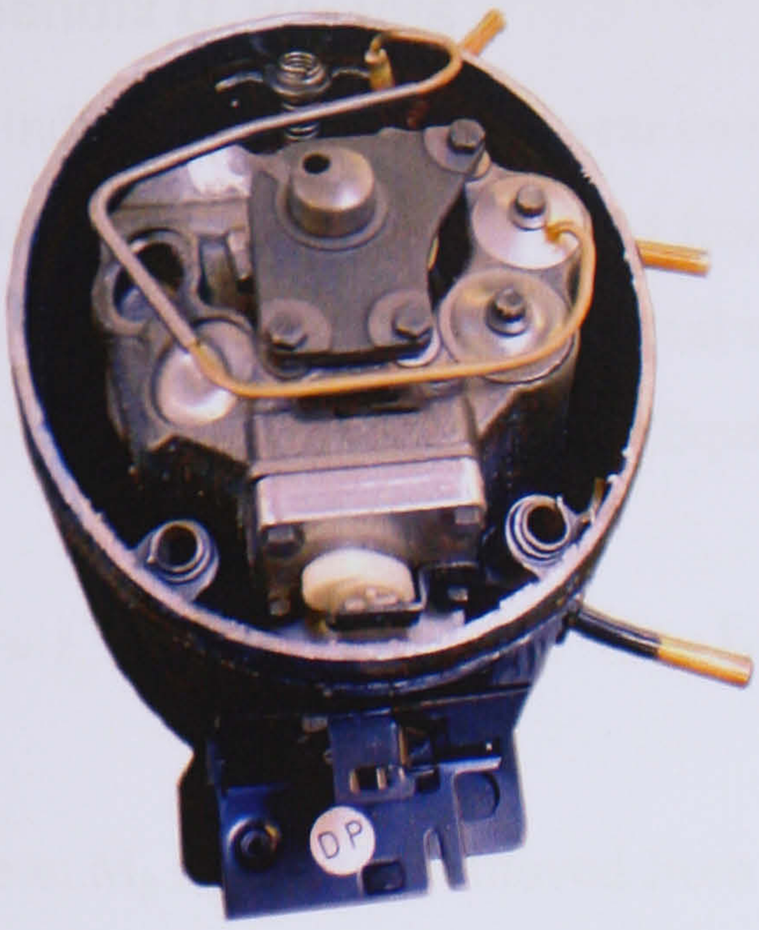

Figure C.1 hermetic compressor assembly (casing separated)

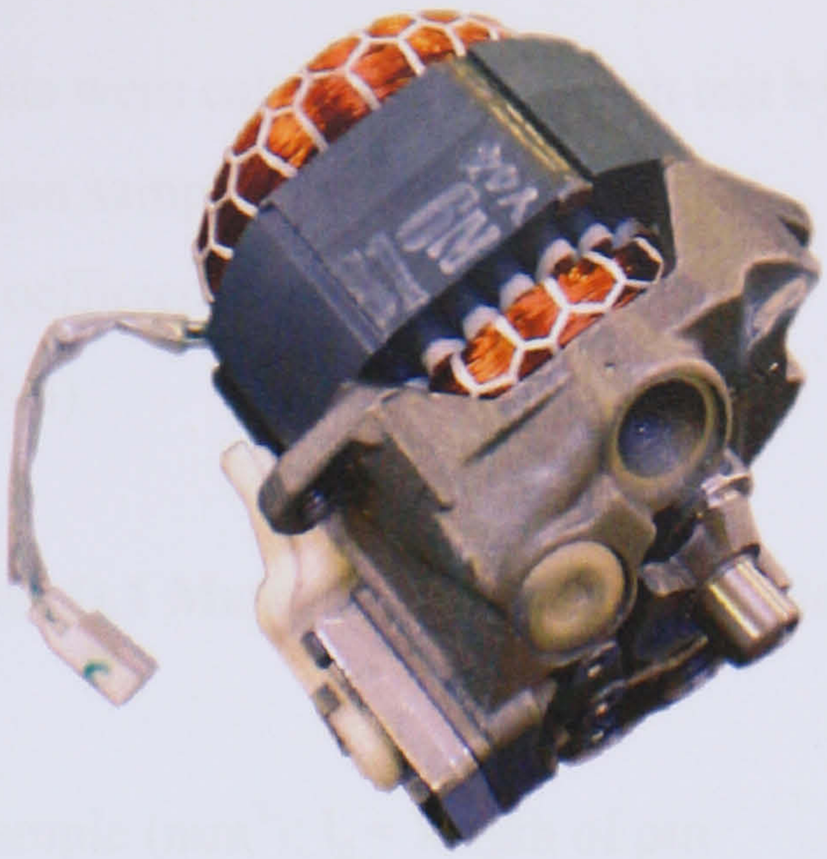

Figure C.2 pump and motor sub-assembly

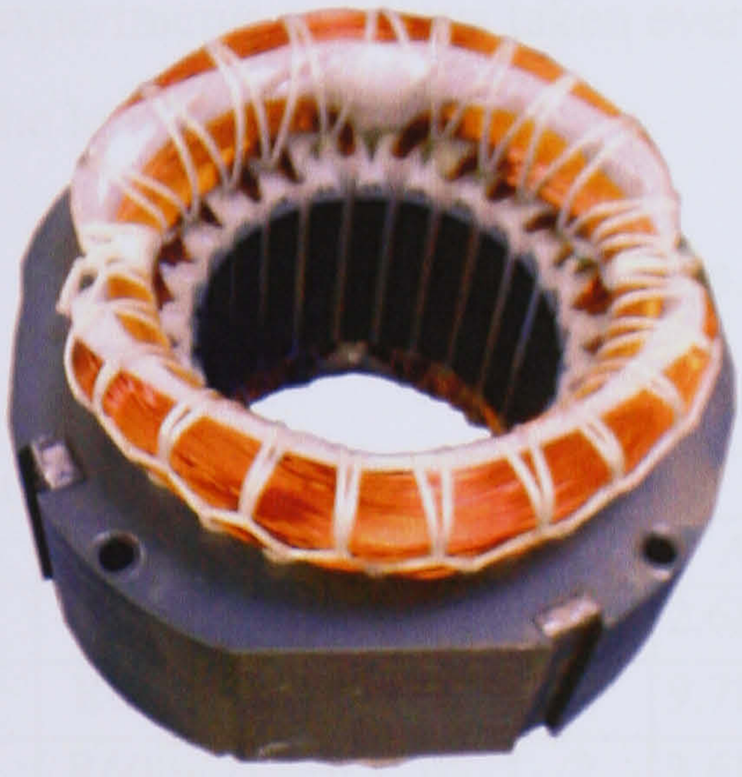

Figure C.3 motor winding assembly

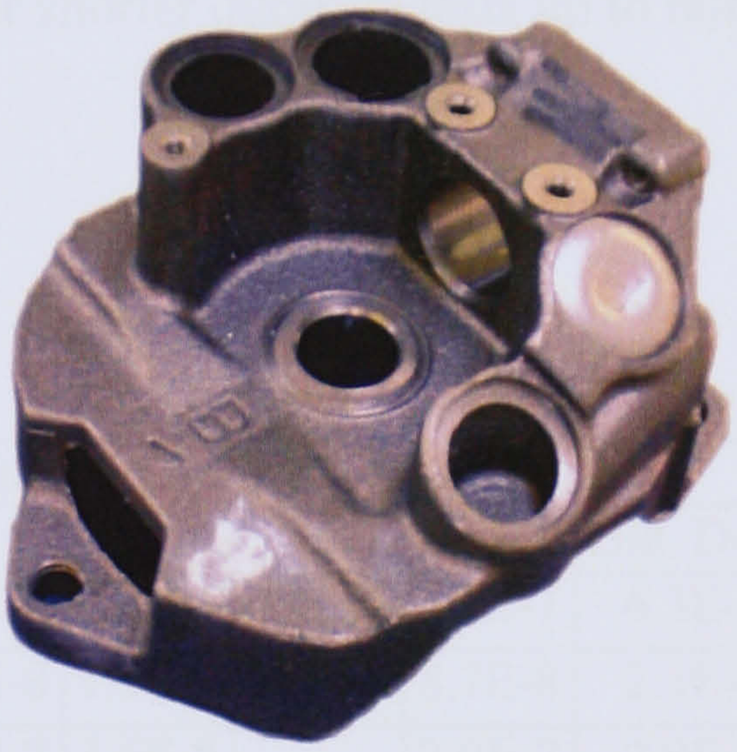

Figure C.4 pump body assembly

Figure C.5 crankshaft

Figure C.6 relative size of connecting rod (2 pence coin)

Appendix D Results

The individual dimensional wear coefficients were calculated after each test by calculating the material removed from the pin sample (Equation D.1), subsequently using the dimensional wear coefficient equation detailed in the main text (1.2.1.2) to provide *k* (Equation 1.3).

$$M_p = l_p^{\,3} \times 0.167$$

Equation D.1 Material removed from pin

Where: M_p = material removed from pin sample (mm^3); l_p = length of pin sample wear scar (mm).

Friction coefficients and contact potentials were recorded in software during the experiments, readings taken every 10s for shorter duration tests up to 60s for the longest duration tests.

D.1 initial 7200s A-type plates, 1-16

Test No.	Charge	Temp °C	Dur. hrs	Dimensional wear coefficient (k)					
				A	B	C	D	Ave.	Std. Dev.
1	R600a/MO	05	2	2.6E-7	1.4E-6	4.2E-8	2.9E-7	5.1E-7	6.3E-7
2	R600a/MO+	05	2	9.7E-8	7.7E-8	1.1E-7	6.3E-8	8.7E-8	2.1E-8
3	R600a/POE+	05	2	3.6E-8	5.3E-7	3.6E-8	-	2.0E-7	2.9E-7
4	R134a/POE+	05	2	2.3E-7	2.0E-7	9.7E-8	-	1.8E-7	7.0E-8
5	R600a/MO	25	2	5.6E-7	9.1E-7	1.3E-6	2.9E-7	7.8E-7	4.6E-7
6	R600a/MO+	25	2	2.3E-6	1.4E-6	1.4E-6	2.8E-6	2.0E-6	1.1E-6
7	R600a/POE+	25	2	3.3E-6	1.1E-5	7.8E-6	-	7.3E-6	3.8E-6
8	R134a/POE+	25	2	3.9E-7	3.3E-7	3.5E-7	-	3.6E-7	4.7E-8
9	R600a/MO	57	2	6.9E-7	3.5E-7	6.9E-7	-	5.8E-7	1.9E-7
10	R600a/MO+	57	2	1.9E-5	2.4E-5	2.4E-5	-	2.2E-5	2.9E-6
11	R600a/POE+	57	2	2.1E-5	2.9E-7	2.6E-5	2.4E-5	1.8E-5	1.2E-5
12	R134a/POE+	57	2	2.3E-6	2.3E-6	9.2E-6	6.0E-6	5.0E-6	3.3E-6
13	R600a/MO	110	2	3.6E-8	1.5E-7	3.6E-8	1.2E-7	8.6E-8	5.9E-8
14	R600a/MO+	110	2	2.9E-7	1.2E-7	9.7E-8	-	1.7E-7	1.0E-7
15	R600a/POE+	110	2	7.8E-6	5.5E-6	1.8E-6	-	5.1E-6	3.0E-6
16	R134a/POE+	110	2	1.6E-6	1.4E-5	1.4E-5	-	1.0E-5	7.3E-6

Table D.1 Wear coefficient, initial 7200s, A-plate tests

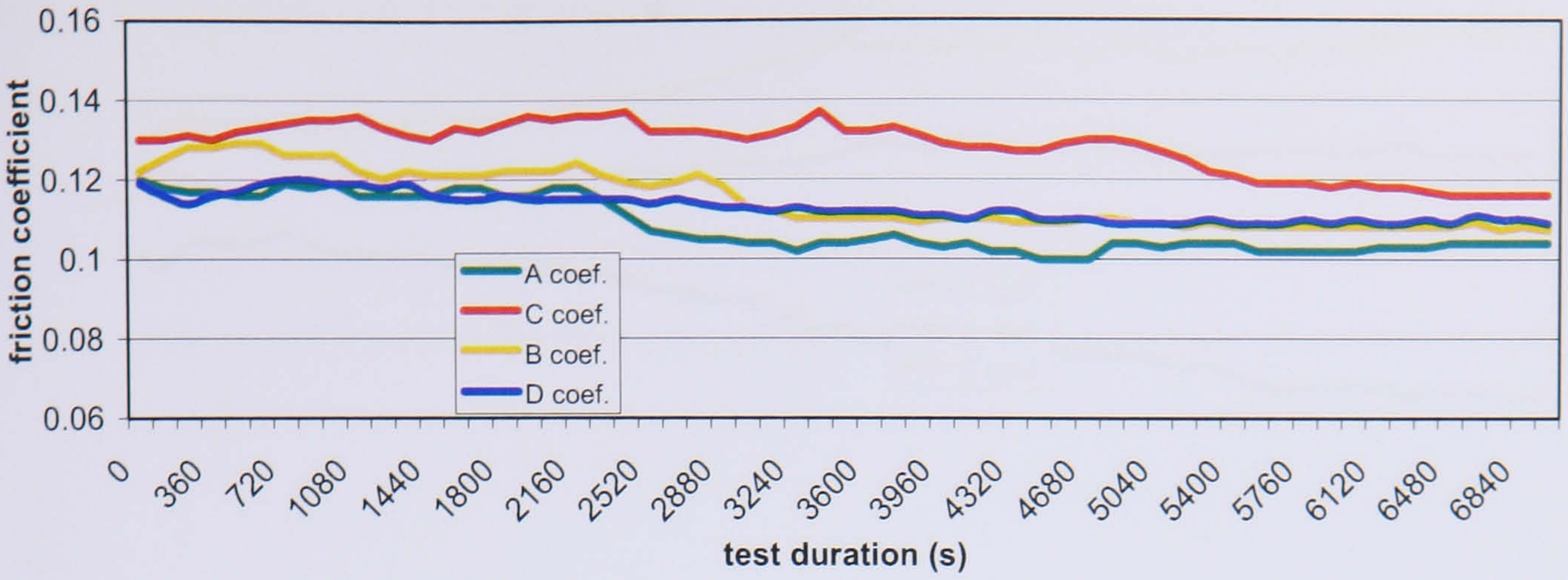

Figure D.1 Friction coefficient, test 1, R600a, MO, 05°C

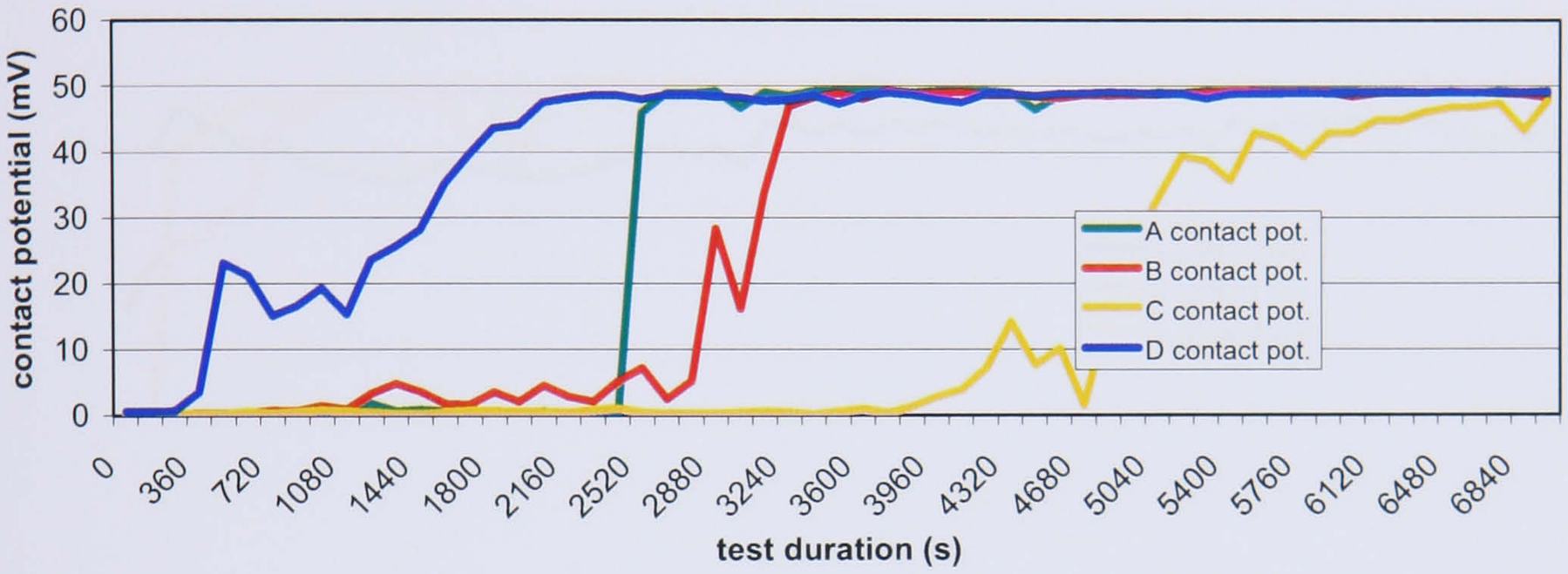

Figure D.2 Contact potential, test 1, R600a, MO, 05°C

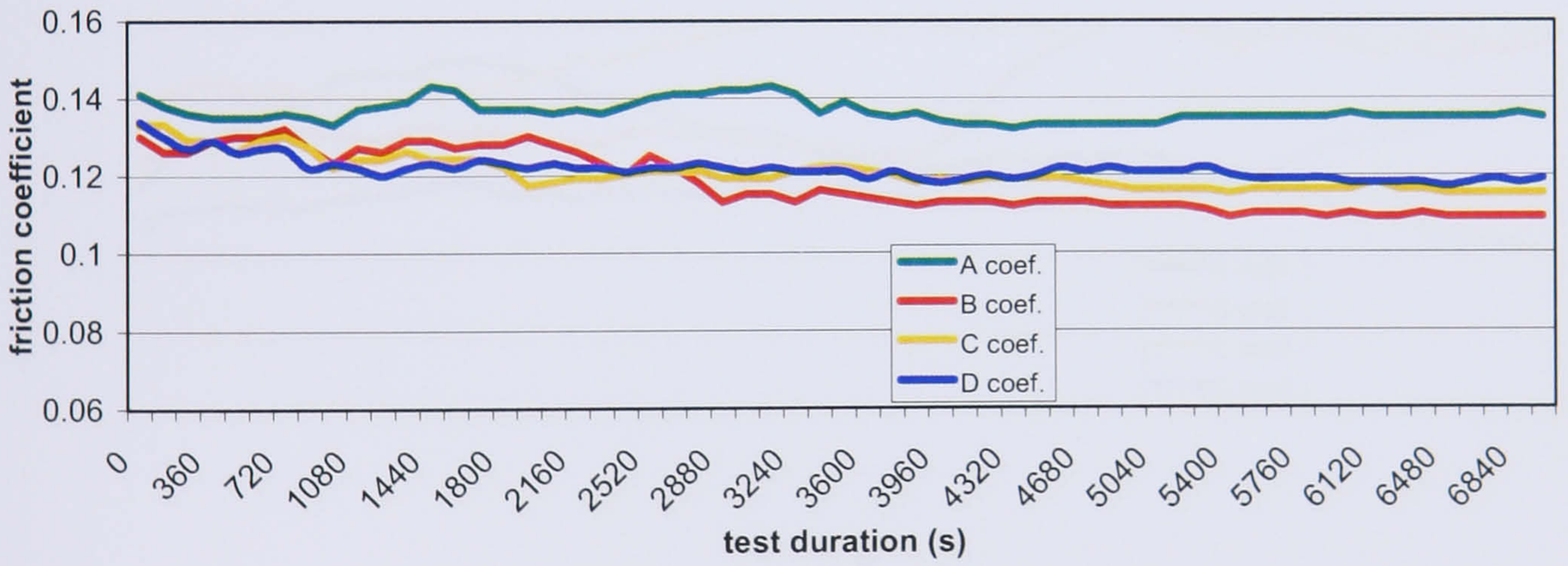

Figure D.3 Friction coefficient, test 2, R600a, MO+, 05°C

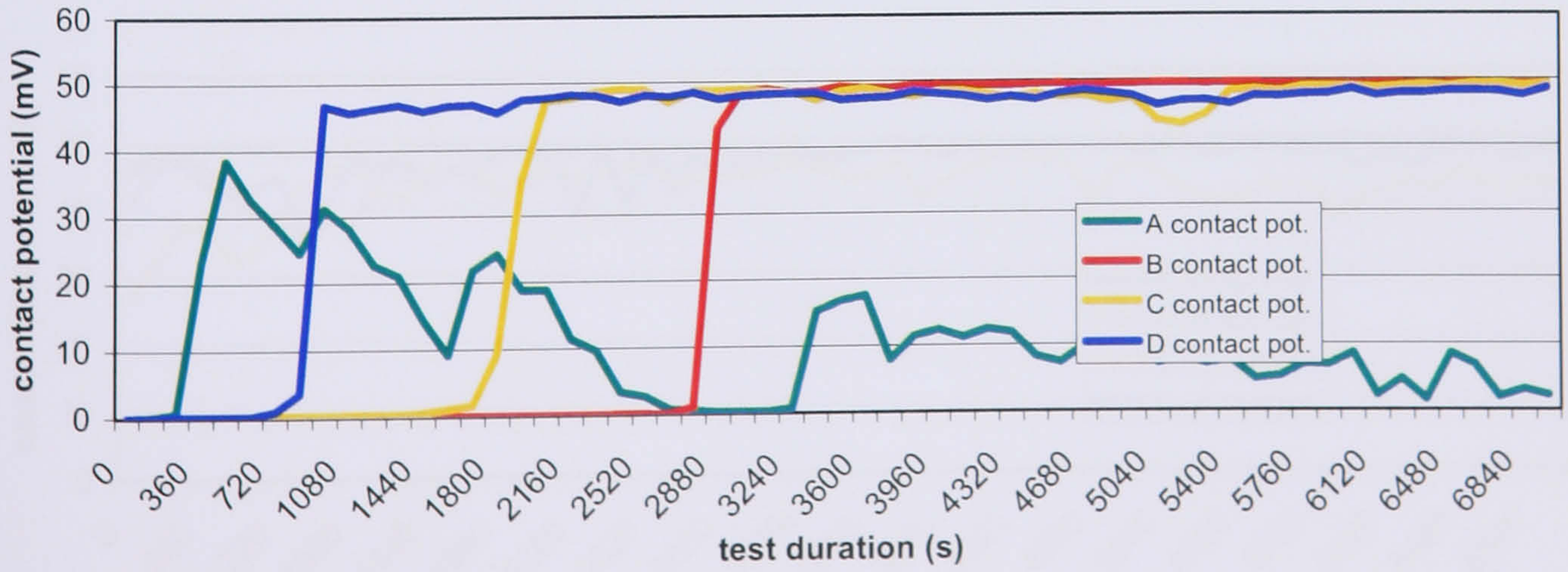

Figure D.4 Contact potential, test 2, R600a, MO+, 05°C

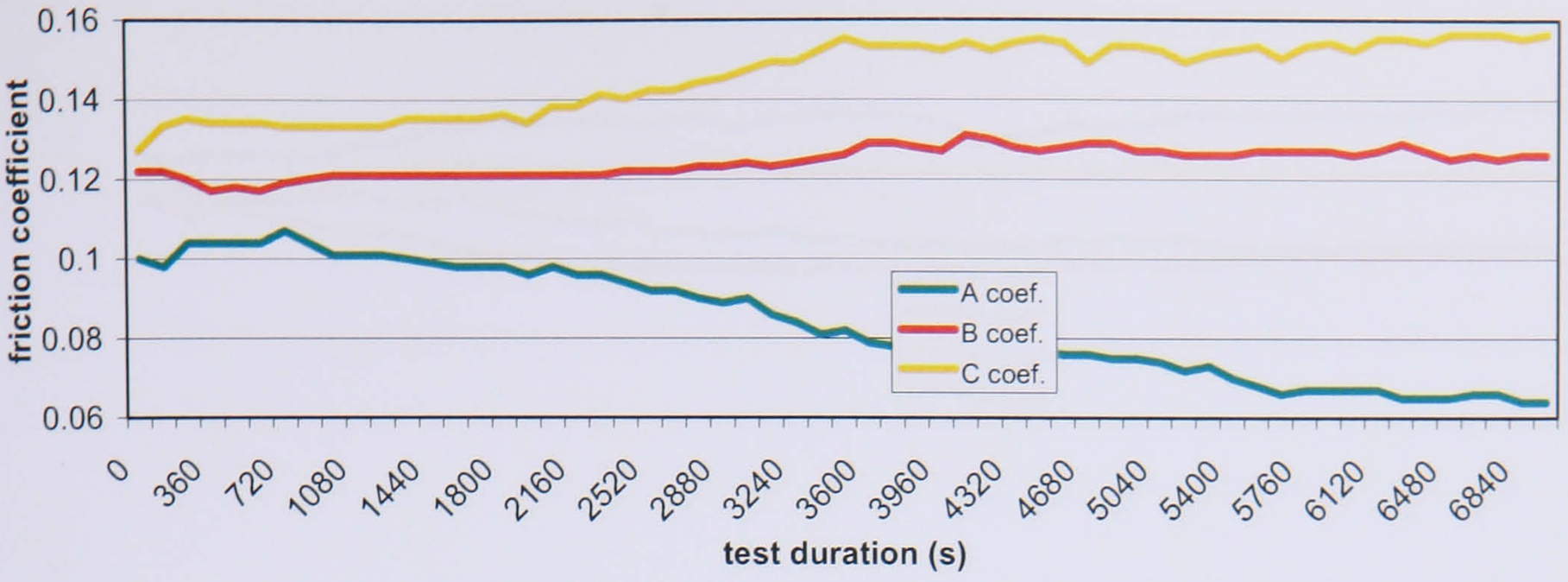

Figure D.5 Friction coefficient, test 3, R600a, POE+, 05°C

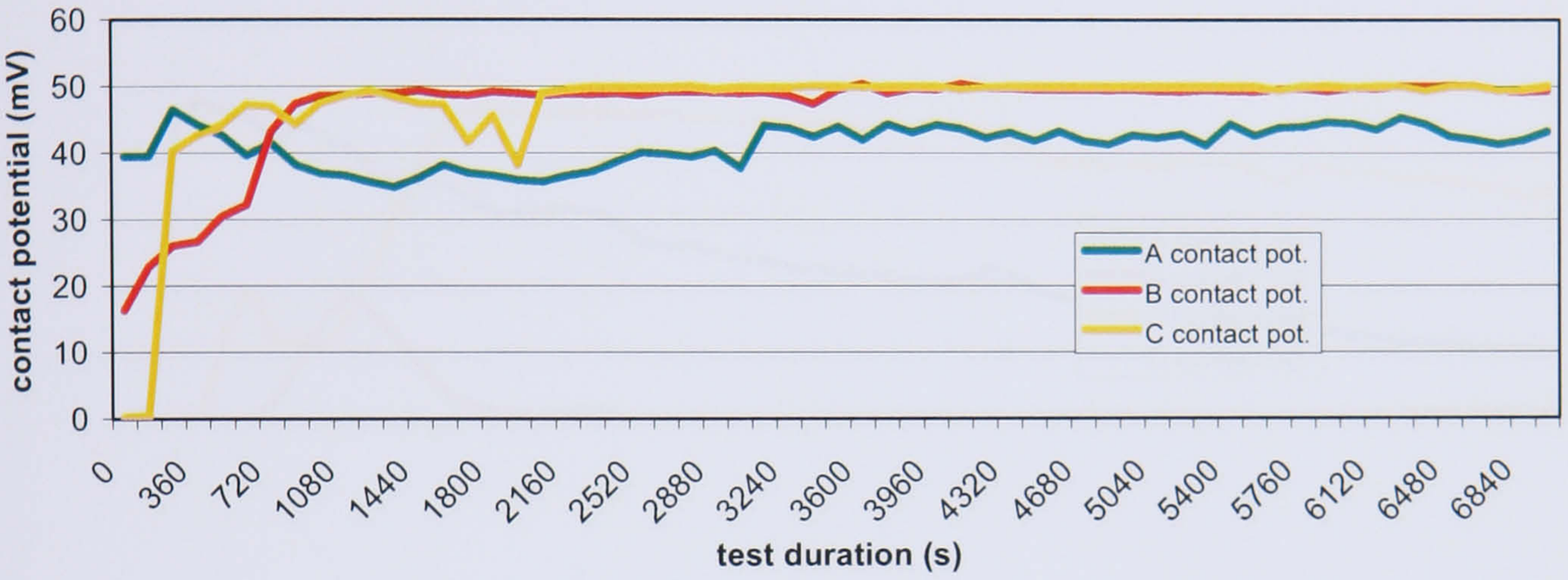

Figure D.6 Contact potential, test 3, R600a, POE+, 05°C

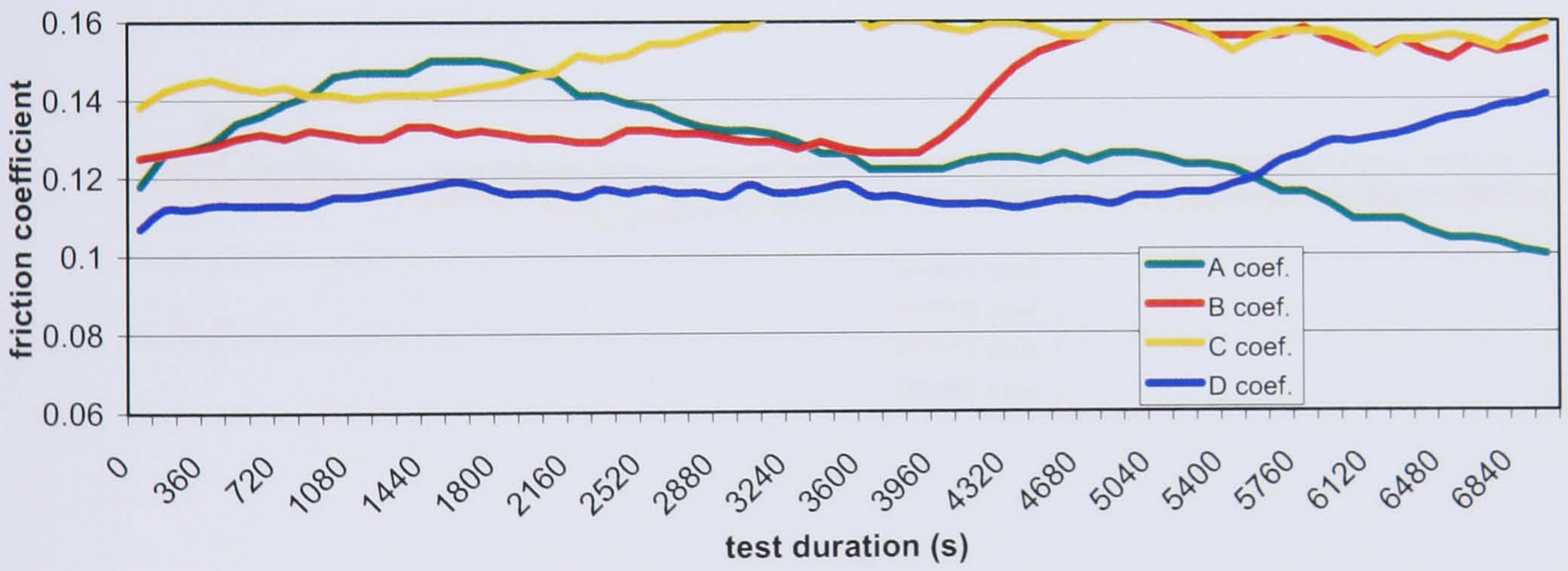

Figure D.7 Friction coefficient, test 4, R134a, POE+, 05°C

Figure D.8 Contact potential, test 4, R134a, POE+, 05°C

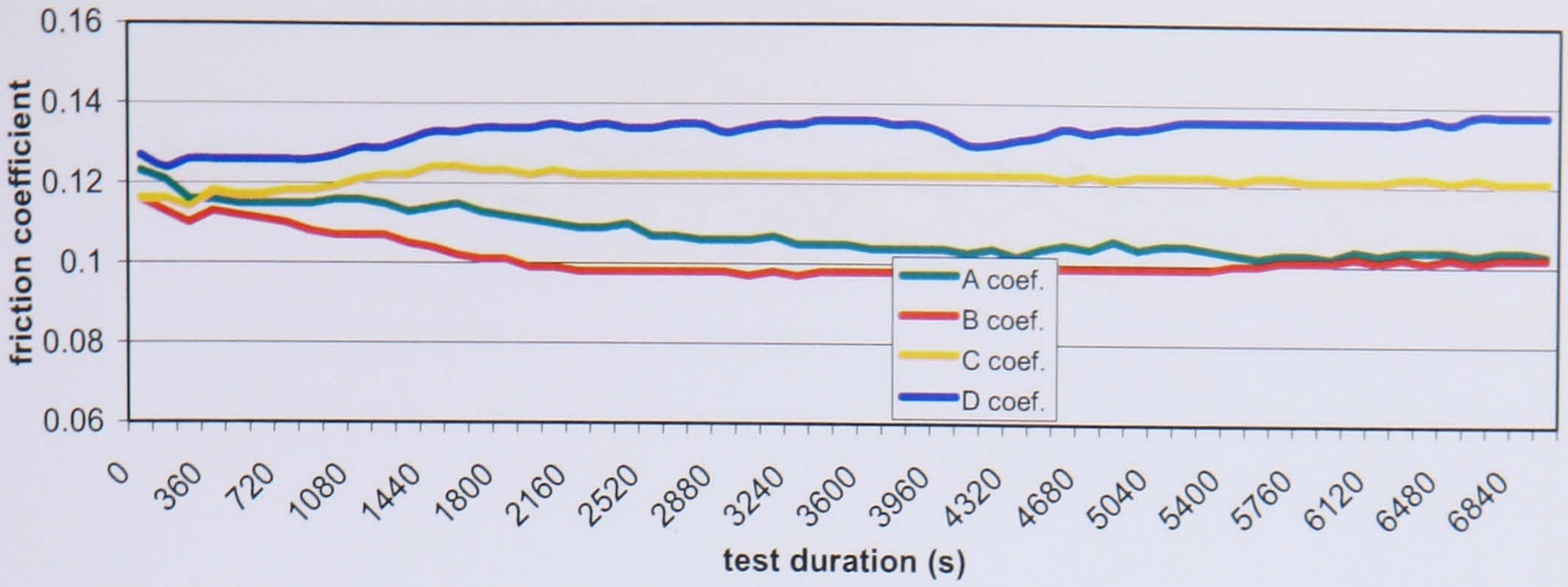

Figure D.9 Friction coefficient, test 5, R600a, MO, 25°C

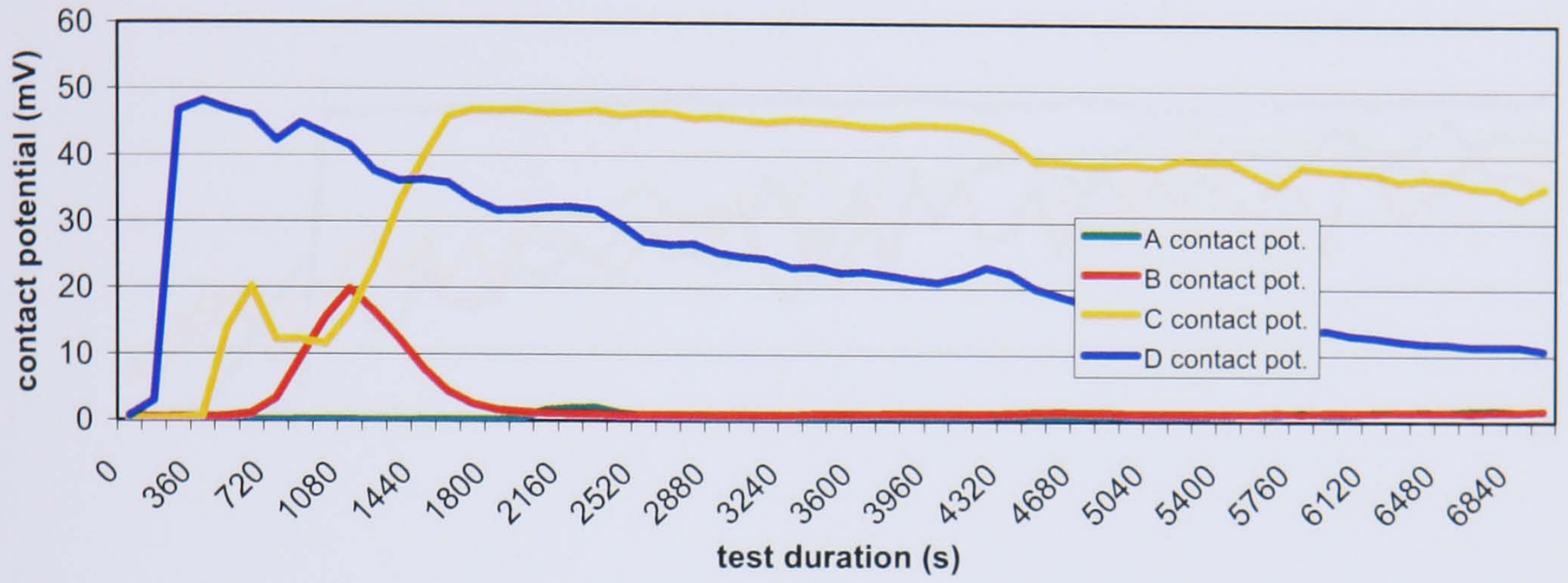

Figure D.10 Contact potential, test 5, R600a, MO, 25°C

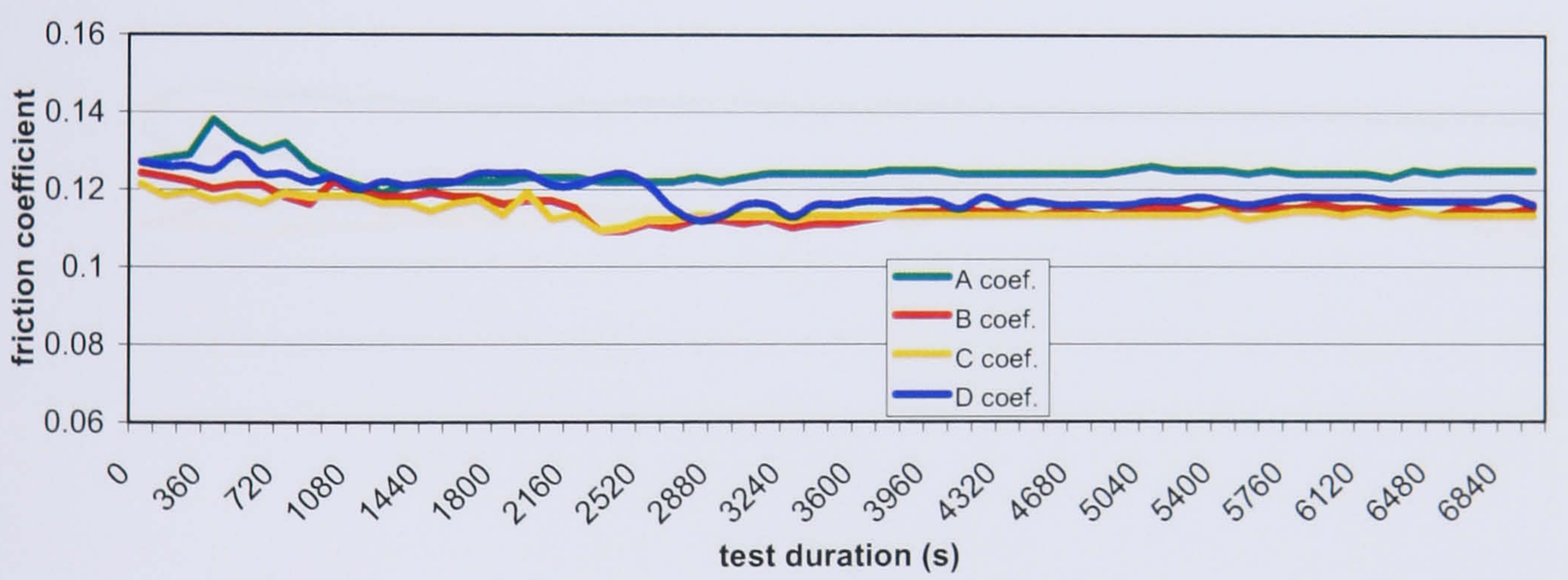

Figure D.11 Friction coefficient, test 6, R600a, MO+, 25°C

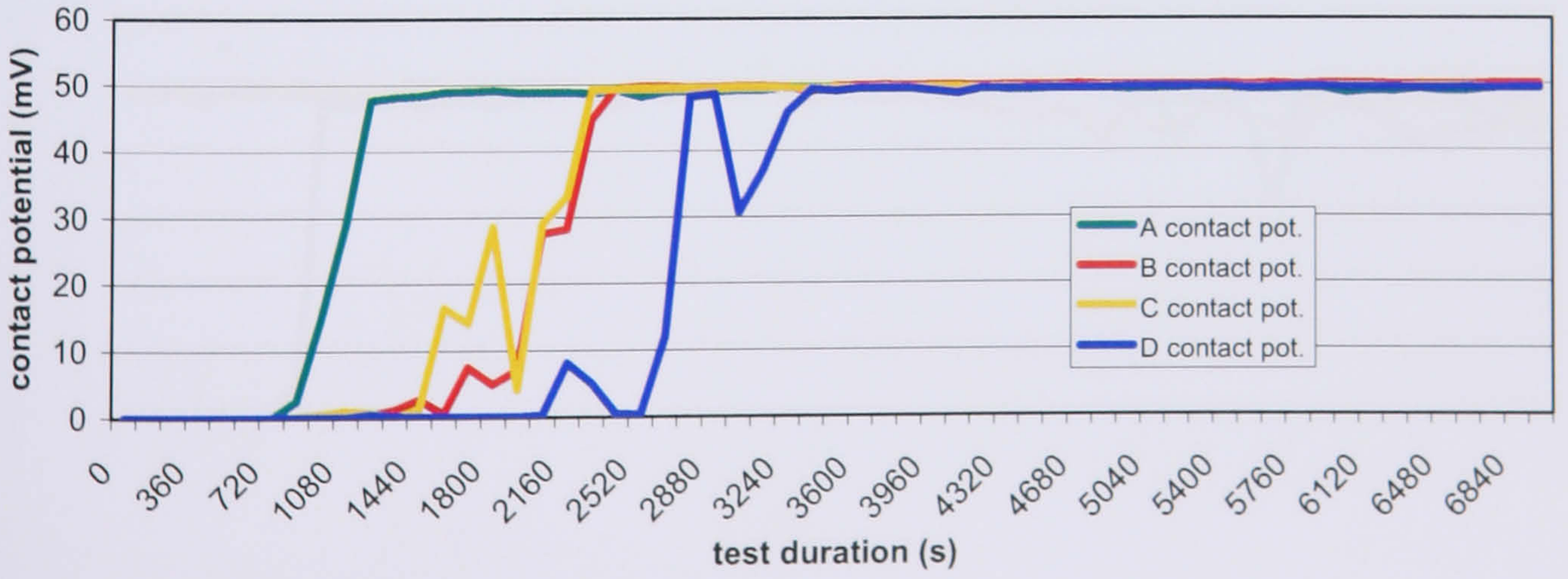

Figure D.12 Contact potential, test 6, R600a, MO+, 25°C

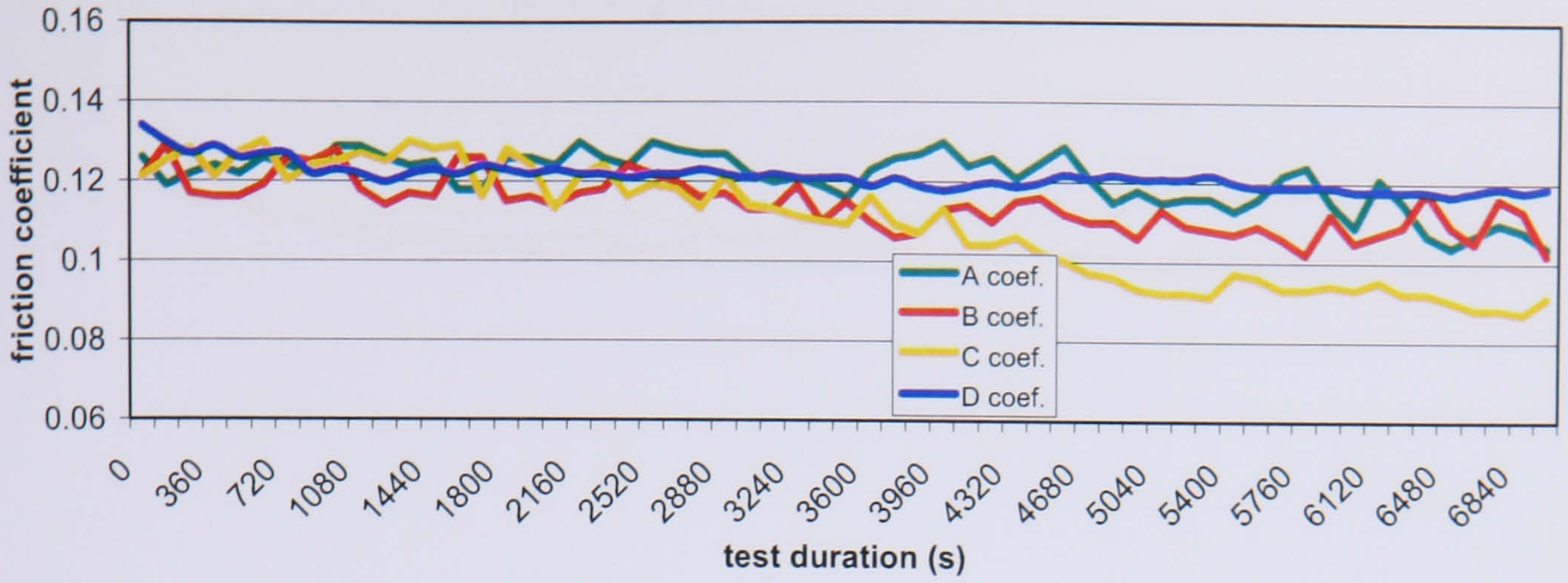

Figure D.13 Friction coefficient, test 7, R600a, POE+, 25°C

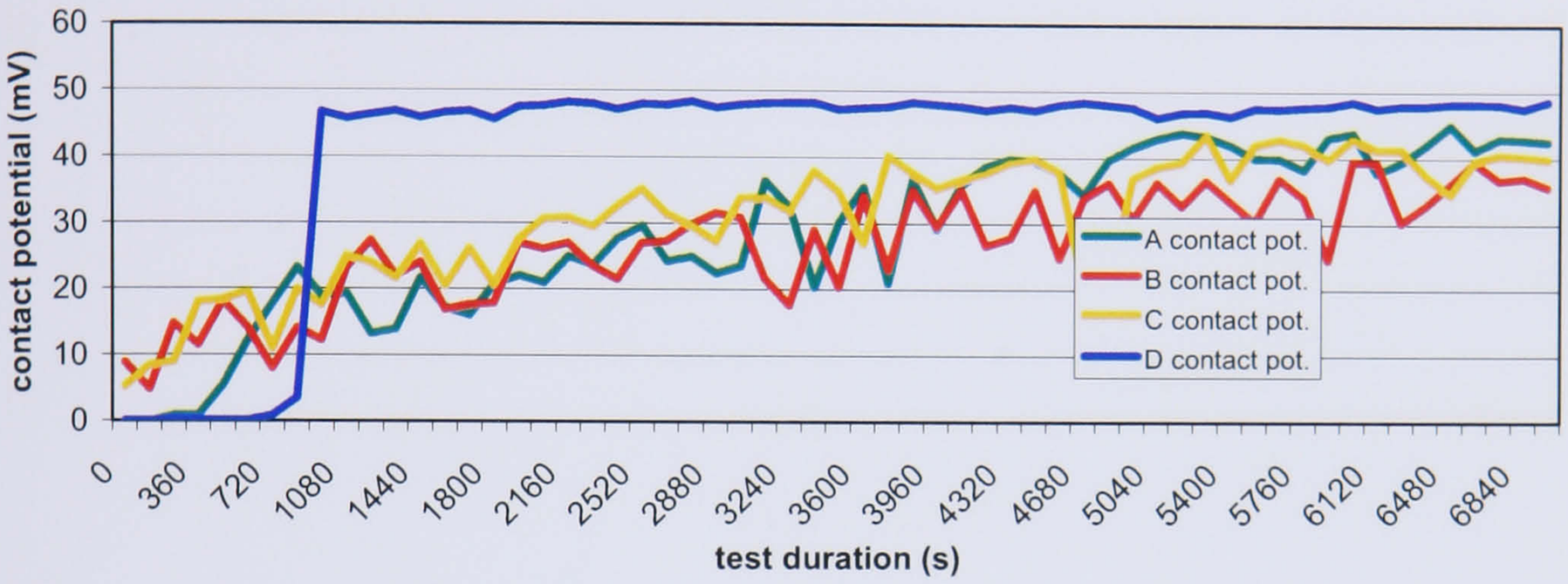

Figure D.14 Contact potential, test 7, R600a, POE+, 25°C

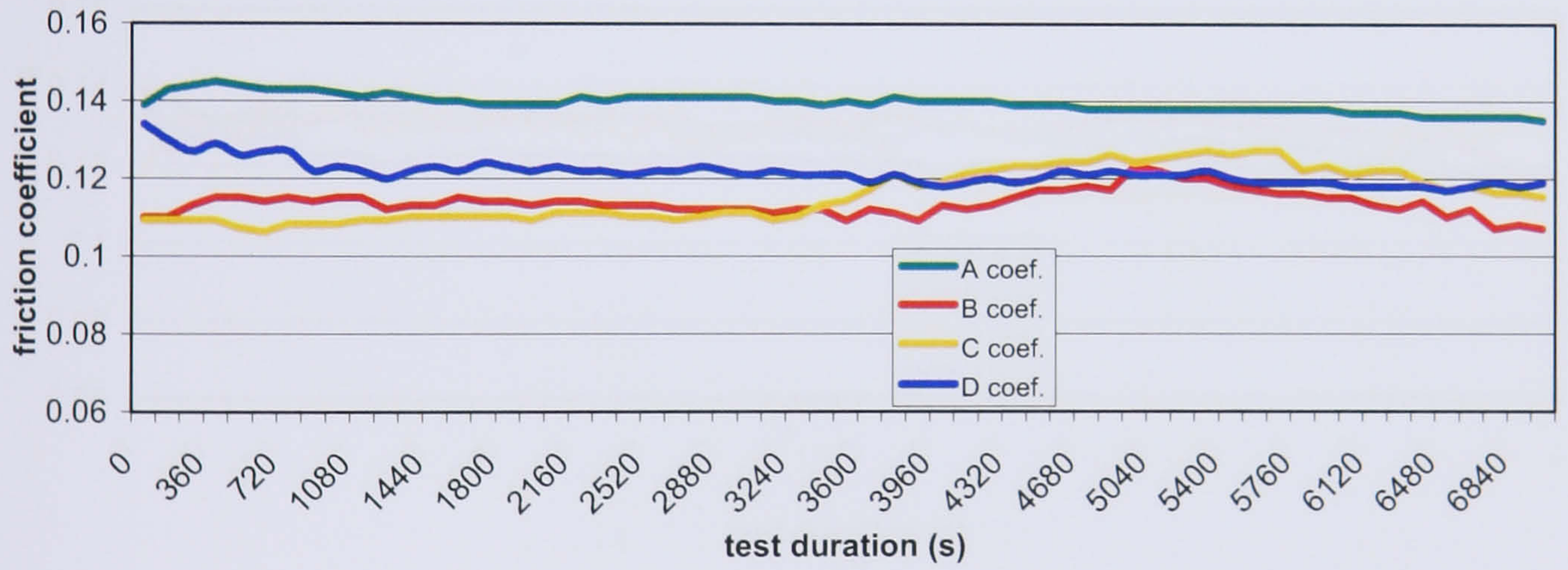

Figure D.15 Friction coefficient, test 8, R134a, POE+, 25°C

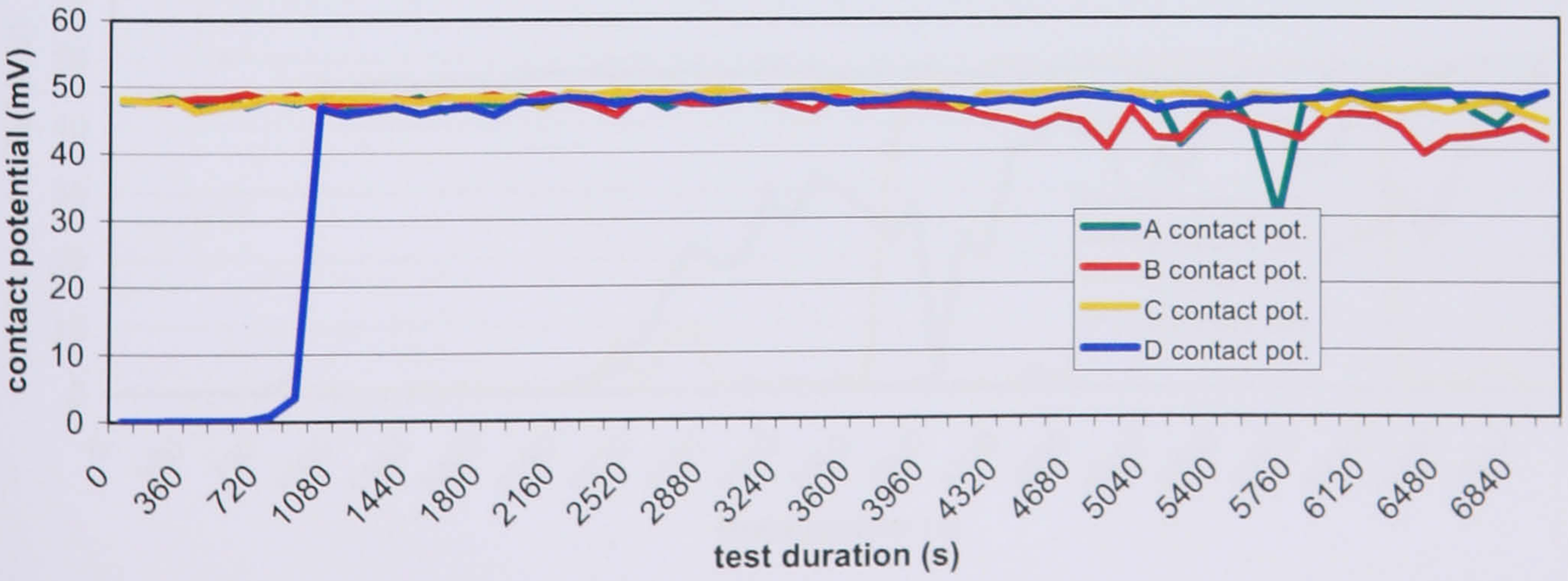

Figure D.16 Contact potential, test 8, R134a, POE+, 25°C

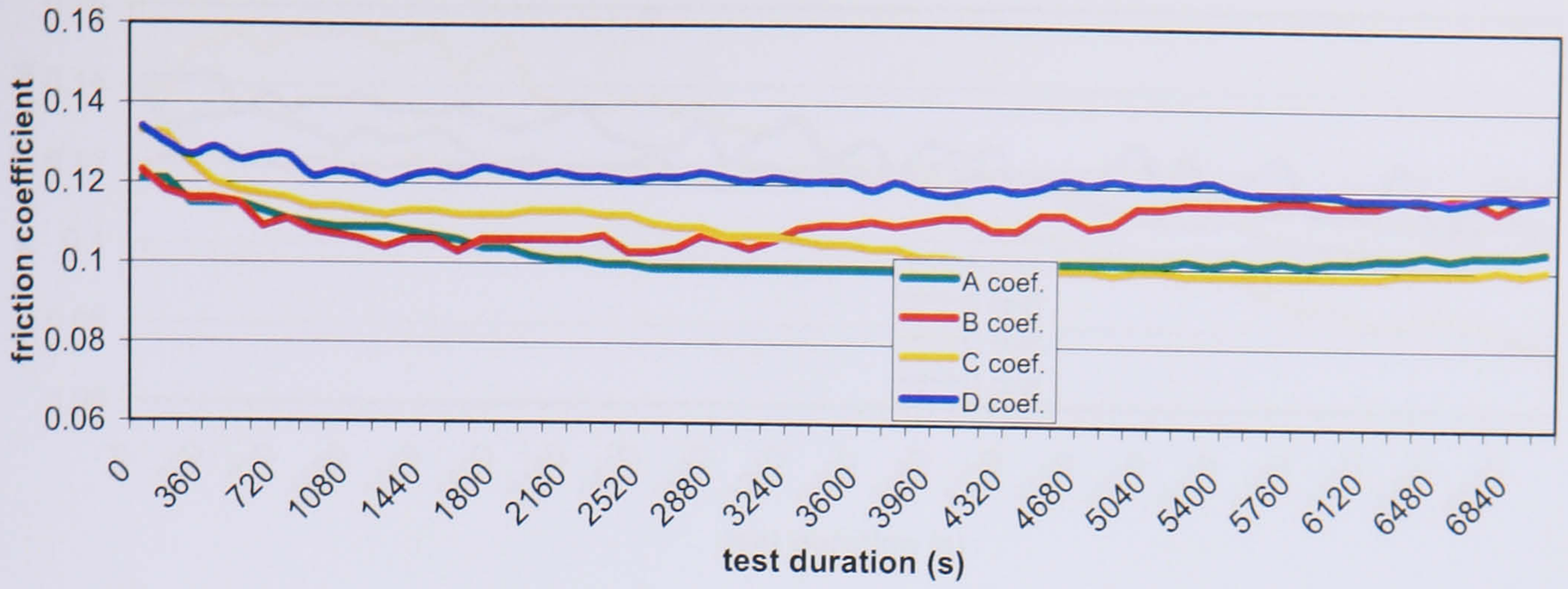

Figure D.17 Friction coefficient, test 9, R600a, MO, 57°C

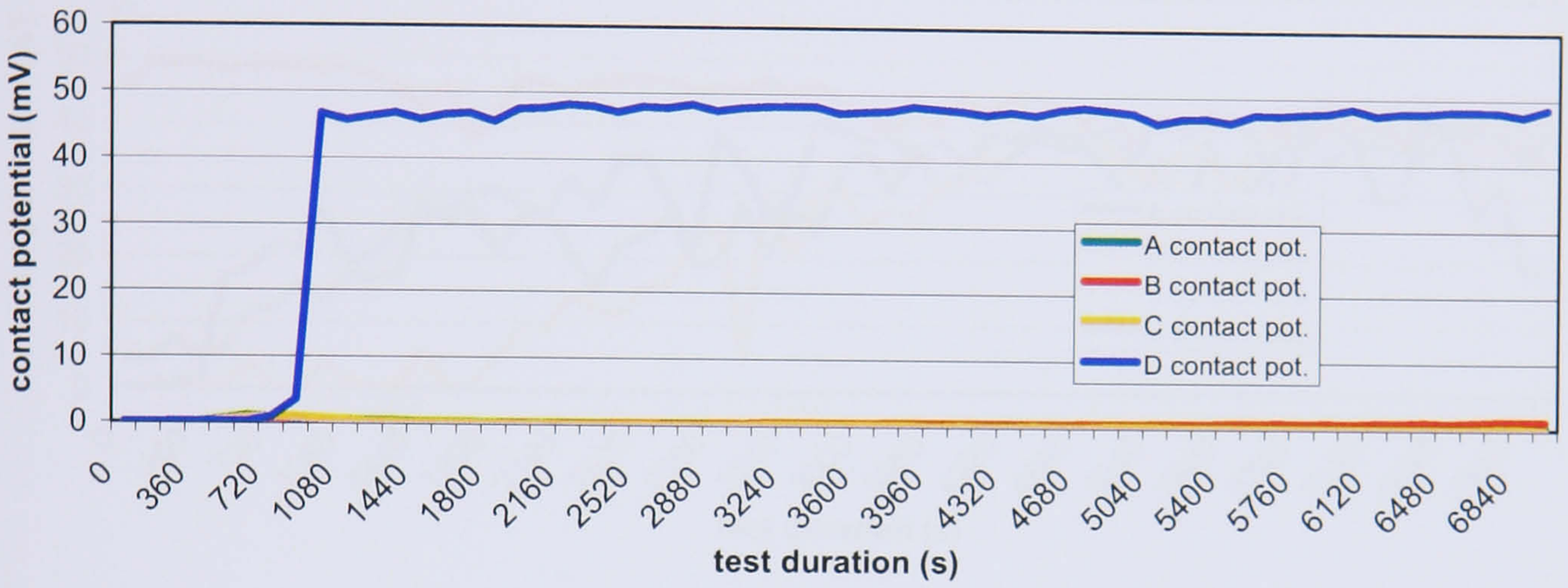

Figure D.18 Contact potential, test 9, R600a, MO, 57°C

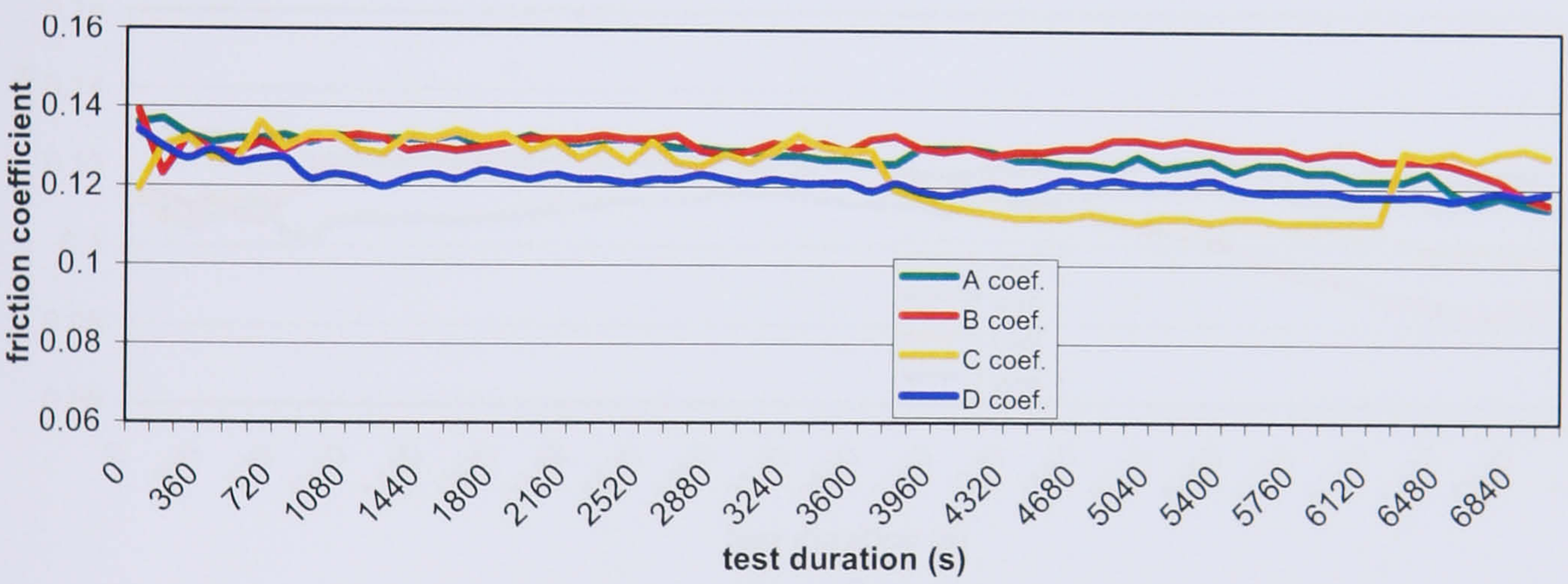

Figure D.19 Friction coefficient, test 10, R600a, MO+, 57°C

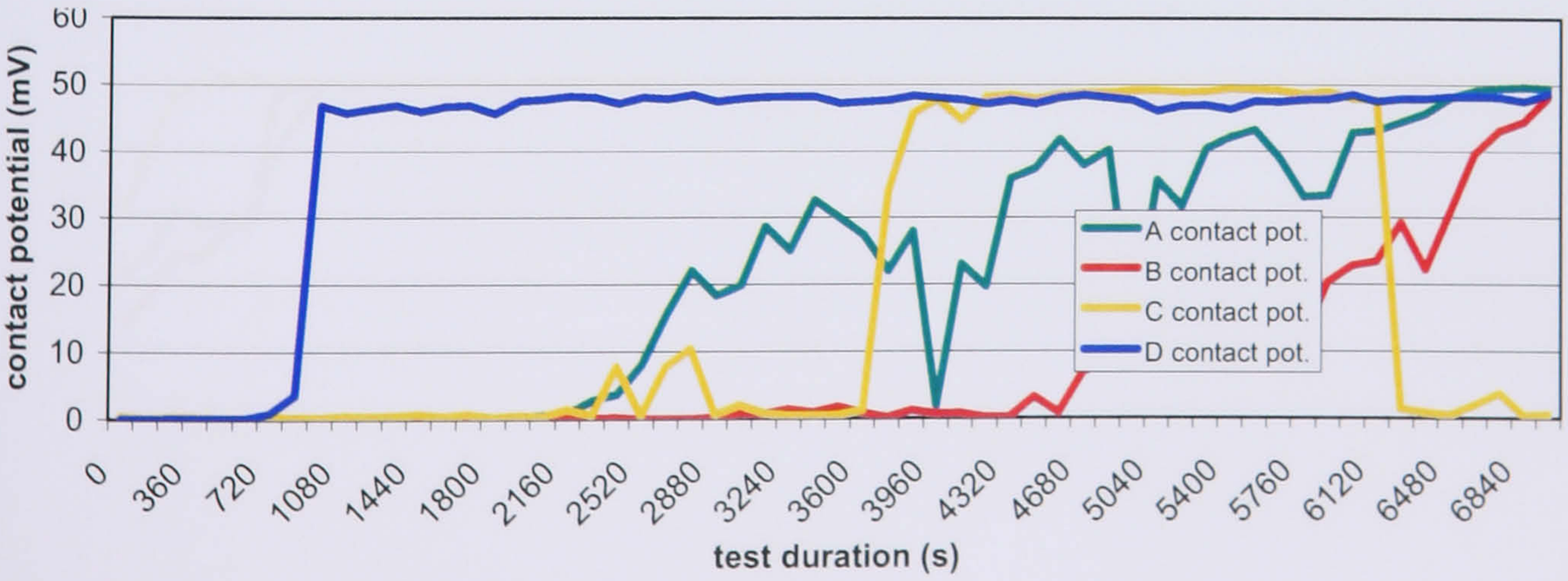

Figure D.20 Contact potential, test 10, R600a, MO+, 57°C

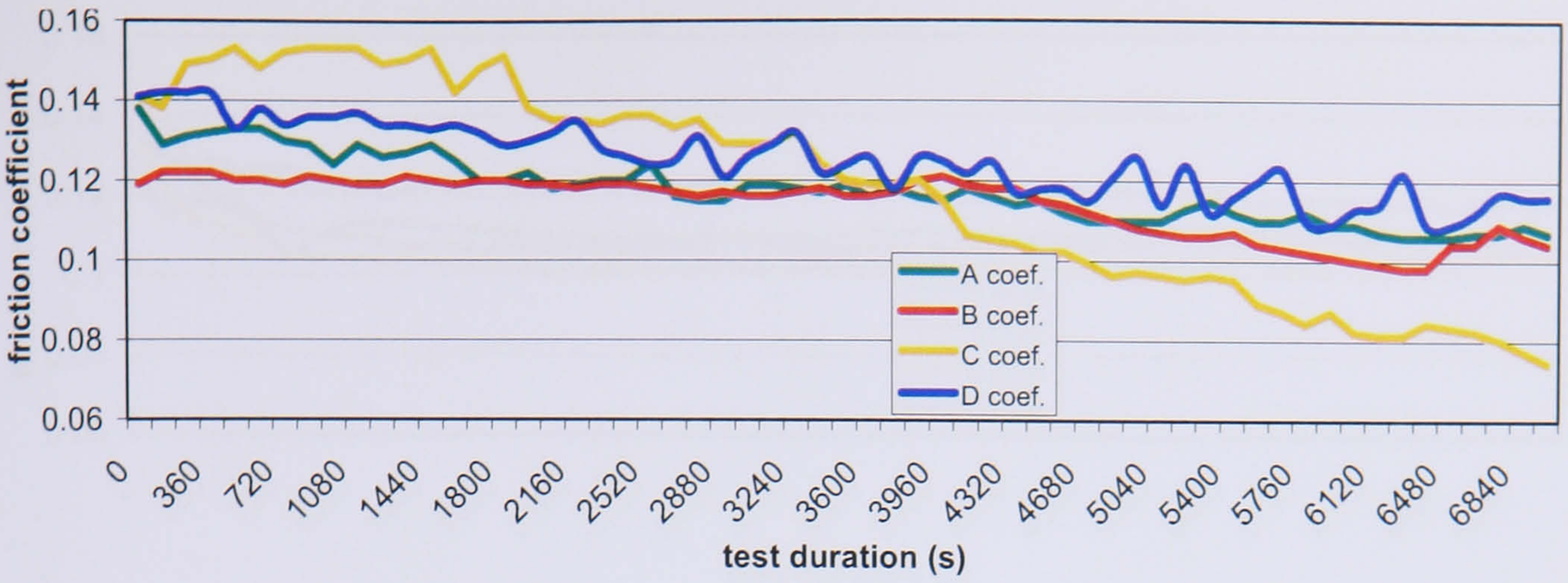

Figure D.21 Friction coefficient, test 11, R600a, POE+, 57°C

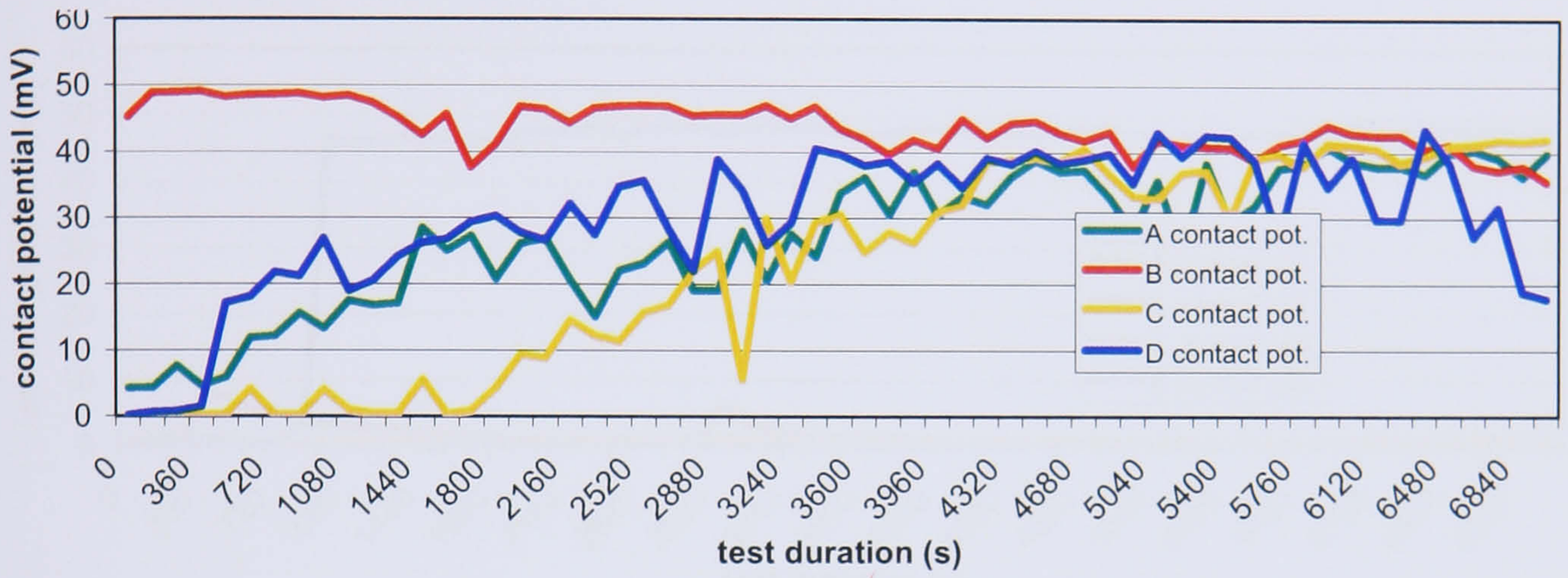

Figure D.22 Contact potential, test 11, R600a, POE+, 57°C

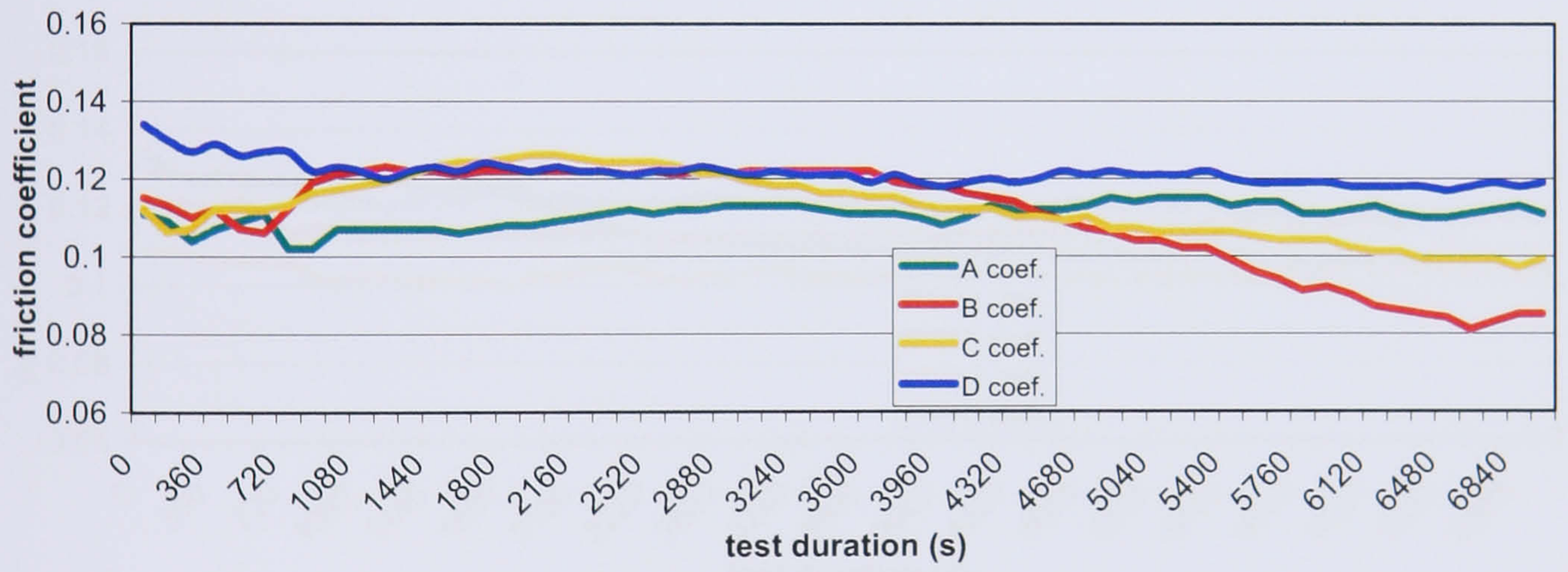

Figure D.23 Friction coefficient, test 12, R134a, POE+, 68°C

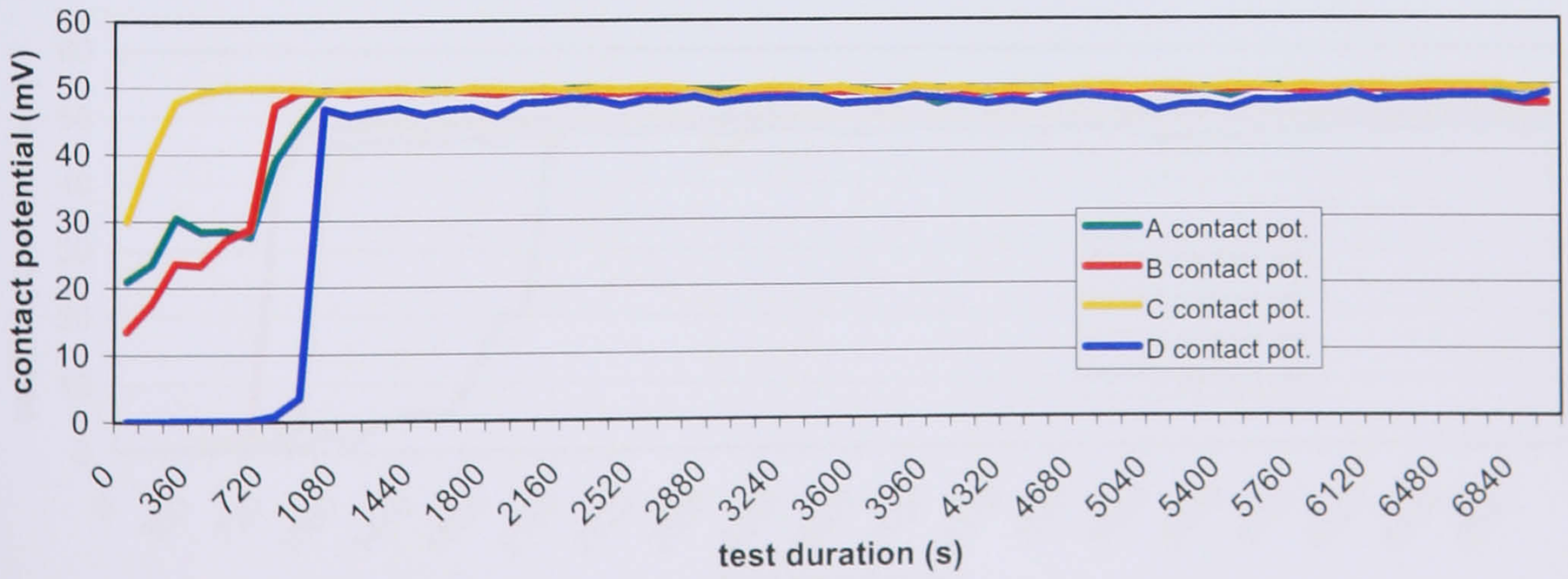

Figure D.24 Contact potential, test 12, R134a, POE+, 68°C

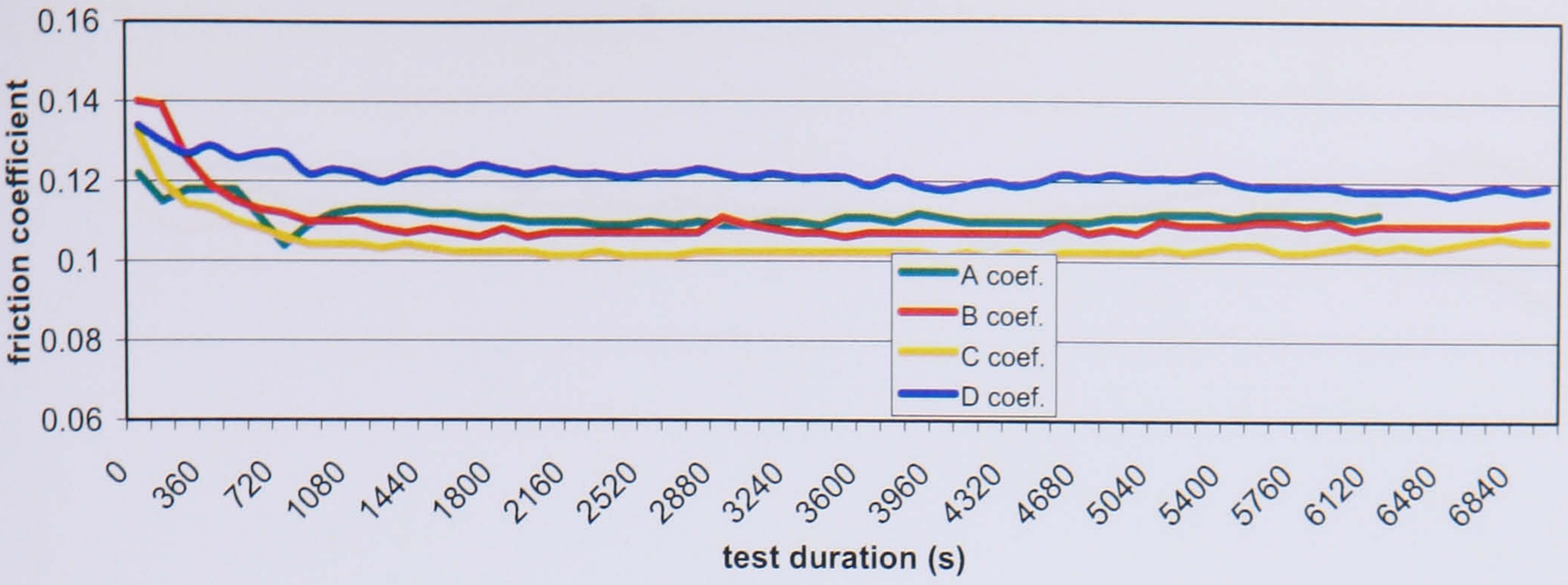

Figure D.25 Friction coefficient, test 13, R600a, MO, 110°C

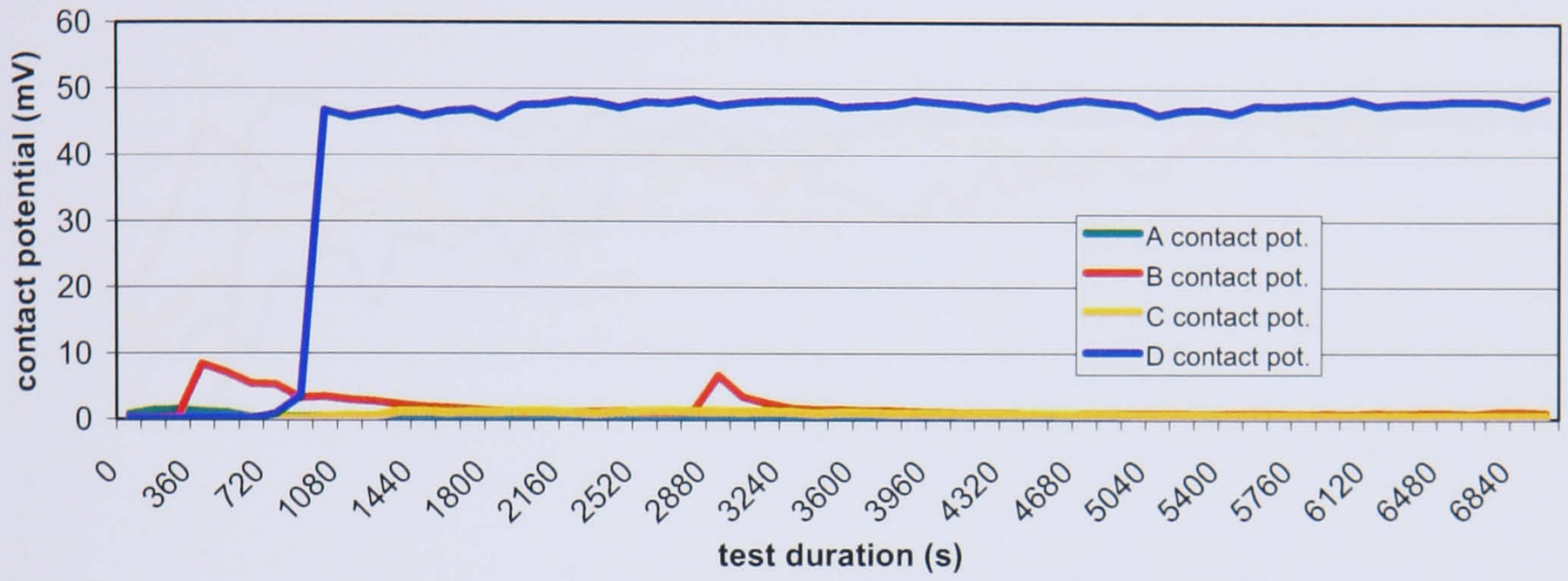

Figure D.26 Contact potential, test 13, R600a, MO, 110°C

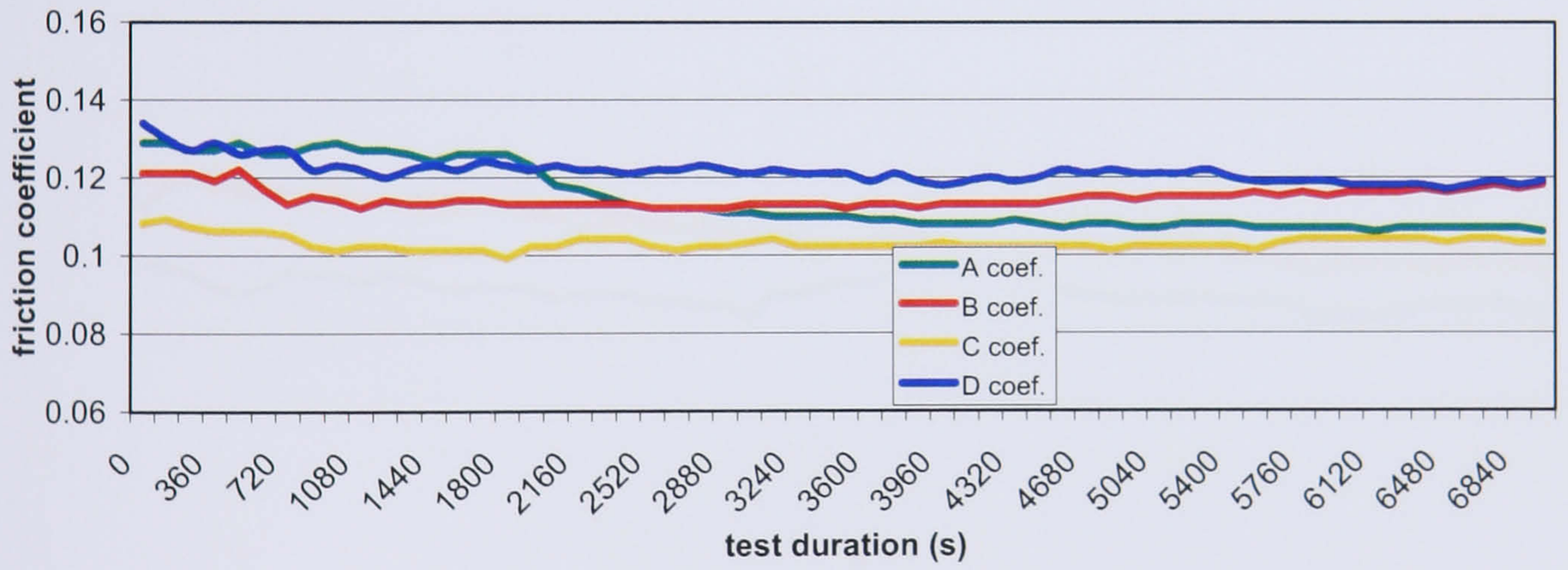

Figure D.27 Friction coefficient, test 14, R600a, MO+, 110°C

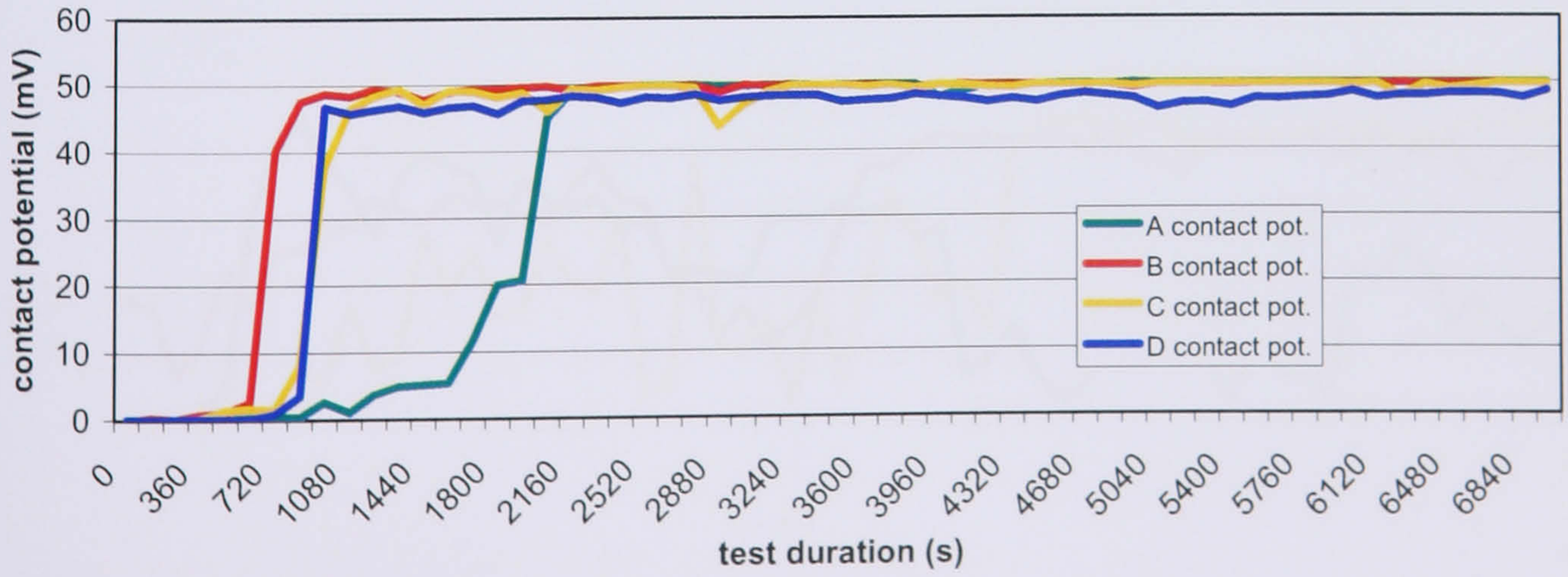

Figure D.28 Contact potential, test 14, R600a, MO+, 110°C

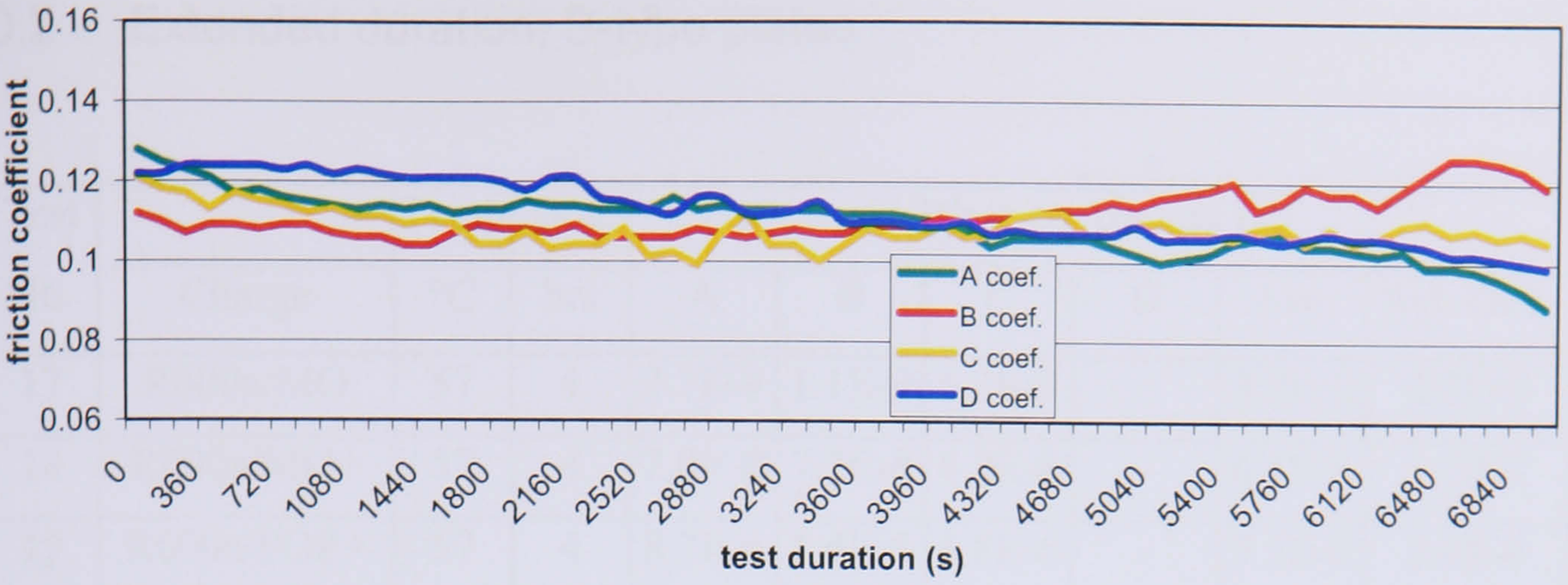

Figure D.29 Friction coefficient, test 15, R600a, POE+, 110°C

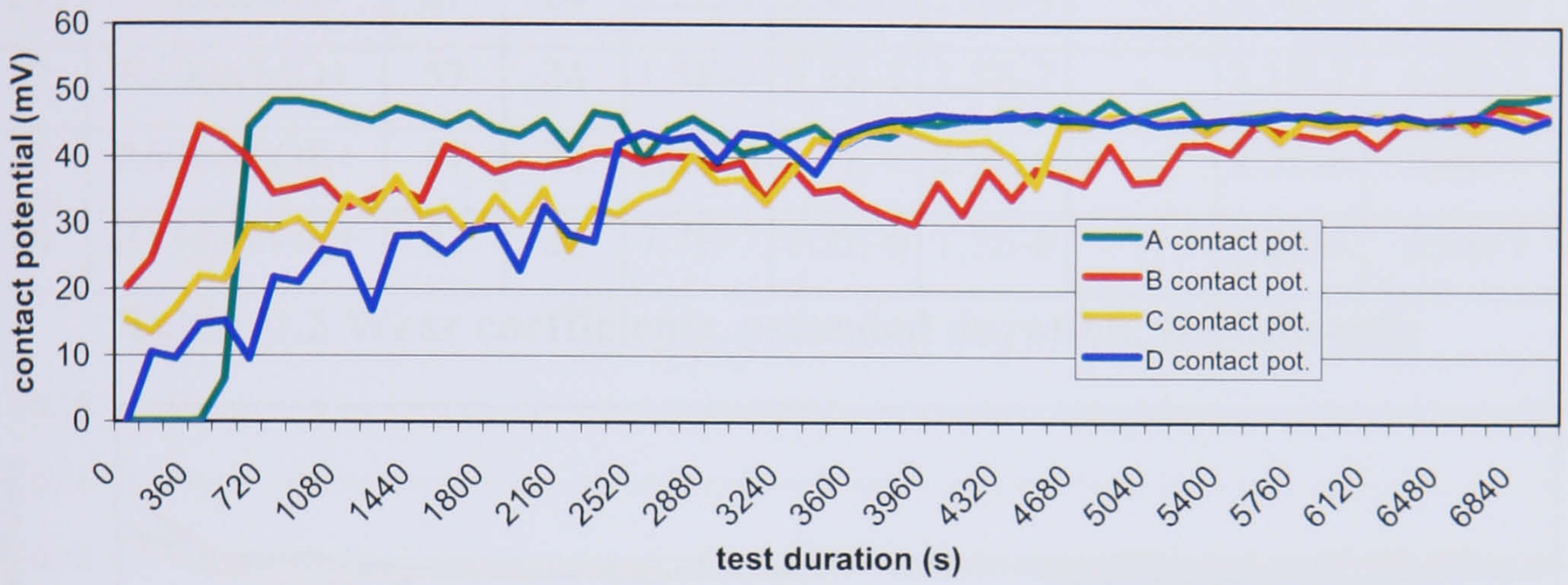

Figure D.30 Contact potential, test 15, R600a, POE+, 110°C

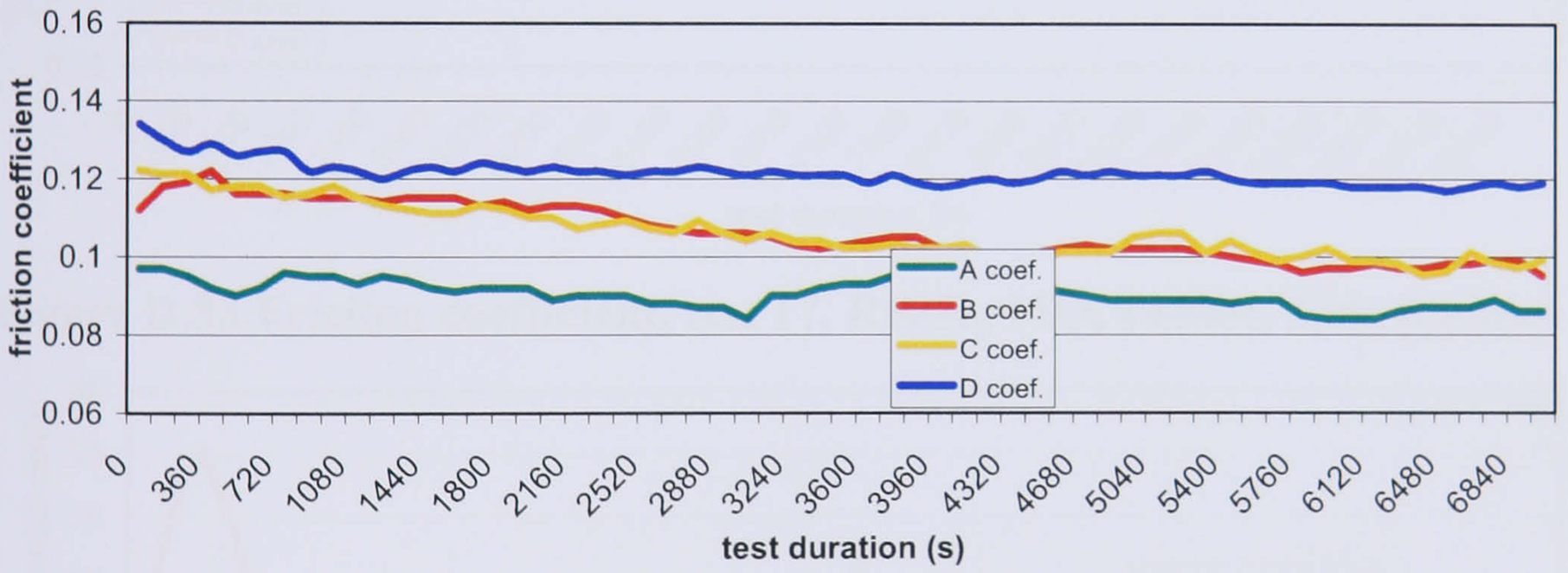

Figure D.31 Friction coefficient, test 16, R134a, POE+, 110°C

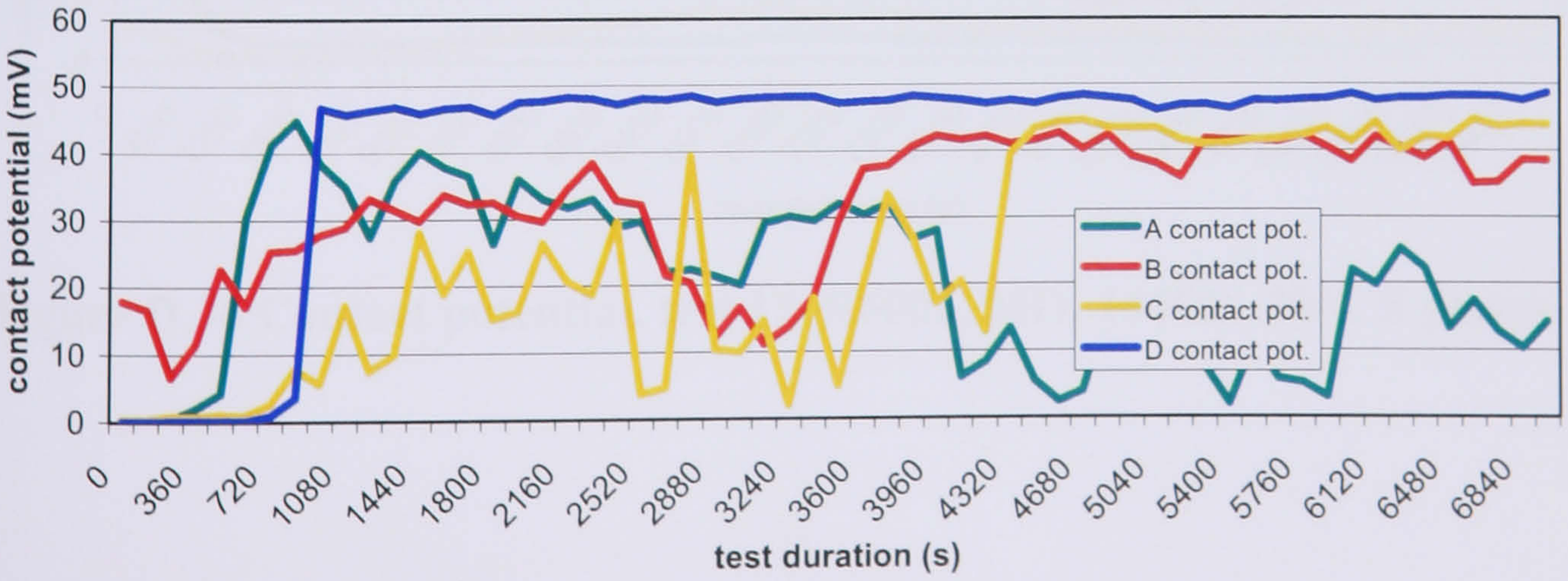

Figure D.32 Contact potential, test 16, R134a, POE+, 110°C

D.2 Extended duration, B-type plates

Test No.	Charge	Temp °C	Dur. hrs	Wear coefficient (k) A	B	C	D	Ave.	Std. Dev.
17	R600a/MO	57	4	3.7E-9	1.1E-9	6.2E-9	-	3.7E-9	2.5E-9
18	R600a/MO+	57	4	7.0E-8	7.2E-8	4.2E-8	-	6.1E-8	1.7E-8
19	R600a/POE+	57	4	8.2E-6	1.4E-5	6.8E-6	-	9.5E-6	3.6E-6
20	R134a/POE+	57	4	7.1E-6	3.4E-6	4.8E-6	-	5.1E-6	1.9E-6
21	R600a/MO	57	24	3.2E-9	3.4E-9	1.5E-9	-	2.7E-9	1.1E-9
22	R600a/MO+	57	24	1.5E-7	3.3E-7	1.5E-7	-	2.1E-7	1.0E-7
23	R600a/POE+	57	24	2.2E-6	1.7E-6	2.9E-6	-	2.3E-6	5.8E-7
24	R134a/POE+	57	24	7.7E-7	1.2E-6	1.5E-6	-	1.2E-6	3.9E-7

Table D.2 Wear coefficients, extended duration, B-plate tests

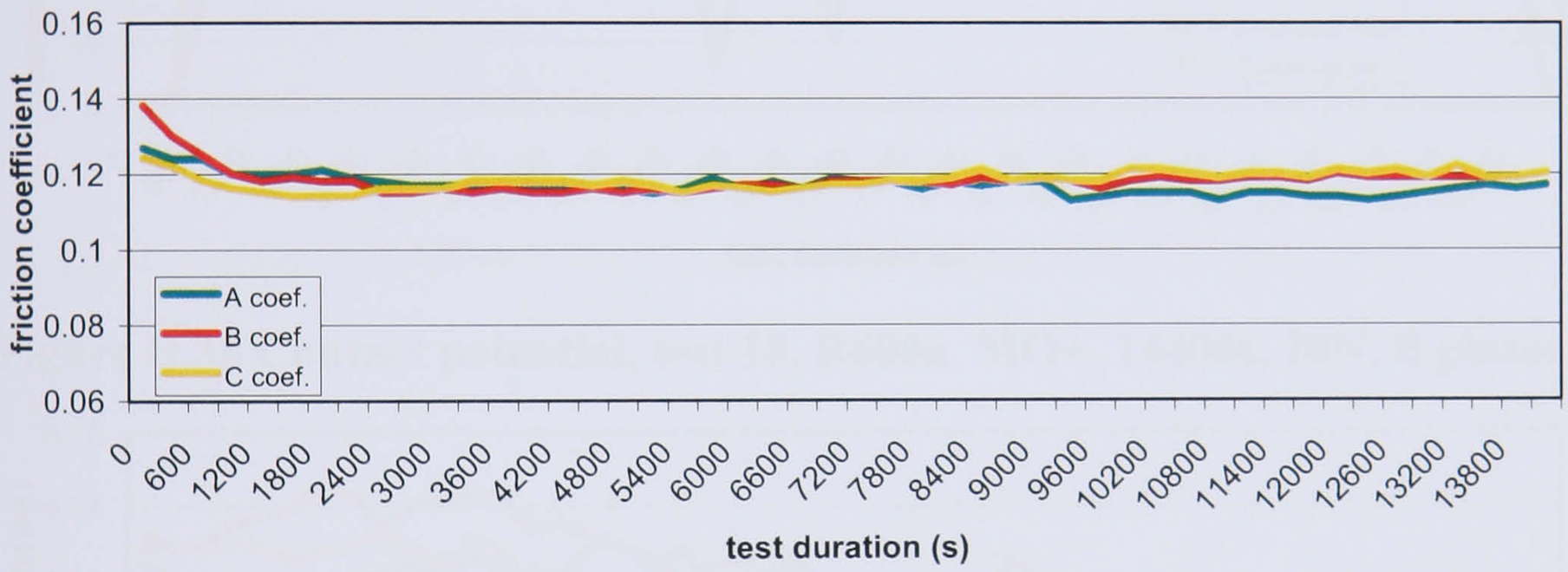

Figure D.33 Friction coefficient, test 17, R600a, MO, 14400s, 20N, B plates

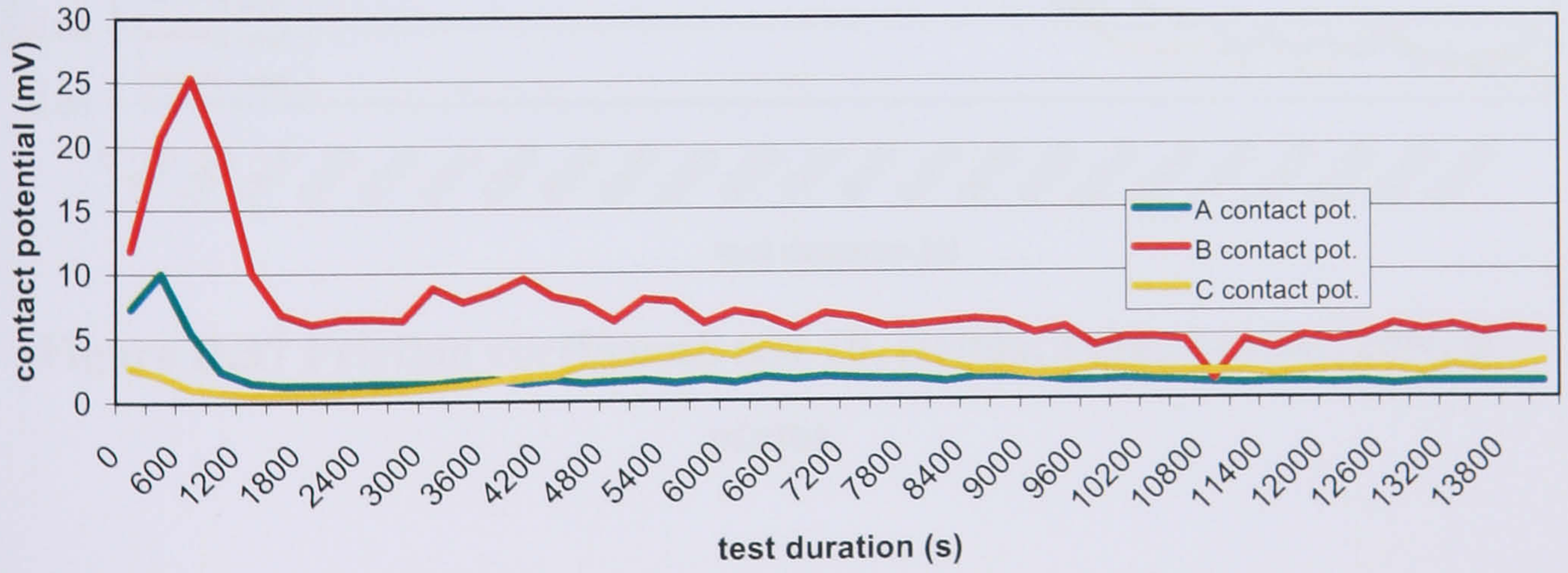

Figure D.34 Contact potential, test 17, R600a, MO, 14400s, 20N, B plates

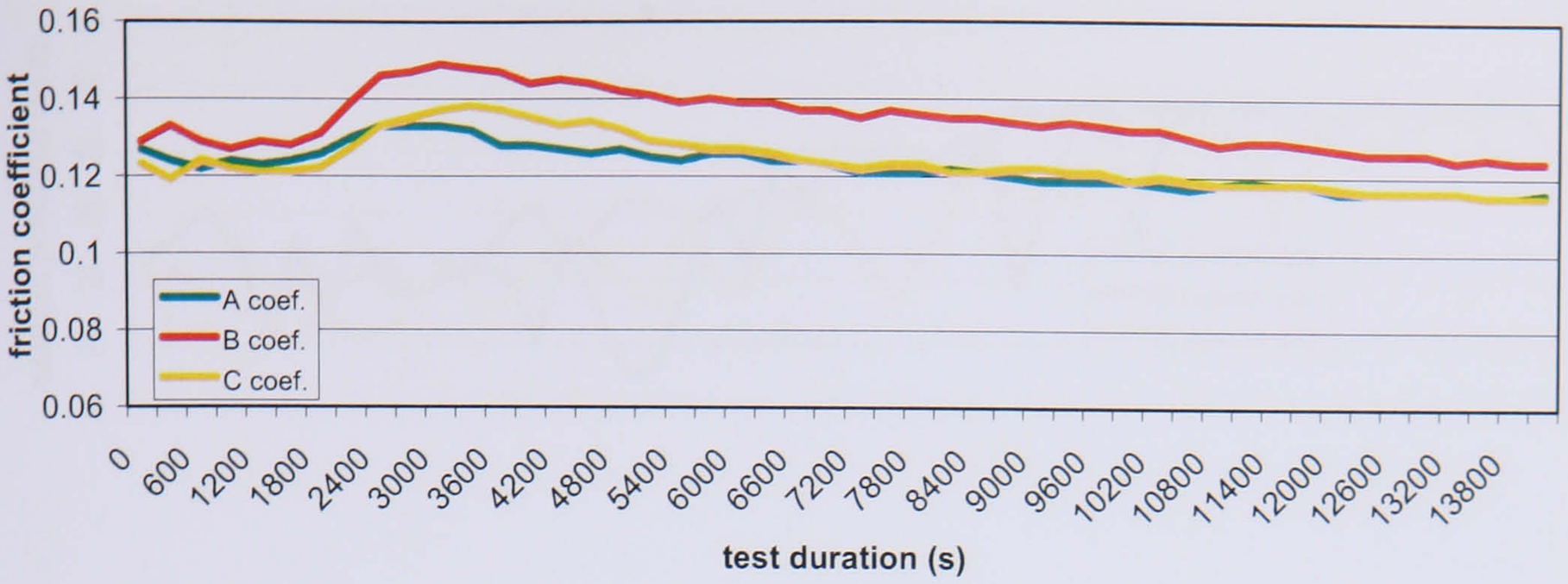

Figure D.35 Friction coefficient, test 18, R600a, MO+, 14400s, 20N, B plates

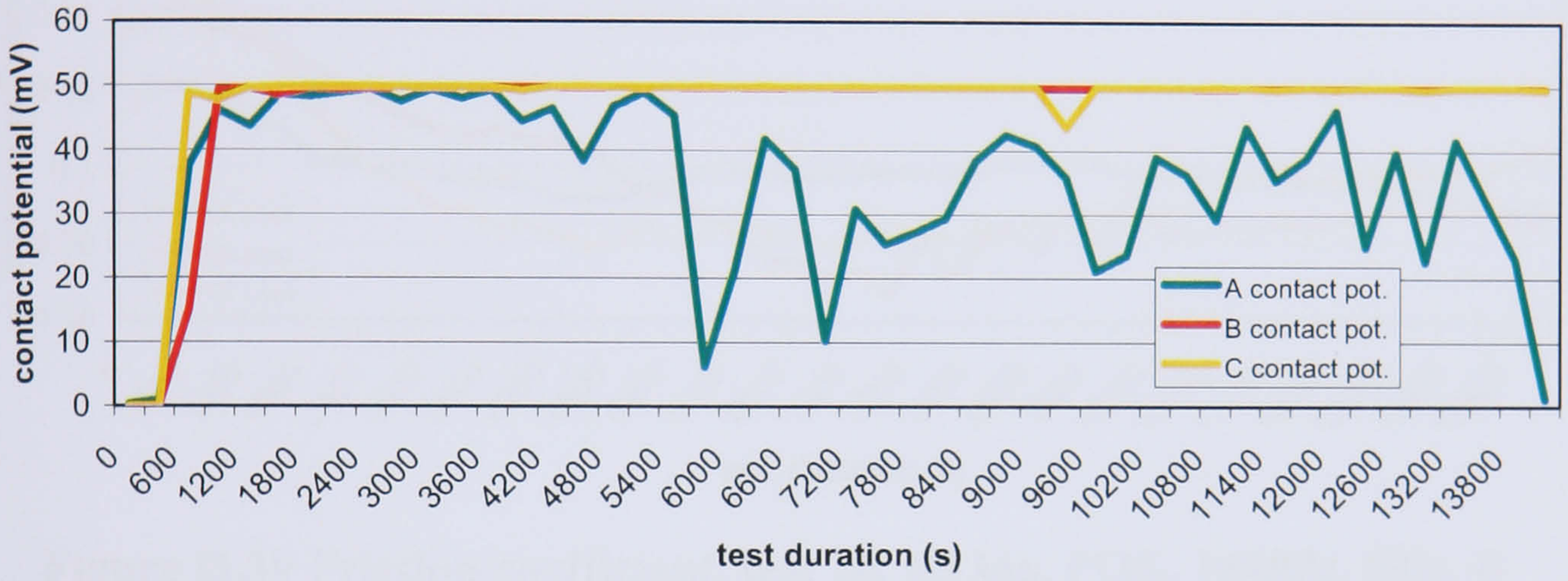

Figure D.36 Contact potential, test 18, R600a, MO+, 14400s, 20N, B plates

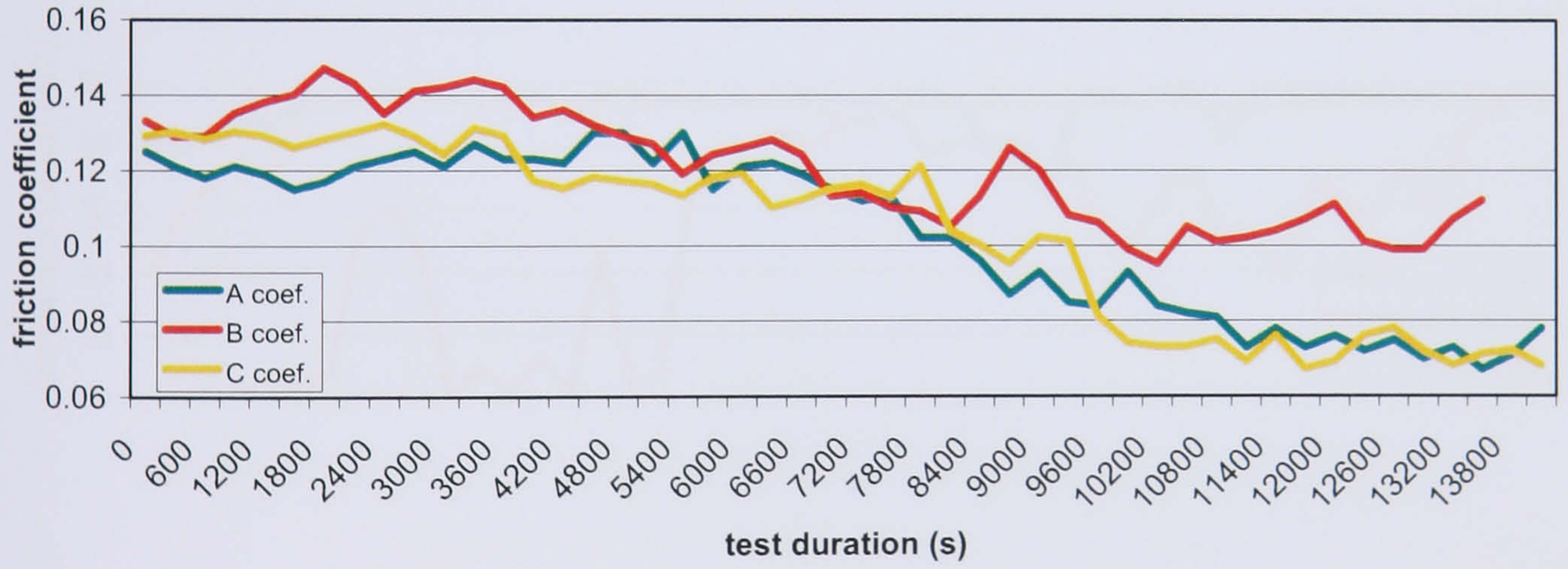

Figure D.37 Friction coefficient, test 19, R600a, POE, 14400s, 20N, B plates

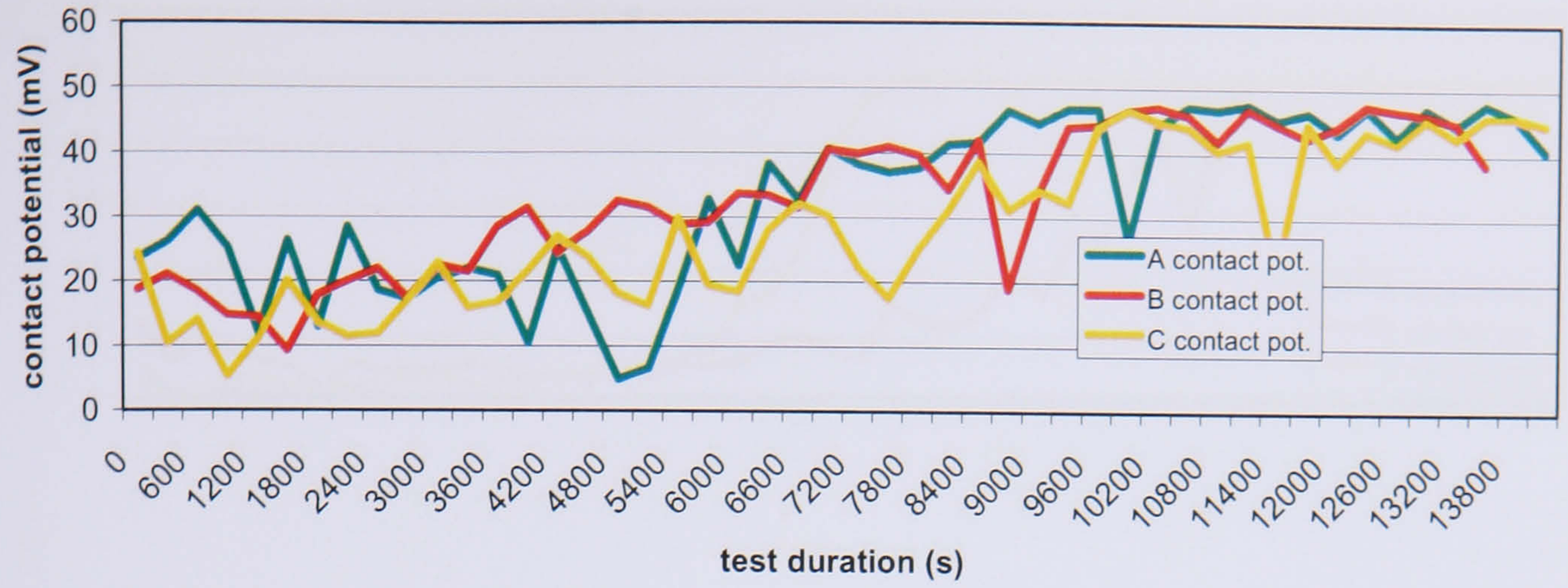

Figure D.38 Contact potential, test 19, R600a, POE, 14400s, 20N, B plates

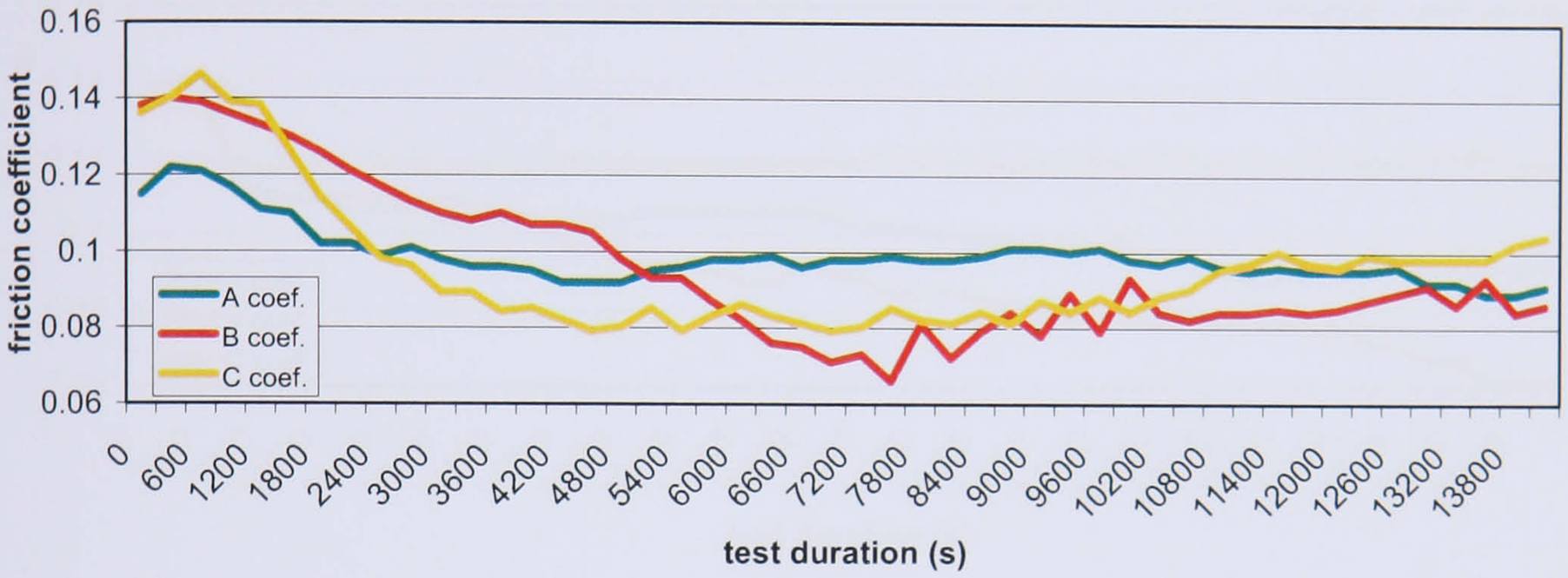

Figure D.39 Friction coefficient, test 20, R134a, POE, 14400s, 20N, B plates

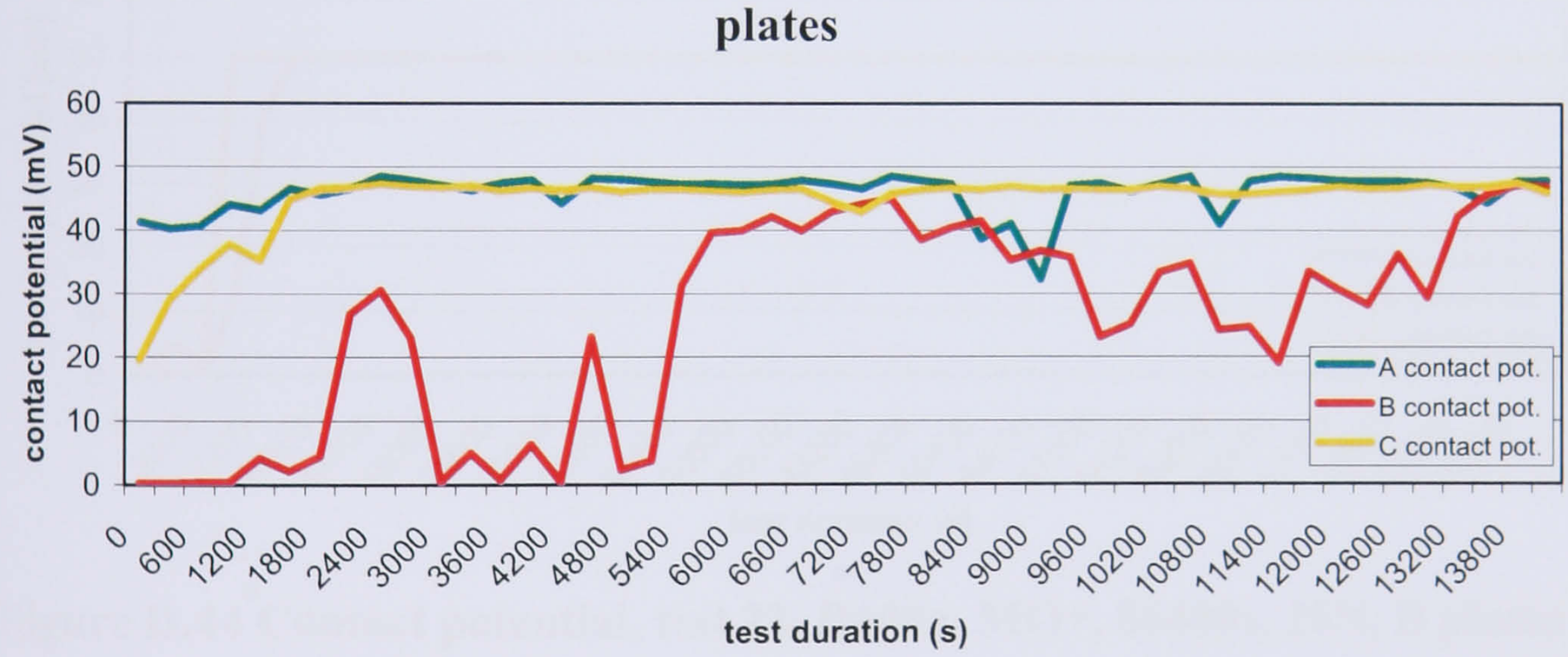

Figure D.40 Contact potential, test 20, R134a, POE, 14400s, 20N, B plates

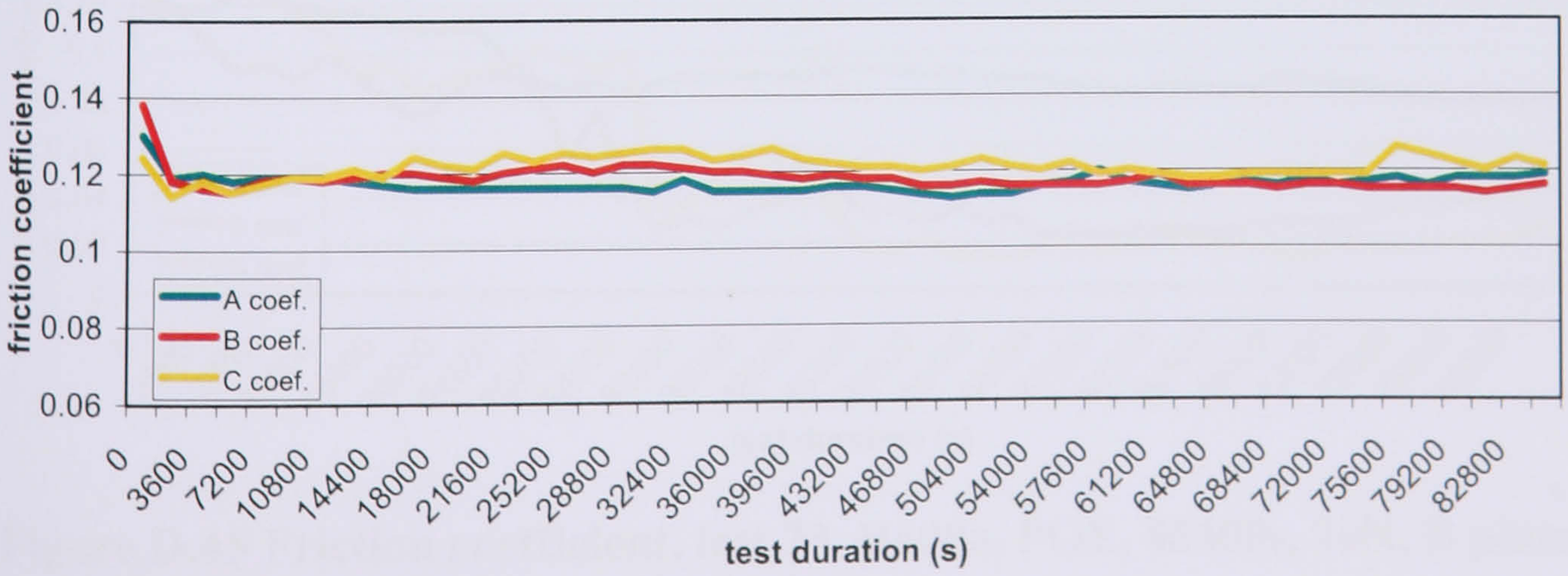

Figure D.41 Friction coefficient, test 21, R600a, MO, 86400s, 20N, B plates

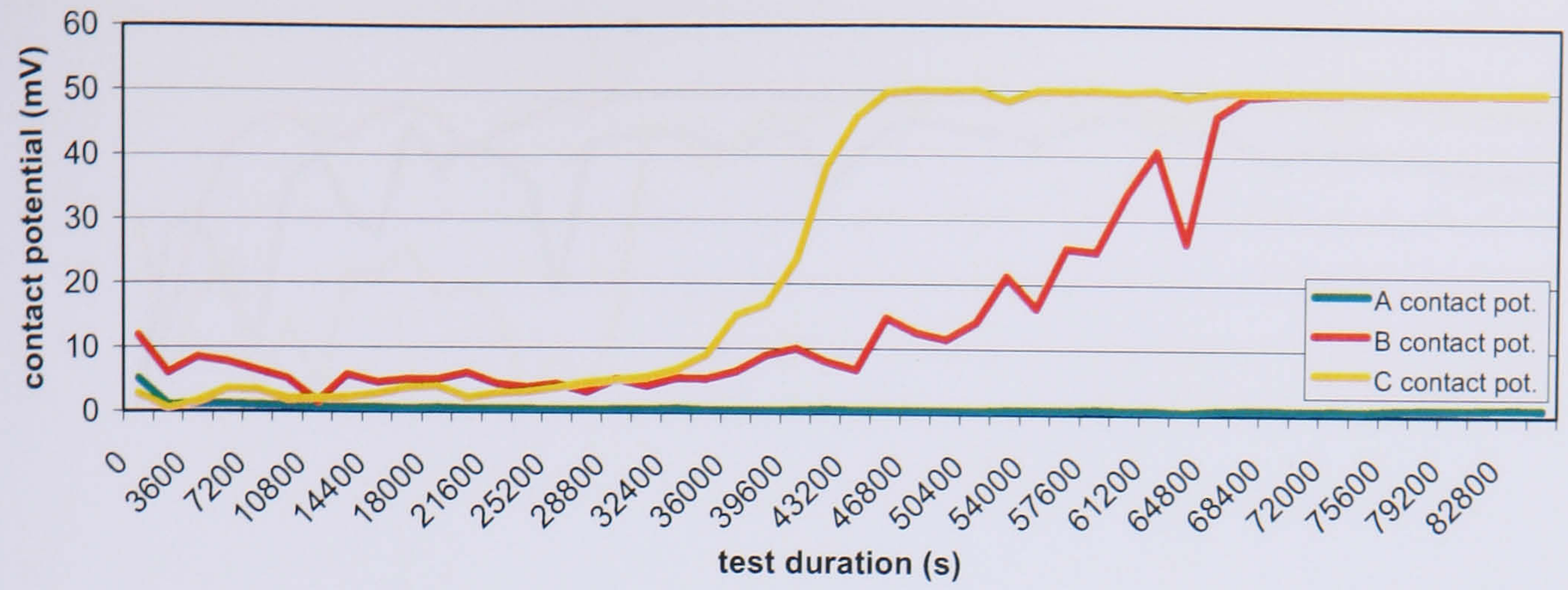

Figure D.42 Contact potential, test 21, R600a, MO, 86400s, 20N, B plates

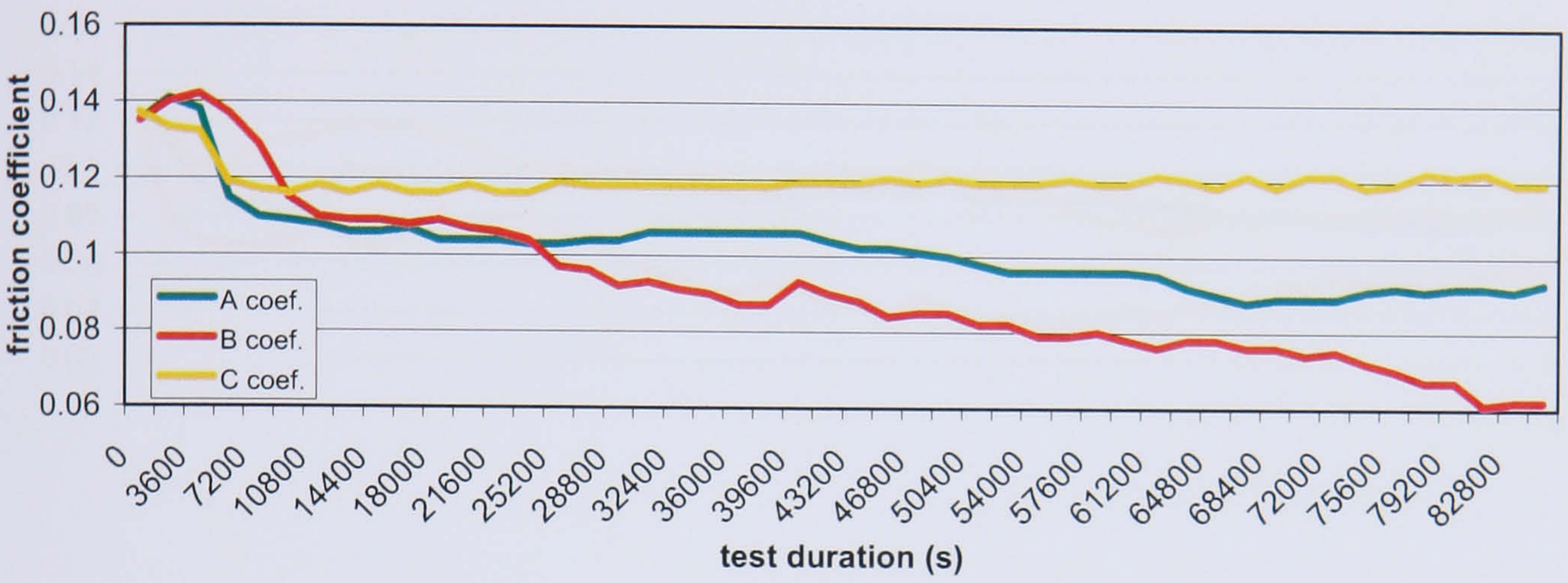

Figure D.43 Friction coefficient, test 22, R600a, MO+, 86400s, 20N, B plates

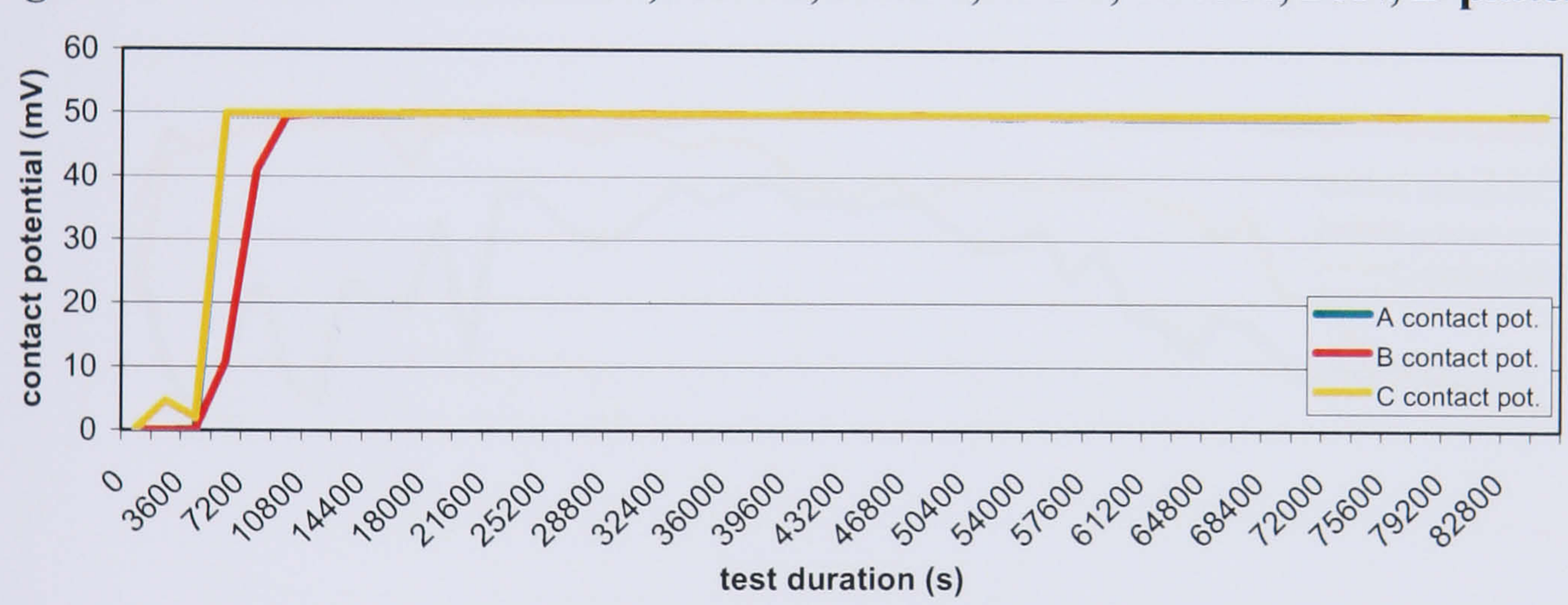

Figure D.44 Contact potential, test 22, R600a, MO+, 86400s, 20N, B plates

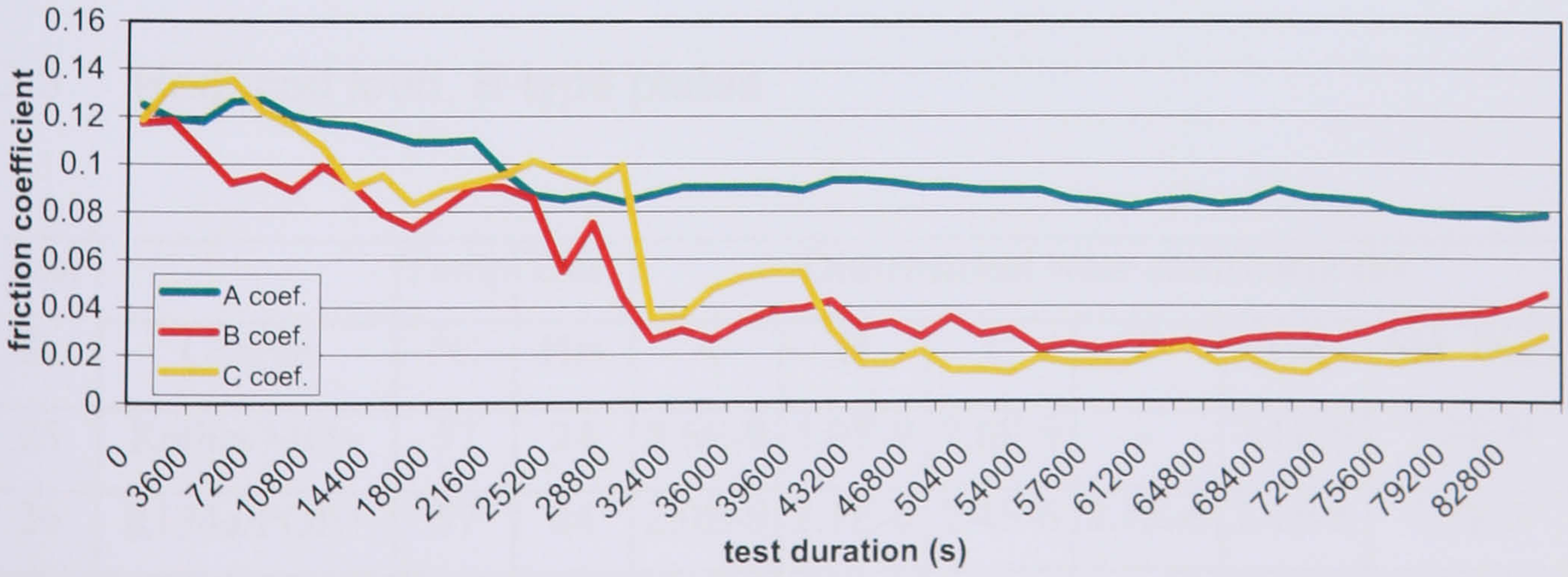

Figure D.45 Friction coefficient, test 23, R600a, POE, 86400s, 20N, B plates

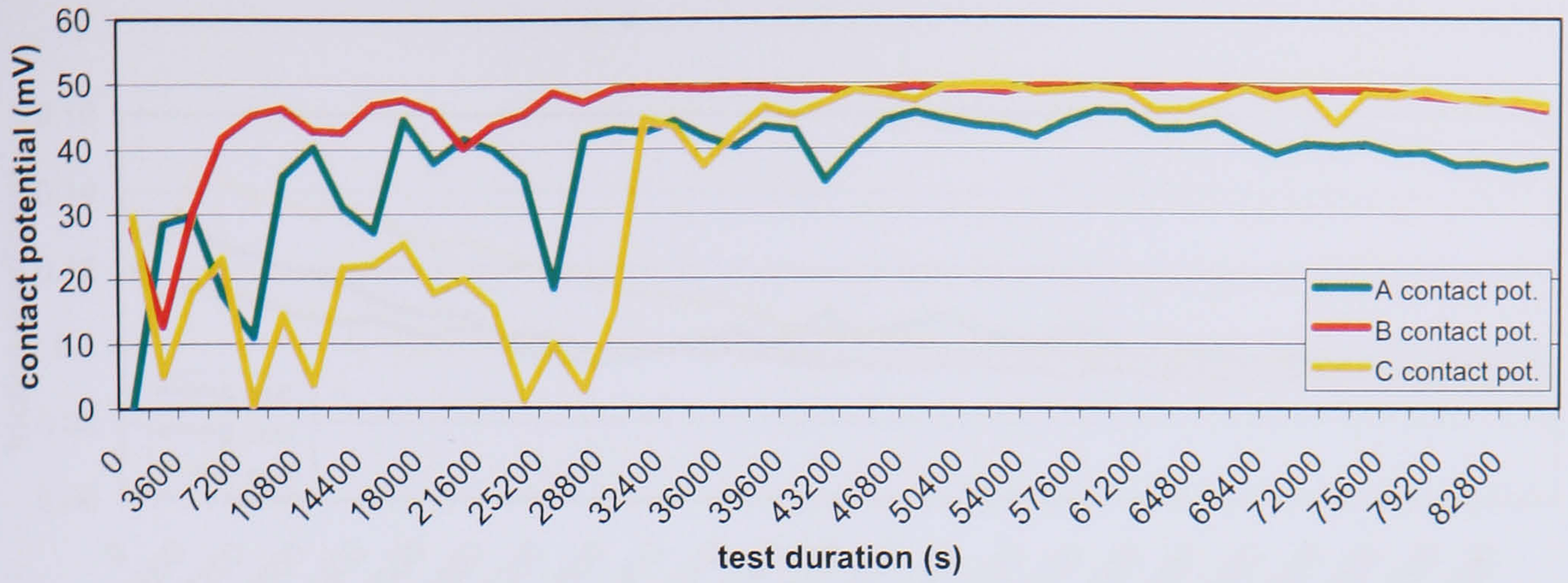

Figure D.46 Contact potential, test 23, R600a, POE, 86400s, 20N, B plates

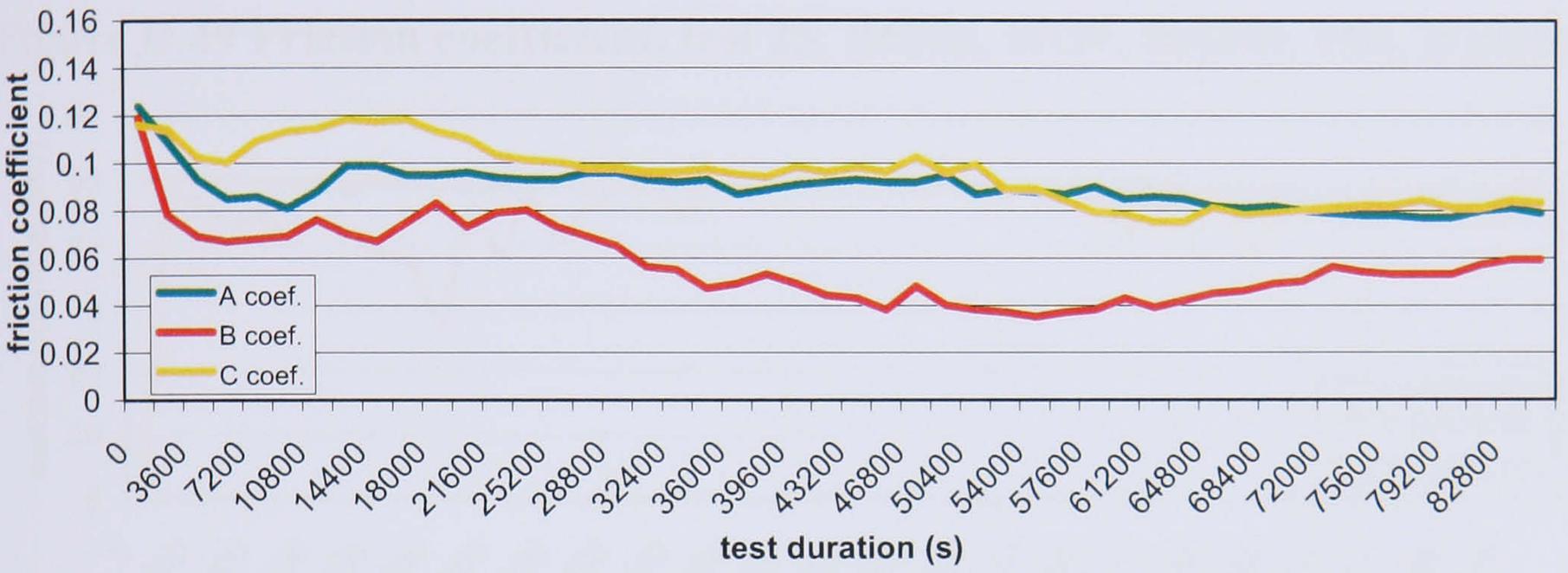

Figure D.47 Friction coefficient, test 24, R134a, POE, 86400s, 20N, B plates

Figure D.48 Contact potential, test 24, R134a, POE, 86400s, 20N, B plates

D.3 Reduced load, B-type plates

Test No.	Charge	Temp °C	Dur. Hrs	Dimensional wear coefficient (k)					
				A	B	C	D	Ave.	Std. Dev.
25	R600a/MO+	57	24	8.6E-9	5.0E-9	7.6E-9	-	7.1E-9	1.9E-9
26	R134a/POE+	57	24	2.0E-6	2.1E-6	2.4E-6	2.1E-6	2.1E-6	1.7E-7
27	R600a/MO+	57	66	1.9E-8	1.0E-8	1.6E-8	-	1.5E-8	4.6E-9
28	R134a/POE+	57	66	7.2E-7	6.6E-7	7.6E-7	1.0E-6	7.9E-7	1.7E-7

Table D.3 Wear coefficients, reduced load, B-plate tests

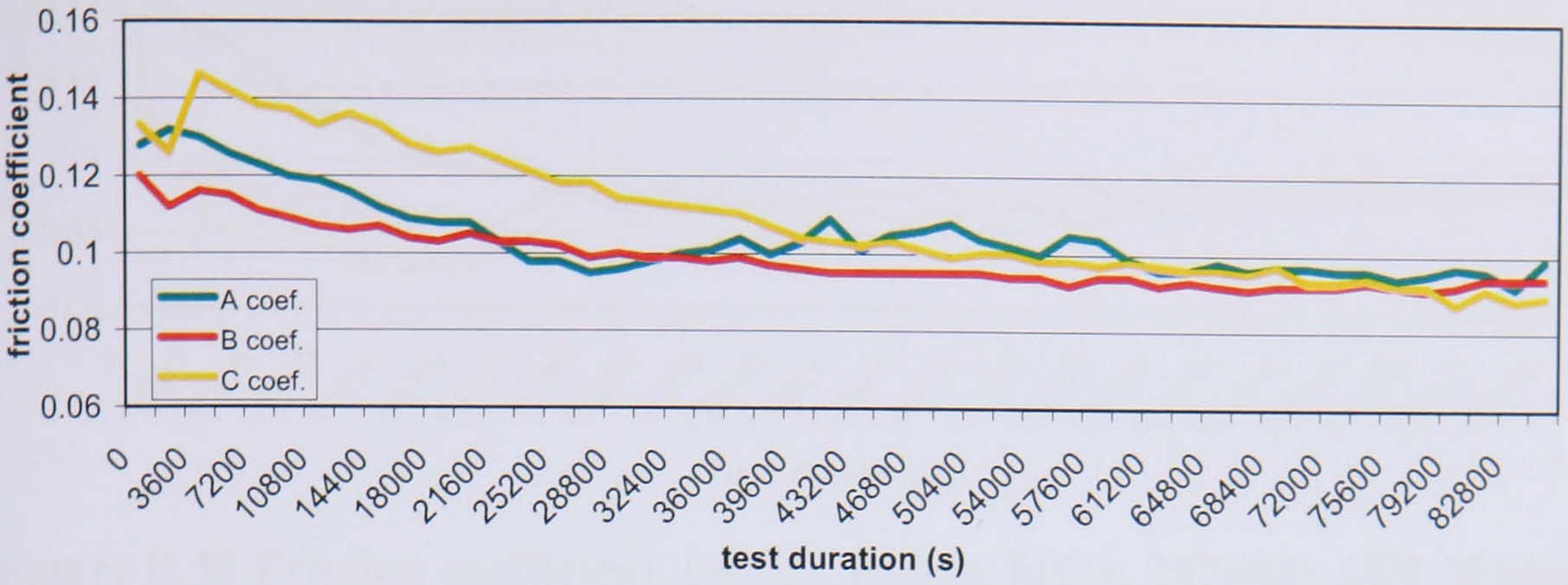

Figure D.49 Friction coefficient, test 25, R600a, MO+, 86400s, 15N, B plates

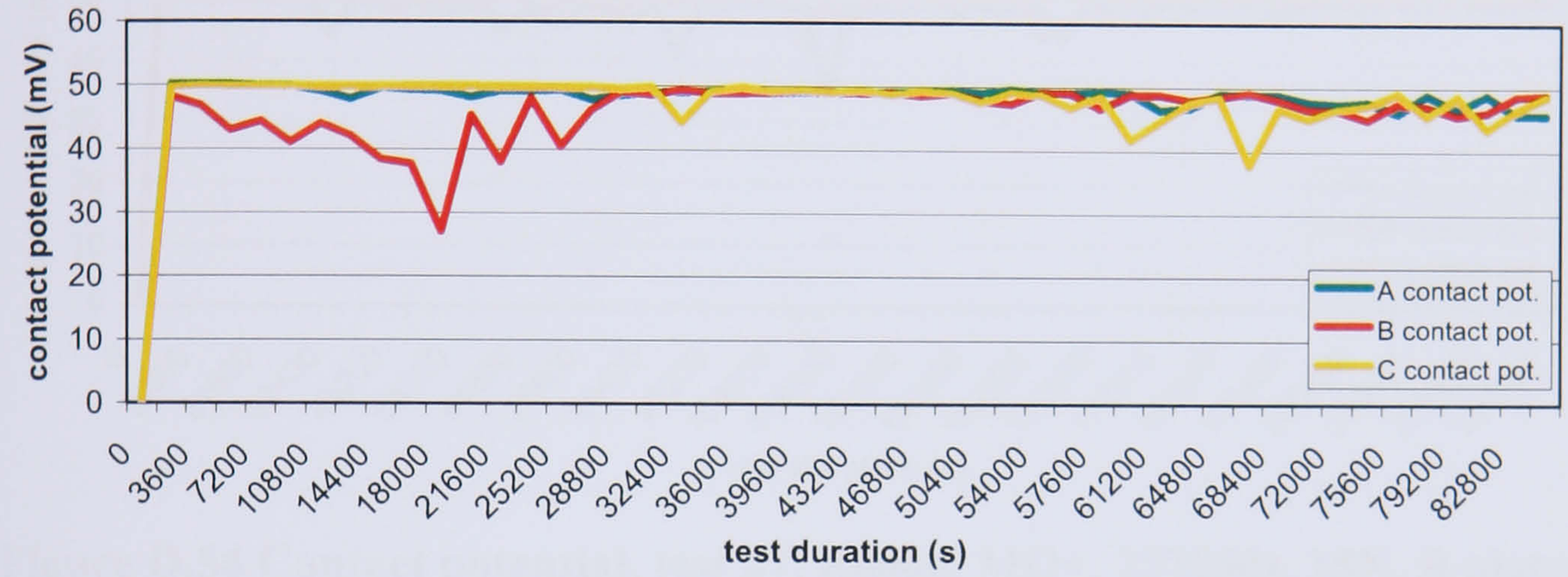

Figure D.50 Contact potential, test 25, R600a, MO+, 86400s, 15N, B plates

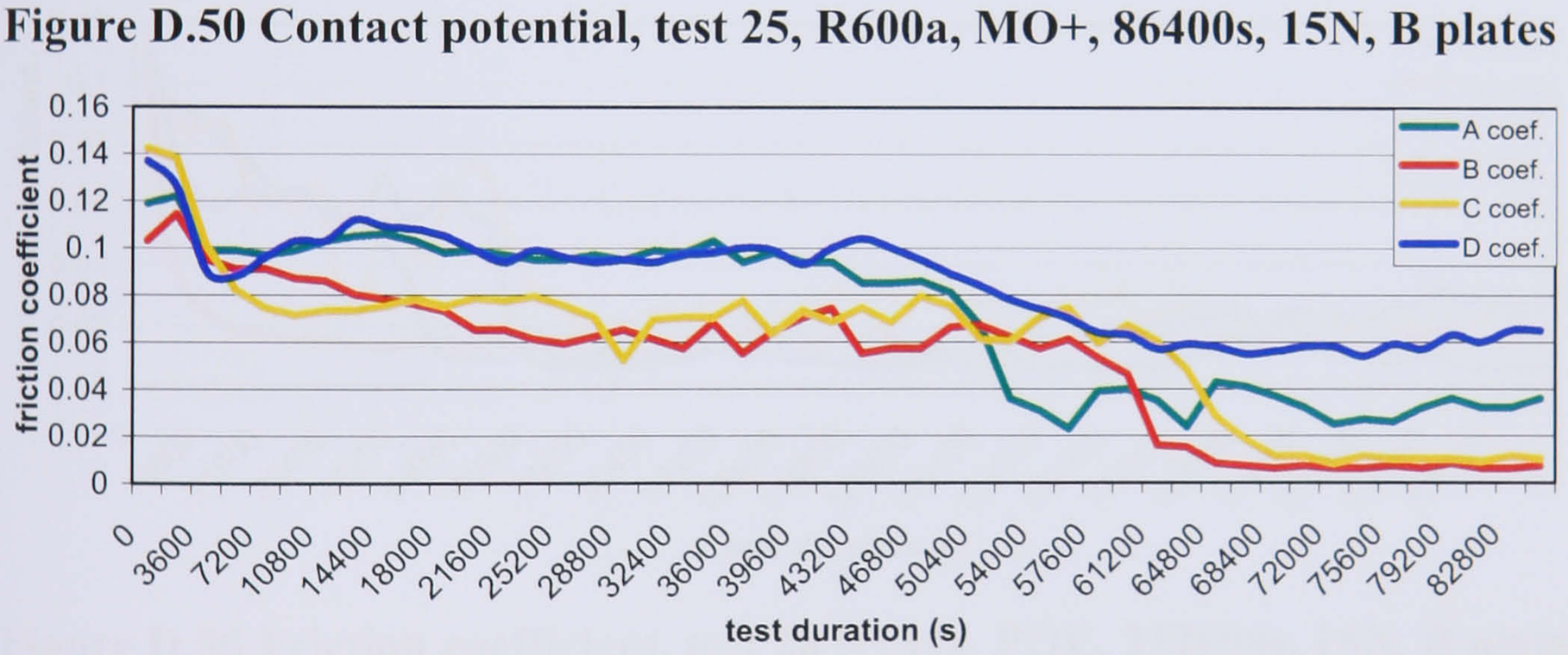

Figure D.51 Friction coefficient, test 26, R134a, POE, 86400s, 15N, B plates

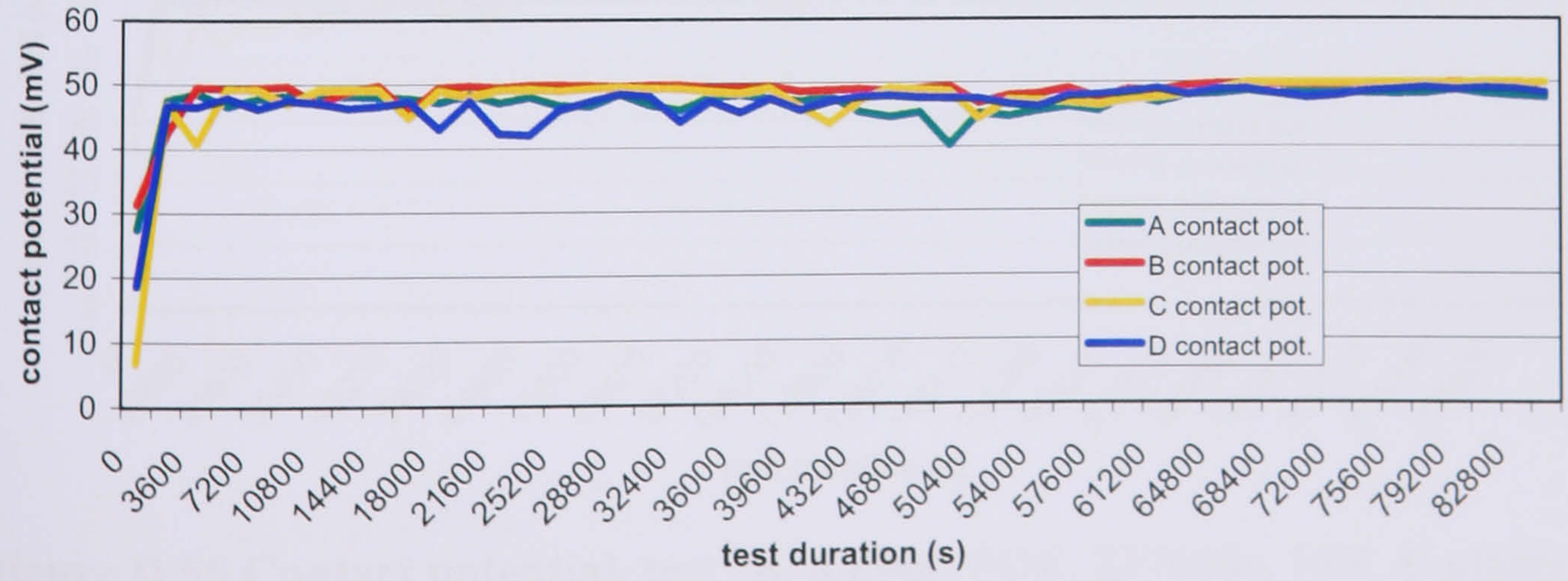

Figure D.52 Contact potential, test 26, R134a, POE, 86400s, 15N, B plates

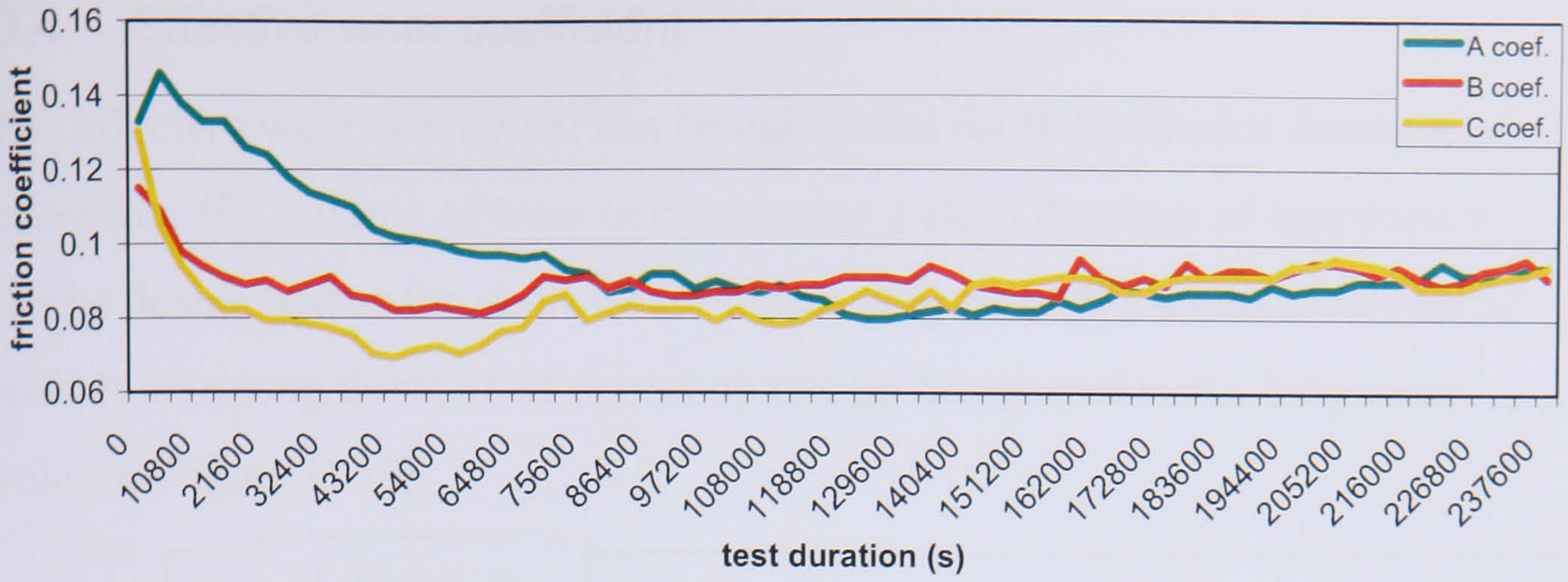

Figure D.53 Friction coefficient, test 27, R600a, MO+, 237600s, 15N, B plates

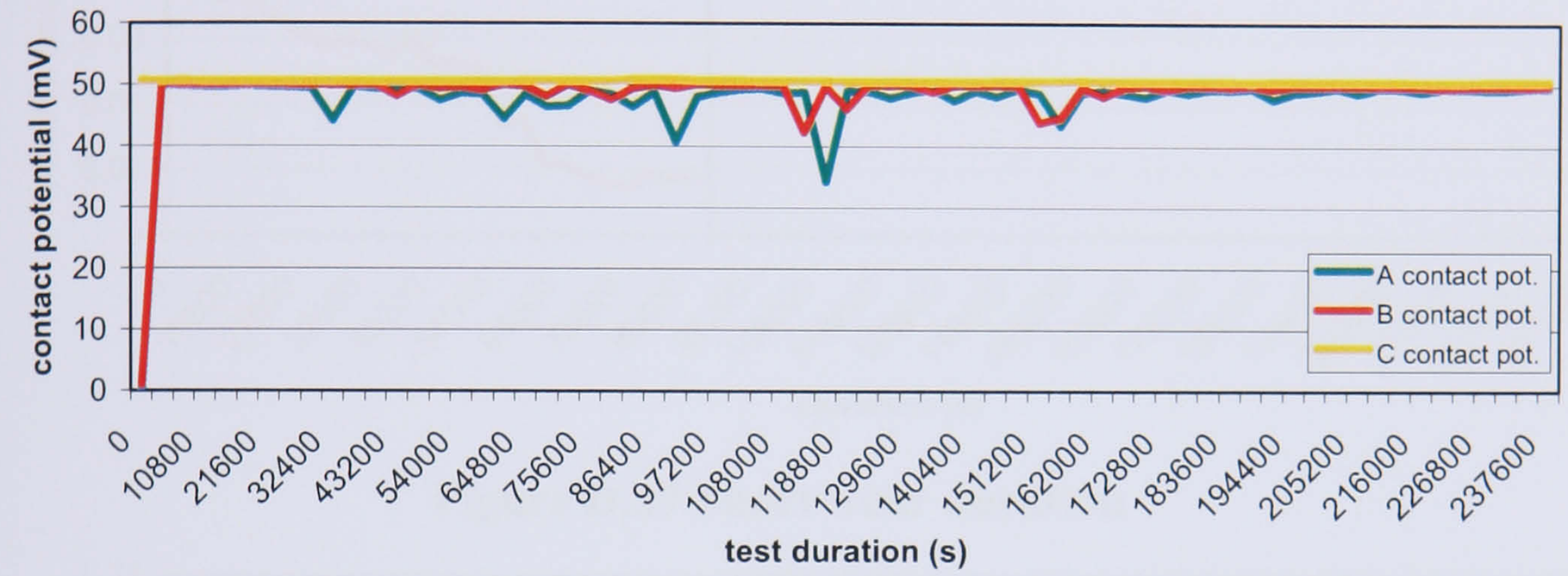

Figure D.54 Contact potential, test 27, R600a, MO+, 237600s, 15N, B plates

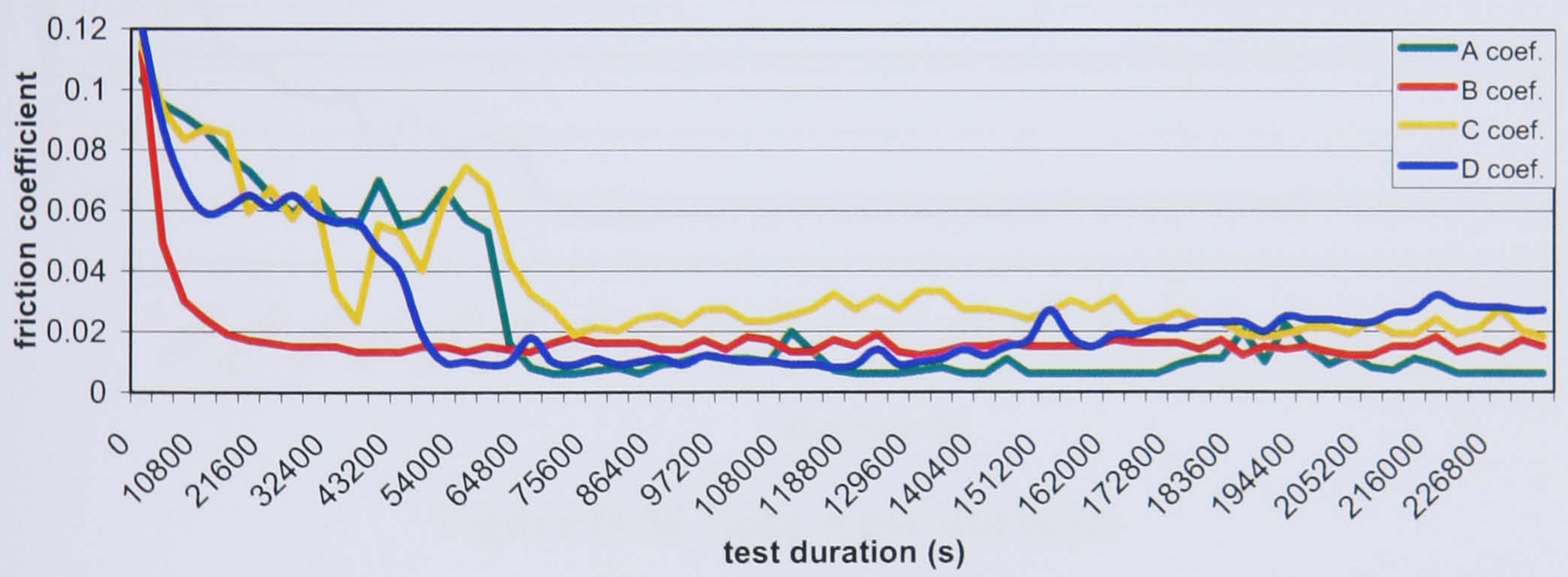

Figure D.55 Friction coefficient, test 28 R134a, POE, 237600s, 15N, B plates

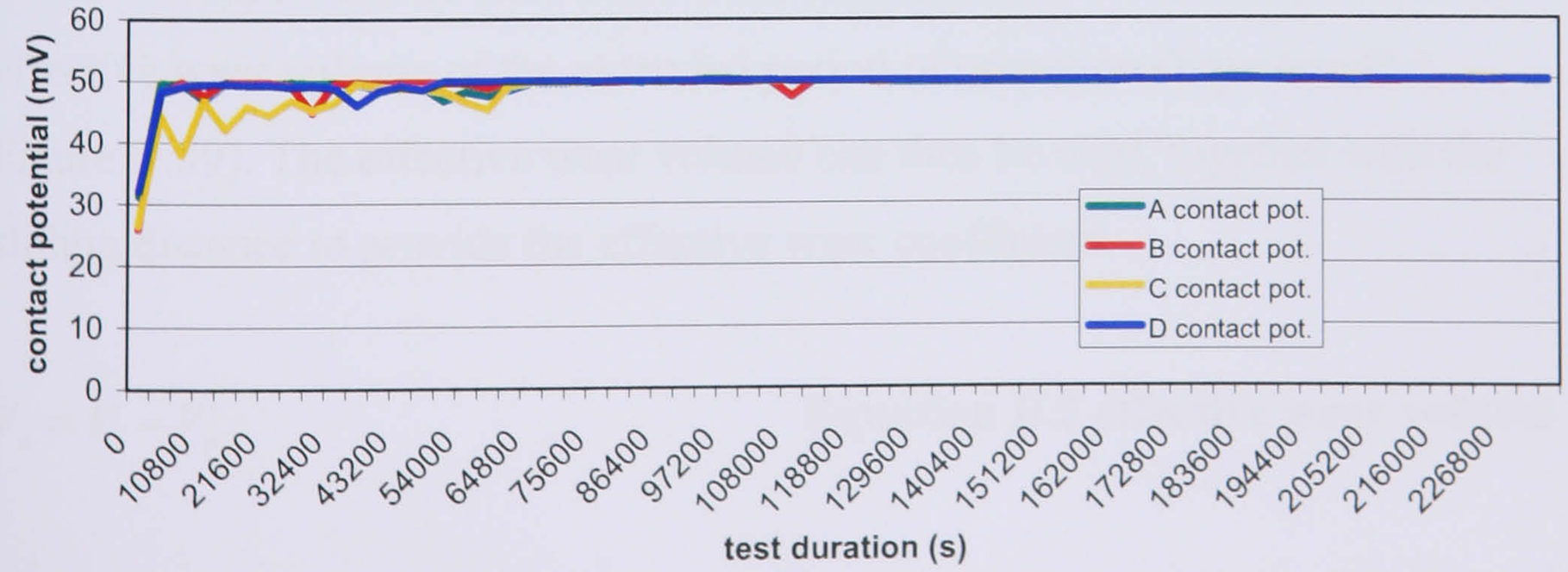

Figure D.56 Contact potential, test 28, R134a, POE, 237600s, 15N, B plates

D.4 Effective wear coefficient

The effective wear coefficient can be calculated for the extended duration of operation. If a volume of wear occurs during a short duration of operation it can be designated as the short wear volume (Figure D.57) whilst a volume of wear from a long duration of operation can be designated as the long wear volume (Figure D.58).

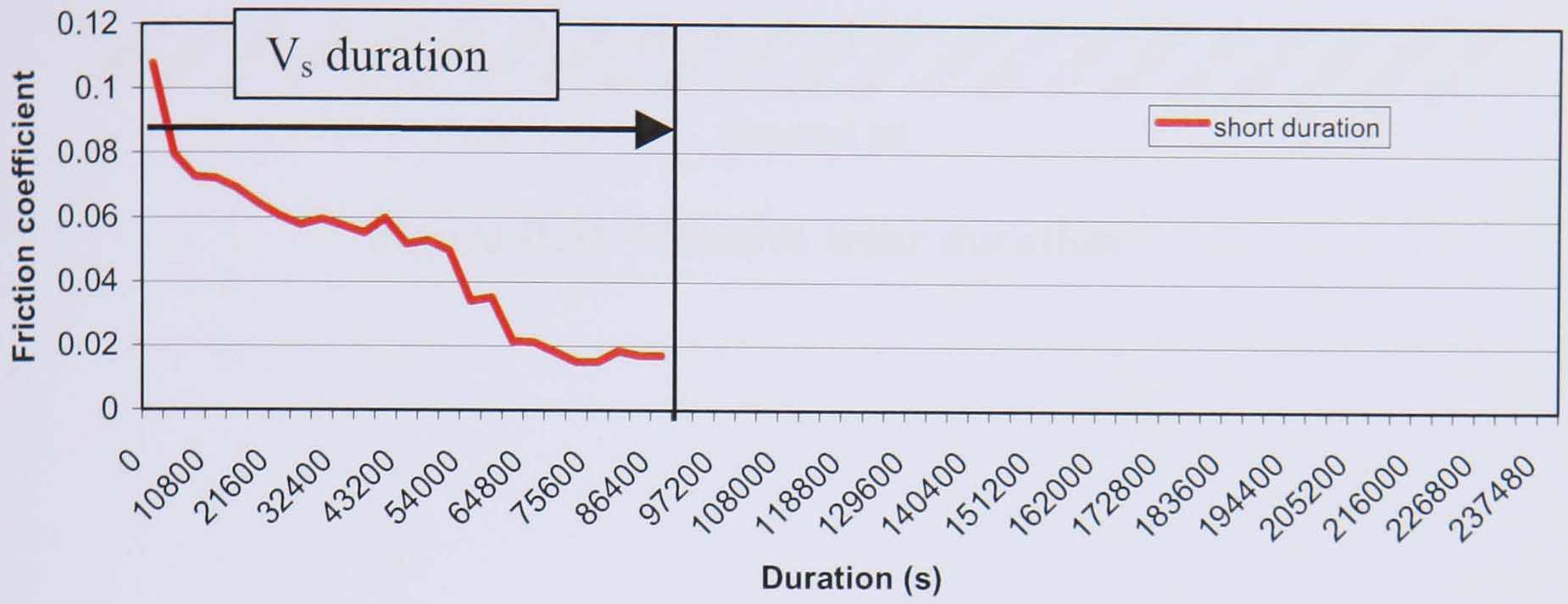

Figure D.57 Short wear duration

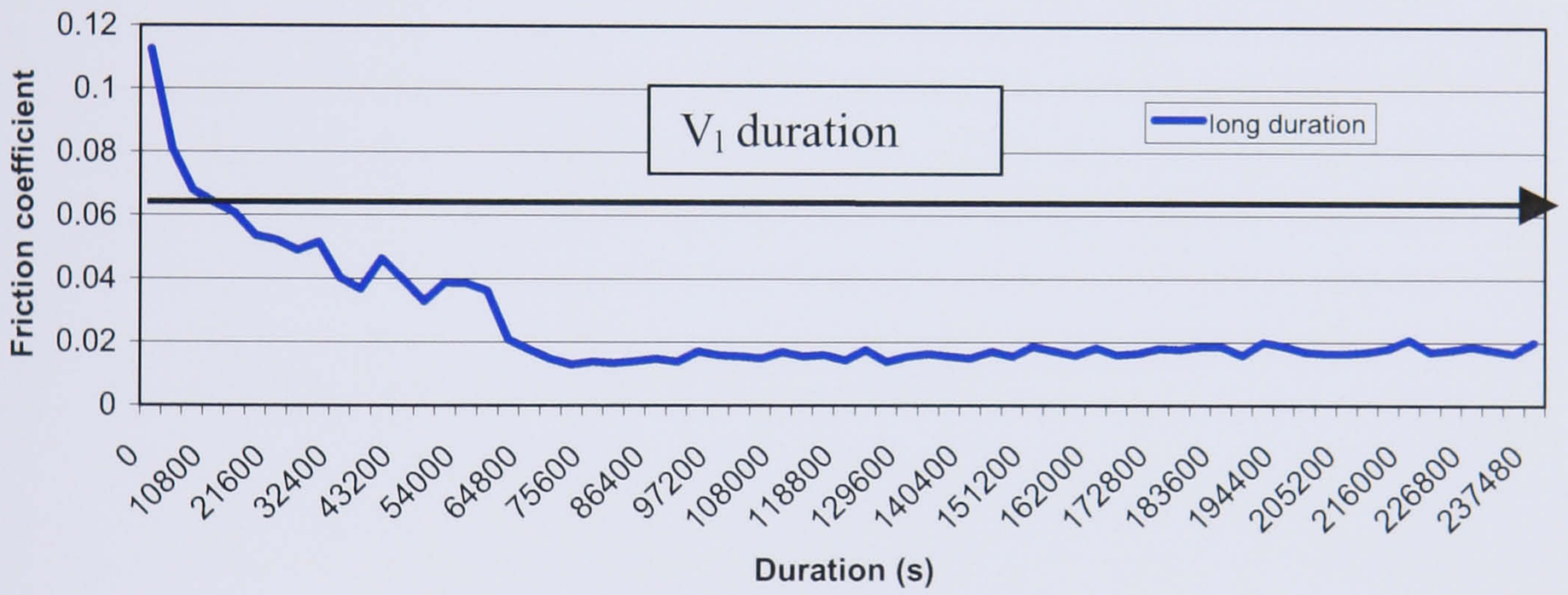

Figure D.58 Long wear duration

Since the difference between the two is limited to duration and wear volume, the short volume can be subtracted from the long wear volume to provide the effective wear volume of the extended period of operation (Equation D.2, Figure D.59). The effective wear volume can then be used, together with the sliding distance to provide the effective wear coefficient.

$$V_e = V_l - V_s$$ **Equation D.2 effective wear volume**

Where: V_e = effective wear volume (mm^3); V_l = long wear volume (mm^3); V_s = short wear volume (mm^3).

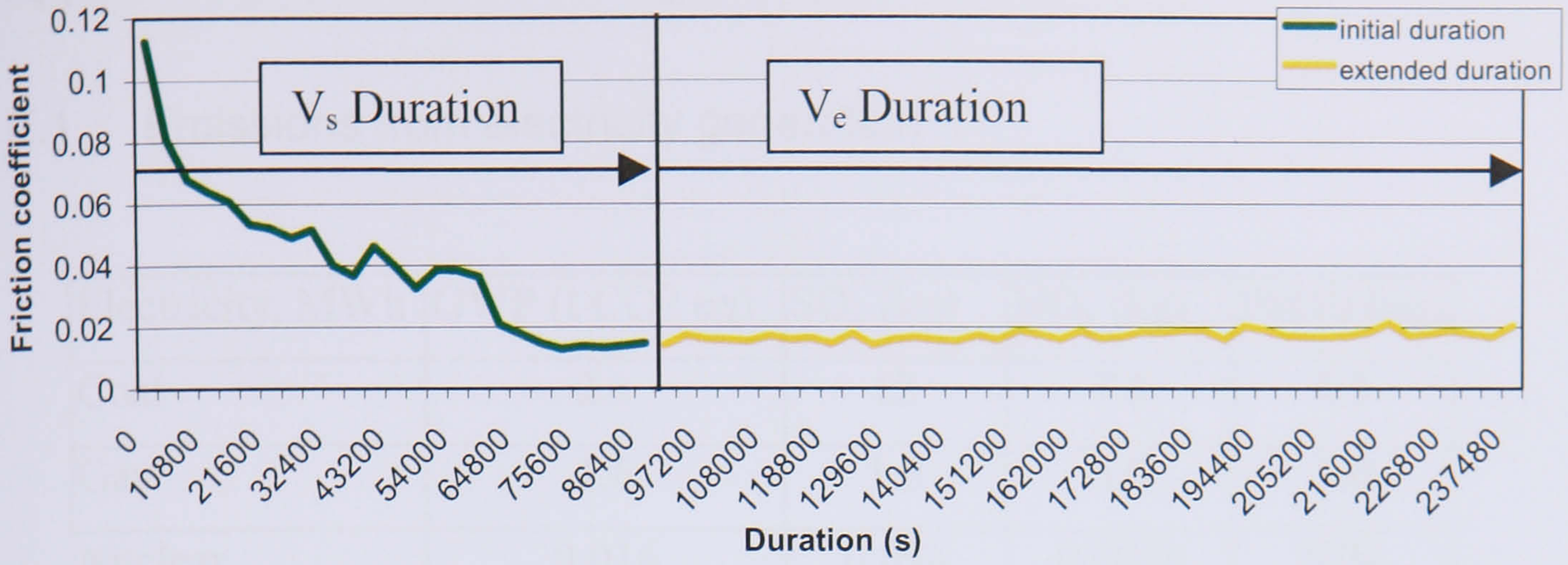

Figure D.59 Effective wear duration

Appendix E Emissions of Key Indicators

E.1 Emissions from electricity generation

Electricity, MWh	GWP (t CO2 eq)	SO_2 (kg)	NO_x (kg)	PM10 (kg)
Coal	2.1	13	7.4	4.5
Gas	1.6	1.5	3.0	1.0
Nuclear	0.016	0.094	0.0058	0.04
Renewable	0.0094	0.03	0.033	0.36

Table E.1 Emissions from generation of electricity, by type

Values for Nuclear power generation are an agregate of data for PWR and BWR reactor types sourced from within Sima-Pro LCA software (Pre-Consultants 2001). Data for emissions from Renewable power generation was sourced as hydro (Nichols and Sturges 1996) from within the PEMS LCA software package. Generation from Gas shares the same source within PEMS whilst Coal fired data (also from PEMS) has an alternative reference point (ETH-ENET 1995).

E.2 Emissions from material feedstock supply

tonne of material	GWP (t CO2 eq)	SO_2 (kg)	NO_x (kg)	PM10 (kg)
Steel	4.8	0.018	0.0097	0.061
Aluminium	45	0.19	0.062	0.12
Copper	11	0.27	0.017	0.076
Polyethylene	2.2	0.015	0.022	0.011

Table. E.2 Emissions from material feedstock, by material type

All data for the material feedstock has been taken from the PEMS LCA software package. Data for polyethylene referenced from an alternative source (Boustead 1993) within the package to that for copper, aluminium and steel (ETH-ENET 1995).

E.3 Emissions from material processing

tonne of material	GWP (t CO2 eq)	SO_2 (kg)	NO_x (kg)	PM10 (kg)
Steel	0.79	3.8	2.1	2.7
Aluminium	2.6	21	5.5	10
Copper	1.2	3.9	2.0	0.21

Table E.3 Emissions from material processing, by material type

Data for aluminium processing has been calculated by substituting the material inputs of "100% recycling aluminium" for the output of the aluminium feedstock. The data reference for the both the aluminium and steel (ETH-ENET 1995) was sourced from within PEMS. The copper processing data (ETH-ENET 1995) was taken from the GEMIS LCA package (Oki Institute).

Appendix F Life Cycle Assessment

F.1 Goal and scope

The goal of the LCA is to ascertain the environmental implications of hydrocarbon refrigerants when used with the domestic hermetic compressor.

- Identify changes to the compressor's lifecycle resulting from changes to material composition of the compressor, refrigerant and lubricant.
- Identify the aspects of the lifecycle most affected by changes in performance and durability.
- Identify the environmental implications of these lifecycle changes.

F.1.1 Scenario

The Scenario for the study is the use of hermetic compressors over a fixed time period. Variables within the scenario include:

- Recycle options for materials.
- Recovery options for refrigerants.
- Power requirements at the use phase of the lifecycle.
- Electricity supply fuel mix.

F.1.2 Environmental problem areas

Prior to the withdrawal of CFCs as refrigerants the primary environmental concern would lay with ozone depletion. The emphasis during late 1990's shifted toward global warming, contributions from the disposal and servicing of refrigerators (subsequent release of HFCs) and, in particular, the in use power consumption of the refrigeration system being the most significant.

F.1.3 Functional unit

For a comparative study of alternative systems and scenarios a point of reference must be established (Pira International 1997). The comparisons should be made on the basis of equivalent function, therefore in an LCA study, the data is calculated back to the functional unit. In the case of the hermetic compressor, there would be little point in using the compressor as the

functional unit since its longevity and material content may be subject to change under alternative scenarios. For the LCA a common function should be derived, in this case the function would be the provision of heat transfer within a domestic refrigerator over a period time. For the purpose of these works, the functional unit will be the provision of heat transfer over 15 years.

F.2 System and system boundaries

The system for the initial LCA model has been developed in accordance with existing standards (ISO-14041 1998) and following the guidelines of the software provider (Pira International 1997). The system follows the material flows from production, through installation and use, into disposal, reuse and recycling. The boundaries for the system exclude commonalties such as the refrigerator itself, energy savings as a result of improvements in technology affecting the refrigerator (insulation performance, etc) or performance enhancements to compressor types. The system schematic (Figure F.1) depicts virgin material stocks flowing through material processing to assembly. From assembly the compressor enters the use phase, consuming the lifetime energy use previously calculated (6.5) for each scenario. After the use phase the compressor is segregated, a proportion disposed off through landfill, with subsequent discharge of refrigerant, the remainder being recycled. The recycled compressors are separated into material stock and fed into the material flow to supplement virgin feedstock.

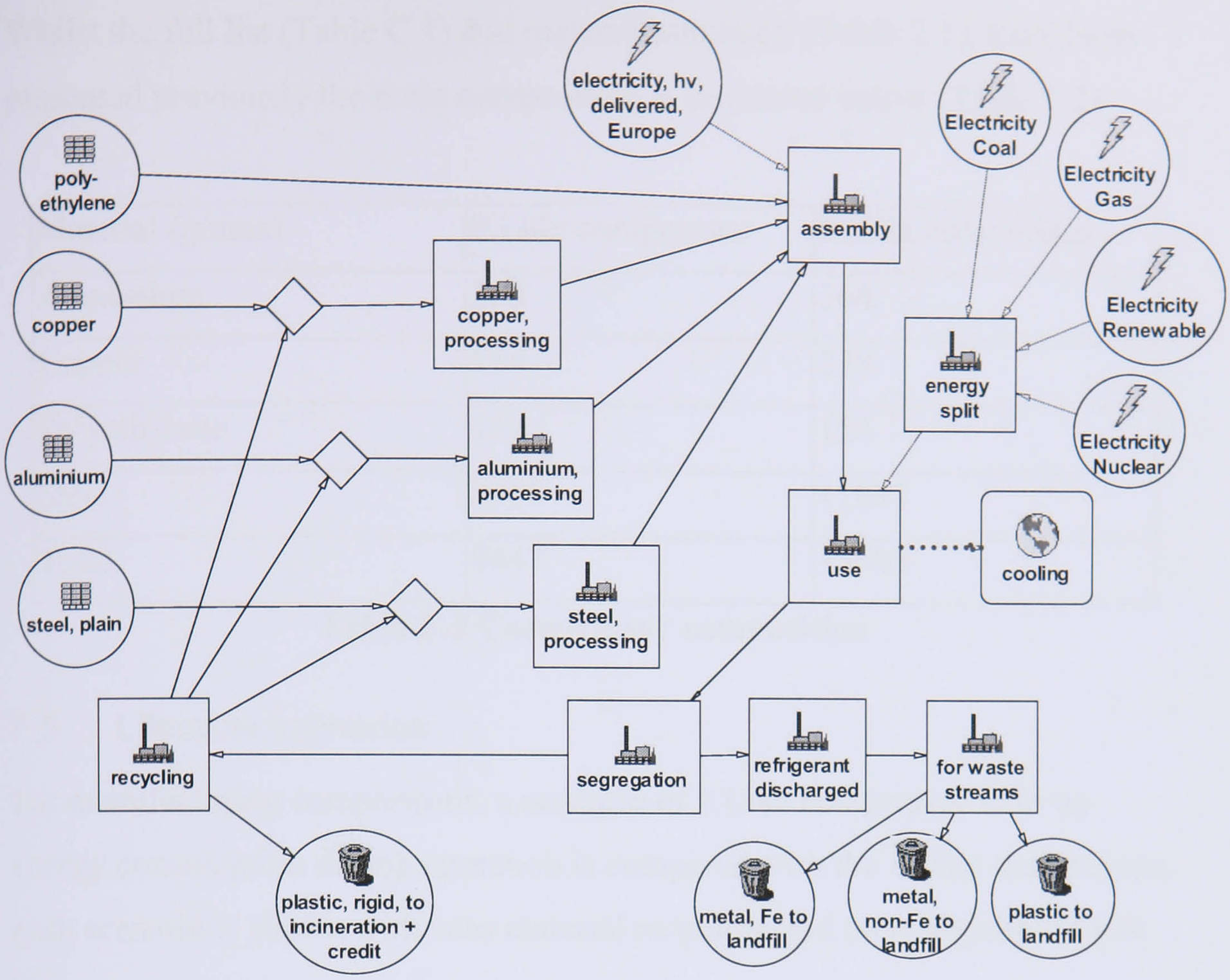

Figure F.1 LCA system schematic

F.3 Data sources

For the LCA a number of sources are used depending on the characteristics of the data set (Table F.1).

Data Type	**Data Source**
Material composition	Physical measurement
Material quantities	Physical measurement
Longevity	Experimental research, wear regime,
In use power	Experimental research, wear regime,
Reuse/Recycling	Existing reports and journal articles
Fuel mix	PEMS, ExternE
Environmental Exchanges	PEMS

Table F.1 LCA Data sources

F.4 Material Inventory

The material inventory data set for the compressor has been compiled by disassembly of a virgin unit, with subsequent weighing at component level.

Whilst the full list (Table C.1) and material summary (Table 2.1), have been presented previously the main composition is presented below (Table F.2).

Material (grams)	R134a compressor	R600a compressor
Aluminium	200	264
Copper	738	738
Polyethylene	154	154
Steel	8355	11847
Total	9447	13003

Table F.2 Compressor composition

F.5 Lifecycle scenarios

For manufacturing comparisons, a scenario of R134a compressor with no energy consumption during operation is compared with the R600a compressor, each scenario is shown with zero material recycling and no refrigerant (Table F.3).

Scenario	Compressor	Refrigerant	recycling	Power
1	R134a	-	-	-
2	R600a	-	-	-
3	R134a	200g R134a	50%	4100 kWh
4	R134a POE	200g R134a	50%	4541 kWh
5	R600a	80g R600a	50%	3942 kWh
6	R600a addit MO	80g R600a	50%	4244 kWh

Table F.3 Compressor lifecycle scenarios

For the full lifecycle scenario a recycling rate of 50% is selected. Each compressor type consumes energy over 15 years at the rates previously calculated (Table 6.18) for the alternative lubricant types and compared with zero wear scenarios. During disposal of non-recycled compressors 100% discharge of refrigerant to atmosphere is assumed. During recycling, 100% recovery is assumed.

F.5.1 Alternative fuel mix scenario

To evaluate the true cost to the environment alternative fuel mix scenarios were utilised (Table F.4). These comprised 2002 UK fuel mix, coal fired generation, and projected 2020 fuel mix (DTI 2004).

Fuel mix	2002 UK	2020 UK
Coal	34%	7%
Gas	38%	60%
Nuclear	25%	9%
Renewables	3%	24%

Table F.4 UK fuel mix for 2002 and 2020

F.5.2 Environmental indicators

To ascertain the environmental impact of the compressor lifecycle, four key environmental indicators were selected. The key indicators, GWP (CO_2), SO_2, NO_x, and PM10 are those used by the EU for energy sector emissions (European Commission 1998) as described previously (1.2.4).

F.6 LCA emission results

F.6.1 Manufacturing emissions

The LCA results for the compressor manufacturing show higher emission levels for the R600a compressor than for the R134a compressor (Figure F.2). The result is not surprising given the higher material content for this compressor.

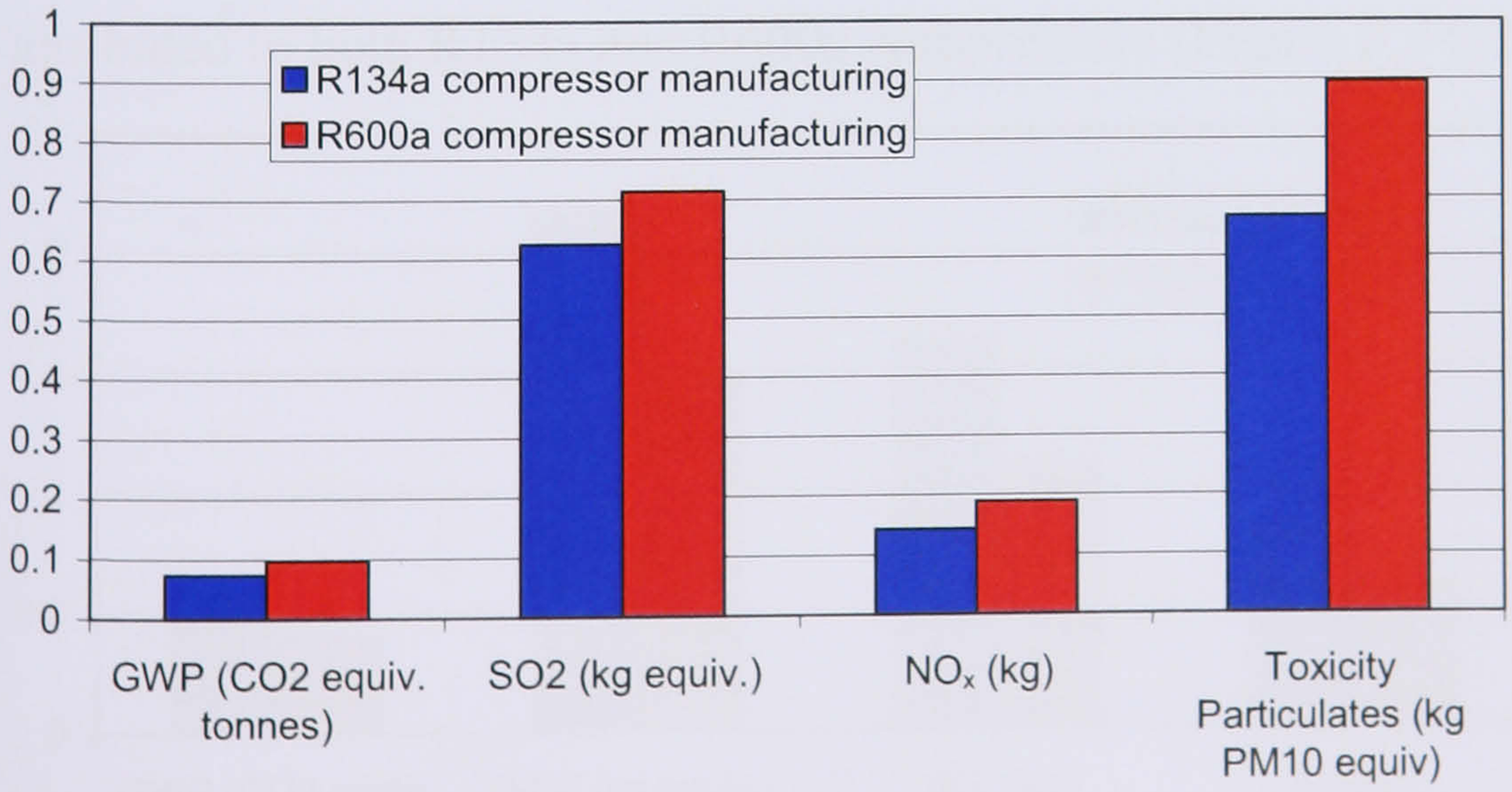

Figure F.2 Manufacturing emissions for R134a and R600a compressors

F.6.2 2002 UK fuel mix lifetime emissions

The LCA results for the two compressor types operating under a 2002 UK fuel mix scenario can be compared (Figure F.3, Table F.5). Under these conditions the R134a has higher emission levels for each of the key indicators than the R600a compressor.

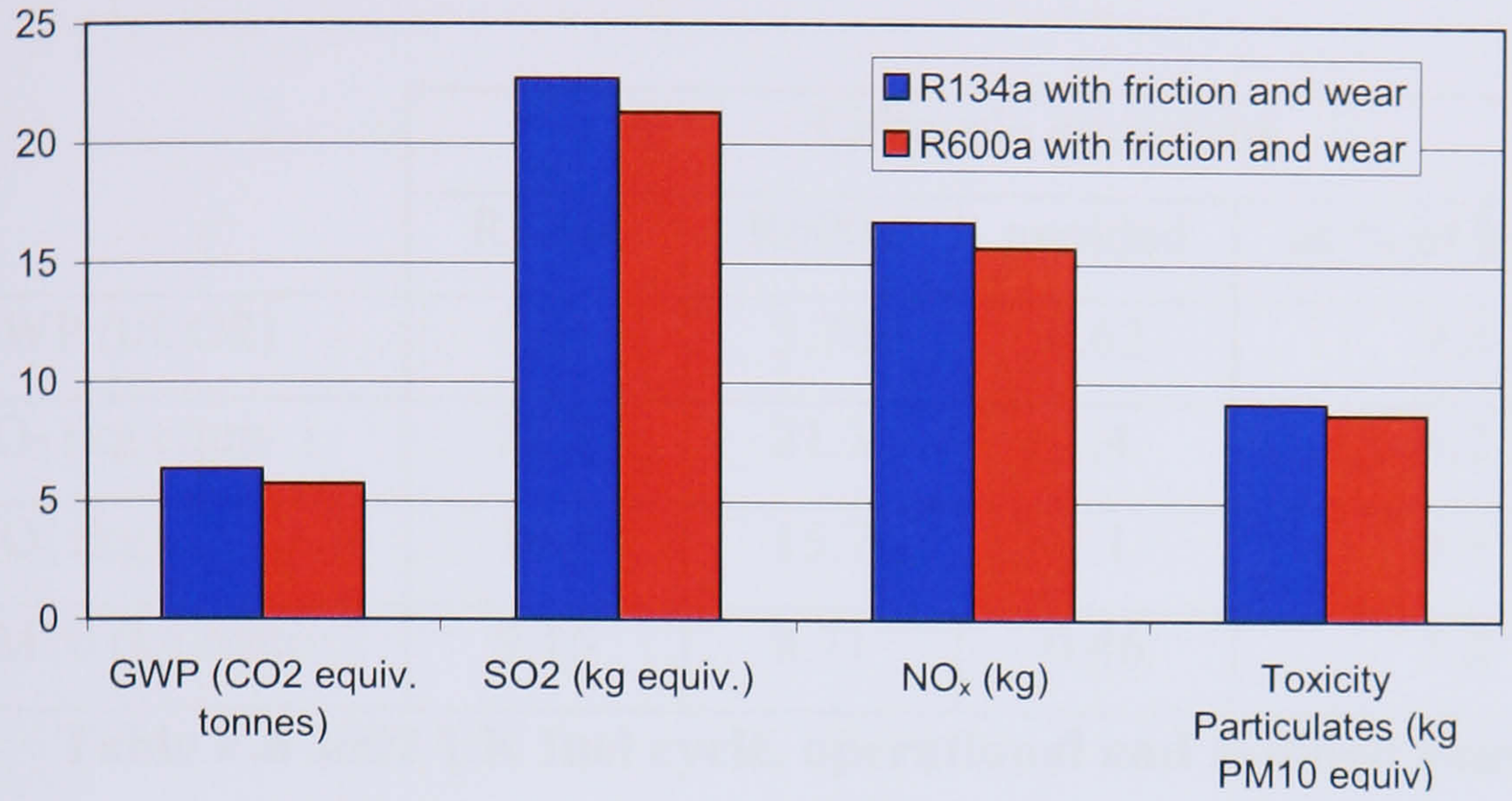

Figure F.3 LCA lifecycle emissions for R134a and R600a compressors

	Lifecycle emissions		friction and wear	
	R134a	R600a	R134a	R600a
GWP (t/CO2)	6.31	5.70	0.59	0.40
SO_2 (kg equiv.)	22.7	21.3	2.2	1.5
NO_x (kg)	16.7	15.7	1.6	1.1
PM10 (kg equiv.)	9.16	8.71	0.85	0.58

Table F.5 2002 UK fuel cycle, emissions attributable to friction and wear

The LCA results for the zero-wear compressor can be subtracted from the operational (with friction and wear) to enable the effects of friction and wear to be attributed to both R134a and R600a compressors (Figure F.4Table F.5).

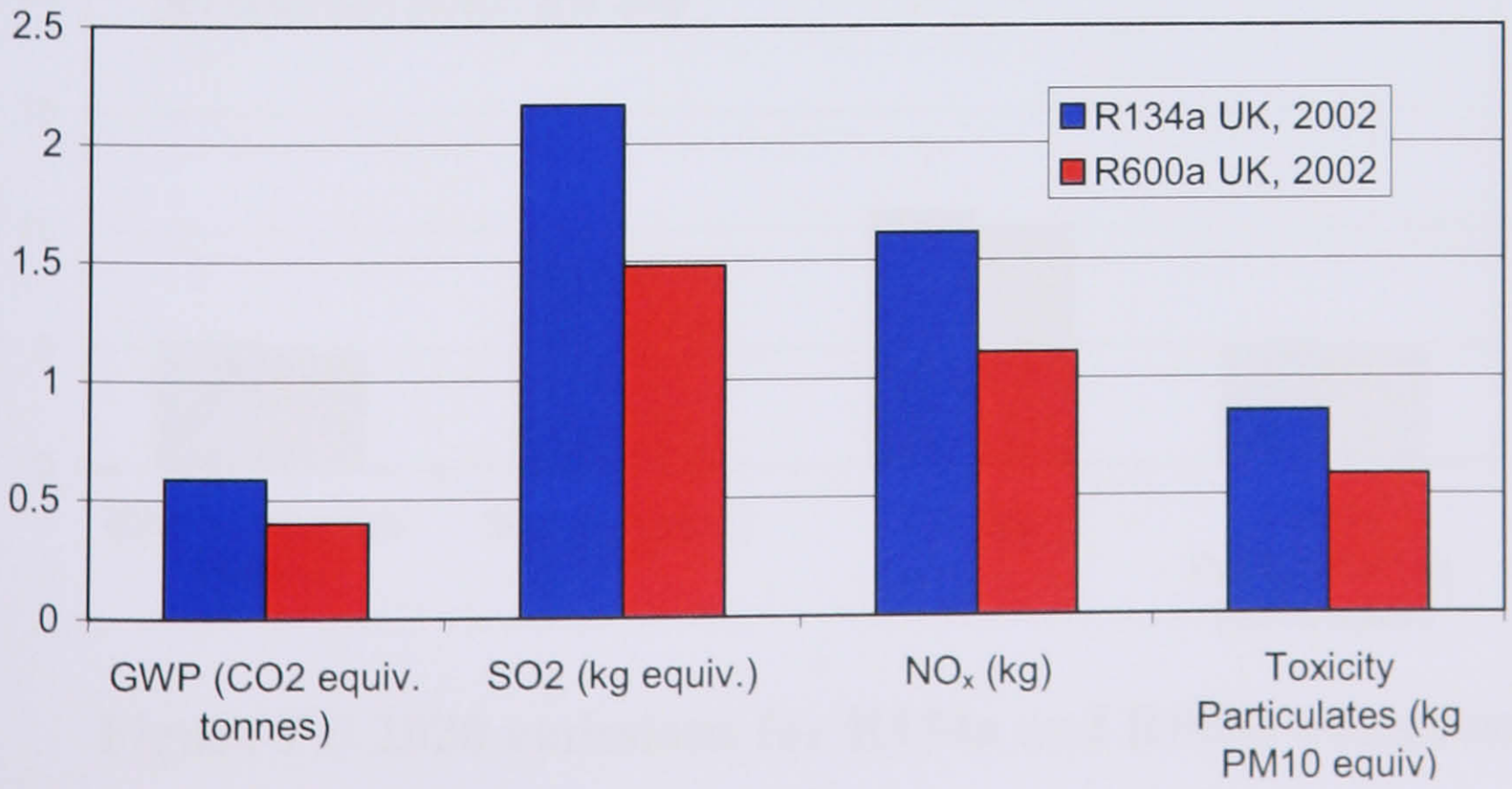

Figure F.4 2002 emissions attributable to friction and wear

The emission levels directly attributable to friction and wear are typically 50% greater for the R134a compressor, this despite having a lower friction and wear coefficients than the R600a compressor. If the operational emissions for the R600a compressor are subtracted from those of the R134a compressor, the emissions attributable to refrigerant type can be shown (Table F.6).

	Lifecycle emissions			
	R134a	R600a	avoided	as % of R134a
GWP (t/CO2)	6.31	5.70	0.62	9.8
SO_2 (kg equiv.)	22.7	21.3	1.4	6.2
NO_x (kg)	16.7	15.7	1.1	6.3
PM10 (kg equiv.)	9.16	8.71	0.46	5.0

Table F.6 2002 UK fuel cycle, operational and avoided emissions

The results indicate a 5-6% reduction in emissions for SO_2, NO_x and PM10 and nearly 10% for GWP. The discrepency between GWP and other emisssions is due to the very high GWP for refrigerant R134a compared to R600a.

F.6.3 2020 UK fuel mix lifetime emissions

For comparison with the current UK electricity supply, the LCA results for the two compressor types operating under a 2020 UK fuel mix scenario are presented (Figure F.5, Table F.7).

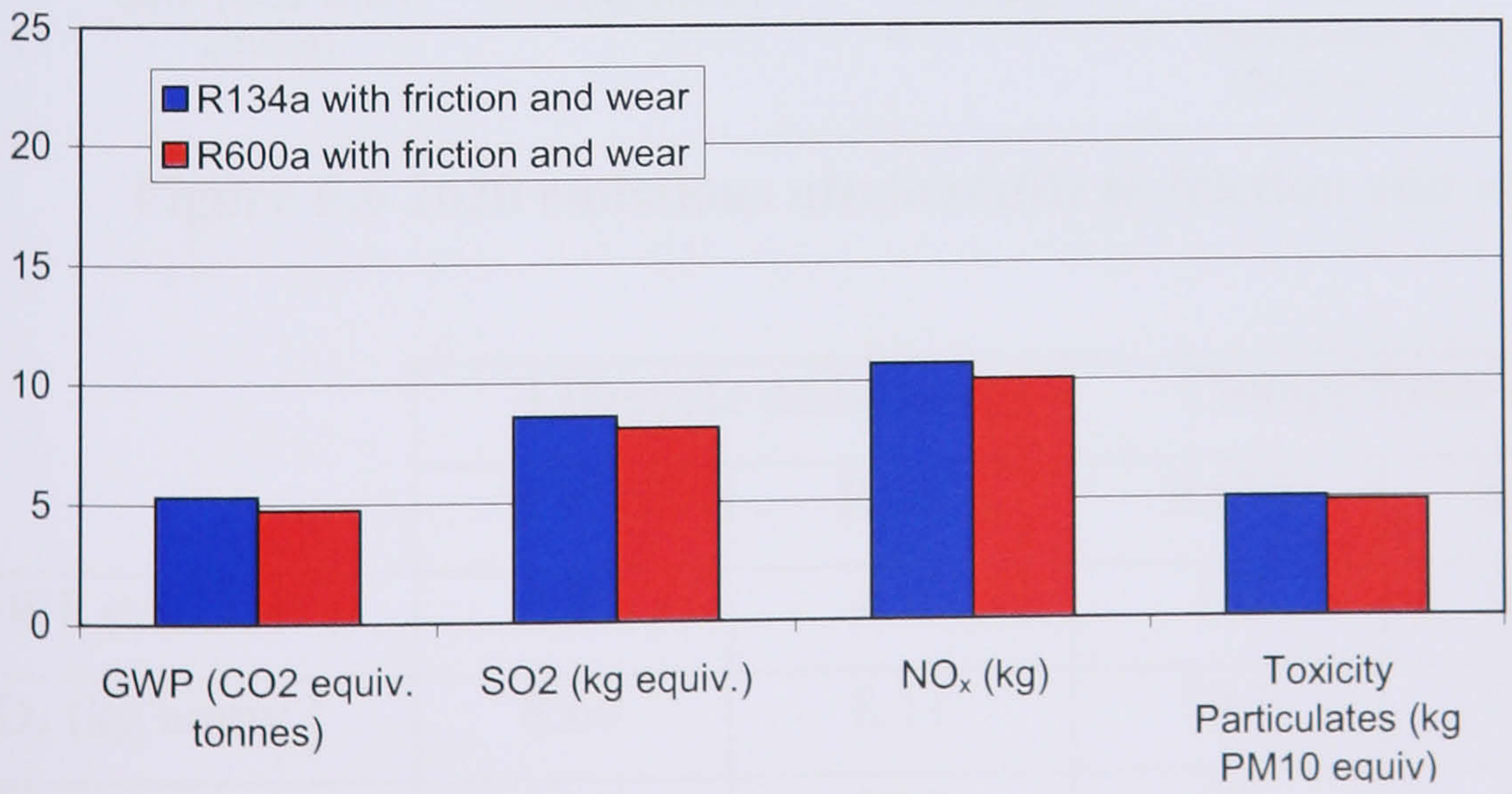

Figure F.5 2020 emissions for R134a and R600a compressors

	Lifecycle emissions		friction and wear	
	R134a	R600a	R134a	R600a
GWP (t/CO2)	5.30	4.75	0.49	0.33
$S0_2$ (kg equiv.)	8.60	8.11	0.79	0.54
NO_x (kg)	10.7	10.0	1.03	0.71
PM10 (kg equiv.)	5.03	4.85	0.45	0.31

Table F.7 2020 UK fuel cycle, emissions attributable to friction and wear

Under these conditions the R134a again has higher emission levels for each of the key indicators than the R600a compressor. The LCA results for the zero-wear compressor can be subtracted from operational (with friction and wear) results to enable the effects of friction and wear to be attributed to both R134a and R600a compressors (Figure F.6, Table F.7). The emission levels directly attributable to friction and wear are typically, as for the 2002 fuel mix, 50% greater for the R134a compressor. The 2020 emissions can also be compared to those for the 2002 fuel mix (Table F.8).

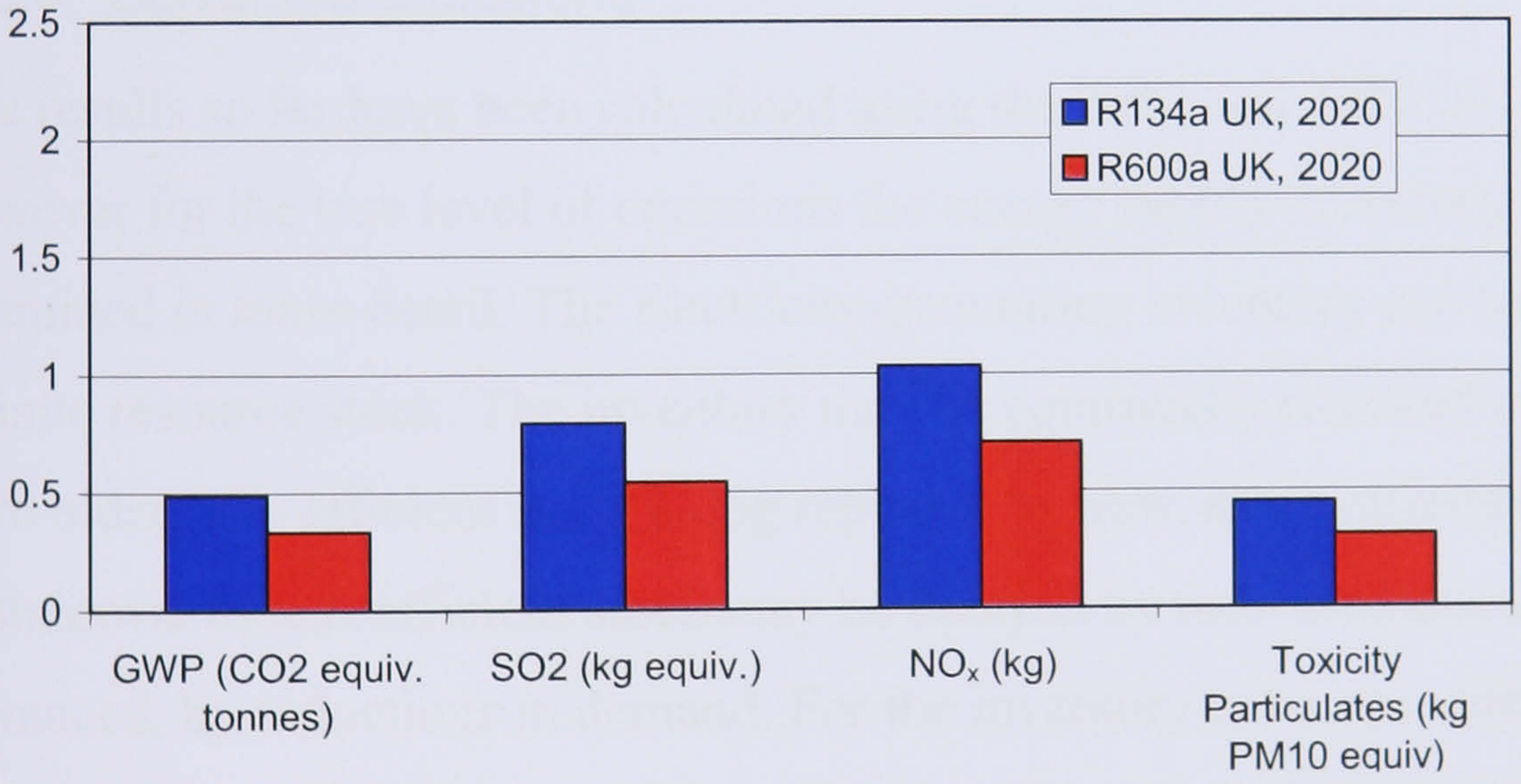

Figure F.6 2020 emissions attributable to friction and wear

	Lifecycle emissions		Change from 2002	
	R134a	R600a	R134a	R600a
GWP (t/CO2)	5.30	4.75	1.0	0.94
SO_2 (kg equiv.)	8.60	8.11	14.1	13.2
NO_x (kg)	10.7	10.0	6.0	5.6
PM10 (kg equiv.)	5.03	4.85	4.1	3.9

Table F.8 2020 UK fuel cycle, change in emissions from 2002

Changes in emission levels from 2002 fuel mix to 2020 fuel mix appear more significant than those attributed to a change in compressor type when operating with the 2002 UK fuel mix. Avoided emmisions attributable to refrigerant type (Table F.9) indicate much lower reductions in emissions for SO_2, NO_x and PM10 but similar reductions to 2002 for GWP. The discrepency between GWP and other emisssions is again due to the very high GWP for refrigerant R134a compared to R600a.

	Lifecycle emissions			
	R134a	R600a	avoided	as % of R134a
GWP (t/CO2)	5.30	4.75	0.55	10.4
SO_2 (kg equiv.)	8.60	8.11	0.48	5.6
NO_x (kg)	10.7	10.0	0.67	6.2
PM10 (kg equiv.)	5.03	4.85	0.19	3.7

Table F.9 2020 UK fuel cycle, operational and avoided emissions

F.6.4 Corrected emissions

The results so far have been calculated using the 2002 and 2020 UK fuel mix, however for the true level of emissions the energy supply inventory should be examined in more detail. The electricity-generating inventory can be viewed as a finite resource stock. The inventory may be continually renewed over time with older, less efficient stock being replaced by new, more efficient stock. The withdrawal of less efficient stock may be delayed by increased demand, or advanced, by reductions in demand. For the inventory to be run with minimum emissions, low emitting stock such as renewables and nuclear would be run at full capacity whilst high emitting stock run as a top-up. Under these operating conditions the difference in energy requirements between the lower consumption R600a compressors and the higher consumption R134a compressors would be met entirely by higher emission stock. In the case of both the 2002 and 2020 UK scenarios this additional requirement would be met by coal fired generation. The additional emissions can be calculated by subtracting the baseline R600a emissions from R134a emissions when operating under a coal fired scenario and can be compared with those calculated for 2002 and 2020 cycles (Table F.10). From the results it is clear

that using this method for the calculation of avoided emissions, the effects of a change in compressor type are much more significant than might be initially envisaged. Although GWP levels are only increased by 38% the other key indicators show much more significant increases of 104-167% over those calculated using the 2002 fuel mix.

	R134a Lifecycle additional emissions		
	2002	2020	Coal
GWP (t/CO2)	0.61	0.55	0.85
SO_2 (kg equiv.)	1.40	0.48	3.7
NO_x (kg)	1.06	0.67	2.17
PM10 (kg equiv.)	0.46	0.19	1.21

Table F.10 Additional emissions from coal cycle, R134a

The additional emissions can be added to the baseline R600a emissions for both 2002 and 2020 fuel cycles to project the corrected whole lifecycle emissions for R134a and compared directly with those for R600a (Figure F.7).

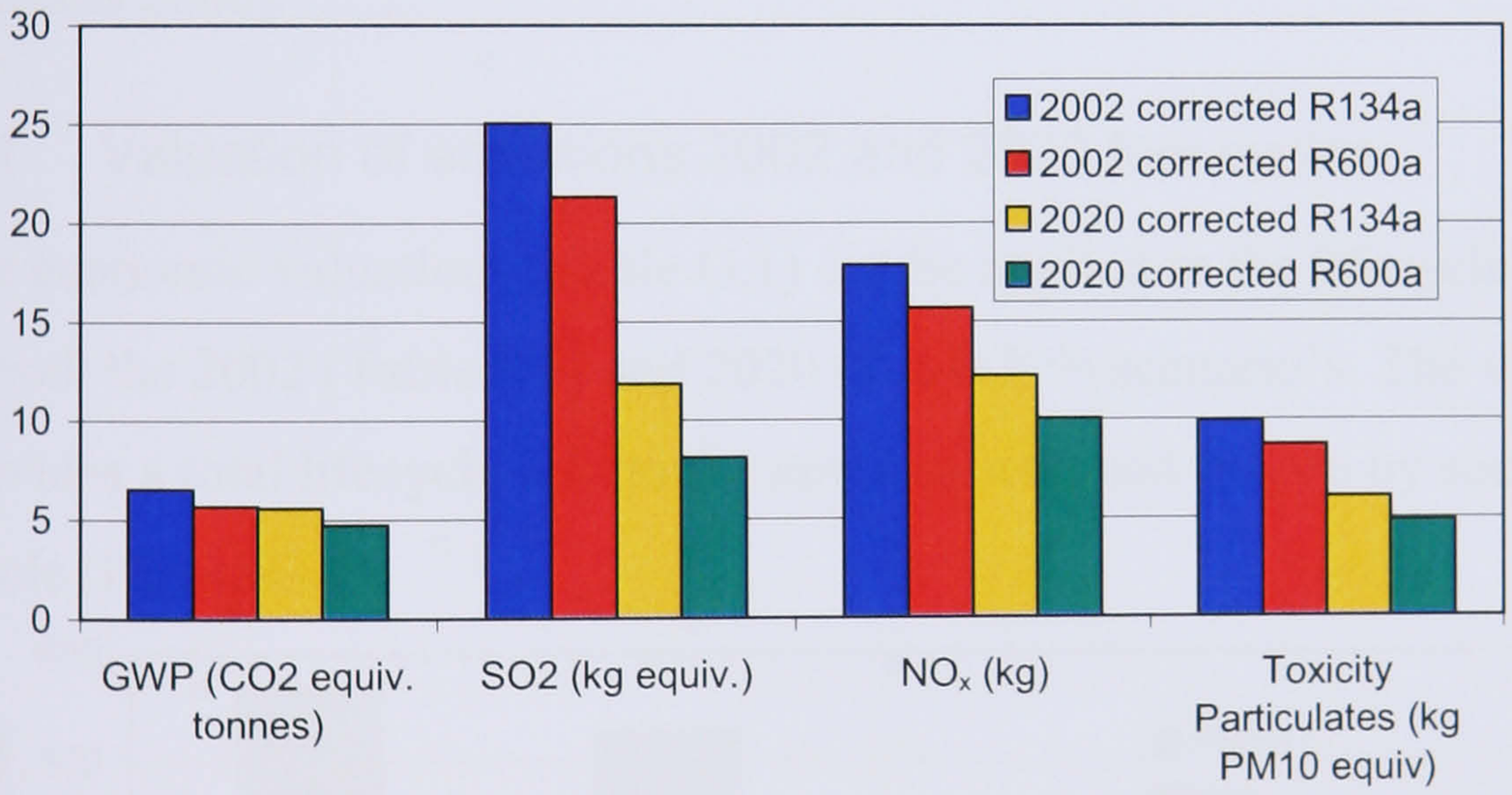

Figure F.7 Corrected emissions, 2002 and 2020 UK fuel cycles

The corrected levels show that change in compressor type from R134a to R600a would lead to significant reductions in emissions. For the 2002 cycle reductions vary from 12% for NO_x emissions to 15% for SO_2 emissions. For the 2020 cycle the reductions vary from 15% for GWP to 31% for SO_2 emissions. These reductions, when expressed as a percentage of the lifecycle emissions, are much more significant than the raw emissions savings for 2002 and 2020 fuel cycles described previously (Table F.9, Table F.6).

Appendix G Economic valuation

For any decision making methodology to be useful, it should compare like with like. Simply relating an avoided emission of 0.85 tonnes of CO_2 to 3.7kg of SO_2 is meaningless until a common denomination is utilised. For the key indicators values can be attached to the quantity of pollutant emitted (Table G.1).

Emission	Units	Valuation (Euros)
GWP	Tonnes CO_2 equiv.	32.60
Acidification	Kg SO_2 equiv.	7.4
Nitrogen oxides	Kg NO_x	2.3
Particulates	Kg PM10	17

Table G.1 Emissions valuation, key indicators

The Values for SO_2, NO_x, and PM10 are taken from the ExternE project (European Commission 1998) as described (Table 1.3) whilst the CO_2 value has been taken from expected trading prices under the EU emissions trading scheme, if the requirements of the Kyoto Protocol are to be met (Capros and Mantzos 2000).

G.1 Valuation of emissions 2002 and 2020 fuel cycles

The economic valuations (Table G.1) can be applied to the lifecycle emissions of both the 2002 (Table F.6) and 2020 (Table F.9) scenario's. The valuation provides a total lifecycle cost to the environment, and is born by society as a whole (Figure G.1).

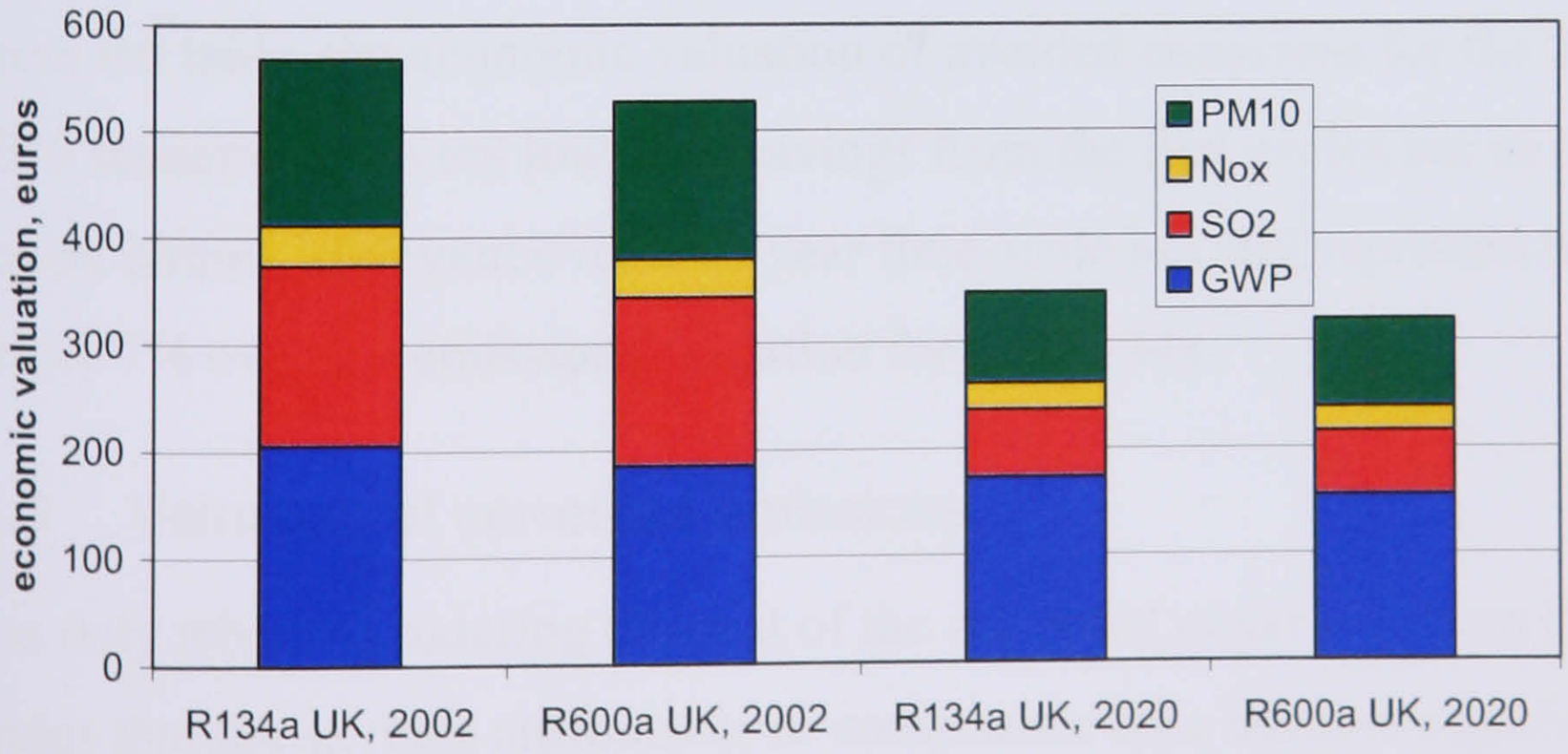

Figure G.1 Lifecycle cost of compressor 2002 and 2020 UK fuel mix

From the chart it is clear that, for the lifecycle cost of emissions, a change in fuel mix scenario has a significant effect. Whilst the costs attributable to CO_2

emissions fall by 16% to €155-173, the most significant saving is for SO_2 emissions, falling by 63% to €60-64 (Table G.2). Total environmental costs over the lifecycle fall by 43% to €320-347, a saving of €207-221.

	2002 cost		2020 cost		Savings from 2002	
	R134a	R600a	R134a	R600a	R134a	R600a
GWP	206	186	173	155	33	31
SO_2	168	158	64	60	104	98
NO_x	39	36	25	23	14	13
PM10	156	148	86	82	70	66
Total	568	527	347	320	221	207

Table G.2 2002, 2020 UK fuel cycle, emission costs, euros

G.2 Valuation of avoided emissions

The avoided emissions calculated for both the UK fuel cycles are used to calculate the value of avoided emissions from utilising the R600a compressor in place of the R134a compressor (Table G.3).

	2002 savings, €	2020 savings, €
GWP	20	18
SO_2	10	3.6
NO_x	2.4	1.5
PM10	7.7	3.1
Total	41	26

Table G.3 Valuation of avoided emissions

From the table, the economic valuation of avoided emissions for the 2002 and 2020 scenarios are very low. The savings from the fuel cycles are so low as to appear almost irrelevant over a 15 year time-scale but still represent savings of nearly 7% over the emissions valuation for the R134a.

G.3 Valuation of corrected emissions

It is only when considering the cost of the corrected emissions from the fuel cycles that the savings attributable to compressor type become significant (Figure G.2). The reduction in costs using the corrected emissions for the R600a compressor over the R134a are also much more significant (Table G.4).

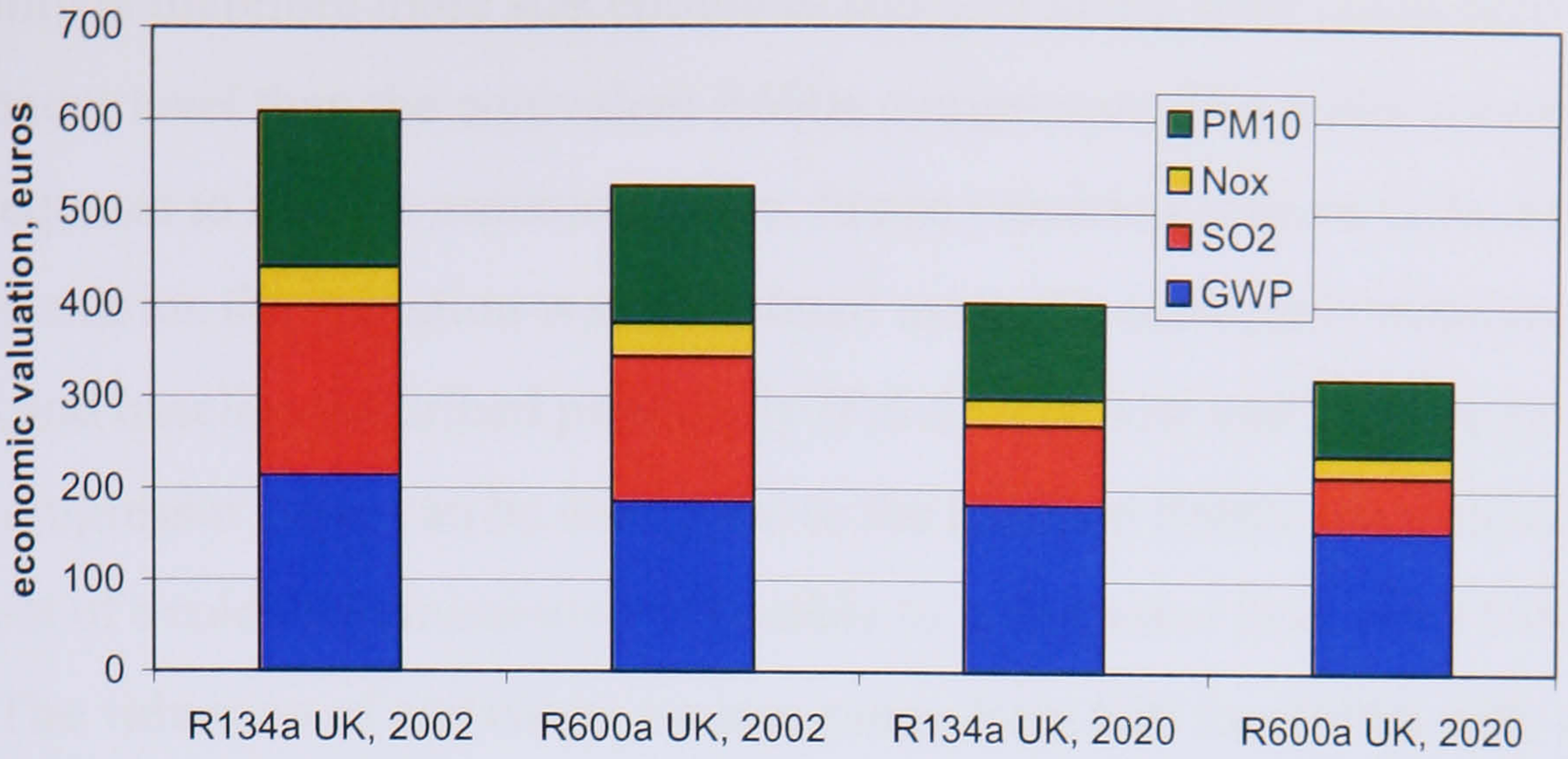

Figure G.2 Corrected emissions valuation, 2002 and 2020 fuel cycles

The value of corrected avoided emissions rises to €81, with the lowest contribution of €5 from NO_x whilst those from GWP and SO_2 the most significant with €28. In percentage terms, savings with the 2002 cycle average 13% whilst those with the 2020 cycle average 21%.

	Savings, €	2002 as % of R134a	2020 as % of R134a
GWP	28	13	15
SO_2	28	15	32
NO_x	5	12	18
PM10	21	12	20
Total	81	13	21

Table G.4 Value of corrected avoided emissions

G.4 Sensitivity analysis

The material wear-rates calculated for the compressor types are only estimates and therefore subject to inaccuracies. To allow for this, further iterations of the LCA model were carried out with energy consumption derived from alternative wear-rates for both the R134a and R600a compressor (Table G.5).

	R134a compressor			R600a compressor		
Range	Low	mid	high	low	mid	high
Wear coef.	$0.8x10^{-8}$	$1.2x10^{-8}$	$1.8x10^{-8}$	$1.5x10^{-8}$	$2x10^{-8}$	$2.5x10^{-8}$
Energy	4360	4541	4980	4167	4244	4334

Table G.5 Energy use for alternative wear-coefficients, sensitivity

The Energy use for the compressors show a wider range for the R134a compressor than for the R600a. The R134a compressor performance and

durability is therefore more susceptible to changes in the wear characteristics at component level than the equivalent R600a compressor. The wider energy range equates to a wider emission range, hence valuation (Figure G.3). For these scenarios the valuation was calculated using the corrected emissions model and baseline described previously (F.6.4). The low and high ranges for both compressor types can be compared to the baseline R600a to calculate the true cost of avoidable emissions attributable to compressor selection (Table G.6). The valuation of emissions savings range from €20 for R600a with a low wear rate, to costs of €194 for high wear rate R134a.

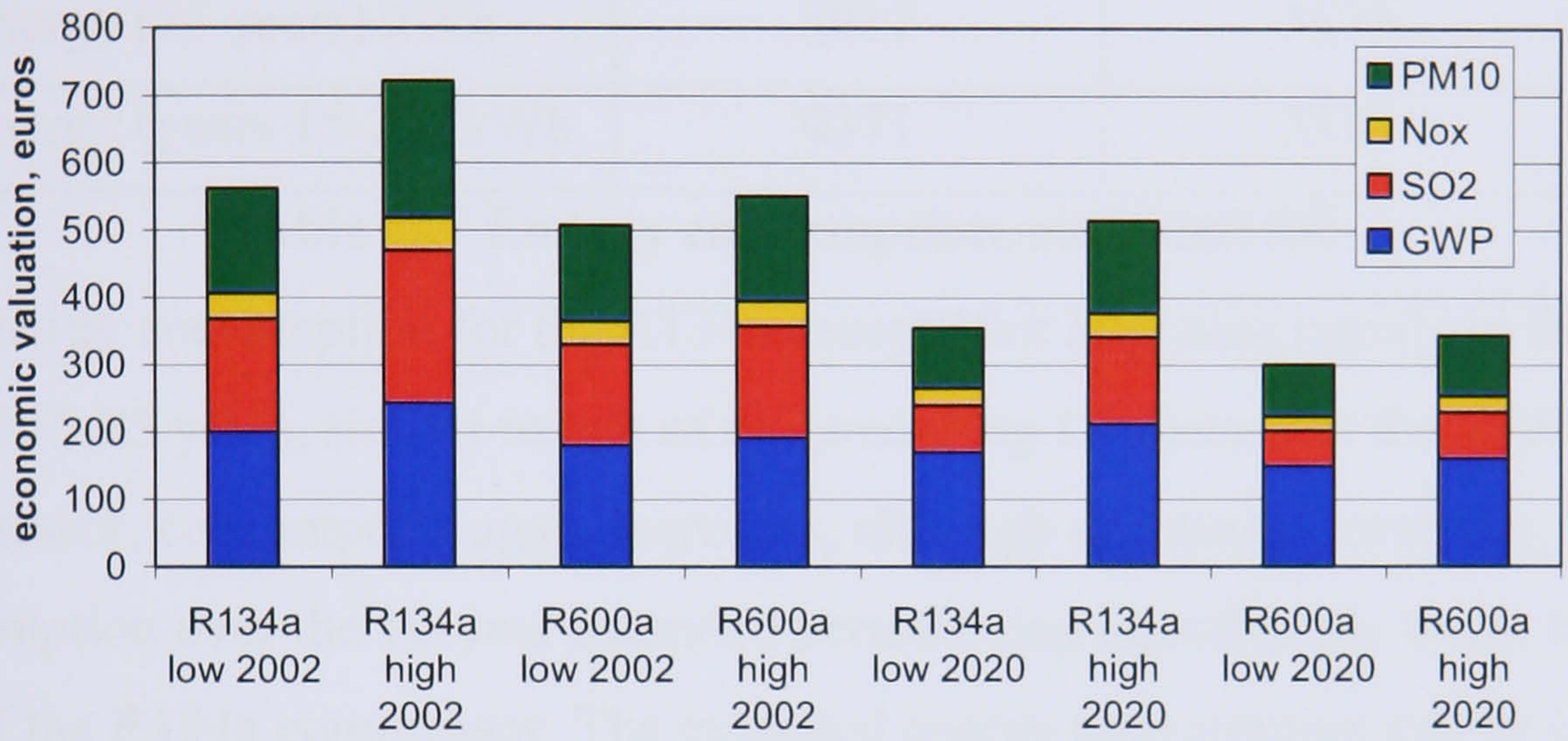

Figure G.3 Corrected emissions valuation, sensitivity

The High wear rate R600a, in contrast, presents additional costs of €23 and the low wear rate R134a costs of €35. In percentage terms, the baseline scenario represents savings of 38% over the high wear R134a and 10% over the low wear whilst savings of 7% are accrued over the high wear R600a and a cost penalty of 7% compared to the low wear counterpart.

	2020 costs (savings) €				Savings, % of total emissions cost			
	R134a		R600a		R134a		R600a	
	Low	High	Low	High	Low	High	Low	High
GWP	15.3	58.3	-5.3	6.2	9%	27%	-4%	4%
SO_2	11	69	-7.3	8.5	15%	53%	-14%	12%
NO_x	1.9	13	-1.3	1.5	8%	35%	-6%	6%
PM10	6.8	54	-5.9	6.9	8%	40%	-8%	8%
Total	34.6	194.0	-19.8	23.1	10%	38%	-7%	7%

Table G.6 2020 avoidable emission costs

G.5 Extended lifecycle

The lifecycles described have been calculated over a 15 year period. However, it is not uncommon for such devices to be operated over an extended life, particularly in low-income households or rented property as second hand or used products. To ascertain the effects of extended life the energy values were re-calculated over a 25 year lifecycle (Table G.7).

	R134a	R600a
Energy (15 years) kWh	4541	4244
Energy (25 years) kWh	8912	7579
Energy (years 15-25) kWh	4371	3335

Table G.7 Energy consumption, extended life

The energy consumption for the R134a compressor increases rapidly in the period 15-25 years, similar to that of the preceding 15 years. For the R600a compressor, consumption again increases, although at a much lower rate. The consumption over the 10-year extended period being significantly lower than that of the R134a compressor. The extended energy consumption can be used to calculate the corrected emissions valuation for the period 15-25 years, this time using emissions of an R600a compressor operated over 0-10 years from new as the baseline (Figure G.4).

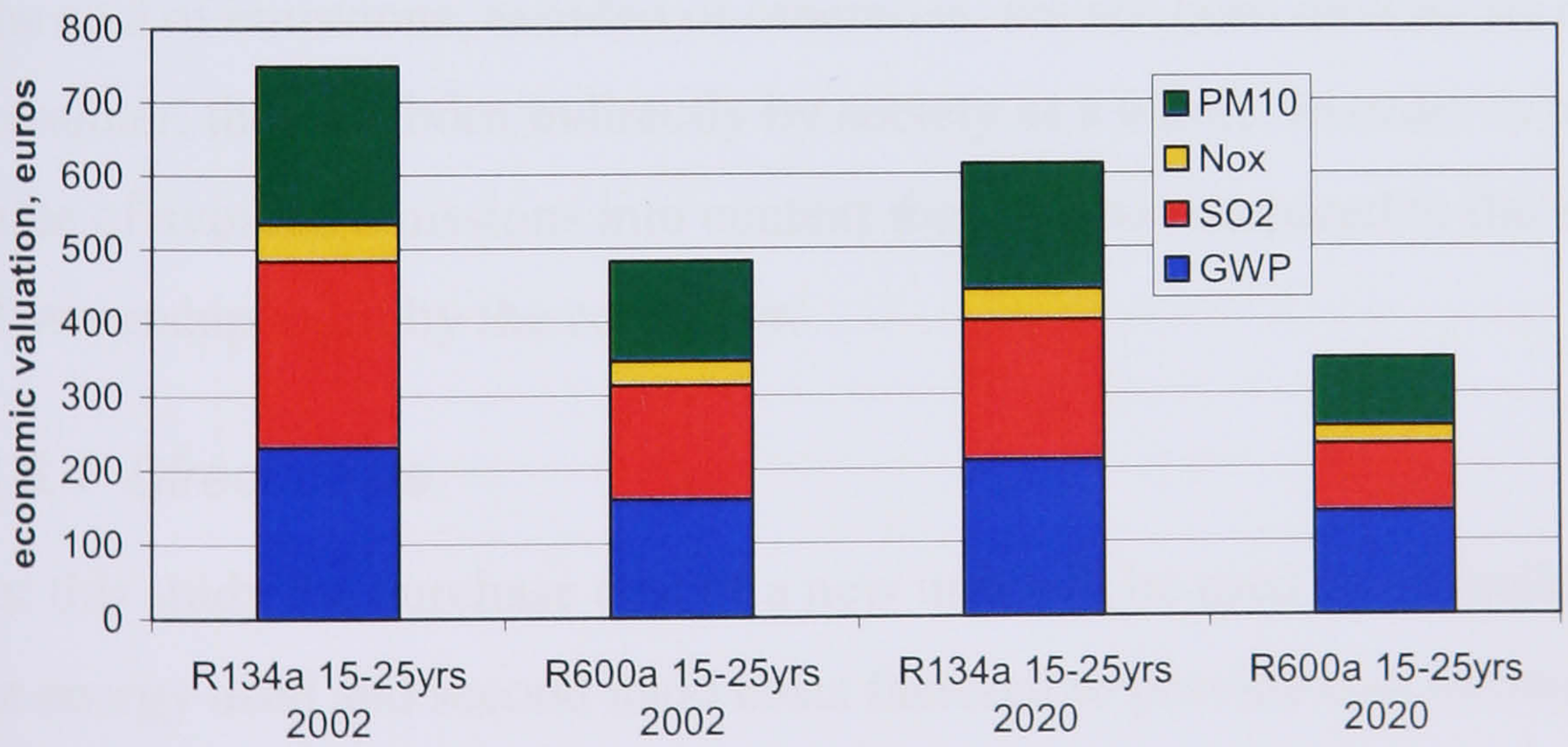

Figure G.4 Valuation of corrected emissions, extended duration

During the extended period of operation the difference in emissions between the R134a and R600a compressors is much more significant. If the used R600a compressor is utilised instead of the used R134a, the value of avoided emissions increases from €81, for the first 15 years, to €266 for the period 15-

25 years. The avoided emissions, when spread across the period of ownership, equate to an average of €5.40 per annum during the first 15 years but increase to €26.60 per annum over the 10-year extended period. If a new R600a compressor is used instead of a used R134a, the value of avoided emissions increases further to €401 over the 10-year period (Table G.8). The emissions presented equate to savings of 54% when using the 2002 fuel cycle rising to 65% for the 2020 scenario. For a new R600a compressor instead of a used R600a compressor over the ten-year period the savings are a modest €134. This represents savings of 28% and 39% over the 2002 and 2020 fuel cycle scenarios respectively.

	Additional costs (savings) €		Savings, % of total emissions cost			
			2002		2020	
	R134a	R600a	R134a	R600a	R134a	R600a
GWP	110	38	48%	24%	52%	27%
SO_2	149	51	59%	33%	79%	56%
NO_x	27	10	54%	29%	64%	39%
PM10	115	36	54%	26%	67%	39%
Total	401	134	54%	28%	65%	39%

Table G.8 Avoidable emission costs 2002 2020, extended duration

G.6 True cost of ownership

The cost of emissions, avoided or otherwise, are not born directly by the consumer, they are born indirectly by society as a whole. In order to place the value of avoided emissions into context they can be compared to the direct cost of ownership, born by the consumer.

G.6.1 Direct costs

For this study the purchase cost of a new unit will be used as a baseline with the energy used and second hand costs factored to provide cost of ownership over the first 15 years and subsequent 15-25 year period (Table G.9). The table shows that for an appliance fitted with the R600a compressor, there is little difference between the direct costs of ownership for the initial 15 years and the subsequent 10 years of extended operation. The direct costs of ownership are in fact marginally lower for the used appliance than the new. For an appliance

fitted with the R134a compressor the cost of ownership over the first 15 years is again similar to that of the R600a appliance. However, the cost of ownership for a used R134a appliance is much higher, even though the purchase price for the used product is much lower than a new appliance. Direct economic savings attributable to compressor selection can be calculated as €44 (€2.93 p.a.) for the first 15 years of ownership and €161 (€16.10 p.a.) for a new R600a appliance compared to a used R134a operating from years 15 to 25.

Operating period, years	0-15		0-10	15-25	
Compressor type	R134a	R600a	R600a	R134a	R600a
Purchase cost, €	220	220	147*	45	45
Energy used, kWh	4541	4244	2758	4371	3335
Energy cost, €0.15/kWh, €	681	637	414	656	500
Total cost of ownership, €	901	857	560	701	545
Costs over new R600a, €	44	-	-	161	5
Average cost per annum, €	60	57	56	70	54.5
Av. Savings per annum, €	3	-	-	16	0.5

*purchase cost for 0-10 years is factored over a 15 year period of ownership

Table G.9 Direct cost of ownership, initial and extended use

G.6.2 Comparisons of direct and indirect costs

The direct cost of ownership scenarios can be compared to their indirect (corrected emissions valuation) environmental costs. The R600a operating over 0-15 years and 0-10 years is used as a baseline scenario for comparison of annual direct and indirect costs. The R600a compressor is compared to the R134a operating over 0-15 years and 15-25 years under the 2002 fuel cycle (Figure G.5).

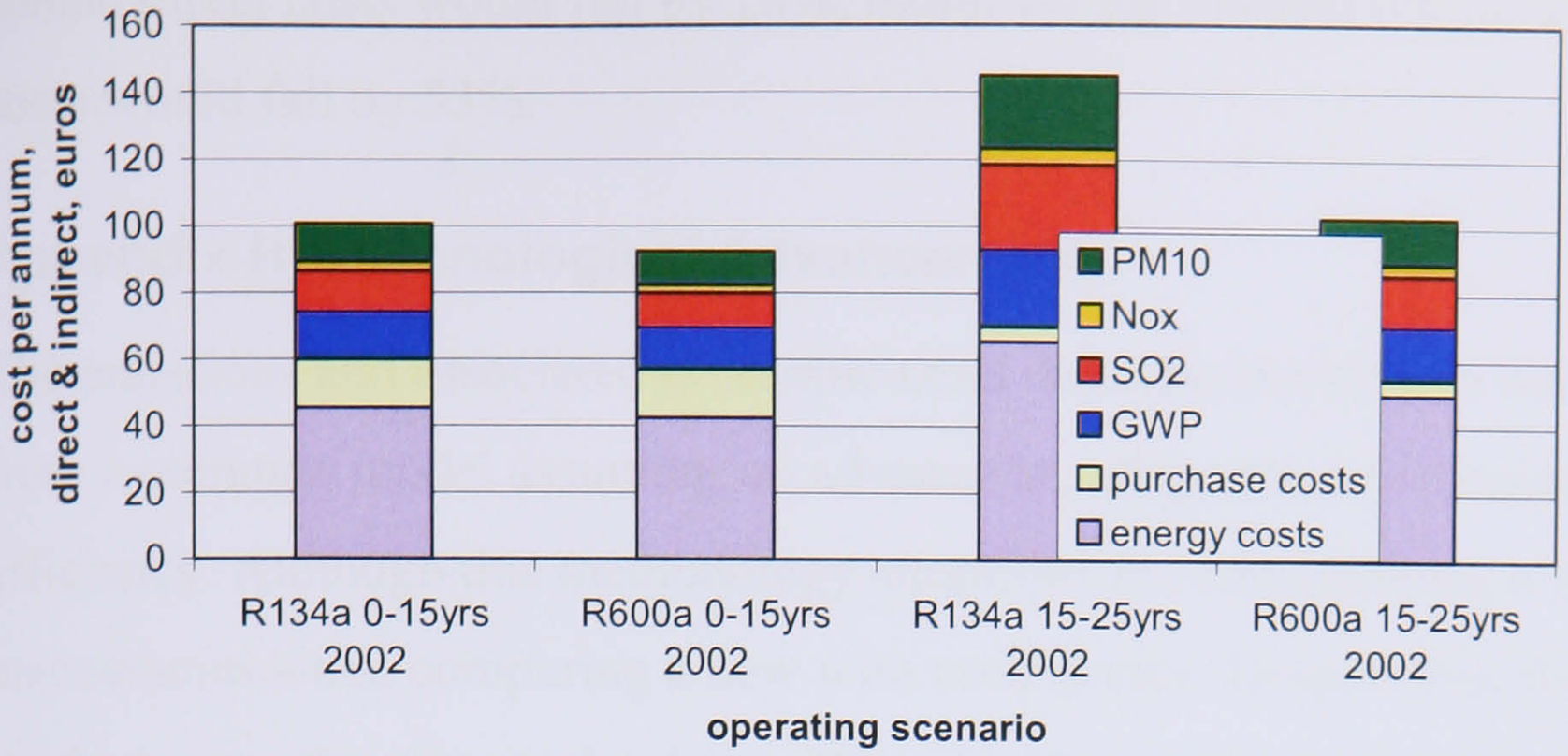

Figure G.5 True cost of ownership, 2002 fuel cycle, per annum

The indirect costs for each of the alternative scenarios varies from 38% of the total for the new R600a product operated over 15 years, rising to 52% for the used R134a. Overall, the direct costs to the consumer are not too dissimilar to the indirect costs, variance primarily being caused by the product purchase price. Most significantly, the consumer's primary consideration when procuring the product is the cost of purchase. In each of the scenarios the purchase price represents only a fraction of the true costs of the product, both to the consumer when compared to energy cost and to the environment when compared to emissions valuation (Table G.10).

Operating period, years	0-15		15-25	
Compressor type	R134a	R600a	R134a	R600a
Purchase costs, €	14.7	14.7	4.5	4.5
energy costs, €	45.4	42.4	65.6	50.0
Emissions costs, €	40.6	35.2	74.8	48.2
total costs, €	100.6	92.2	144.9	102.7

Table G.10 Total costs, direct and indirect, 2002 fuel cycle, per annum

The purchase costs represent only 15-16% of annual costs for a new product and just 3-4% of costs associated with selecting a used appliance. Total avoidable costs can be found by subtracting the best case (baseline) scenario from each condition. The avoidable costs range from €8.40 per annum for the new R134a, €10.40 for the used R600a compressor, all attributable to increased emissions, up to €52.60 for the used R134a of which €39.70 is due to emissions. By replacing a used R134a device with a new R600a device, the

annual direct costs would fall by 18%, moreover the indirect (environmental) costs would fall by 53%.

Appendix H Technological Advancement

The emissions and associated economic costs described have been derived from a common model assuming no advance in refrigeration technology or efficiency. Although this methodology simplifies the comparisons, it leads to inaccuracies when comparing a new with used device. Despite this, the new product using the same technology offers significant savings to both the consumer and environment. Advancements in product efficiency made during the course of this project and are projected to continue in the near future. For the compressor itself, advancements in material selection, anti-wear coating and lubricant viscosity should lead to increased efficiency and reduced wear. For the target appliance, improvements in insulating materials and technologies will reduce the burden placed upon the compressor, hence reduced operating cycle, compressor size and energy requirement.

H.1 Improvements in Energy Requirements

During the progression of the project, on going improvements have been made to the efficiency of refrigeration products. At the outset of the project, energy requirements for a range of typical fridge-freezers and refrigerators were recorded and subsequently compared with equivalent units as the project progressed (Figure H.1, Figure H.2).

Figure H.1 Comparison of 2001 and 2004 fridge freezers

Figure H.2 Comparison of 2001 and 2004 refrigerators

The fridge freezers ranged in size from 215 to 305litres for standard models and from 295 to 325 litres for frost-free models. To allow for variance in appliance volume, unit cost and energy requirements are divided by the internal volume. For 2001 models a range of appliances rated at "A" and "B" efficiency were selected, for 2004 only "A" rated appliances were selected. This criteria is a reflection of the range of appliances offered by retailers and provides for a generalised spread of data. The actual change in energy requirements for a typical device has dropped significantly between 2001 and 2004 as energy efficiency standards improved and older, less efficient models, were dropped from manufacturers product offerings (Table H.1).

2001	Cost, €	Volume, Litres	Energy, kWh/yr
Fridge-freezer, standard	440	266	428
Fridge-freezer, frost free	515	259	487
Refrigerator, 145ltr	214	148	216
Refrigerator, 290ltr	335	288	210
2004			
Fridge-freezer, standard	391 (-11%)	264 (-1%)	317 (-26%)
Fridge-freezer, frost free	463 (-10%)	279 (+8%)	343 (-30%)
Refrigerator, 145ltr	240 (+12%)	141 (-5%)	151 (-30%)
Refrigerator, 290ltr	364 (+9%)	294 (+2%)	166 (-31%)

Table H.1 Comparison of 2001 and 2004 energy requirements

For fridge freezers, product costs have fallen by an average of 10-11% whilst technological improvements have brought about energy savings of between

26% for standard fridge-freezers to 30% for frost-free models.Frost-free models have historically used up to 50% more energy than standard models (DETR 1999). The 2004 frost-free models surveyed for this project showed a much lower penalty of 8%, compared with 14% for 2001, much of which can be attributed to the increased internal volume. For refrigerators, product costs have risen by 9-12% whilst technical improvements have resulted in energy savings of 30% compared to 2001 models. Interestingly, the energy requirements of the 290 litre refrigerator models are very similar to those of the 145 litre units.

H.2 Energy efficient refrigeration

The most efficient models available in 2001 can also be compared with the most efficient of 2004 (Table H.2). For the most efficient models, technology produces improvements of 33% for fridge-freezers and 10% for refrigerators.

	Volume, litres	Energy, KWh/yr	Energy Saving against	
2001			*2001 typical*	-
Fridge-freezer	284	205	223 (52%)	-
Refrigerator	222	175	35 (17%)	-
2004			*2004 typical*	*2001 efficient*
Fridge-freezer	284	137	180 (57%)	68 (33%)
Refrigerator	255	157	9 (5%)	18 (10%)

Table H.2 Comparison of the most efficient models, 2001 & 2004

For fridge-freezers, the most efficient 2004 model available represents an energy saving of 180kWh per annum or 57% compared with a typical 2004 product. For refrigerators, the improvements are more modest, representing a saving of just 9kWh over a typical unit.

H.2.1 Annual efficiency improvements

From the data presented it is clear that improvements in efficiency run at approximately 30% every three years for typical refrigeration appliances of all types except the most efficient refrigerators which improve at approximately 10%. For the purposes of this project technological improvement will be rated at 30% every three years or 9% per annum for complete appliances of which 4.5% attributable to compressor technology.

H.3 Application of technological advancement

The compressor model described assumes an increasing rate of energy use over time. If this is compounded with an advance in technology providing ever more efficient replacement products then replacement becomes increasingly attractive both to the environment and the consumer.

H.3.1 Alternative compressor replacement strategy

The indirect, environmental, costs can be compared over time for both the R600a (Figure H.3) and R134a (Figure H.4) compressors assuming a technical improvement rate of 4.5% per annum. The baseline 25-year extended operational duration can be compared with replacement scenarios of 15 years and 8 years.

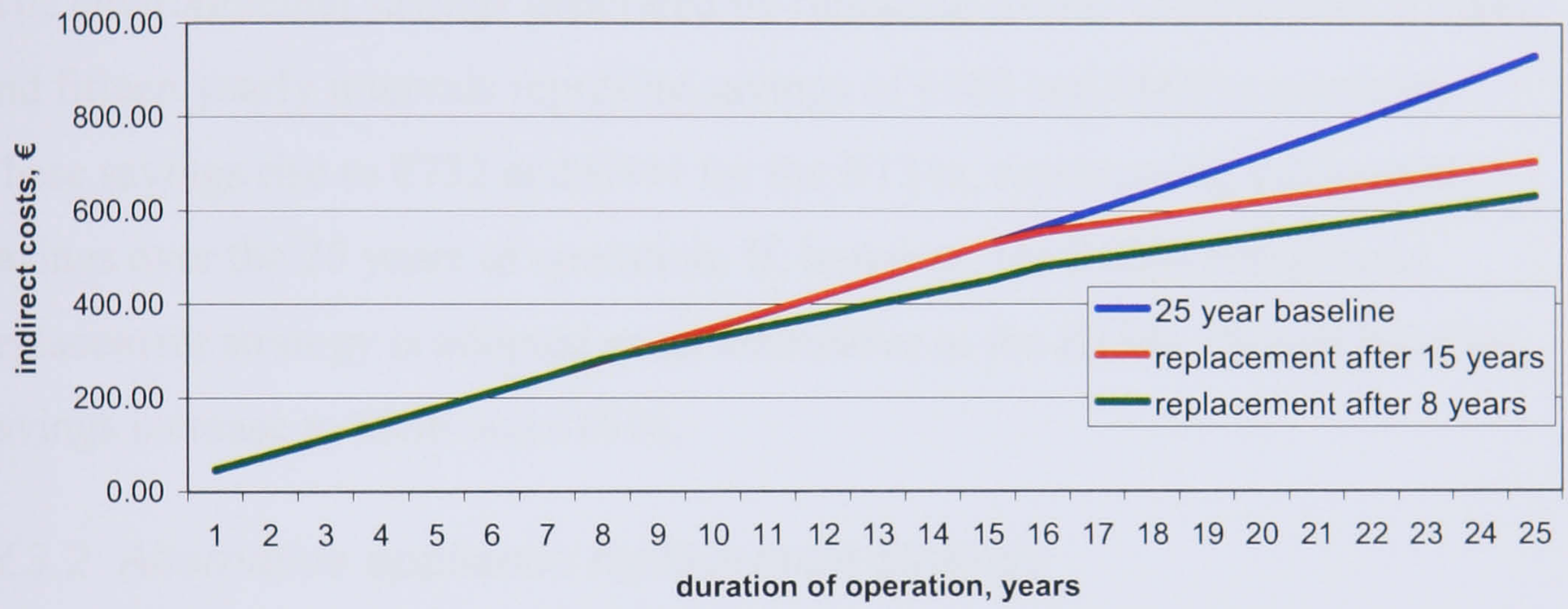

Figure H.3 Comparison of compressor replacement scenarios, R600a

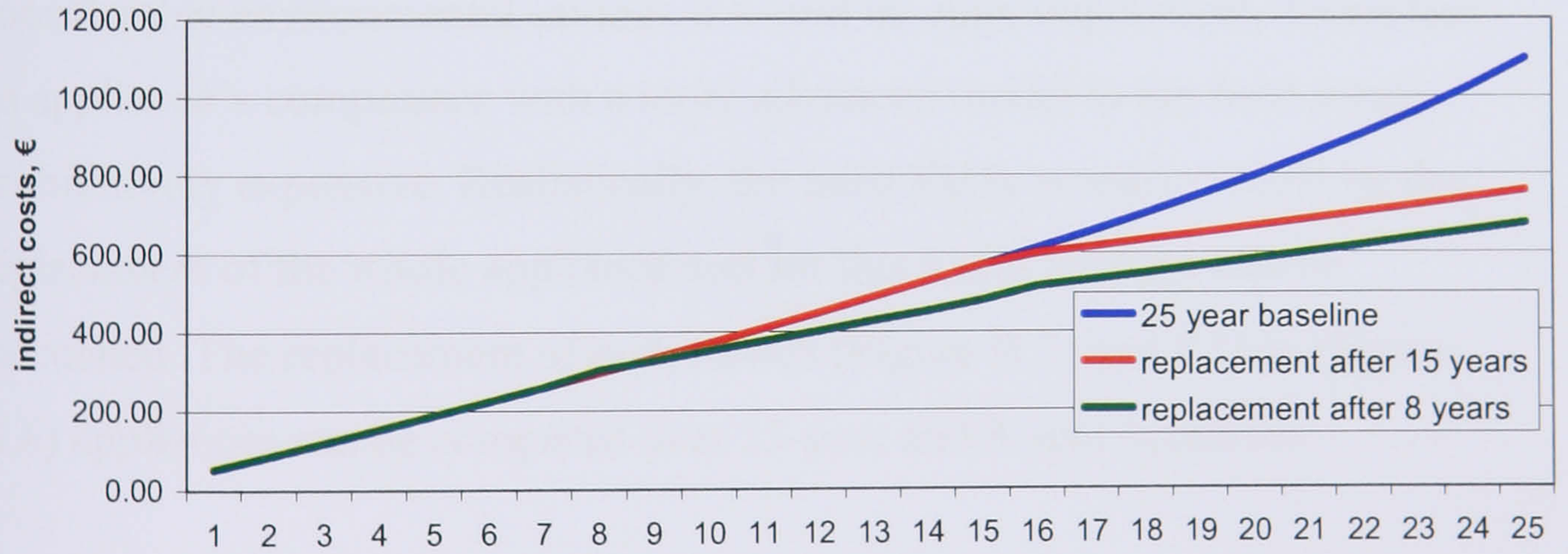

Figure H.4 Comparison of compressor replacement scenarios, R134a

For both compressor types, replacement after 15 years of operation provides for significant environmental savings over the 25-year baseline while replacement at 8-year intervals offers further improvement.The environmental costs of each scenario can be compared to their respective baselines (Table

H.3) to provide environmental savings valuations using the corrected emissions described previously (F.6.4).

	Environmental savings over 25yrs, €					
	R600a replacing R600a 25yr		R134a replacing R134a 25yr		R600a replacing R134a 25yr	
	8yr	15yr	8yr	15yr	8yr	15yr
GWP	134	184	193	247	233	284
SO_2	181	249	272	354	306	374
NO_x	33	46	49	65	56	68
PM10	141	190	217	279	241	290
Total	488	669	732	944	836	1016

Table H.3 Environmental savings, alternative compressor replacement

The environmental savings generated by replacing R600a compressors at eight and fifteen yearly intervals represent savings of €488 and €669 respectively. These savings rise to €732 and €944 for the R134a, representing substantial savings over the 25 years of operation. If, however, the R600a compressor replacement strategy is adopted as an alternative to the R134a 15-year baseline, savings increase to €836 and €1016.

H.3.2 Alternative appliance replacement strategy

Although the compressor replacement strategy highlighted above offers considerable environmental savings it would be quite impractical. To replace an appliance's compressor with a more advanced model in the field seems prohibitively expensive. Realistically, the most likely scenario would be the replacement of the whole appliance and for this a new strategy can be calculated. The replacement of both R600a (Figure H.5) and R134a (Figure H.6) appliances can be compared over 15-year and 8-year scenarios.

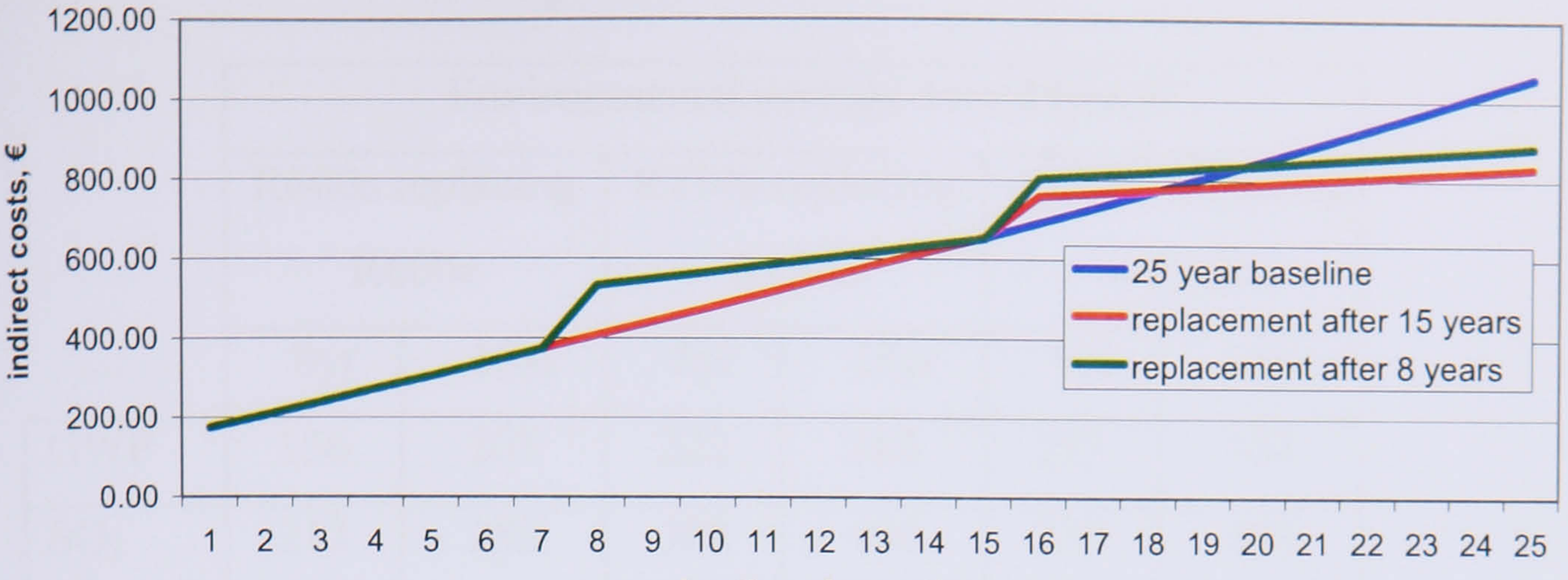

Figure H.5 Comparison of appliance replacement scenarios, R600a

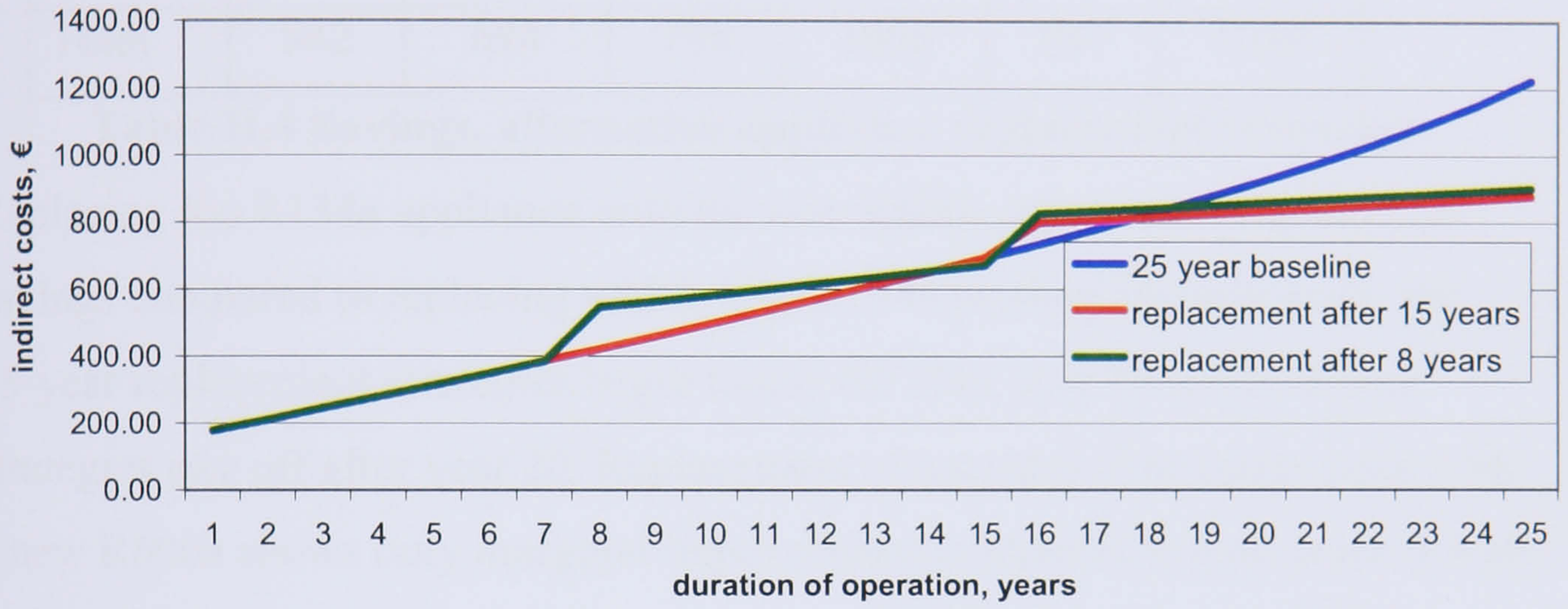

Figure H.6 Comparison of appliance replacement scenarios, R134a

For these scenarios the rate of technological improvement is assumed to be 9% per annum. Even with the higher environmental burden of refrigerator manufacturing and recycling compared to that of the compressor, 15-year replacement still shows the significant environmental benefit it did for compressor replacement alone. For the R600a appliance, replacement after 8-years instead of 15 shows a significant environmental burden whilst for R134a the burden is marginal. As with the compressor, the environmental costs of each scenario can be compared to their respective baselines (Table H.4) to provide environmental savings (or costs) valuations using the corrected emissions described previously (F.6.4). The environmental savings generated by replacing R600a appliances at fifteen and eight yearly intervals represent saving of €694 and a cost of €542 respectively. These savings rise to €1006 and €798 for the replacement of the used R134a, representing more significant savings over the 25 years of operation.

	Environmental savings over 25yrs, €					
	R600a replacing R600a		R134a replacing R134a		R600a compared to R134a	
	8yr	15yr	8yr	15yr	8yr	15yr
GWP	156	208	222	284	253	304
SO_2	213	283	308	400	339	408
NO_x	41	56	58	77	63	78
PM10	132	148	211	246	232	247
Total	542	694	798	1006	887	1039

Table H.4 Savings, alternative appliance replacement scenarios

Replacing the R134a appliance with the new R600a represents only modest savings compared to replacing with a new R134a product. Significantly, the 15-year replacement strategies begin to pay off after year 18 whilst 8-year strategies pay off after year 20. Replacement of a used R134a compressor with a new R600a shows only marginal improvement compared to replacement with a new R600a compressor. The advancement of technology during 15 years leading up to replacement closing the performance gap between technologies.

H.3.3 Appliance replacement strategy, costs to the consumer

The costs to the environment do not necessarily correlated to the costs born by the consumer. The replacement strategies described above are examined for direct costs to the consumer through both the purchase price and energy costs. Scenarios for the replacement of R600a (Figure H.7) and R134a (Figure H.8) appliances are examined whilst technological advancement is again assumed to be at a rate of 9% per annum.

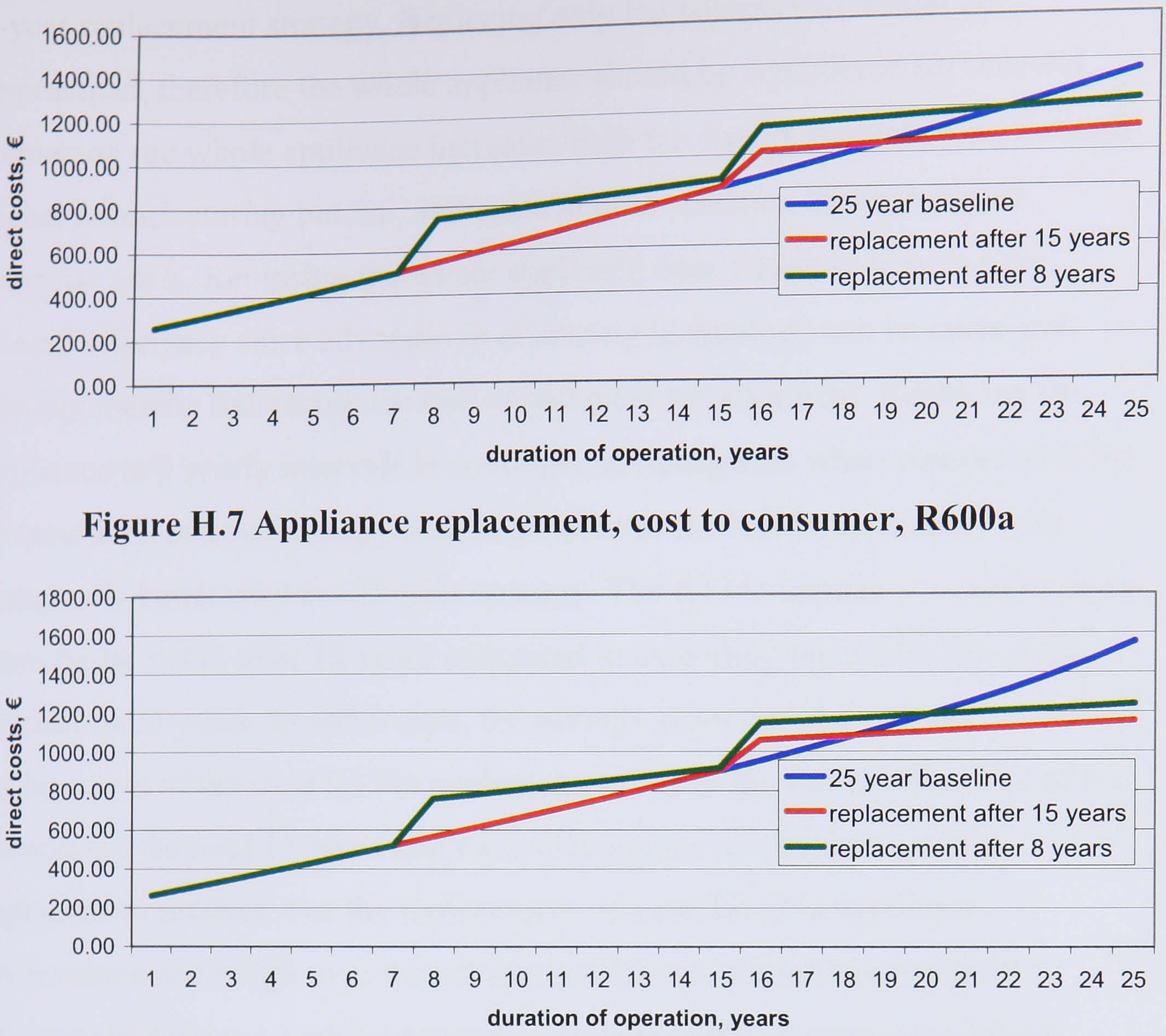

Figure H.7 Appliance replacement, cost to consumer, R600a

Figure H.8 Appliance replacement, cost to consumer, R134a

For the R600a appliance, the 8-year replacement strategy provides only modest savings to the consumer and in-fact represents additional costs to the before year 22 or some 14 years after the first replacement. The 15-year replacement scheme provides more significant overall savings and breaks even after 19 years or 4 years after replacement. The R134a 8-year replacement strategy provides more significant savings than that of the R600a, with overall costs being very similar. The scheme provides savings over the 25-year baseline after 20 years, still some 13 years after the first replacement. The 15-year strategy provides marginally improved savings but, more significantly, does so after year 19 or 4 years after replacement.

H.4 Technical advancement, summary of implications

Technical advancement, in the form of improved energy efficiency, can offer the inducements of lower emissions, reduced energy costs, and quicker payback. When examining the compressor alone, environmental savings over time can be quite significant, offering greatly reduced emissions, even for the

8-year replacement strategy. Replacing only the compressor would be impractical, therefore the whole appliance should be considered for renewal. Replacing the whole appliance increases both the environmental costs, through higher manufacturing burden, and costs to the consumer, through higher purchase costs. Replacing the whole appliance does however improve the overall efficiency since advances in insulating technology can be taken into account thereby increasing the rate of technical advancement. Replacing the appliance at 8 yearly intervals is no longer advantageous when compared to the 15-year replacement strategy and, in the case of the R600a appliance, only marginally better than the 25-year strategy. The R134a appliance benefits most from replacement after 15 years compared to extending the useful life of the product to 25 years. In either case, the savings generated through the replacement of the used R134a appliance are due to the fall in efficiency of the compressor beyond 15 years and the technological advancement of the replacement product. For the replacement of a used R134a appliance environmental savings over the subsequent 10-year period run to €1039 (average of €104 p.a.) whilst economic savings to the consumer total €400 (average of €40 p.a.). To place this into context, The UK used market for cold appliances represents 700000 units sold at an average age of 15 years and kept for a further 7.5 years. If these 700000 units were instead replaced with new products, the environmental savings would run to €72.8M per annum whilst economic savings would be €28M.